(CMP における材料除去メカニズムに関する研究)

Study on the Material Removal Mechanism for CMP characteristics

Mohammed A. Y. A. Bakier

Abstract

The modality for the estimations of the material removal is the core of this study. Through the identification of the mechanisms deduced to the considered models, we could achieve that. We have studied different models due to the chemical mechanical polishing (CMP) area which is under the usage from the plenty of fields from which the several applications branches. Therefore, these applications cannot be counted but it is possible to reduce them to the fundamental effective factors which play a crucial role anyhow the followed mechanism or field.

Firstly, we referred to the basic conventional methods which were handled by the previous researchers (chapter 1) which reflex how they tried to deeply understand the material removal process based on the accuracy of predictions and estimations because this operation has taken place at the microscale. Hence it is very sensitive to chemical activity especially between the wafer surface and the slurry. Moreover, the mechanical effect plays an important role in motivating the CMP parameters. Without exaggeration, we can say that the mechanical power represents the left and right hands for polishing assignments. So that, any defect at it, gets the CMP is not capable to arrive at its target.

For the material removal rate (MRR) at the particle scale, the researchers concentrated on a theoretical study (chapter 2) of the relative tools such as the atomic interactions and the molecular dynamics. Consequently, building the theoretical model is based on denoting the relationships between two CMP characteristics such that the left properties change slightly and are considered uniform during the CMP processing. For example, at Sec. 2.1, we show the estimation methods of MRR based on the relation between particle-wafer, Polishing Pad-wafer, slurry-wafer, … and so on.

After that, we shed the light on the particle agglomeration phenomenon which is a landmark at the wafer-scale mechanisms. In chapter 3, we clarified that the agglomeration based on the Smolochowski approach (Sec.3.1) is built on the bridge which connects CMP and nanofluids. Hence, we set to derive the proposed model and the verification of it (Sec. 3.2.5). Therefore, we extracted the results that help us to identify the general MRR behavior as a dependent variable to the movement of the primary particles concentration and the time. For the deep agglomeration tracking, we take care about the ways of measurements, more specifically, the functions of particle size distributions which are plotted based on the data generated from the dynamic light scattering (DLS) technology. We offered the distinctive features for the used method from the relationships between the agglomeration and each of (pH, concentration, Down-load, and velocity). Since the material removal mechanism is an open topic, many speculations are raised. So, we preferred to be acquainted with the most effective methods of the balance between the results validity and the reality of the assumptions. That is the numerical simulation (chapter 4) where we have studied the material removal mechanism at the pattern trapped model. After we had narrative some of the computational approaches and how the finite element method is implemented for model description, we have explained the Cu-damascene process in which we will concentrate on one of its steps related to Cu-CMP. The model settings for the model under study are presented in section 4.3. The results that we inferred enhance the possibility of prediction of the required CMP steps to achieve the smooth surface for the microelectronic chip (Sec 4.4). Such criterion possesses high attention due to the problems yield from the overpolishing. The pressure at the slurry and the stress at the copper material coincide with each other and enhance a great interaction based on the controlling of the boundary conditions. As the mass of the copper pattern

reduces, the normal stress intensively grows up, which accelerates: Copper removing process, Achieving the planarization criterion, and Justifying the size of manufacturing consumables. In the conventional methods, the pressure on the patterns was considered to have a uniform effect to avoid its complexity. The merit of this study is that the pressure distribution, as well as the slurry flow field, are spatial-time-dependent quantities. A classification from fluid dynamics is supported in chapter 5, and the highlight effects which are noticed in the current study are raised in the final chapter 6.

Acknowledgment

Chapter 1: Background

Chapter 2:

Removal Mechanisms from Conventional Models

Chapter 3:

Removal Mechanism and the Agglomeration

Chapter 4:

Removal Mechanisms at Pattern Trapping Model

Chapter 5: Classification by Fluid Dynamics

Chapter 6: Essence points and Summary

Chapter 1: Background

Chapter 1: Background

1.1 Chemical Mechanical Polishing

Chemical mechanical polishing (CMP) is a process of wafer surface smoothing and planarization. The extreme smooth and flat surface of wafer without subsurface damage, deformations and scratches can be produced by using the CMP process. The CMP process combines chemical reactivity and mechanical action on the wafer surface (Fig. 1).
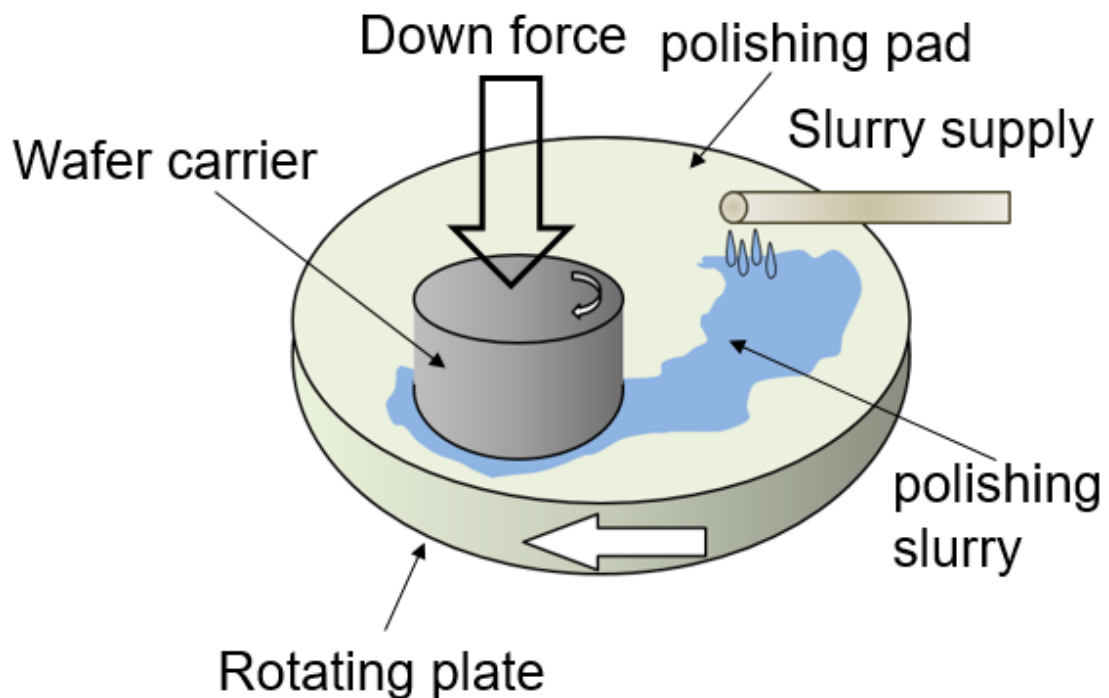
Fig. 1 Schematic graph for chemical mechanical polishing.

Normally, the wafer is held by the polishing head, the wafer surface is attached to the backing film. The down-force pressure is applied to the polishing head to press the wafer surface on the polishing pad during the slurry is released to the polishing pad at the near centre point of the polishing pad. When the platen and polishing head are rotated, the slurry with the abrasive particles spread to the polishing pad and are carried between the

wafer surface and the polishing pad. The slurry with the abrasive particles chemically reacts with the wafer surface. The reacted layer forms on the wafer surface. This reacted layer is soft or passivated so it could be mechanically reacted with the abrasive particles and can be removed from the wafer surface by the both sliding and rolling abrasive particles.

However, the performance of polishing process can be simple expressed by Preston's equation which is direct proportion to the pressure of the wafer and velocity of the polishing pad as in equation:

$$MRR = K_p P \frac{\partial s}{\partial t} (1)$$

Where Kp is the Preston coefficient, P is the down force pressure, and $\frac{\partial s}{\partial t}$ is the linear velocity of the polishing pad. Recently, CMP process has been widely used for achieving a global planarization and very smooth surface in semiconductor devices manufacturing such as integrated circuits (IC), light emitting diodes (LEDs), etc. the CMP market size rapidly increased from about $ 300-400 millions in 1997 to $ 3.32 billion in 2014 [1]. The CMP process requires the several consumables. The slurry cost is a major component of the overall cost in CMP consumables [2]. Furthermore, we can see that the CMP consumable of slurry market is growing at a higher value than the polishing pad and the trend is constantly increasing. Many researchers focused on the development of abrasive particles in slurry.

There are some model which focus on the equilibrium between chemical reaction kinetics and the abrasion as HKMG Al-CMP model introduced by Xu and Chen [3]. At this approach, the wafer surface composites of unreacted (Γ) and reacted materials, randomly

3

distributed. The formation of a composite layer of a wafer surface is a dynamic chemical process. Therefore, the abrasion action directly depends on size of embedded particles on pad through particle adsorption/desorption from the pad.
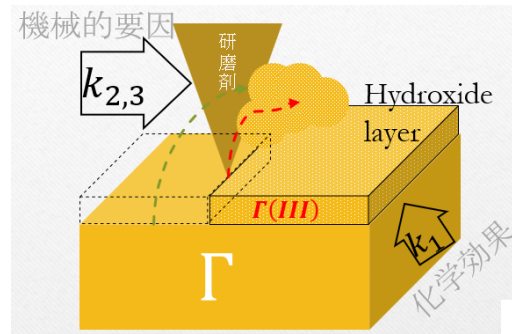
Fig. 2 Effect of chemical reactivity on removal mechanism [3].

The abrasion basically is supported from the friction effect which is generated from the contact areas of the asperities of polishing pad and from the active abrasive particles dispersed at the slurry flow.
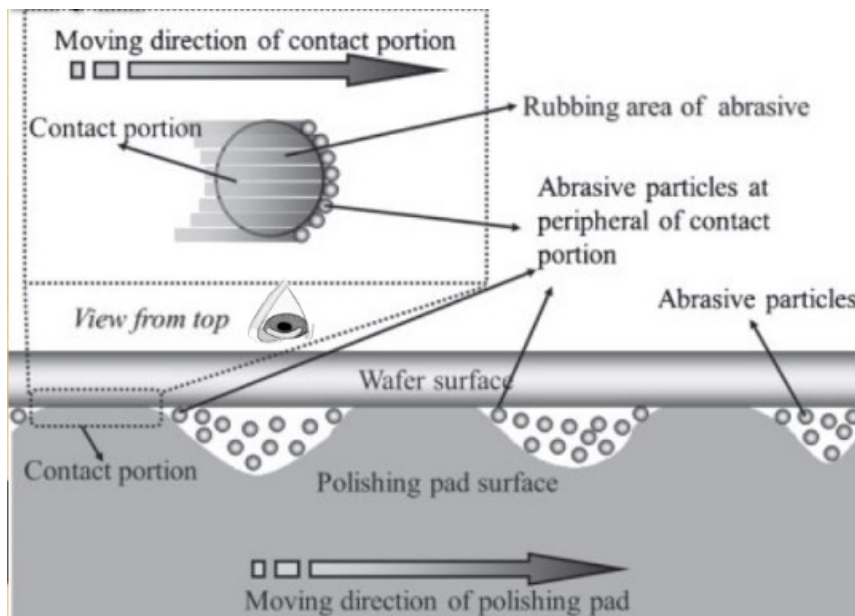
Fig. 3 Effect of mechanical factors on removal mechanism [4].

Isobe et al. [4] have explained the stages required for achieving the effective pressure

4

(contact pressure) which implies to the suitable material removing. The pressure progress enhances the direct contact area of polishing pad asperities, which in turn supply the number of active abrasive particles on the wafer surface. The relation correlates between mechanical factors (pressure and velocity) and the material removal rate is denoted from general Preston equation

$$\text{MRR} = kP^{\alpha}V^{\beta} \quad (2)$$

1.2 Agglomeration mechanisms and MRR

The high-speed development at the feature size and device geometry of modern integrated circuits (IC) implies chemical mechanical polishing (CMP) has become the most important process choice for the surface planarization in the fabrication of advanced multilayer ICs in the microelectronic industry. Thus, a confrontation is forced with an estimation of CMP consumables, and the slurry is on the top of the list. The collusion that occurred between mechanical and chemical effects enhances the crucial role of slurry. Therefore, any deviation at slurry nature inevitably pushes to CMP characteristics and results. Agglomerates production represents the most challenging issue for slurries, in which it could sometimes flip the outcomes inversely to what is planned for. Hence researchers take care of study the relative circumstances of agglomeration especially that these are nano-scale incidents. Therefore, they are subjected to different mechanisms from that at the normal metric space. This the reason gets agglomeration dominates great ambiguity in its phenomena and effects. Hence, we sought in this review article to shed light on the private nature of agglomerates, how scientists are capable to estimate them, their robust relation with surface finishing, and the attempts of agglomeration control.

1.2.1 Electrostatic surface force performance

The introduction of the mathematical concept of fractals permits a quantitative description of the structure of aggregates, which in the past was generally considered to be too complicated. The fractal concept also has contributed to a better understanding of the kinetics of the aggregation process (Table 1). The picture that evolved is based on the existence of two regimes of irreversible aggregation [5-8]. The clusters in both regimes are fractal, but their fractal dimensions, D, are different. For diffusion-limited aggregation D = 1.8, while for reaction limited aggregation D = 2.0-2.1 (denser). In addition, the time dependence of the average cluster size, R, is different in both regimes. The existence of both aggregation regimes has been demonstrated for silica [9-15] colloids. Aggregation in these systems is controlled by electrostatic Coulomb forces that cause a repulsive energy barrier between approaching particles. When a salt is dissolved in the dispersion, the height of the repulsion barrier can be reduced.

At sufficiently high electrolyte concentrations the repulsive barrier can be completely removed and diffusion-limited aggregation results. By contrast, at low electrolyte concentrations when the potential barrier is still several k_{BT}, reaction-limited aggregation results. Where the aggregate produced from collision two masses [16]; M-K and K, N_0 initial concentration, η: viscosity, k_B: Boltzman's constant, U: repulsive pair potential energy between the two abrasive particles at a distance r, $k^{-1} = \sqrt{\frac{\varepsilon k_B T}{4\pi n q^2}}$:

Debye–Hückel screening length, Ze and q: charges, n: charges concentration, ε: the solvent dielectric constant.

Table 1. The kinetics of the agglomeration processes

diffusion-limited regime (DLA)	reaction-limited regime (RLA)
very rapid	much slower
The rate is limited solely by the diffusional motion of the aggregating particles	Particles/clusters have a low sticking probability due to plenty of barriers
$R \propto t^{1/D}$	$R \propto e^{\alpha D}$
Particles are uncharged. Thus, they have no kinetic barriers to agglomeration collision between the two clusters they stick and the resulting cluster has the sum of the mass of either cluster. The driving force is the reduction of surface area or free energy upon sticking $$\frac{dN_M}{dt} = \frac{1}{2}\sum_{k=1}^{n-1} aN_{M-K}N_K - \sum_{k=1}^{\infty} aN_M N_K$$ $$a = \frac{8k_B T N_0}{3\eta} = \frac{1}{t_0}$$	charge-stabilized particles. The agglomeration of these abrasive particles is prevented because a substantial repulsive energy barrier exists between them arising from the repulsive electrostatic energy of like charges. $$\frac{dN_M}{dt} = \frac{1}{2}\sum_{k=1}^{M-1} a_1 N_{M-K}N_K - \sum_{k=1}^{\infty} a_2 N_M N_K$$ $$a_1 = a_1(M-K, K)$$ $$a_2 = C\frac{(M^{1/3} + K^{1/3})^2}{M^{1/3} + K^{1/3}} e^{-U/(k_B T)}$$ $$U(r) = -\frac{Z^2}{\varepsilon}\left(\frac{e^{kr_1}}{1+kr_1}\right)\left(\frac{e^{kr_2}}{1+kr_2}\right)\frac{e^{-kr}}{r}$$ $$C = \frac{8}{3}k_B T N_0$$

Besides, for slurries in which the particles are at their isoelectric point, the particle aggregates can grow from a nanometres to micrometres size in a relatively short time [16] due to the effect of particle surface forces. Such large particles can be the cause of undesirable, deep scratches on the wafer surface [18]. The basic surface forces are attributed to firstly, the van der Waals force which is formulated for the contact of one rigid spherical particle with radius r_p and one rigid flat surface can be found by using [17]:

$$f_{vdW} = \frac{A_{wsp}}{6d_0^2} r_p, A_{wsp} = (A_w^{\frac{1}{2}} - A_s^{\frac{1}{2}})(A_p^{\frac{1}{2}} - A_s^{\frac{1}{2}}) \quad (3)$$

$$\kappa^2 = \left(\frac{e^2}{\varepsilon\varepsilon_0 kT}\right)\sum_i z_i^2 n_{i\infty}, n_{i\infty} = 1000 N_A M_i \quad (4)$$

Secondly, the double-layer interaction force f_{dl} between one spherical particle with radius rp and flat surface and zeta potentials Ψ_1, Ψ_2 under a constant surface charge assumption (HHF-CC) [18,19] is given as a function of the separation distance d0 as follows:

$$f_{dl}(d_0) = -2r_p\pi\varepsilon_0\varepsilon_r(\Psi_1^2 + \Psi_2^2)\frac{\kappa e^{-\kappa d_0}}{1-e^{-2\kappa d_0}}\left(\frac{2\Psi_1\Psi_2}{\Psi_1^2+\Psi_1^2} + e^{-\kappa d_0}\right) \quad (5)$$

The double-layer force between two spherical particles can be computed based on the CA [22] as follows:

$$f_{dl}(d_0) = \frac{-4r_p\pi n_\infty kT}{\kappa}\left[2\bar{y}\ln\left(\frac{B + \bar{y}\coth\left(\frac{\kappa d_0}{2}\right)}{1 + \bar{y}}\right)\right]$$

$$+ \frac{-4r_p\pi n_\infty kT}{\kappa}\ln\left(\frac{1}{\bar{y}^2} + \cosh\kappa d_0 + B\sinh\kappa d_0\right) + \kappa d_0 \quad (6)$$

where $n_\infty = \sum_i n_{i\infty}, \bar{y} = y_1 + y_2, y = \frac{ze\Psi}{kT}, B = (1 + \bar{y}^2 csch^2(\kappa d_0/2))^{1/2}$

1.2.2 Chemical activities

(a) The Reaction Time and the Slurry Additives

Brahma and Talbot [22] have correlated between the aggregation nature and the reaction history in which the chemical contents were reacting with each other. The pH was ~8, near the iso-electric point (IEP), such that aggregation was occurring at a measurable rate. Initially, reaction-limited aggregation was observed, characterized by exponential growth of aggregate sizes, for the majority of suspensions tested.
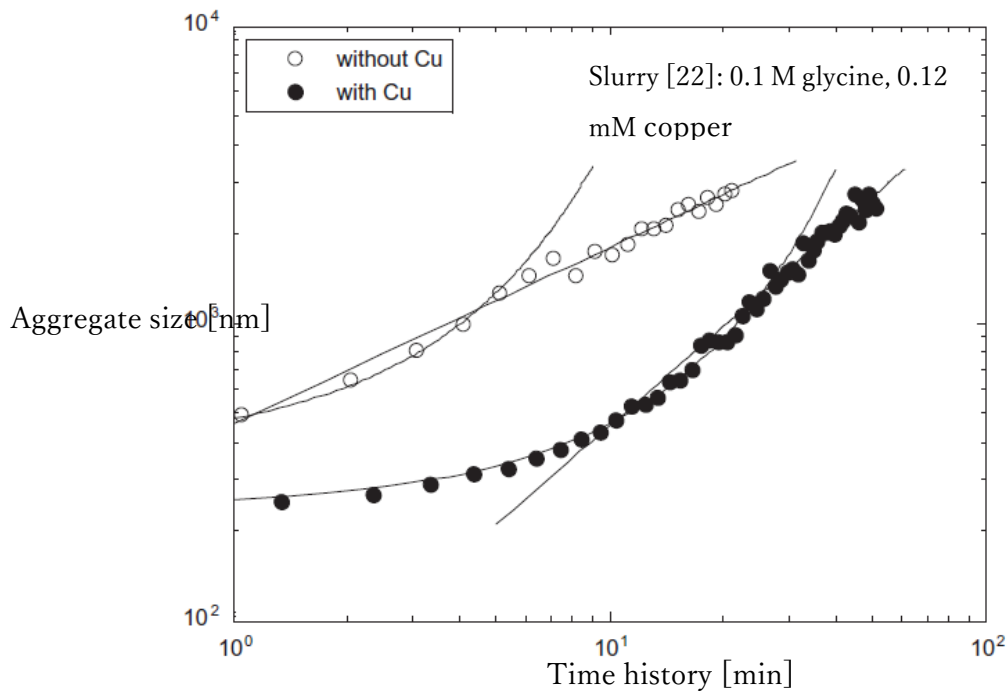
Fig. 3 Histogram of Aggregation growth at the used slurry [22]
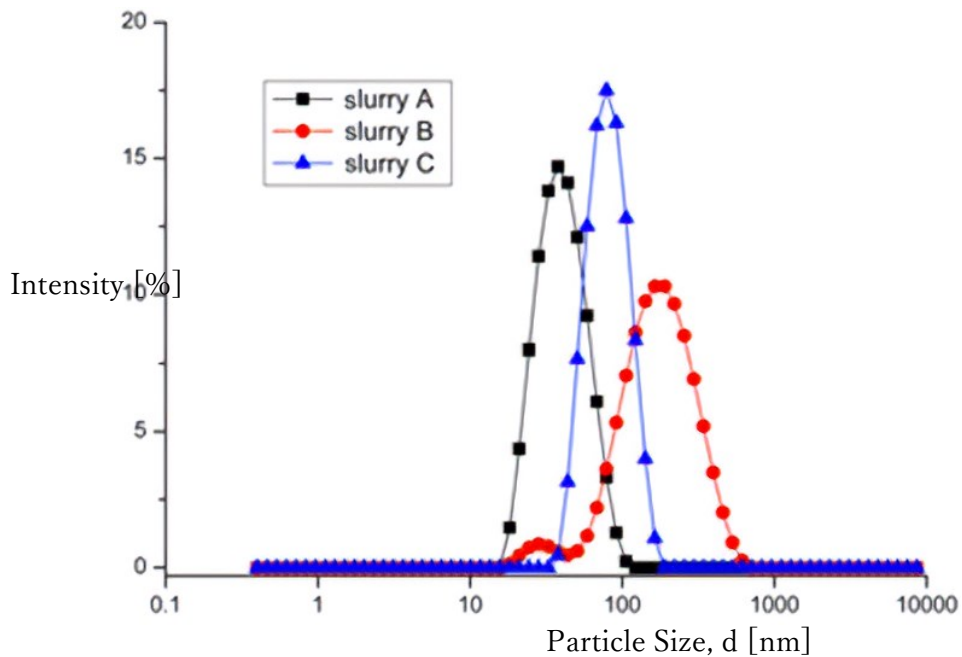
Fig. 4 Particle distributions at Slurry A (15%Silica+1%EDA), Slurry B (Slurry A+3%HPMC), Surry C (Slurry B + 0.2% dispersant); HPMC: hydroxypropyl methyl cellulose [23].

It was observed that once aggregate sizes reached ~500 nm, the aggregate size growth followed a power law, suggesting a shift to diffusion-limited aggregation. This shift is likely caused as a cluster–cluster aggregation dominated over particle–cluster aggregation. Moreover, the suspensions which are without copper exhibited power-law growth from the beginning of measurements. Meaning that these suspensions display high agglomeration action.

(b) Chemistry of the dispersants

Gaopan Chen et al. [23] had noticed that the Organic alkali additives in slurry react with silicon wafer and forms a more stable soft layer (silicate) on the silicon surface which would minimize the damage caused by silica abrasives particles during the polishing. So, they had used ethylenediamine (EDA) as a chemical etchant. But They found that the addition of polymer celluloses would bring serious colloidal silica agglomeration. Therefore, in order to get more stable and well-dispersed slurries, it is necessary to add a

dispersant to reduce the agglomeration of particles (Fig. 4). they had arrived that the compounds with fluorocarbon or polyacrylic function group give some enlightenment that the dispersant with both fluorocarbon and polyacrylic groups will have better dispersibility. Thus, the dispersant with the chemical composition of pre-neutralized fluorocarbon-modified polyacrylic supplied by AFCONA Additives Sdn Bhd is selected.

1.2.3 Functionality of the texture (hardness)

In practical applications, however, there may be a few oversize particles in the slurries in the form of larger size particles (hard agglomerates) due to insufficient filtration [5], or the agglomerates of the primary slurry particles (soft agglomerates) due to poor stability. Hence generation of such agglomerates in the CMP slurries results in unequal distribution of the applied head load on the abrasives, which may lead to surface deformations [25].

(a) Hard Agglomerates

Although the presence of hard agglomerates was suspected to result in major surface deformations [24,25] their impact on polishing performance was only recently quantified in a systematic study [26]. Polishing tests conducted in the presence of hard agglomerates at the established detection limits verified significant degradation in the polishing performance. Surface analysis of the silica wafers polished with spiked slurries showed increased surface roughness, and more surface deformations relative to the baseline polishing as illustrated by the AFM images in Fig.5 a and b. In addition, significant variations were detected in the material removal rate response in the presence of hard agglomerates indicating that they have to be removed from the slurries not only to protect the surface quality but also to achieve a consistent material removal rate.
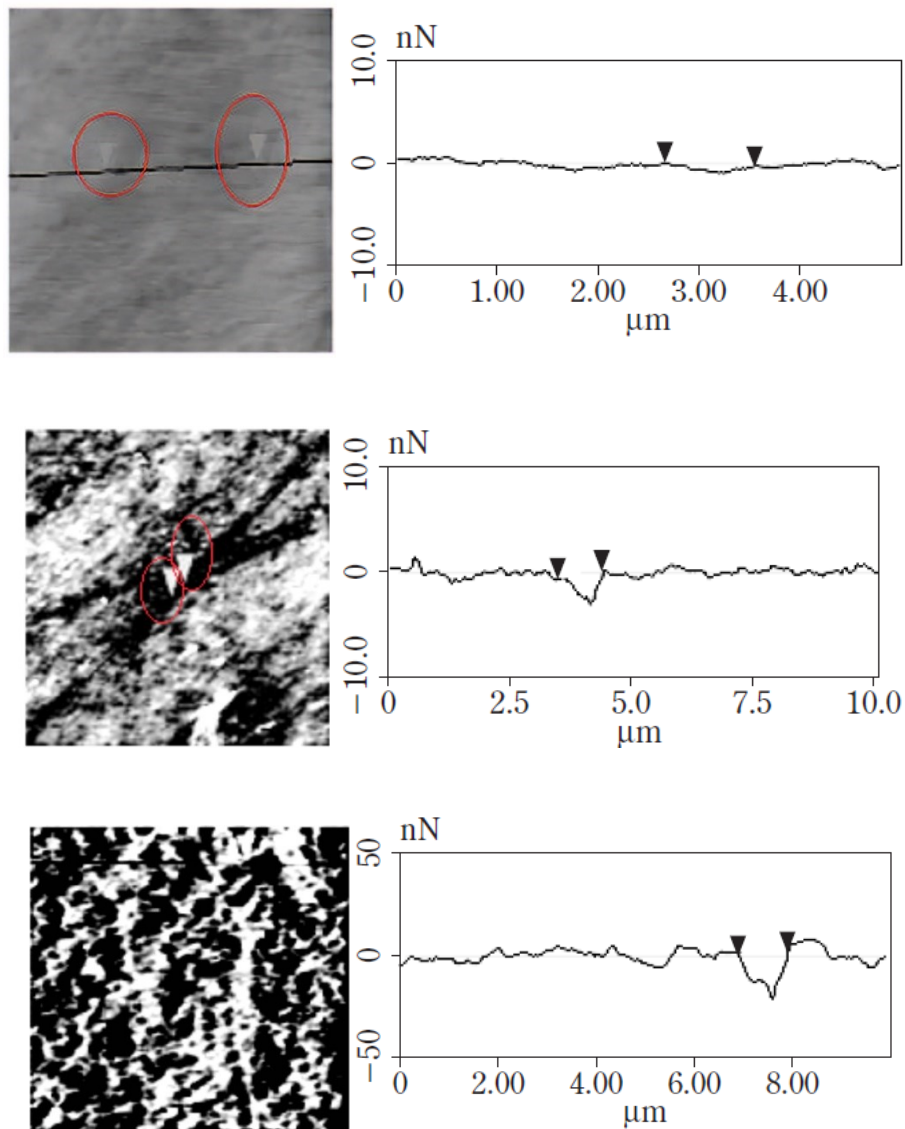
Fig. 5 AFM images of a polished surface due to different agglomerated slurries [48].

(b) Soft Agglomerates

To remove coarser particles, filtration of CMP slurries is commonly practiced. Nevertheless, even after filtering the slurries, the defect counts on the polished surfaces are often observed to be higher than expected [27]. It has been suspected that some of the defects are created by the agglomerate formation during the CMP operations. A study conducted on a silica-silica system [28] by substituting a fraction of baseline slurry with

1 2

dry aggregated, polymer flocculated, and salt coagulated particulates have shown that even the agglomerates, which breakdown under the applied load can result in major surface deformations (Fig.5; bottom figure). These observations indicate that CMP slurries must remain stable during polishing to obtain optimal polishing performance.

1.2.4 Slurry shear Effect

Feng-Chi et al. [29] have shown that high shear-inducing pumps used for slurry delivery cause a significant increase in the concentration of the agglomerates if the magnitude of shear is large enough. Therefore, particles can overcome inter-repulsive forces between them. This is the mechanism -as they thought- by which shear induces the agglomerates in the CMP slurries [30-32]. However, Khanna et al. [33] have concluded that the shear does not cause a significant change in the primary particle size of the abrasives in CMP slurry. But when salts and surfactants are added to the slurry, which changes the slurry chemistry, resulting in an increased rate of formation of agglomerates in the slurry [34]. The decrease in the inter-particle repulsive forces with the reduction in pH further explained the increase in the extent of agglomeration as the pH was reducing from pH~10 (basic) to pH~2 (acidic) conditions.
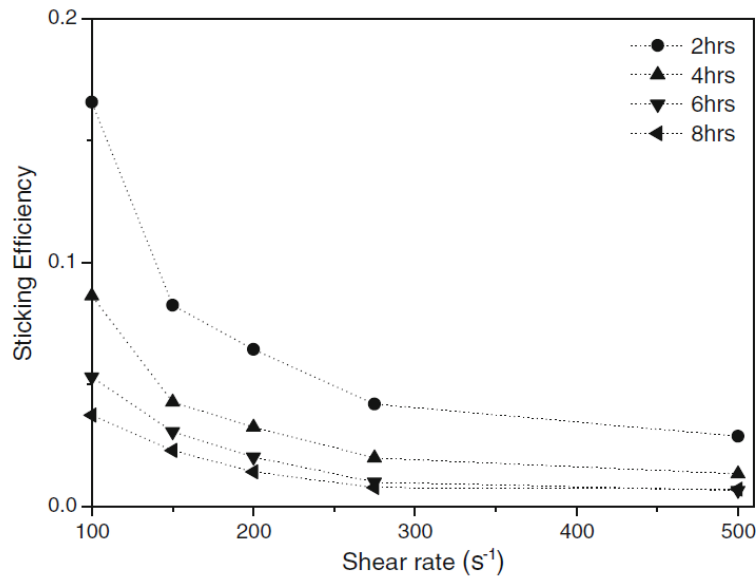
Fig. 6 Time effect on shear-induced agglomerates [35].

In the context, the perspective of Dogon and Golombok [35] was that they had tried to couple between a fluid property (shear) and the fracture size which yields the aggregate growth as follows:

• The shear is proportional to fracture width and therefore is larger in large fractures than in smaller ones.

• Suspensions of small particles have agglomerated faster under high shear conditions in the process of ''orthokinetic agglomeration''.

Consequently, the sticking efficiency (ratio of agglomeration rate to shear-induced collision rate), which reflects the cohesion/strength degree of the generated aggregate from orthokinetic collisions (Fig. 6), offers the destructive effect of shear as time increasing (in hours) because bridging ions creating the agglomerates are depleted, then the sticking efficiency decreases (subjected to surface conditions).

1.2.5 Size-ionic relationship

Brahma and Talbot [22] proved that the dominance effect of aggregation comes from pH by interpreting the effect of ionic strength on aggregation size. However, they ascertained that [37] shear force could not break up aggregates (contrary to Khanna et al. [33]). Where they adopted an exclusive definition for "soft/hard" aggregation. Anyway, the imperfection point here is that they did not associate between the characters of diffusion-limited aggregation DLA/ reaction-limited aggregation RLA and soft/hard agglomerates. It may be some kind of limitation that the used abrasives are Alumina particles (150 nm) at Cu-CMP which rises the incompatibility at slurry constituents of abrasives. Also, they had implemented some additives to the slurry which stimulate the agglomeration to be forced created, consequently, it will be unsound to say that agglomeration has resulted only from CMP.

1.2.6 Based on the indirect inference

Due to the much-complicated conditions of polishing-induced agglomerates and the tracking methods are not easy, many researchers restore to elicit the generation of aggregations certainly due to just polishing operation from their tangible implications either at the consumable slurry or at the produced polished surface. Such an indirect sense of aggregation development could be very suitable as an easy predictable approach. Crawford et al. [36] have investigated the shear thickening of a 25 wt.% fumed silica slurry with 0.15 M KCl and its impact on polishing performance and subsequent surface damage. The thickened slurry displays a ~5-fold increase in viscosity with an increasing shear rate. As the shear rate is reduced back to zero, the slurry continues to thicken showing a final viscosity that is ~100×greater than the initial viscosity. It was deduced
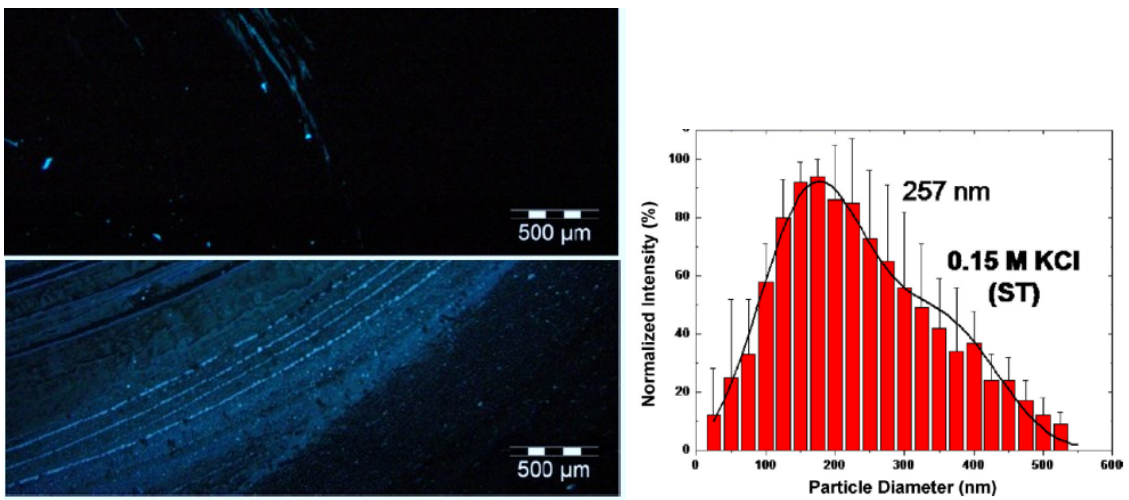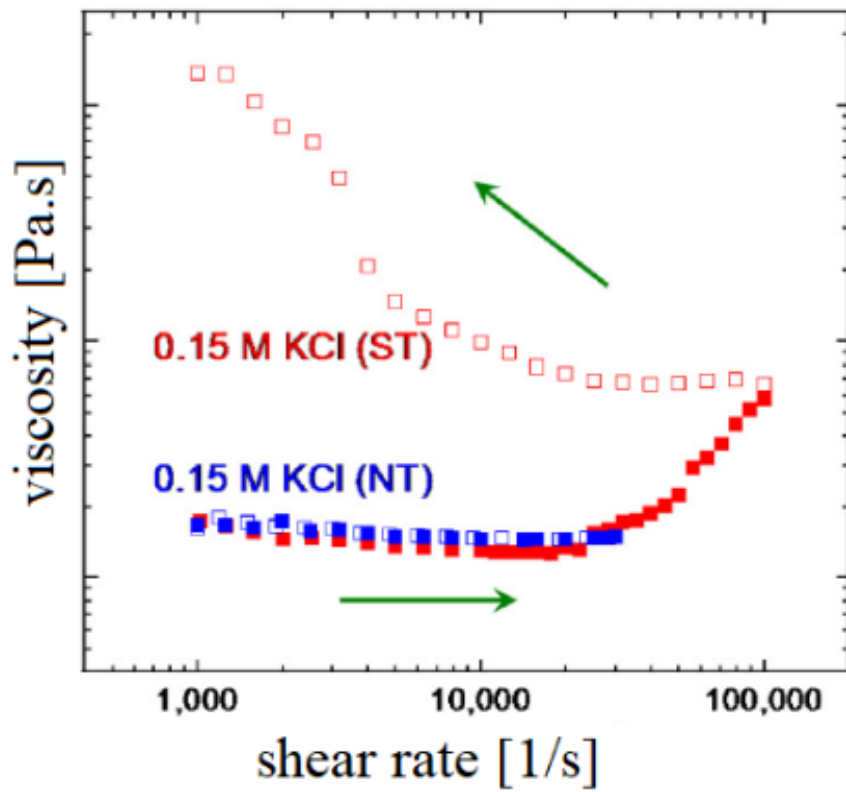
Fig. 7 ST: shear-thickening case, NT: not the thickening case, the solid symbols (top figure) refer to shear rate ramp while the open symbols refer to the reduction, (0.15 M KCl) salt concentration, slurry concentration: 25 wt.%, temperature 25 0C, solid curve (bottom figure) an Edgeworth–Cramer dual-peak function, where mean particle size (257 nm) became much larger than primary case (175 nm) [36].

that the slurry thickening and surface scratching were associated with a dramatic increase in the population of the agglomerates. They were able to correlate changes in slurry viscosity, specifically shear thickening, with the formation of surface scratches during polishing. Then the relation between surface defects and the changes in the slurries 'particle size distribution could be inspired.

1.3 Surface finishing and material removal mechanisms

1.3.1 The agglomeration size and the friction force

The importance of particle size distribution is coming from the frequency of abrasion to expect the surface topography and improve the surface finishing process. It is noticed that the important reason for the discrepancies in many pieces of research describing a relation between MRR and particle size where they attributed that to the type of CMP process. When Luan et al. [46] investigated the effect of low silica concentration slurry (2~5) %, the MRR was directly proportional to the concentration (Fig. 8). On the other hand, they did not distinguish between the initial and instantaneous concentrations along the time of polishing itself while Bakier et al. [38] depicted the reliance between concentration and MRR regarding the differentiation between initial and instantaneous cases. Also, they [46] correlated between the concentration and the particle motion styles as two types; rolling and sliding. Yet, if we consider the contact area mechanism, the relationship will be reserved. Besides, they deduced that for the negligible indentations, as concentration increases, consequently, a rolling mechanism is dominant by particles meaning that the friction decreases. As for the agglomeration, they characterized it into two types; the hard type comes only from contamination (insufficient filtration), while the soft agglomerates are generated from the instability of primary particles during CMP operations.
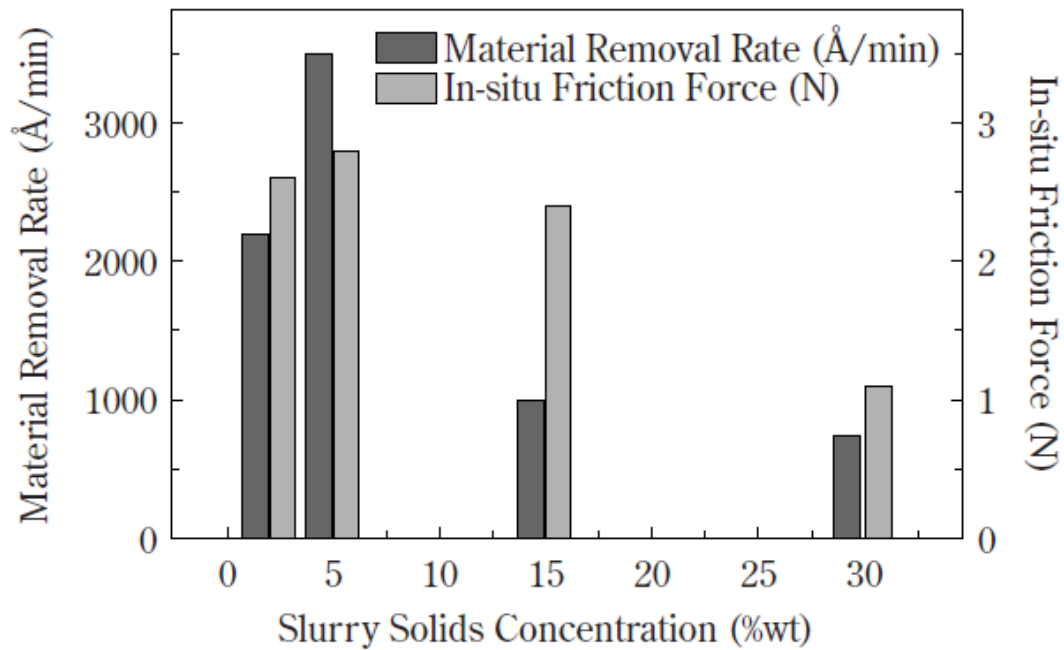
Fig. 8 Material removal rate and friction force of silica as a function of solids loading of 0.5μm silica abrasives [46].

1.3.2 The mixture aggregates

(a) The composite abrasives and MRR

In principle, all constituents in the mixture (more than one kind of abrasives) may coexist as independent entities, or they can mutually attract. Therefore, that yields either hetero-aggregates or smaller particles that can adhere to the larger ones. In the latter case, one may also have the core/shell entities in a mixture with independent small components, present in excess. Figure 9, introduced by Matijevic and Babu [47], demonstrates that the mixed abrasives caused a significant increase in the removal rate and lesser roughness of silicon nitride, as compared to using each abrasive component separately [39]. (as shown in Table 2) which clearly demonstrates the enhanced removal rates [5] when mixed abrasives were employed [40].
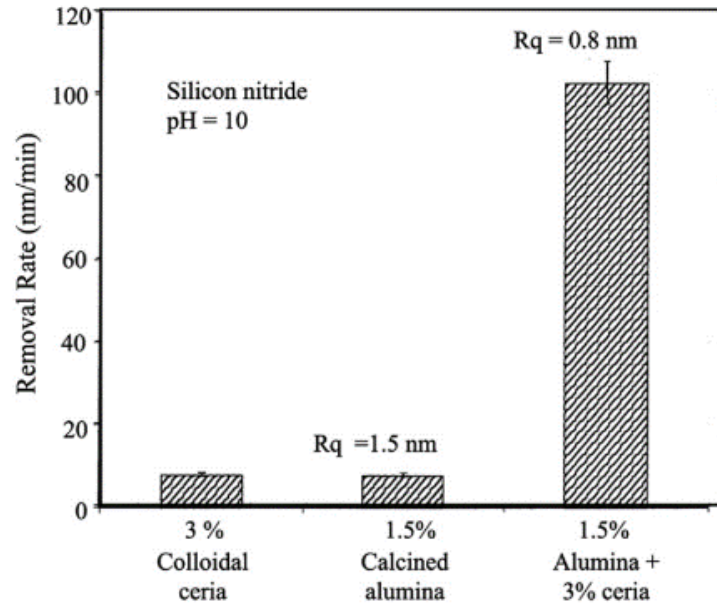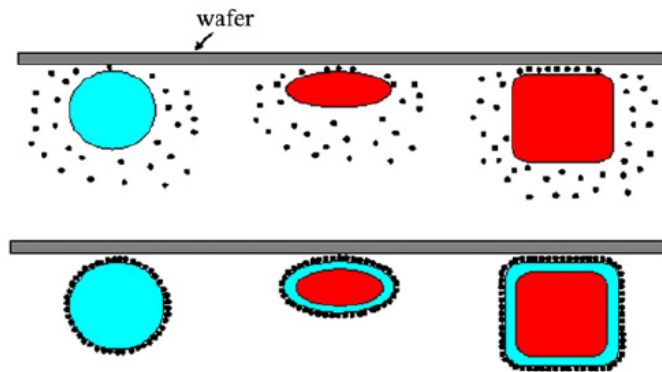
Fig. 9 Effect of mixed abrasives on material removal mechanism [47].

Table 2. Comparison polishing rates for different slurries types [5].
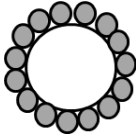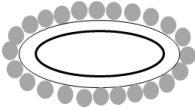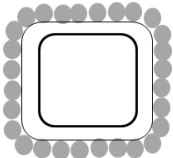
slurry	appearance	Polish rate(nm/min)
1.5 wt% nanosized ceria (Nyacol) at pH 4		~0
3wt % cubic hematite (700 nm) at pH 4		17
3wt % silica (400 nm) + 1.5 wt% ceria at pH 4		22±2
3wt % ellipsodoil hematite (450 nm) + 1.5 wt % ceria (Nyacol) at pH 4		67±2
3wt % cubic hematite (700 nm) + 1.5 wt% ceria (Nyacol) at pH 4		96±19

Table 3. Relation between surface roughness and slurry type [41].

Slurry	Appearance	Polishing rate (nm/min)	Surface roughness (nm)
3wt % colloidal silica (300 nm) coated with nanosized ceria		34±3	1.3~1.6
3wt % hematite (400 nm) encased with silica, coated with nanosized ceria		120±12	1.3~1.5
3wt % hematite (700 nm) encased with silica, coated with nanosized ceria		121±3	0.9~1.1

(b) The composite abrasives and surface roughness

Data in Table 3 show that such coated particles further accelerate the polishing process [42], without having an adverse effect on the surface roughness [40, 47]. In mixtures, they are pressed against the wafer (or disc) by the larger ones, whereby the shape of the latter plays a significant role in the process. As stated by Xu et al. [42] that these polymers act as micro polishing pads.

Finally, using uniform particles consisting of a polymer latex encased with inorganic shells proved beneficial in the CMP of Cu, resulting in reduced dishing and erosion [43].

References

1. NATTHAPHON BUN-ATHUEK, "Novel Characteristics of sub-10 nm Silica Particles for Hybrid Fine Particles in Chemical Mechanical Polishing of Sapphire", PhD Thesis, Computer Science and Systems Engineering, Kyushu Institute of Technology, 2019.

2. M. Bahr, Y. Sampurno, R. Han, A. Philipossian, "Slurry Injection Schemes on the Extent of Slurry Mixing and Availability during Chemical Mechanical Planarization", Micromachines, Vol. 8 (6), pp. 170, 2017.

3. Q. Xu, L. Chen, "A Material Removal Rate Model for Aluminum Gate Chemical Mechanical Planarization", ECS Journal of Solid State Science and Technology, Vol. 4 Number 3, P101-P107, (2015).

4. A. Isobe, M. Akaji, S. Kurokawa, "Proposal of New Polishing Mechanism Based on Feret's Diameter of Contact Area between Polishing Pad and Wafer", Japanese Journal of Applied Physics, Vol. 52, 126503, (2013).

5. L. L. HOEKSTRA, R. VREEKER, W. G. M. AGTEROF, "Aggregation of Colloidal Nickel Hydroxycarbonate Studied by Light Scattering", Journal of Colloid and Interface Science, Vol. 151, Issue 1, pp. 17-25, 1992.

6., H. Eugene Stanley, N. Ostrowsky (Editors), "On Growth and Form, Fractal and Non-Fractal Patterns in Physics", ISBN 978-94-009-5165-5, Nijhoff, Dordrecht, 1986, Spain.

7. C. Domb, J. L. Lebowitz, (Editors), "Phase Transitions and Critical Phenomena", Vol. 18, eBook ISBN: 9780080538754, 2000, Academic Press, New York.

8. P. Meakin, "Fractal aggregates", Advances in Colloid and Interface Science., Vol. 28, pp. 249-331, (1987).

9. D. W. Schaefer, J. E. Martin, P. Wiltzius, D. S. Cannell, "Fractal Geometry of Colloidal Aggregates", PHYSICAL REVIEW LETTERS, Vol. 52, pp. 2371 (1984), DOI: https://doi.org/10.1103/PhysRevLett.52.2371.

10. C. Aubert, D. S. Cannell, "Restructuring of colloidal silica aggregates", PHYSICAL REVIEW LETTERS, Vol. 56, pp. 738, (1986).

11. J. E. Martin, "Slow aggregation of colloidal silica", Physical Review A, Vol. 36, pp. 3415, (1987).

12. P. Tang, D. E. Colflesh, B. Chu, "Temperature effect on fractal structure of silica aggregates", J. Colloid Interface Sci. Vol. 126, pp. 304-313, (1988).

13. P. W. Rouw, C. G. de Kruif, "Adhesive hard-sphere colloidal dispersions: Fractal

structures and fractal growth in silica dispersions", Physical Review A, Vol, 39, pp. 5399, (1989).

14. J. E. Martin, J. P. Wilcoxon, D. Schaefer, J. Odinek, "Fast aggregation of colloidal silica", Physical Review A, Vol. 41, pp. 4379, (1990).

15. M. Carpineti, F. Ferri, M. Giglio, E. Paganini, U. Perini, "Salt-induced fast aggregation of polystyrene latex", Physical Review A, Vol. 42, pp. 7347, (1990).

16. Rana Biswas, Yingying Han, Pavan Karra, Peter Sherman, Abhijit Chandra, "Diffusion-Limited Agglomeration and Defect Generation during Chemical Mechanical Planarization", Journal of The Electrochemical Society, 155, 8, D534-D537 (2008).

17. Dinçer Bozkaya, and Sinan Müftü, "A Material Removal Model for CMP Based on the Contact Mechanics of Pad, Abrasives, and Wafer", Journal of The Electrochemical Society, 156 ,12, H890-H902, 2009.

18. D. Maugis, "Contact, Adhesion and Rupture of Elastic Solids", ISBN: 978-3-662-04125-3, (2000), Springer-Verlag, Berlin, Germany.

19. G. R. Wiese and T. W. Healy, "Effect of particle size on colloid stability", Trans. Faraday Soc., Vol. 66, pp. 490 (1970).

20. S. J. Usui, "Interaction of electrical double layers at constant surface charge", J. Colloid Interface Sci., Vol. 44, pp. 107-113, (1973).

21. J. Gregory, "Interaction of unequal double layers at constant charge", J. Colloid Interface Sci., Vol. 51, pp. 44-51, (1975).

22. Neil Brahma, Jan B. Talbot, "Effects of chemical mechanical planarization slurry additives on the agglomeration of alumina nanoparticles II: Aggregation rate analysis", Journal of Colloid and Interface Science, Vol. 419, pp. 25–30, 2014.

23. Gaopan Chen, Guihai Luo, Guoshun Pan, Yuhong Liu, Haimen Luo, "Influence of colloidal silica dispersion on the decrease of roughness in silicon chemical mechanical polishing", Micro & Nano Letters, Vol. 11, Issue 7, pp. 382–385, 2016, doi: 10.1049/mnl.2015.0592.

24. L. M. Cook, "Chemical processes in glass polishing", J. Non-Cryst. Solids, Vol. 120 Issues 1-3, pp. 152-171, (1990).

25. J. Schlueter, presented at SemiCon Southwest 95 (1995).

26. G. B. Basim, J. J. Adler, U. Mahajan, R. K. Singh, B. M. Moudgil, "Effect of Particle Size of Chemical Mechanical Polishing Slurries for Enhanced Polishing with Minimal Defects", J. Electrochem. Soc., Vol. 147, 3523, (2000).

27. R. Ewasiuk, S. Hong, V. Desai, "Chemical Mechanical Polishing in IC Device

Manufacturing III", (Arimoto Y. A., Opila R. L., Simpson J. R., Sundaram K. B., Ali I., Homma Y.; Editors.), p. 408, Electrochem. Soc. Proc. 99-37, (1999), Pennington, NJ.

28. G. B. Basim, B. M. Moudgil, "Effect of Soft Agglomerates on CMP Slurry Performance", Journal of Colloid and Interface Science, Vol. 256, Issue 1, p. 137-142, December (2002).

29. F.C. Chang, S. Tanawade, R.K. Singh, "Effects of stress-induced particle agglomeration on Defectivity during CMP of low-k dielectrics", J. Electrochem. Soc., Vol. 156, H39–H42, 2009.

30. A.J. Khanna, S. Gupta, P. Kumar, F. Chang, R.K. Singh, "Study of agglomeration behavior of chemical mechanical polishing slurry under controlled shear environments", ECS Journal of Solid State Science and Technology, Vol.7 (5), P238–P242, (2018).

31. M. Elimelech, J. Gregory, X. Jia, W. RA, "Particle Deposition and Aggregation Measurement, Modelling and Simulation", ISBN: 978-0-7506-7024-1, 1995, Elsevier, https://doi.org/10.1016/B978-0-7506-7024-1.X5000-6.

32. R.J. Hunter, "Foundations of Colloid Science", ISBN: 9780198505020, 2001, Oxford University Press.

33. Aniruddh J. Khanna, Sushant Gupta, Purushottam Kumar, Feng-Chi Chang, Rajiv K. Singh, "Quantification of shear induced agglomeration in chemical mechanical polishing slurries under different chemical environments", Microelectronic Engineering, Vol. 210, pp. 1–7, 2019.

34. F.C. Chang, "Externally induced agglomeration during chemical mechanical polishing of metals and dielectrics", Materials Science & Engineering, Vol. Ph.D, University of Florida, Gainesville, Florida, pp. 1–123, 2008.

35. David Dogon, Michael Golombok, "Particle agglomeration in sheared fluids", Journal of Petroleum Exploration and Production Technology, Vol.5, pp.91-98, 2015, DOI 10.1007/s13202-014-0121-2.

36. Nathan C. Crawford, S. Kim R. Williams, David Boldridge, Matthew W. Liberatore, "Shear thickening and defect formation of fumed silica CMP slurries", Colloids and Surfaces A: Physicochem. Eng. Aspects, Vol. 436, pp. 87– 96, 2013.

39., M.G. Song, J. Lee, Y.G. Lee, J. Koo, "Stabilization of gamma alumina slurry for chemical–mechanical polishing of copper", J. Colloid Interface Sci., Vol. 300, pp. 603– 611, (2006).

38. Mohammed A. Y. A. Bakier, Keisuke Suzuki and Panart Khajornrungruang, "Study on relationship between nano particle agglomeration action and polishing characteristics in CMP", Extended Abstracts of the 2020 International Conference on Solid State Devices and Materials, pp. 139–140, 2020.

2 4

39. A. Jindal, S. Hegde, S.V. Babu, "Chemical Mechanical Polishing of Dielectric Films Using Mixed Abrasive Slurries", Journal of The Electrochemical Society, Vol. 150, G314, (2003).

40. Z. Lu, S. Lee, V.R.K. Gorantla, S.V. Babu, E. Matijevic, "Effects of mixed abrasives in chemical mechanical polishing of oxide films", J. Mater. Res., Vol. 18, 2323, 2003.

41. K. Cooper, J. Cooper, J. Groschopf, J. Flake, Y. Solomentsev, J. Farkas, "Effects of Particle Concentration on Chemical Mechanical Planarization", Electrochemical and Solid-State Letters, Vol. 5 Number 12, G109, 2002.

42. Xue Feng Xu, H.F. Chen, H.T. Ma, B.X. Ma, Wei Peng, "The Mechanism of Polymer Particles in Silicon Wafer CMP", Materials Science Forum, Vols. 626-627, pp 231-236, 2009.

43. N. Kawahashi, M. Hattori, title not found, Mater. Res. Soc. Symp. Proc., 671, M.2.2.1, 2001.

44. Tayyab Suratwala, Rusty Steele, Philip E. Miller, Lana Wong, Joel F. Destino, Eyal Feigenbaum, Nan Shen, Michael Feit, "Influence of partial charge on the material removal rate during chemical polishing", Journal of American Ceramic Society, Vol. 102, pp. 1566–1578, 2019.

45. Aniruddh J. Khanna, Feng-Chi Chang, Sushant Gupta, Purushottam Kumar, and Rajiv K. Singh, "Characterization of the nature of shear-induced agglomerates as hard and soft in chemical mechanical polishing slurries", Journal of Vacuum Science & Technology B, Vol. 37, 011207, (2019); doi: 10.1116/1.5065516, https://doi.org/10.1116/1.5065516.

46 Xiaodong Luan, Yuling Liu, Baoguo Zhang, Shengli Wang, Xinhuan Niu, Chenwei Wang, Juan Wang, "Investigation of the barrier slurry with better defect performance and facilitating post-CMP cleaning", Microelectronic Engineering, Vol. 170, pp. 21-28, 2017.

47. E. Matijevic, S.V. Babu, "Colloid aspects of chemical–mechanical planarization", Journal of Colloid and Interface Science, (2008), vol. 320, pp. 219–237.

48. G. Bahar Basim, Brij M. Moudgil, "Slurry Design for Chemical Mechanical Polishing", KONA Powder and Particle Journal, Vol.21, pp. 178-184, (2003).

Chapter 2:

Conventional Models

of Material Removal

Chapter 2: Conventional Methods of Material Removal

2.1 Theoretical Discussion

When the wafer rigidly contacts the pad surface with a high normal pressure and low relative velocity, the effect of lubrication will be negligible and the friction force at the interface will be high. This contact is known as direct contact. As the normal pressure decreases or the relative velocity between the wafer and the pad increases, the thickness of lubrication increases and the wafer will slide without much friction on the pad surface. This is called hydroplane sliding contact. Semi-direct contact is in the transition between direct and hydroplane sliding contact.

2.1.1 Particle-Wafer interaction

The most famous material removal equation is the experimental Preston's Equation [1], which was initially introduced for glass polishing,

$$MRR= K_e PV \quad (1)$$

where MRR is the material removal rate, K_e an all-purpose coefficient, P, the down pressure and V the relative velocity over the wafer-pad interface. It demonstrates a linear dependency of material removal rate on the pressure and velocity. An equivalent equation is the Archard's equation [2] in the area of *wear*. Not all experimental MRR data in CMP, specially, in metal CMP, supports the linear pressure times velocity dependency. Revised Preston's equations were therefore proposed by different researchers. For example, considering that the material removal rate does not extrapolate to zero, Maury et. al. [3] introduces a fitting parameter MRR_0 into Preston's equation:

$$MRR= K_e PV + MRR_0 \quad (2)$$

Later, the nonlinear experimental equation

$$MRR = K_e P^\alpha V^\beta \text{ (3)}$$

where where α, β are two fitting parameters, was proposed by Wrschka et. al [4] to get a better fit of the experimental data.

The major problem with Preston's equation and its revision is that consumable and wafer parameters are not included explicitly. Therefore, the process window in terms of consumable effects cannot be obtained. By extending Brown's model [5] of the metal polishing to the silicon polishing, Cook [6] developed a physical model to address this limitation. The interactions between the abrasive particles and the wafer surface is proposed as a Hertzian elastic penetration [7] of a spherical particle under uniform pressure P into the wafer surface, sliding along the surface with a velocity V and removing glass volume proportional to the penetration. The MRR formulation was proposed as:

$$MRR = (2E)^{-1}PV \text{ (4)}$$

where E is the Young's modulus of the wafer materials. This model can be taken as a theoretical verification of the Preston's equation since it supports the linear dependency of MRR on pressure and velocity. The relationship between the wafer surface roughness Ra and the down pressure P and abrasive size can also be obtained based on this model:

$$R_a = 3/4 \, x (P/2k_1 E)^{2/3} \text{ (5)}$$

where $k1$ is the particle concentration and unity for a fully filled close hexagonal packing [6] and x the diameter of the slurry particles. A similar model was developed by Liu et. al. [8] based on the statistical method and Herzian elastic

penetration. Besides the wafer material parameter including wafer hardness H_w and wafer Young's modulus E_w, this model includes pad hardness H_p and abrasive Young's modulus E_s:

$$MRR = C_e \left(\frac{H_w}{H_w+H_p}\right)\left(\frac{E_S+E_w}{E_S E_w}\right) PV \quad (6)$$

where Ce is a coefficient to account for the effects of slurry chemicals and other consumable parameters. This model, similar to Cook's model, suggests that the material removal is proportional to the applied pressure and relative speed.
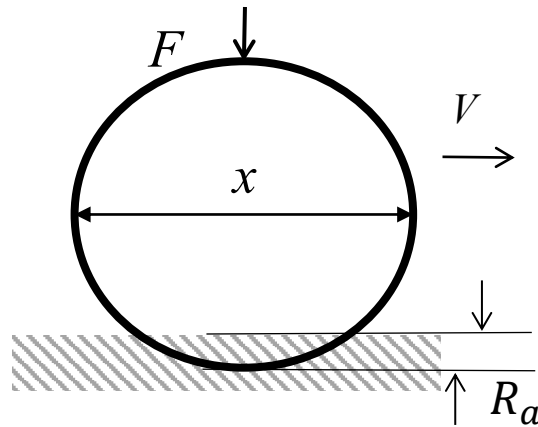
Fig.1 Mechanics of particle/glass contact (from Cook [6]).

The advantages of Cook's and Liu's models over Preston's equation are that they provide insights into the roles and interactions of the consumable parameters. The contributions of the slurry abrasives and pad, for example, have been attributed to their size and hardness. An additional benefit is that not only material removal rate, but also surface quality issue such as roughness, can be addressed using these models. In Cook's and Liu's models, the mechanical removal by abrasive particles is the dominant mechanism. Some

researchers, instead, believe that the material removal is due to a mechanical-enhanced erosion.

In Runnels' model, the hydroplane sliding contact mode was assumed to be a physical phenomenon occurring in CMP. In hydroplane sliding contact mode, only the hydrodynamic lubrication film supports the load between two surfaces. Under the assumption that the slurry exhibits Newtonian behavior and the pad and the wafer are rigid and flat, the behavior of the slurry film was explained using Navier-Stokes equations for incompressible Newtonian flow. Runnel et. al. [9] follows this and developed an erosion-based model for CMP. They assumed that a fluid film exists between the wafer and pad interface, which affects the erosion/material removal rates at each single point through the fluid stress tensors over there:

$$MRR = C_e \sigma_t \sigma_n \quad (7)$$

where C_e is an all-purpose coefficient, σ_t is the shear stress due to the slurry flow and σ_n the normal stress. Runnel's model has been integrated into several particle-scale models by researchers including Tseng and Wang [10] and Zhang and Busnaina [11]. Tseng and Wang attributed the normal stress at the particle-wafer contact to the elastic indentation of the particle into the wafer surface, which is similar as that proposed by Cook [6], and calculated the normal stress over the wafer-particle interface as

$$\sigma_n = \frac{F}{\pi r_c^2} \quad (8)$$

where F is the force acting on the spherical particles, which is proportional to the pressure P,

$$r_c = \left(\frac{3}{4} F \left(\frac{d}{2}\right) \left[\frac{(1-v^2)}{E} + \frac{(1-\acute{v}^2)}{\acute{E}}\right]\right)^{1/3} (9)$$

3 0

the radius of wafer-particle contact, d the diameter of particles, υ and υ' the Poisson's ratios of wafer surface and the particle and E and E' the elastic modulus of the wafer and particles, respectively. The shear stress due to the slurry flow can be approximated as:

$$\sigma_t = C_e\sqrt{\mu V P A_0} \qquad (10)$$

where μ is the dynamic viscosity of the slurry and A_0 the area of wafer surface. Substitution of equations (8) and (10) into (7) yields:

$$MRR = K_e P^{5/6} V^{1/2} \quad (11)$$

where Ke is the parameter to account for material properties, slurry abrasive concentration and chemical processes. This model demonstrated a non-linear relationship between the material removal and the pressure times velocity. In comparison to the Cook's and Liu's model, Tseng's model is attempting to connect the elastic indentation to the erosion rate instead of the mechanical abrasion. While the down pressure dependency (an exponent of 5/6) is still close to a linear dependency, the velocity dependency (an exponent of ½) is quite nonlinear. This is because the contribution of velocity has been attributed to the slurry flow instead of a sliding of abrasives. Recently, the suitability of the Preston's equation was examined [10] and a modified Preston's equation was proposed based upon the combined solid and fluid mechanics. Cook's, Liu's and Tseng and Wang's models attributed the penetration of the abrasive particles to Hertzian elastic contact. Zhang and Busnaina [11] estimated the contact pressure between the particle and the contact surface and found that it is larger than the yielding stress of the polished materials. Therefore, they proposed that plastic deformation is a more likely deformation mechanism of polishing surfaces.

The contact pressure over the particle-wafer interfaces is suggested to be equal to the hardness H_w of the wafer materials. Replacing the normal stress (Eq. 8) in Tseng and Wang's model with the hardness H_w yields the following material removal rate formulation:

$$MRR = K_e(PV)^{1/2} \quad (12)$$

where K_e is the parameter to account for materials properties, slurry abrasive concentration and chemical processes. Both Tseng and Wang and Zhang and Busnaina's models suggest a nonlinear pressure times velocity dependency of material removal rate. However, Zhang and Busnaina attributes all the non-linearity to the fluid flow while part of the non-linearity in Tseng and Wang's model is from the elastic indentation of the abrasives. Moreover, it is noted that besides the external force applied on the particles from the pad, they also proposed that an adhesion force, either van der Waals force or electrostatic force depending on the separation distance between the particle and the wafer, contributes to the indentation. This has been integrated into another particle-scale model by Zhang et.al [12]. In a series of papers by Ahmadi and Xia [13] and Mazaheri and Ahmadi [14,15], a thermodynamic work parameter Wa of adhesion is used to account for its effects on the indentation of abrasive particles. Lately, Mazaheri and Ahmadi [15] introduced a double layer (dl) force into the indentation force, whose magnitude is a function of the zeta potential of the abrasives and the wafer. Beside the abrasive wear, Ahmadi and Xia [13] also consider the adhesion wear of wafer in their model. Moreover, while most of the models treated the abrasives as spherical shape, Mazaheri and Ahmadi [14, 15] treated them as spheres with a number of hemispherical bumps around their surface. The penetrations of slurry abrasives are modeled as the penetrations of the bumps.

The above models imply that the abrasives are embedded into the pad and indented into the wafer surface. Beside these kinds of 'two-body' based models, it is noted that there are modeling efforts which assume that the abrasive particles float in the slurry and impact the wafer surface from time to time. It is these impacts that remove the materials. One model on this aspect has been proposed by Su [16], assuming a three-body abrasion of materials. Models similar to that by Tseng and Wang, attributing the material removal to the erosion enhanced by the 'three-body' abrasive impact, instead of a 'two-body' indentation, may be developed.

2.1.2 Polishing Pad-Wafer interaction

The pad is assumed to be smooth in the earlier particle-wafer interaction models. It has been observed that the pad topography and pad material play an important role in material removal process. For example, the material removal rate increases with the pad surface roughness [17]. A softer pad yields larger material removal rate [17]. Without conditioning of the polishing pad surface, the material removal rate decreases exponentially with polishing time [18]. In consideration of this, Yu et. al. [19] developed a pad-based model. They approximated the peaks on the pad surface by hemispherical asperities with constant radius β. The asperity height is assumed to follow a Gaussian distribution $\Phi_Z(\mu_Z, \sigma_Z)$ where μ_Z is the mean value and σ_Z is the standard deviation of the asperity heights. Based on the model, the real contact area is smaller than the nominal contact area and proportional to the down pressure. Steigerwald et. al [20] proposed that the material removal rate is proportional to the number of abrasive particles over the contact area. Combining this argument with Yu's model yields a linear dependency of the material removal rate on the down pressure. This agrees with Preston's Equation. Zhao

and Shi [21] also proposed a model based on the wafer-asperity contact. Unlike Yu's model [19], the model does not consider the Gaussian distribution of the asperity heights. The contact area between an asperity and the wafer is given by $A_a \propto P^{2/3}$ based on Hertz elastic contact theory. By combining Steigerwald's argument, the material removal rate formulation can be obtained as

$$MRR = K(V)P^{2/3} \quad (13)$$

where $K(V)$ is a function of the relative velocity V and other CMP parameters. It is further considered by Zhao and Shi [21] that when the particles are rolling against the wafer surface, their contribution to material removal will be negligible. They argued that whether the particle is rolling or not is determined by the surface friction between the particles and the wafer, and only when the down pressure P is larger than a threshold down pressure P_{th}, the pure rolling can be avoided. This leads to the following material removal rate formulation:

$$MRR = \begin{cases} K(V)\left(P^{2/3} - P_{th}^{2/3}\right), & P \geq P_{th} \\ 0, & P < P_{th} \end{cases} \quad (14)$$

Besides the above analytical models, it is also noted that recently numerical models based on finite element method have been used to investigate the wafer-pad contact [31]. The fundamental difference between the above pad-based models in this section and the particle-based models by Cook and others is that pad-based models attribute the material removal rate to the number of abrasive particles captured by the polishing pad while the later attributes the material removal rate to the interaction between a single abrasive and the wafer. Therefore, the nonlinear pressure dependency in Yu et. al [19] and Zhao and Shi's models [21] is due to the pressure dependency of the contact area

while in the particle-based models it is due to the pressure dependency of the indentation of a single abrasive. Neither of them may be sufficient. A complete model should consider that the material removal rate is equal to the number of abrasives times the material removed by a single abrasive. A particle-pad interaction model is critical for this purpose considering that the function of the polishing pad is to hold the abrasive particles, transmit load forces to the particle-wafer surface, and conform to the wafer being polished.
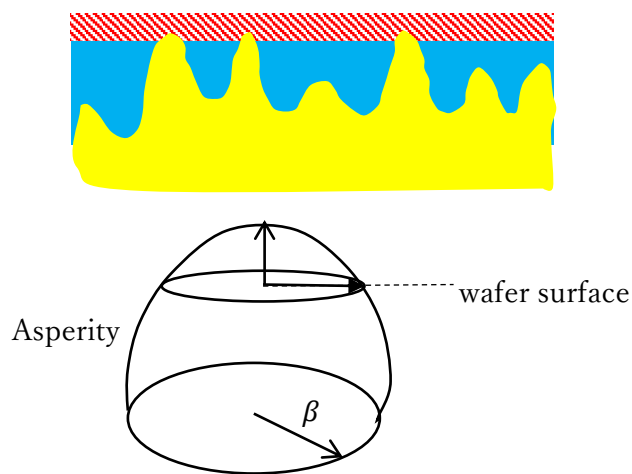
Fig. 2 Wafer-pad contact model (Yu et. al [19])

2.1.3 Particle-Polishing Pad Interaction

Since the force supported by the 'cutting tools'-slurry abrasives is critical to determine the material removed by a single abrasive and it is obtained from the polishing pad or slurry film, a successful particle-pad interaction model should first be able to evaluate the force. Several possible contact modes between the particles and pad exist. The first mode is that a slurry film is formed over the wafer-pad interface and therefore the particles are never embedded into the pad but impact the pad only. In this case, the pad contributes to the force through the slurry film.

Detailed fluid mechanics model considering the topography and deformation of the

pad is needed to evaluate this force. Su's model [16] may be helpful on this aspect.

The second possible mode is that the abrasives are embedded into the polishing pad.

This is the case of the 'two-body' removal of materials. Cook's model [7] suggested

a closely packing of spherical abrasives into the pad. It is assumed that the wafer and

pad are separated completely by the abrasives and no pad-wafer direct contact exists.

The force applied on a single abrasive under these assumptions is given by

$$F = \frac{2\sqrt{3}Px^2}{k_1} \quad (15)$$

where P the polishing pressure, x the abrasive size and k_1 is the particle fill fraction

on the pad. This particle-pad interaction model has been integrated into the material

removal model of Cook [7]. It is also used by Ahmadi and Xia [13] to evaluate

the force on a particle in their case of a hard-pad and larger concentration of abrasive

particles. Later, Zhao and Shi [21] proposed that when the pad is soft enough, the

abrasive particles will be embedded into the pad deeply and the force from the wafer

is supported by the pad and abrasives together. This idea has been applied by Luo and

Dornfeld [22, 23, 24] and Fu et. al [25] in their integrated material removal model. Luo

and Dornfeld's model [22, 23, 24] suggested that this force is proportional to the contact

pressure times the abrasive size by assuming that the abrasives are closely packed to each

other and these closely packed abrasives are enwrapped by the pads so that the effective

contact area between wafer and pad is equal to that without abrasives. Moreover, the size

of the abrasives that may be captured by the pad is a function of abrasive size distribution

and pad properties. Fu et. al [25] later assume that the abrasives are dispersed evenly over

the pad surface and use a beam model to evaluate the wafer pad direct contact between

each two single abrasives. The force supported by a single abrasive can be obtained from

the beam model and is a function of abrasive size, down pressure and pad material properties [25]. Besides the force, the second purpose of an abrasive-pad interaction model is to evaluate the number of abrasives involved in the material removal process. Is this number simply proportional to the wafer-pad contact area, as that in the pad-wafer contact model by Yu et. al [19] and Zhao and Shi [21], or buried in more complicated scenarios. Fu et. al [25] simply took the number as an independent parameter in their model. This may be misleading considering that various parameters, say, the abrasive weight concentration and abrasive size, may have an influence on the number [22, 23, 24]. Luo and Dornfeld [22, 23, 24] considered more complex scenario and suggested that only a portion of abrasives are involved in the material removal process. Similar as the size of the active abrasives, the portion is a function of the abrasive size distribution and pad topography and material properties. In summary, the pad-abrasive interaction is one of the most important interactions in CMP process. One of the two material removal components, namely, the abrasive number is a direct output of this interaction. The other, namely, the material removed by a single abrasive, is an output of the interaction through the wafer-abrasive interaction. An accurate model on this interaction will be critical for a successful particle-scale material removal model. There are not many modeling efforts on this aspect before Luo and Dornfeld [23, 24] and more attention should be paid on it in the future.

2.1.5 Slurry Chemical-Wafer interaction

The contribution of slurry chemicals to the material removal is either neglected in earlier models or represented by an all-purpose coefficient. Cook [6] suggested a complete but complicated scenario of the chemical effects. Besides the mechanical removal, it is proposed that the surface removal during polishing should include the following five

chemical processes: (1). the slurry chemical diffusion into the wafer surface; (2). the subsequent wafer material dissolution under the load imposed by the abrasive particles; (3) the adsorption of the dissolution product onto the surface of the polishing grain; (4) the re-deposition of the polishing materials back onto the wafer surface; and (5) the corrosion rate between particle impacts. These steps are not considered in most of the early models for two reasons: first, they are hard to model quantitatively, and second, the contribution of these processes on the total material removal rate is believed to be minimal. From the knowledge of the authors, a recent model by Osseo-Asare [26] is the first to treat the adsorption rate of the dissolution product onto the surface of the polishing abrasives.

The major contribution of slurry chemicals on the material removal process has been attributed to the formation of a surface layer. This idea is well demonstrated by Kaufman et al. [27] in their Tungsten CMP model. They used the following formulation to describe this tungsten passivation in the presence of ferricyanide, an oxidizer:

$$W + 6Fe(CN)_6^3 + 3H_2O \rightarrow WO_3 + 6Fe(CN)_6^{-4} + 8H^+ (16)$$
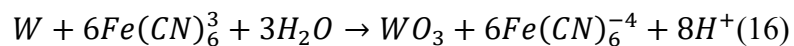
Kaufman et. al. proposed that this passivation layer is removed by slurry abrasives and the fresh tungsten surfaces are exposed, which is subsequently passivated and removed. This mechanism of passivation-removal-repassivation can be used to explain the copper, aluminum and other metal CMP as well. Similar mechanism of surface modification-removal-remodification is supposed to work at silicon, silicon oxide and low-k material CMP. Paul [28] and Zhao et. al [29] have proposed detailed surface kinetics models to connect the slurry chemical concentrations and fresh metal surface sites available to the

formation rate of the surface layer. Their models can explain the material removal rate as a function of chemical and abrasive weight concentration.
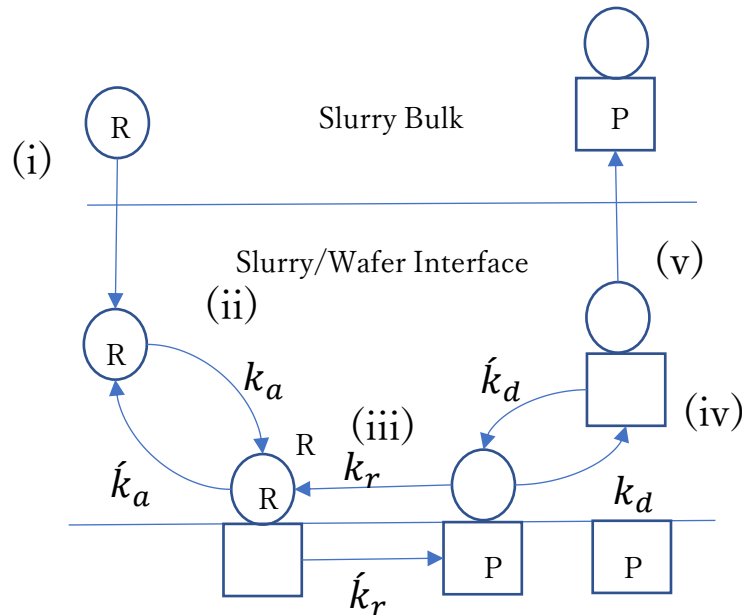
Fig. 3 The five-step kinetics model [30]

Recently, Borst et. al [30] have proposed a five-step model for CMP of SiLK dielectrics: (i). mass transport of reactant from the slurry to the slurry/wafer interface, (ii) adsorption of reactant to available surface site, (iii). reaction between adsorbed reactant and specific wafer surface to form an altered wafer surface layer, (iv). mechanical removal of the altered wafer surface layer, and (v). mass transport of removed material to the bulk slurry. This five-step mechanism is shown in Figure 3 schematically. In their work, formulations to cover the steps (i), (ii) and (iii), which relate the mass transportation, slurry chemical concentration and reaction rate to the formation of the surface layer were presented. This detailed model is supposed to be able to be extended to the CMP of other materials.
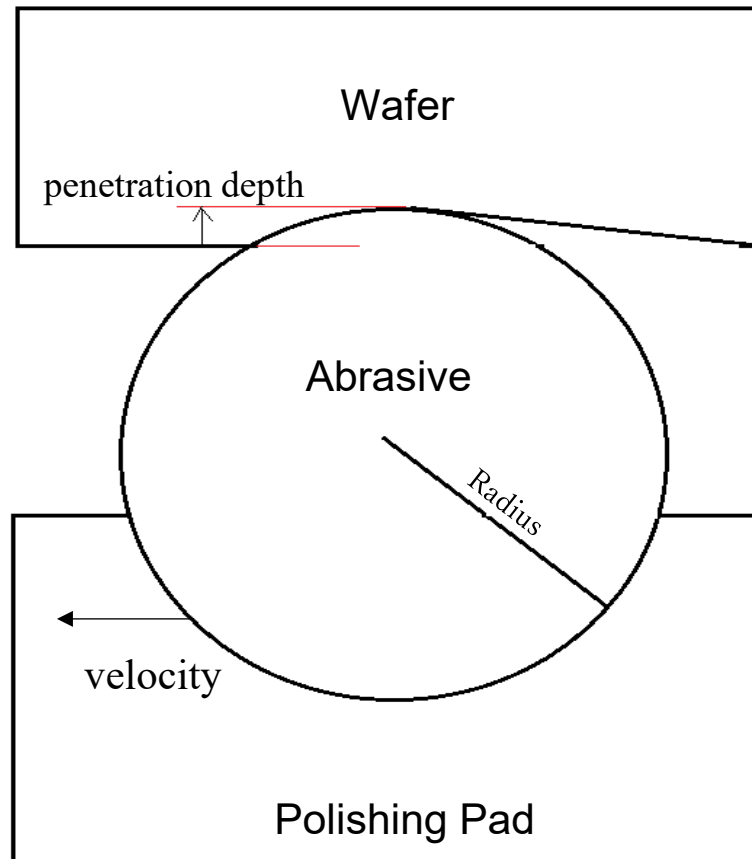
Fig. 4 Abrasive contact schematic at wafer and pad

The idea of the surface modification, removal and re-modification has been applied in Luo and Dornfeld's model [24] as well. They extended Kaufman's model by proposing that the surface layer is a bi-layer structure, one, softer hydrated layer and the other harder bottom layer. They did not cover the details on how the formation rate of the surface layer is affected by the slurry chemicals. However, they do connect the mechanical removal and chemical passivation rate together and propose *MRR* formulations as a coupling function of the surface generation rate, abrasive weight concentrations and wafer-pad contact area.

2.1.6 Particle-Scale material removal mechanism

A model based on elastic theory and statistical method was proposed to explain the

wear mechanism by abrasive particles by Liu *et al.* [8]. It was assumed that the depth of penetration of the abrasive particles into the pad surface is greater than that into the wafer surface, and the particles are in direct contact with the wafer surface during polishing.

The depth of penetration is determined by the hardness of the abrasive and the wafer surface using Hertz's contact theory. By considering the duration of the penetration and the deformation of the surface, the material removal rate (MRR) is defined as,

$$MRR = CAV\left(\frac{HV_{wafer}}{HV_{pad}+HV_{wafer}}\right)\left(\frac{E_{abrasive}+E_{wafer}}{E_{abrasive}E_{wafer}}\right)\frac{F}{A} \quad (17)$$

where V is the relative velocity, HV_w and HV_p are Vickers' hardness numbers for the wafer surface and the pad, respectively. where E_a and E_w are Young's moduli for the abrasive particle and the wafer surface, respectively, and *C* is a constant, A is the area of the wafer, and F is the normal force. The constant C includes the effect of the slurry chemical under the assumption that the chemical and the mechanical actions are independent.

The chemical interaction between the abrasive and the oxide surface was well defined by Cook [6]. In his glass polishing model, the factors determining the rate of mass transport during glass polishing are defined as <u>the rate of water diffusion into the glass surface</u>, the dissolution of the glass under the applied load, the adsorption rate of the dissolved material onto the abrasive surface, the re-deposition of the dissolved material onto the surface of the workpiece, and the aqueous corrosion between particle impacts.

He also considered the material removal process as a plowing process by abrasive particles traveling across the wafer surface. Hertzian contact was assumed to be an

indentation process by the abrasives and its contact stress was calculated from the theory of elasticity.

The electrochemical effect and material removal mechanism in metal CMP were proposed by Kaufman and Sainio [28, 31]. In metal CMP, the chemical action by the slurry chemical dissolves the metal surface and forms a passivating film preventing the isotropic chemical etching process on the wafer surface. By the mechanical action of the abrasive particles and the polishing pad, the passivated film is removed, achieving a degree of global planarization that is unmatched by the chemical etching process. In general, the dissolution rate of the metal surface was found to be two orders of magnitude lower than the polishing rate.

2.1.7 Triple-sided interaction of Slurry Chemicals, Particles, and Pad

The slurry chemicals affect not only the wafer but also the slurry abrasives and polishing pad. Their contribution to material removal is therefore not only reflected through the surface kinetics, but also through the alteration of the abrasive and pad properties such as the abrasive shape, abrasive size and pad Young's modulus. There are not many modeling efforts on these two interactions yet. One of the efforts on the chemical-abrasive interaction is by Mazaheri and Ahmadi [15]. They had proposed that the indentation of abrasives into the wafer surface is determined not only by the load from the pad but also the double layer (dl) forces F_{Ψ}, which are a function of abrasive size d and abrasive zeta potential Ψ. They proposed experimental equations of abrasive zeta potential Ψ as a function of slurry pH values for three different abrasive materials, namely, tantalum penoxide, alumina and silica.

The zeta potential value can be substituted into the formulation of double layer forces

to evaluate the material removed by a single abrasive using the indentation model. A recent model by Castillo-Mejia et. al [32] tried to explain the effect of water-pad interaction in CMP. The water is proposed to plasticize the polishing pad and reduce its elastic modulus. A formulation on the ratio of the Young's modulus of wet pad to the dry pad is suggested. This Young's modulus is then used in a wafer-pad contact model to evaluate the material removal.

2.1.8 Interaction among all

Most of the earlier models have been concentrated on one or two interactions of the CMP processes. They are useful for identifying the input parameters. However, they may not be sufficient for understanding the whole material removal process. The effects of the same input parameters may be contrary to each other when acting in different interactions. For example, in the abrasive-particle interaction, larger abrasive sizes yield larger indentation depth and therefore benefit material removal rates, while in the abrasive-pad interaction, a larger abrasive size, however, may yield smaller number of abrasives and therefore smaller material removal rate. Relying on either the abrasive-wafer model or the abrasive-pad model to explain the effects of abrasive size may be misleading.
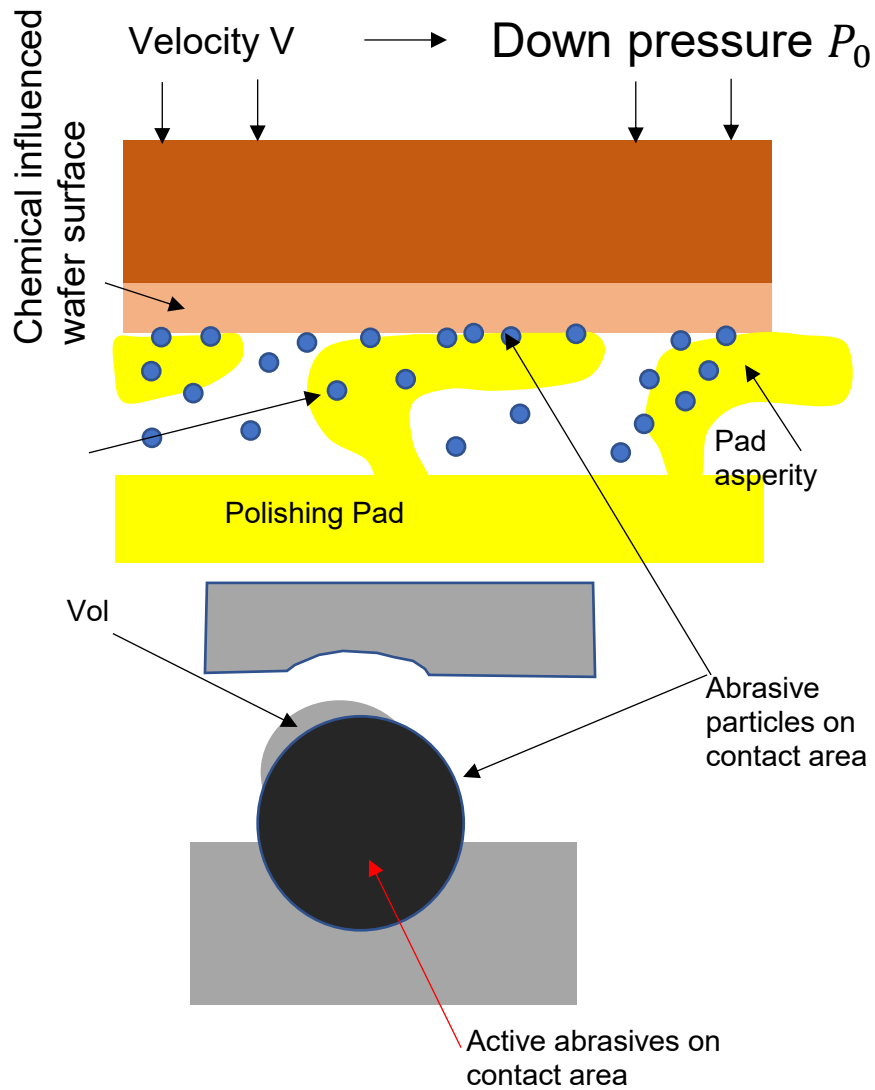
Fig. 5 Interactions among wafer, abrasives and polishing pad [22].

A comprehensive model of CMP integrating the six interactions together is therefore needed. In this section, several integrated modeling efforts at the particle-scale are discussed. Some of them have been mentioned earlier in above sections. Xie and Bhushan [33] were one of the first to consider the comprehensive effects of mechanical elements including the abrasive particles and polishing pad topography in the polishing process.

However, the slurry chemicals are not considered. The model cannot explain the effects of abrasive size distribution either.

The overall picture of the model can be described briefly here, Fig. 4. The slurry is delivered into the wafer-pad interface, with slurry chemicals reacting with the wafer materials and forming a passive layer over the wafer surface. Since the pad surface is rough, few parts of the pad asperities contact the wafer. These set of pad asperities captures the slurry abrasives which are deeply embedded into the pad and share the down force with the pad. These captured abrasives, called *active* abrasives, then remove the chemically influenced surface layer plastically. Among the four interactions, the wafer-abrasive interaction is modeled as a plastic indentation; the wafer-pad interaction is modeled as an elastic Hertz contact of sphere with a half space by assuming a uniform distribution of pad asperities; the abrasive-pad interaction is the key part of the model. The pad plays a role as a filter and only abrasives large enough can be captured; and the chemical wafer interaction is modeled as a process of passivation, removal and re-passivation.

One key idea of the model is that the material removal rate can be decomposed into two parts: one, the number N of the *active* abrasives, and the other, the material removed by a single abrasive per unit time. The advantage of separating the material removal into two parts is that the physical meanings of them are more apparent and therefore it is easier to identify and connect the input parameters to them. An additional benefit is that the connections between the four interactions can be easily obtained through their contribution to these two parameters. A framework of integrated particle-scale modeling connecting the interactions has been proposed. The abrasive-chemical and pad-chemical

interactions are not included in the model yet. However, they are put in the framework for the purpose of completeness.

It is noted that following work of Luo and Dornfeld [22], similar integrated models has been proposed by Fu et. al. [25], Zhao and Chang [34] and Ahmadi and Xia [13]. Works by Mazaheri and Ahmadi [14, 15] are an extension to the modeling efforts of Ahmadi and Xia [13]. They are all based on the idea that the material removal can be separated into the number of abrasive particles and material removed by a single abrasive. Besides the elastic Hertz contact of wafer and pad, they further consider the possibility of a plastic contact between the polishing pad and wafer. The adhesion force and dl forces are included in their models as well to calculate the material removal by a single abrasive. Following Luo and Dornfeld [22] and Fu et. al [25], Bastawros et. al [35] further proposed that three contact modes exist between the slurry particles and polishing pad: full contact mode, partial contact mode, and non-contact mode. However, unlike Luo and Dornfeld's model, none of them explore the effects of chemical surface passivation and abrasive size distribution (or pad-abrasive interaction) on the material removal process.

2.2 CMP and Abrasion approach

2.2.1 Introduction to different views of points

The understanding of the material removal mechanism in chemical mechanical planarization (CMP) should be based on understanding the roles of the cutting tools, or namely, the abrasives, and their interactions with other important input values such as the pad, chemical and wafer materials. The effect of abrasive size distribution in chemical-

mechanical planarization has long been observed [26, 37-43, 46]. For example, experimental results show that there is an inverse proportional relationship between the abrasive size and the material removal rate (*MRR*) [38-39]. Connections between the size distribution and the scratching of wafer surface have also been observed and reported [41-42]. Beside the experimental research, however, there is a general lack of models which can accurately predict the performance of consumables, and specially, the abrasive particles. This limits the application of the experimental results for the optimization of the CMP process.
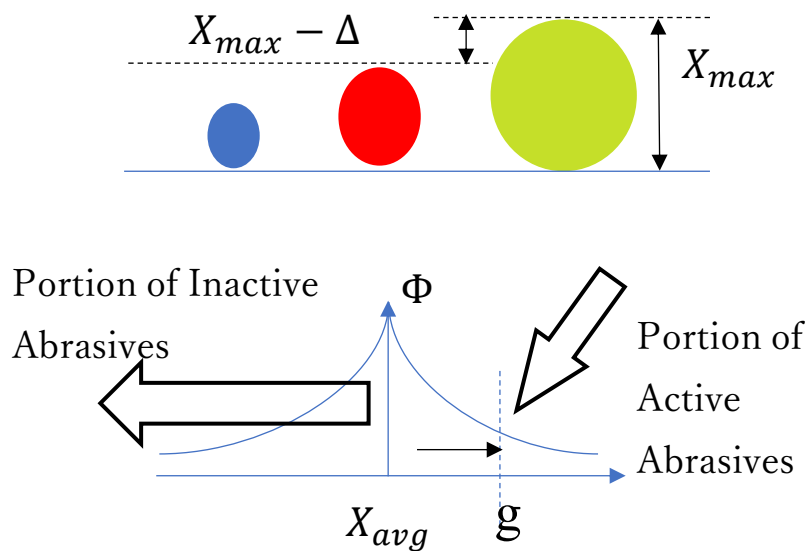
Fig. 6 Abrasive Size Distribution

It is principally based on three assumptions: a regularly periodic pad topography, normal distribution of abrasive size and plastic deformations over the wafer-abrasive and pad-abrasive interfaces (two-body abrasion). The key idea of the model is that the effects of the consumables on material removal can be attributed to two sources. One is the number

of active abrasives, and the other the material removed by a single abrasive, which is a function of the abrasive size. Based on the model, only part of the abrasives, or namely, the *active* abrasives are involved in the material removal process, Figure 6 ([23]). An '*active*' abrasive must satisfy two conditions. First, it should be located on the contact area between wafer and pad. The number of abrasives there is proportional to the weight concentration of abrasives in the slurry. Second, the abrasive should be large enough. This contradicts with view of point adapting the inverse proportional between MRR and particle size. The wafer will contact the largest abrasives first when a force is applied on the wafer top surface. A gap is formed between the pad and wafer surface in the neighborhood of the larger abrasives. Only abrasives larger than this gap can participate in material removal.

Apparently, the distribution function affects both the size of active abrasives, and therefore, the volume removed by a single abrasive, and the number of active abrasives. To fully verify the roles of the abrasive size distributions proposed in the material removal model, however, experimental results of *MRR* as a function of abrasive size distribution are needed. Recently, tungsten (W) CMP experiments have been done by Bielmann et. al. [39] using five different kinds of abrasive size distributions, which were measured using the dynamic light scattering technology. Five different material removal rates are obtained. This chapter discusses the correlation of the model prediction with these experimental results. A detailed view of wafer-abrasive-pad contact is proposed to explain the roles of the abrasive size distribution. Material removal rate formulation as a function of abrasive size distribution was developed and verified.

2.2.2. Vital roles of Luo's approach for the Removal Mechanism [44]

2.2.2.1 Effective Contact

First, it is proposed that only part of the pad contacts the wafer directly. This part of the pad is called the contact area. This view of wafer-pad contact is shown schematically in Fig. 7 (a). The relationship between the down pressure P, contact pressure Pc and contact area A can be obtained based on a contact model. The contact area A and contact pressure Pc are functions of the down pressure, pad topography and pad materials. The abrasive geometry is assumed to be spherical. The *active* abrasives involved in the two-body abrasion will locate on the contact area, Fig. 7 (b)-(e). When there is no abrasive, the wafer and pad contact area A is a function of the wafer-pad topography and wafer-pad materials. Since the nano-scale *active* abrasives are much smaller than the micro-scale features of the pad topography and the pad surface is quite soft related to the abrasive and wafer surface, the final *effective* contact area A and contact pressure Pc in the situations where abrasives are embedded into the contact area, should be approximately equal to those without abrasives, Fig. 7 (e). The trend of this contact, which makes the effective contact area between the wafer and pad as close as possible to that without abrasives (may be pores), is called 'stable contact'. There are four stages, Figs. 7 (b) – (e), from the point that the wafer begins to contact the pad and abrasives to where the final 'stable contact' is realized. When there is no down pressure applied on the wafer top surface, the abrasives will disperse on the pad contact area randomly, Fig. 7 (b). The number of abrasives located on the contact area is proportional to the abrasive weight concentration in the slurry. The wafer and pad are separated by abrasives and the gap g between them is equal to the size of the largest abrasives, Fig. 7 (b). Once down pressure is applied on the wafer

top surface, the wafer will initially be supported by abrasives only (could be very sharp criterion), Fig. 7 (c). The *effective* contact area is approximately equal to $0.25\pi(x_{avg})^2 n$, where n is the number of abrasives and x_{avg} the average size of abrasives. The forces applied on each single abrasive are quite large, and all the abrasives are embedded deeply into the pad. A very small gap is formed between the pad and wafer, Fig. 7 (c), which is a function of the pad hardness and force applied on the abrasives. The trend for wafer and pad to contact directly will push the abrasives to agglomerate. In this stage, some part of contact area is due to the direct contact between the wafer and pad, while another part of contact area is occupied by abrasives with closer relative locations, Fig. 7 (d). The *effective* contact area, equal to the direct contact area (new case after applied pressure) between the wafer and pad plus the area $0.25n\pi(x_{avg-a})^2$ occupied by the abrasives, becomes closer to that without abrasives (before the applied pressure), Fig. 7 (d). The force applied on each single abrasive becomes smaller and therefore the gap g' between the wafer and pad becomes larger. Abrasives smaller than this gap g' are pushed off the contact area, indicating the number n of abrasives is decreasing. The process increasing the direct contact between wafer and pad will continue until all the abrasives are finally packed closely (Agglomeration), as shown in Fig. 7 (e). The *effective* contact area, A_1+A_2, between wafer and pad in this stage is approximately equal to that without abrasives. The direct contact area A_1 will not increase and a stable gap g is finally formed, Fig. 7 (e). From the above discussion, it can be seen that only a portion of the abrasives is involved in the material removal process and the portion of these *active* abrasives is determined by the gap g, which is the lower bound of the *active* abrasive size.

(a)

(b) Without Down Pressure

(c) With Down Pressure

(d) Increase direct contact area

(e) Stable Contact

(f) Abrasive indentation into the Pad
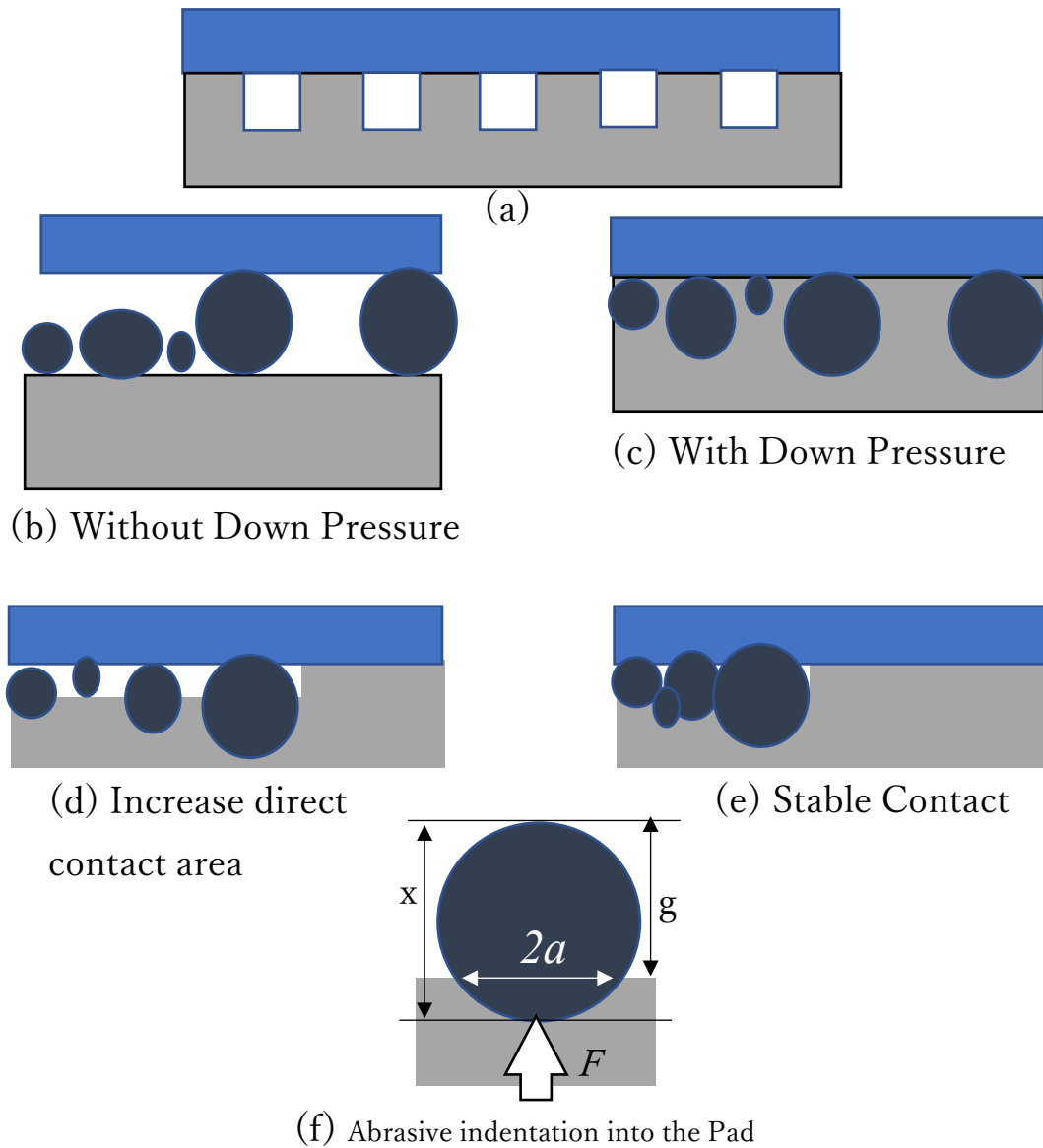
Fig. 7 Abrasive-pad contact mechanism

In most situations the distribution of abrasive particles sizes (i.e. diameters), x, satisfies a normal probability density function

$$p\{x = x_a\} = p\left(\frac{x-x_a}{\sigma}\right) = \frac{1}{\sigma\sqrt{2\pi}}e^{-\frac{1}{2}(\frac{x-x_{avg}}{\sigma})^2} \quad (18)$$

$$p\{x \le x_a\} = \Phi\left(\frac{x-x_a}{\sigma}\right) = \frac{1}{\sqrt{2\pi}}\int_{-\infty}^{\frac{x-x_{avg}}{\sigma}} e^{\frac{-1}{2}t^2} dt \quad (19)$$

where x_{avg} is the mean abrasive diameter and σ the standard deviation. Then the area occupied by the abrasives in Fig. 7 (e), is approximately equal to

$$A_2 = n \int_g^\infty p(x)0.25\,\pi x^2 dx = 0.25 n\pi \int_g^\infty p(x)x^2 dx \approx n[1 -$$

$$\Phi(g)]0.25\,\pi x_{avg-a}^2(g) \quad (20)$$

where n is the number of abrasives on the pad asperities before down pressure is applied (i.e. number of abrasives in Fig7 (b)), and x_{avg-a} (g), a function of g, is the average size of *active* abrasives which is larger than the gap g. The total force F_{total} supported by the abrasives should be equal to the contact pressure P_c times the area A_2 (solid-solid contact), or

$$F_{total} = n[1 - \Phi(g)]0.25\pi x_{avg-a}^2(g)P_c \quad (21)$$

Note that $n[1-\Phi(g)]$ in Eq. (21) is actually the number of *active* abrasives larger than g. The *active* abrasives are indented into the pad surface under forces F, Fig. 7 (f). The indentation depth Δ into the pad surface is x-g for a single active abrasive with size x. The indentation depth of abrasive into the wafer surface has been neglected here since it is much smaller than that in the pad surface (may be this rise an important question about the validity of calculating material removal rate based on abrasive effect). Then the projected area of the indentation into the pad surface is approximately equal to

$$\pi a_2^2 = \pi x(x - g) \quad (22)$$

where a_2 is the radius of the projected area of the indentation. Note here that the indentation depth Δ is much smaller than the abrasive size x. Assuming the indentation leads to a fully plastic deformation, [23], the force applied on the single abrasive with size x can be obtained as (Area) x (Pressure);

$$F(x) = \pi a_2^2 H_p = \pi x(x - g)H_p \quad (23)$$

where H_p is the hardness of the pad (It's worthy to mention here that particle force comes from pad). From Eq. (23) it is seen that the force on an abrasive with size g is zero. The force supported becomes larger for larger abrasives.

2.2.2.2 Aggregation thresholds and Force Field

Once the force applied on each single abrasive is known, the total force supported by all abrasives larger than gap g can be calculated as

$$F_{total} = n \int_g^\infty p(x)F(x)dx = nH_p\pi \left[\int_g^\infty p(x)x^2 dx - g \int_g^\infty p(x)x dx \right] \approx$$

$$n[1 - \Phi(g)]H_p\pi[x_{avg-a}^2 - gx_{avg-a}](23)$$

By performing mathematical manipulation, it is obtained that

$$g = \frac{H_p - 0.25P_c}{H_p}\left(x_{avg-a}(g)\right) = \frac{H_p - 0.25P_c}{H_p}(x_{avg} + \frac{\sigma p(g)}{1 - \Phi(g)}) \quad (24)$$

For a specified abrasive size distribution, the gap g can be obtained by solving Eq. (24); the gap is a function of pad hardness, contact pressure (function of down pressure, pad topography and pad materials) and abrasive size distribution. the material removal rate can be written as the product of the *active* abrasive number $N= n[1-\Phi(g)]$ and the volume removed by a single abrasive $c(x_{avg-a})^2V$ per unit time, where V is the relative velocity of wafer to pad and c a constant independent of the abrasive sizes;

$$MRR = \underbrace{n}_{part1} \underbrace{\left[1 - \Phi\left(\frac{g - x_{avg}}{\sigma}\right)\right]}_{part2} c \underbrace{x_{avg-a}^2}_{part3} V =$$

$$cn[1 - \Phi(\frac{g - x_{avg}}{\sigma})][x_{avg} + \frac{\sigma p(\frac{g - x_{avg}}{\sigma})}{1 - \Phi(\frac{g - x_{avg}}{\sigma})}]^2 V \quad (25)$$

5 3

From Eq. 25, it could be seen that the role of the gap g on material removal is twofold. When the g is increased, Fig. 6, the number of active abrasives is decreased, while the size of active abrasives is increased. Gap g is a function of the contact pressure, pad hardness, and abrasive size distribution, (Eq. 25). Therefore, the roles of contact pressure, pad hardness, and abrasive size distribution on material removal are also twofold. It is noted that it is difficult to obtain an accurate analytical solution of Eq. (25). An approximate determination of gap g is preferred. The contact pressure should be much smaller than the pad hardness so that the indentation depth x-g into the pad is much smaller than the abrasive size x. Therefore, the *active* abrasive size larger than g is usually located in the tail of the distribution function. For a small change of gap g in this region, the average size of *active* abrasives $x_{avg-a}(g)$ may be approximately taken as a constant value of $x_{avg}+3\sigma$. Then the gap g is approximately

$$g = \frac{H_p - 0.25P_c}{H_p}\left(x_{avg} + 3\sigma\right) \text{ (26)}$$

Substituting the approximate solution of gap g (Eq. 26) into Eq. (25) and considering that the number n of abrasives on the contact area before down pressure is applied is proportional to the weight concentration of the abrasives over the mean volume of a single abrasive, we obtain

$$MRR = \underbrace{\frac{C_6}{x_{avg}^3}}_{part1} \underbrace{\left(1 - \Phi(3 - C_7[\tfrac{x_{avg}+3\sigma}{\sigma}])\right)}_{part2} \underbrace{\left[\left(x_{avg} + \frac{\sigma p(3 - C_7[\tfrac{x_{avg}+3\sigma}{\sigma}])}{\Phi(3 - C_7[\tfrac{x_{avg}+3\sigma}{\sigma}])}\right)\right]^2}_{part3} \text{(27)}$$

where the C_6 and $C_7 = 0.25P/H_p$ are two parameters representing the effects of other consumable parameters including the weight / volume concentration of the abrasives, and process parameters including the down pressure and velocity. The first part of the

5 4

equation represents the effect of the abrasive size on the total number of abrasives. The $x_{avg}{}^3$ is proportional to the average volume of a single abrasive and C_6 includes a term for the weight concentration of abrasives. For the same weight concentration, when the average abrasive size is larger, the total number of abrasives on the contact area is small, leading to a small material removal rate. It is noteworthy that there is an upper limit for the weight concentration. When the weight concentration is so large that the total contact area is occupied by abrasives, the material removal will saturate and the above formulation needs revision (Saturation state) [25]. The second part of Eq. 27 is a proportional function, representing the effect of abrasive size distribution on the number of *active* abrasives. The value of the proportion is smaller than 1, indicating that only part of the abrasives on contact area is *active*. The third part represents the effect of the average size of *active* abrasives on the material removal. (Note that the material removal is proportional to the square of the average size of abrasives) The average size of the *active* abrasives is larger than the average size x_{avg} of all abrasives, including *active* and *inactive* abrasives. If the size distribution function of abrasive size is not considered, the *MRR* can be written as a function of the average size x_{avg}:

$$MRR = C_6/x_{avg} \qquad (28)$$

Here, part 2 in Eq. 27 is equal to one, and part 3 of *active* abrasive size is equal to $x_{avg}{}^2$, indicating that all abrasives on the contact area are involved in the material removal process. It is noted that recently Bastawros et. al. [39] have proposed three contact modes between the pad and abrasive particles, namely, the full contact mode, the partial contact mode, and the non-contact mode. The partial contact mode and the non-contact mode can be found in Fu et. al. [26] as well. The contact mode proposed in this paper, which is from

the concept of 'stable contact', e.g. the *effective* contact area between the wafer and pad with abrasives approximately equals that without abrasives, does not fall in these three modes. In the proposed partial contact and non-contact mode, similar to that in stage 3 of Fig. 7 (d), there is still room for abrasives to be packed close to each other (Agglomeration) so that the '*effective*' contact area is approximately equal to that without abrasives. An extreme case of the 'stable contact mode' is that the total contact area is occupied by the abrasives and therefore there is no direct wafer-pad contact; [25]. This is different from the 'noncontact mode' by Bastawros et. al. [39] and Fu et. al. [26]. In the 'non-contact mode' proposed in [39, 26], there is no need for abrasives to be closely packed to each other (agglomeration), which may be the case for a hard pad due to the small pad deformation [26].
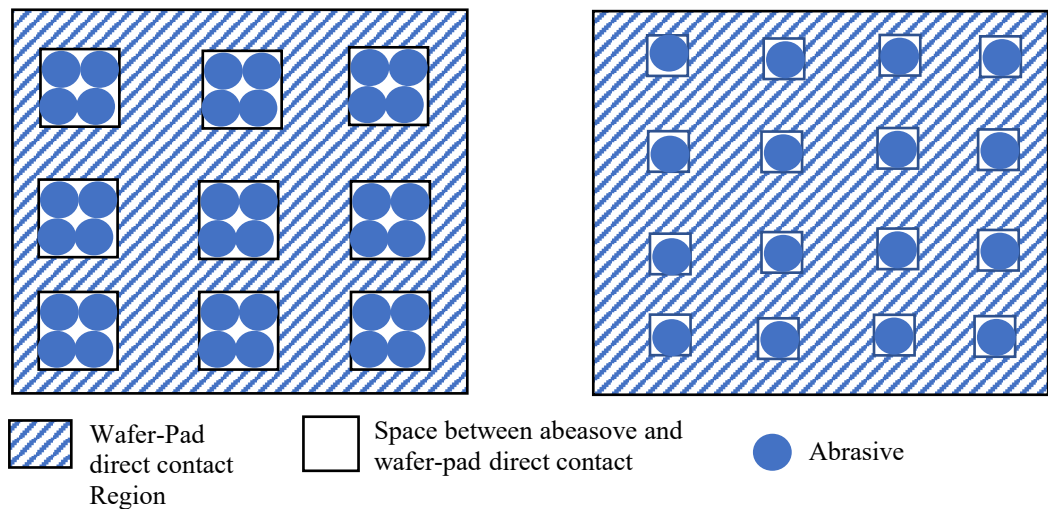
Fig. 8 A comparison with the partial contact mode and full contact mode

In our extreme case, the abrasives should be closely packed to form a mono abrasive layer. The contact mode in this study [26] separates the contact area into two different regions: one, the direct wafer-pad contact region, and the other, the closely packed region

of abrasives. It is necessary to point out that the wafer-abrasive-pad contact shown in Fig. 7 (e) is just one representative part of this contact mode. The top view of the contact between wafer, abrasive and a single pad asperity contact these representative regions dispersing randomly on the contact area is shown schematically in Fig. 8 (left) as a comparison with the partial contact mode and full contact mode of Bastawros et. al. [39] and Fu et. al. [26], Fig. 8 (right). The 'full contact mode', in which each single abrasive is fully wrapped by the pad material as proposed in [10], is an extreme case of the contact mode proposed here. It is also worthy to point out that when developing the material removal rate formulations (15) and (25) in [26], Fu et. al [26] does not consider that the number N of abrasives may be a function of abrasive size, which is proportional to $n[1-\Phi(g)] \propto (1/x_{avg}^3)\Phi(x_{avg},\sigma)$ in this study. Therefore, while the model on the whole is quite reasonable, any experimental verification of material removal rate formulations (15) and (25) in [26] as a function of the abrasive size might lead to some confusion.

2.2.2.3 Experimental verifications

Bielmann et. al. [39] did extensive tungsten CMP experiments using five different distributions of abrasive size. This experimental data is used for model verification. Figure 9 shows SEM/TEM pictures of three of the five abrasives [39]. The size distribution is measured using dynamical light scattering technology and is shown schematically in Figure 9 [39].
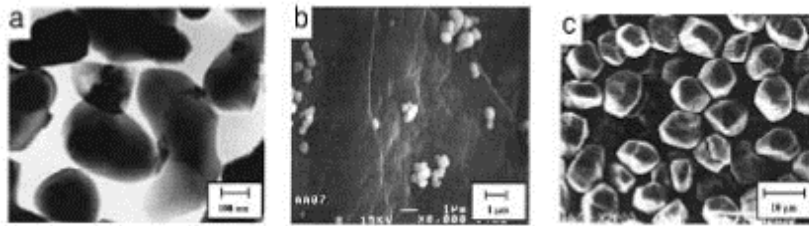
Fig. 9 SEM/TEM pictures of abrasives [39]
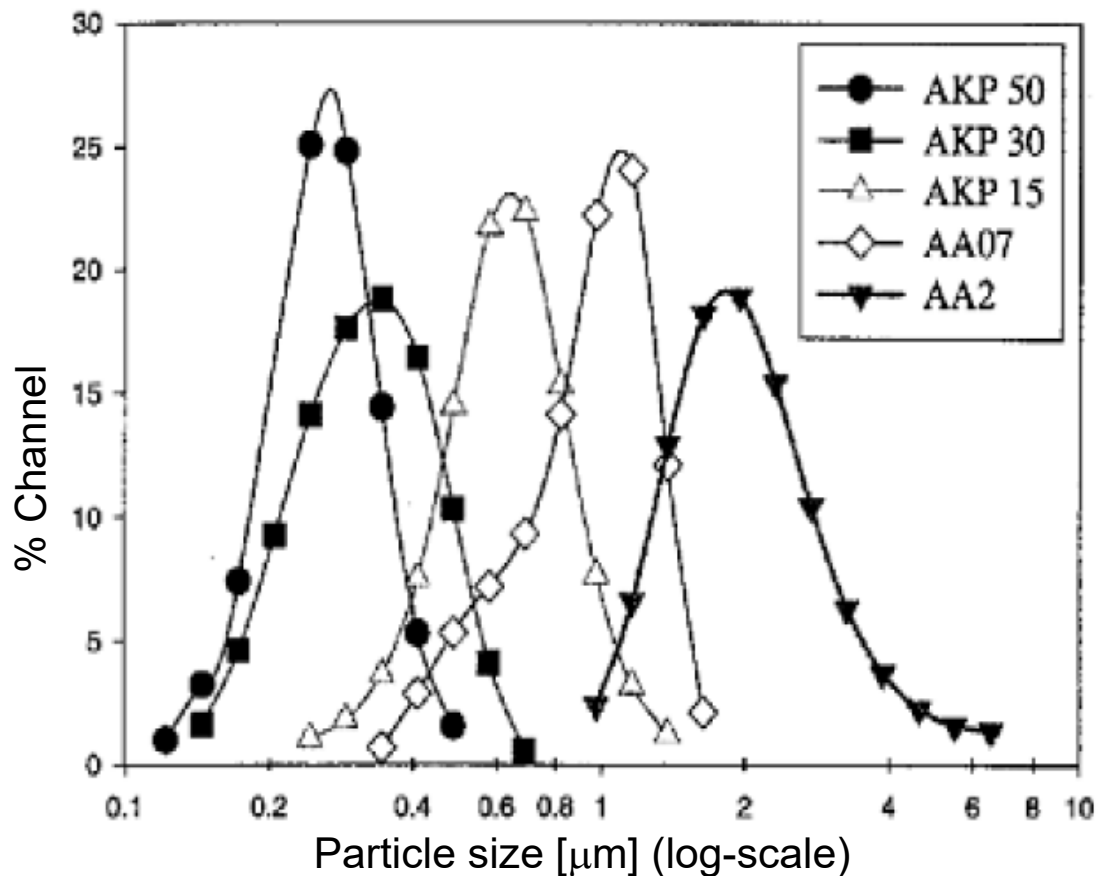
Fig. 10 Abrasive size distribution [3]

The average sizes of the five kinds of abrasives (AKP50, AKP30, AKP15, AA07 and AA2) used by Bielmann [39] were 0.29μm, 0.38μm, 0.60μm, 0.88μm and 2μm, respectively. By assuming that the size distribution satisfies a normal distribution, the standard deviation of the size distribution can be obtained using the measured data in Fig.

5 8

9 and are listed in Table 1. Bielmann [39] changed the weight concentrations of abrasives from 2% to 15% and obtained the material removal rate as a function of median abrasive size under four concentrations.

The *MRR* is also plotted as a function of weight concentration (Fig. 10). The material removal rate saturates for a concentration larger than 10% for abrasive sizes 0.29μm, 0.38μm and 0.60μm. It is concentrated here on the linear region, concentration smaller than 10%. The perfect correlation between the experimental results (average values of the experimental data under the three concentrations 2%, 5% and 10%) and the model predictions of Eq. 27. It is found that with an increase in abrasive size, the decrease in material removal rate can be fit with a power function (agree with my model; chapter 3). We can see this is due to the exponent –3 in the term x_{avg}^3 of part 1 and coefficient C_7 in parts 2 and 3. The C_7 value is a function of consumable values including pad hardness, pad topography and down pressure, but independent of the weight concentration. This implies that the weight concentration does not affect size dependence of material removal rate. Experimental results support this conclusion.

Table 1. The mean size and standard deviation of the abrasive size distributions

Abrasive Type	Mean Size [μm]	Standard Deviation [μm]
AKP50	0.29	0.702
AKP30	0.38	0.1189
AKP15	0.6	0.2106
AA07	0.88	0.2888
AA2	2	1.0562
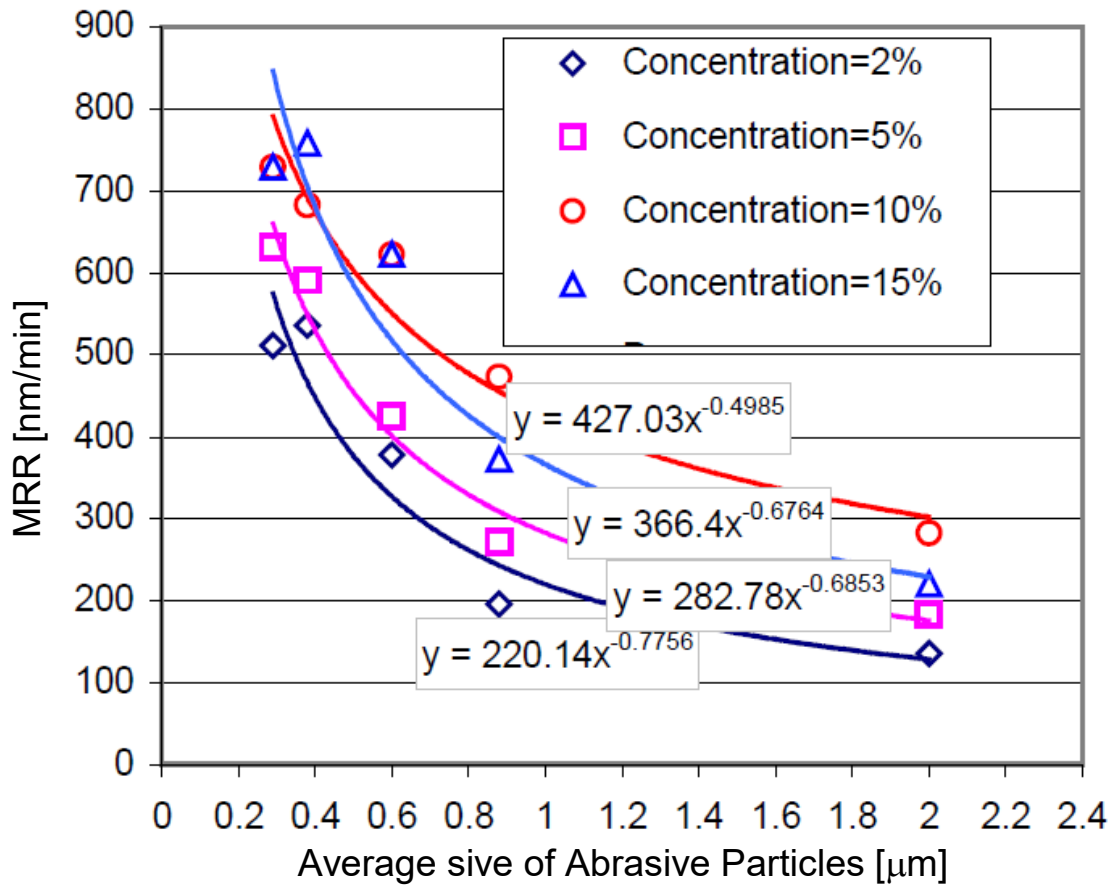
Fig. 11 MRR as a function of abrasive size distribution [39]

Three values of the exponent– -0.6764, -0.6853 and –0.7756, essentially equivalent, were obtained for slurry concentrations 10%, 5% and 2%. When the weight concentration is 15%, the value –0.4985 of the exponent is much larger. This is because C_6 representing the effect of weight concentration is no longer a constant. Its value for concentration 15% is smaller for the smaller abrasive sizes (0.29, 0.38 and 0.6μm) than for the larger abrasive sizes (0.88 and 2μm). This contributes to the increase of the fitted exponent value. Moreover, it is noted that the distribution function of abrasives does play a significant role in the material removal from the fitted exponent values. Otherwise, the values should be equal or close to –1 as indicated by Eq. 28, instead of –0.67~ -0.78.

From the fitting process described above, it is found that only a small portion of abrasives are involved in material removal. The order of the portion (0.1% - 0.4%) contributes significantly to the order of the material removal rate as mentioned in previous. Otherwise, the order of material removal rate prediction may be much larger. Table 2 lists the portion and the range of *active* abrasive size determined by fitting to the experimental data. The portion of *active* abrasives is close for the five size distributions in these experiments and the average sizes of active abrasives are close to $x_{avg}+3\sigma$, as assumed in approximate estimation of the gap g in Eqs. 26 and 27.
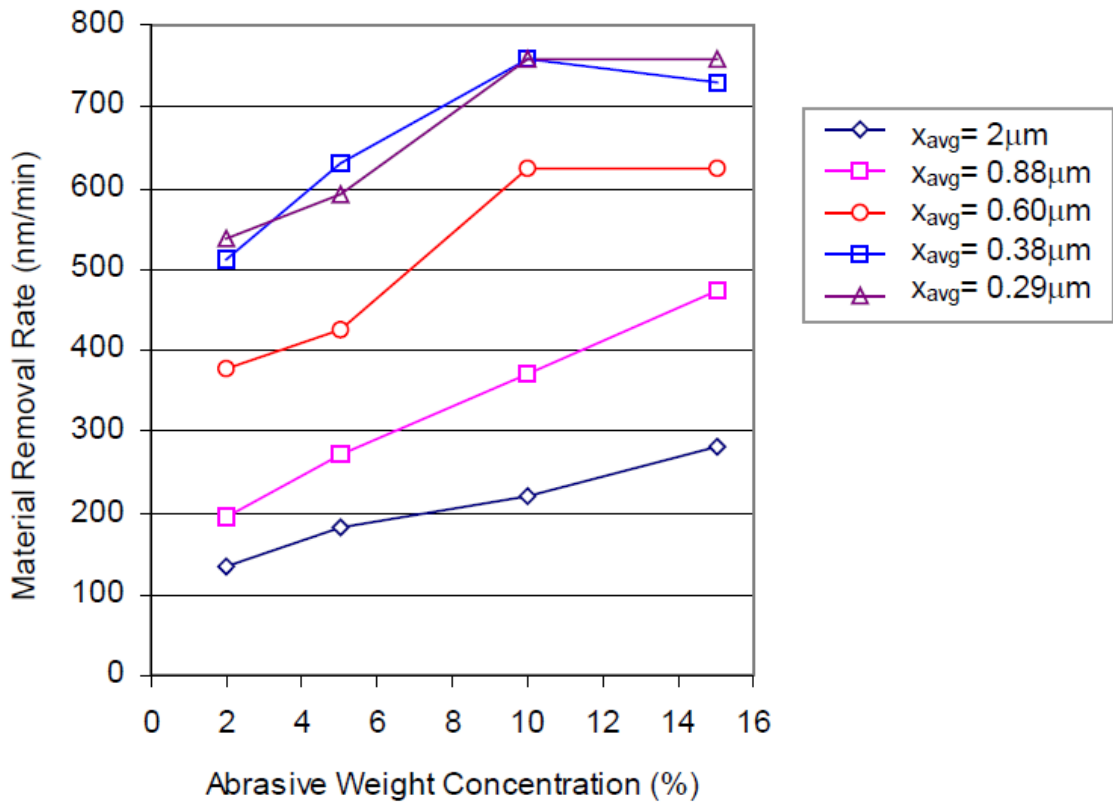
Fig. 12 MRR as a function of abrasive weight concentration [39]
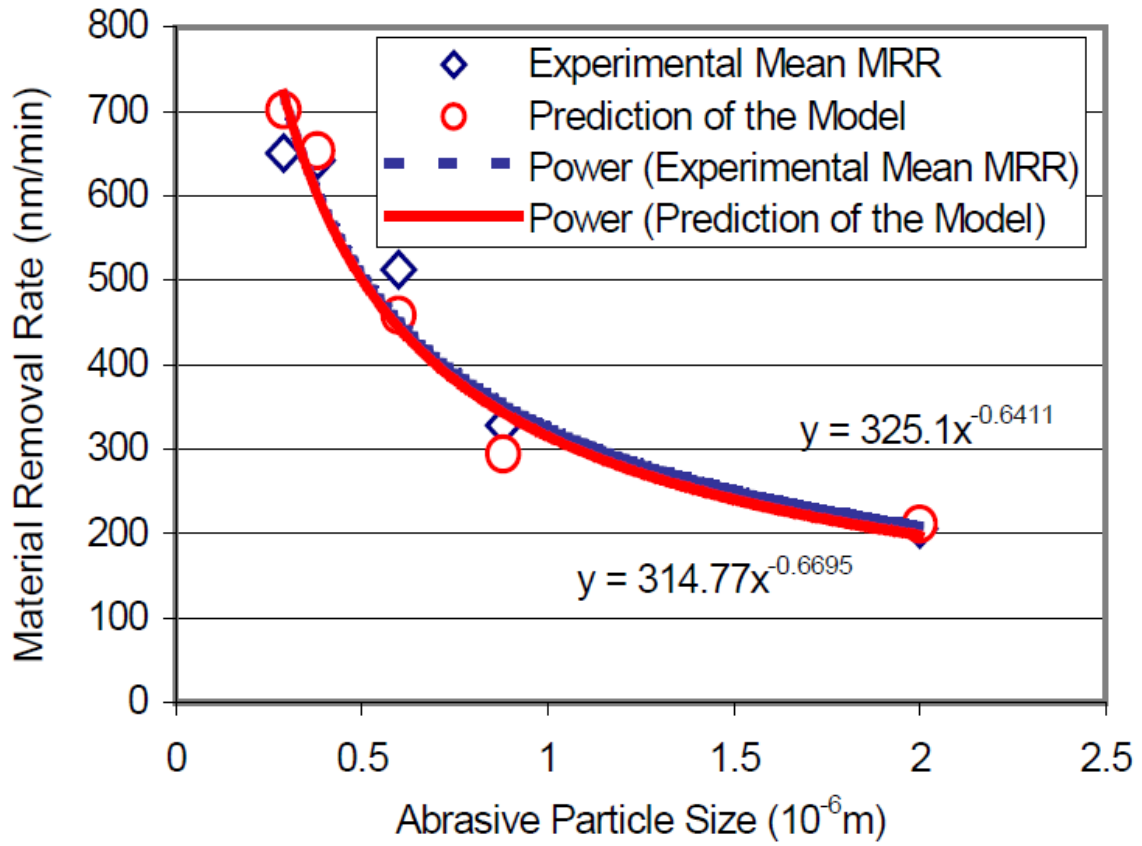
Fig. 13 MRR as a function of abrasive size distribution [22-24].

Table 2. The fraction of active abrasive and range of active abrasive size

	Fraction of Active Abrasives [%]	Range of Active Abrasive size [um]	Average Size of Active Abrasives
AKP50	0.19195	0.490~0.500	0.495
AKP30	0.18270	0.726~0.737	0.731
AKP15	0.17980	1.213~1.231	1.220
AA07	0.18150	1.720~1.746	1.730
AA2	0.17190	5.091~5.169	5.125
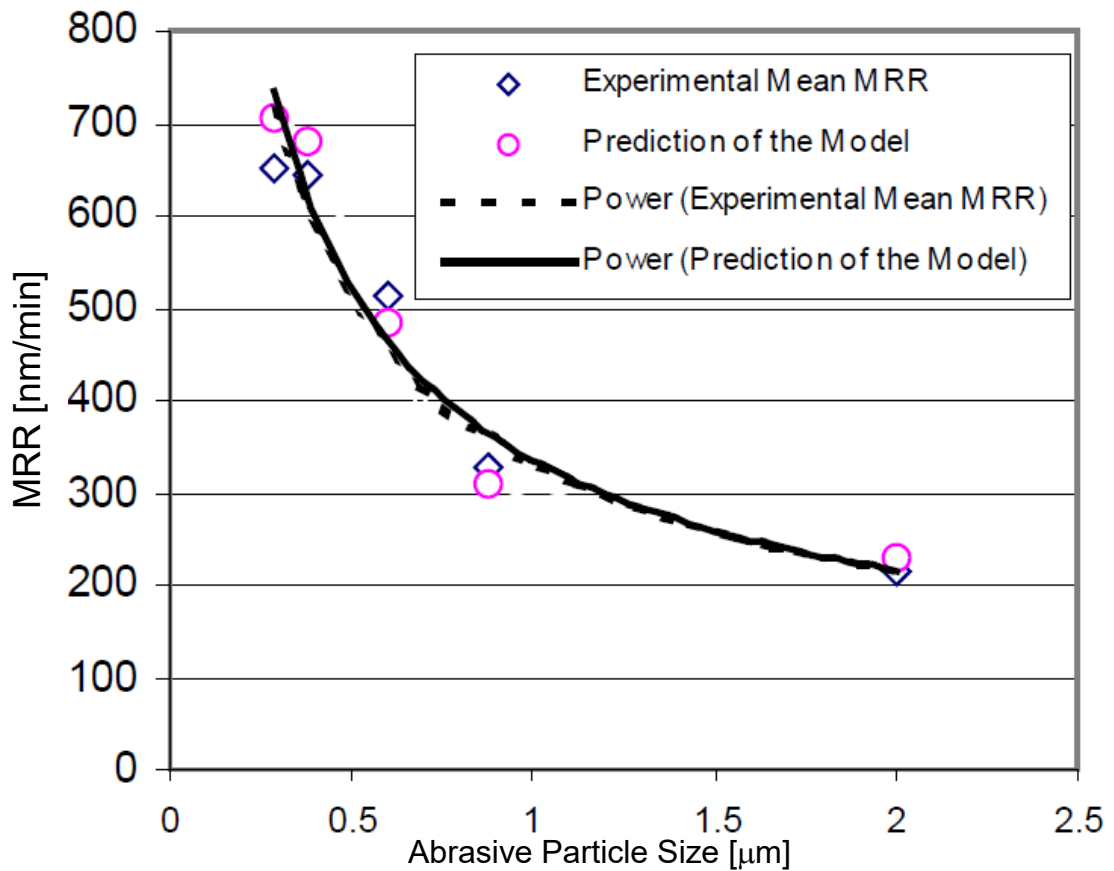
Fig. 14 Precondition of MRR by the simplified formulation.

Therefore, a simplified relationship between the material removal rate and abrasive size distribution may be written as

$$MRR = \frac{(X_{avg} + 3\sigma)^2}{x_{avg}^3} \quad (28)$$

This formulation also fits the experimental results quite well. The model predicts that the cutting depth of the abrasives into the wafer is proportional to the abrasive size. It is noted from experimental results in [39] that the tungsten wafer roughness after polishing is independent of the abrasive size. However, this is not in contrast with the model. The roughness due to the chemical reactions in tungsten CMP, including etching, dissolution and re-deposition, which are independent of the abrasive size, may be larger than that due

to the abrasion (smaller than 1nm). This indicates that the final roughness of polished tungsten wafer is due to the chemical reaction but not exclusively the mechanical abrasive removal. The roughness is mainly a parameter related to the material removal by a single abrasive or chemical reaction. The total material removal is equal to the number of abrasives times the material removed per single abrasive/ chemical reaction. Even though the roughness due to the chemicals is larger than that due to the abrasion, the material removal process is not necessarily a chemical dominant process. It is also noteworthy that smaller abrasive sizes do not always benefit material removal rate. The material removal rate is equal to the number of *active* abrasives times the material removed by a single *active* abrasive. When the cutting depth predicted by the model is smaller than 0.1nm, the material removed by a single abrasive may be minimal. In this case, even if the abrasive number is large, the total material removal rate may be still negligible. Therefore, the cutting depth, a function of abrasive size, wafer-pad contact area and down pressure, set the lower boundary for abrasive sizes under a certain combination of down pressure and polishing pads. Recently, experimental evidences supporting this have been reported by Zhou et. al. [46].

2.2.2.4 Essences and Summary

The work in this section shows that the distribution of the abrasive size plays an important role in the material removal process. The effect of the standard deviation on material removal can be predicted using Eq. 27. The prediction for five mean abrasive sizes schematically is depicted as (Fig. 7). It is found that for each single size, a unique value of standard deviation exists. On the right side of the figure, the material removal rate increases with the standard deviation. And on the left side, the material removal rate

decreases with the standard deviation. The right-side region is called the 'size dominant region', since on this side, the average size of the active abrasives (part 3 in Eq. 27) increases with the standard deviation and the increase is much faster than the decrease of the *active* abrasive number (part 2 in Eq. 27). The left side region is called the 'number dominant region', since in this region the decrease of the number of active abrasives is
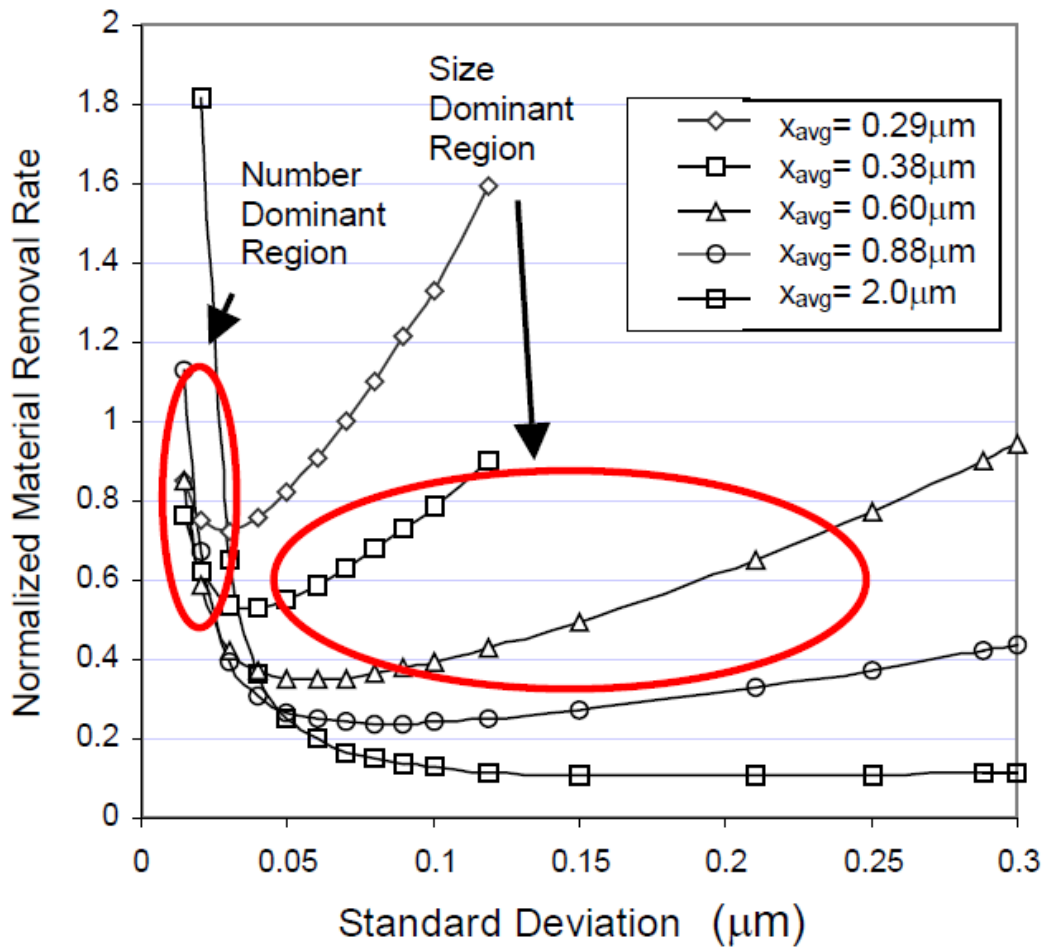
Fig. 15 Material removal as a function of standard deviation of abrasive size distribution.

much faster than the increase of the active abrasive size. In normal cases, the standard deviation will fall in the 'size dominant region' since it is quite difficult to manufacture fine abrasives with small standard deviations falling in the 'number dominant region'.

6 5

This means that decreasing the standard deviation, or using fine abrasives, may not lead to larger material removal rate, if the standard deviation is not in the number dominant region. In practice, filtering is sometimes used to remove the large abrasives to minimize scratching. While the number of surface scratches is reduced, it is usually found that the material removal is reduced as well. Based on the model, this is due to the reduction of the standard deviation in the size domain region. An optimal standard deviation, may be obtained based on the model, satisfying the requirements for minimum surface scratching, and large material removal rate simultaneously.

The abrasive size distribution plays an important role in the material removal in CMP. Basically, it influences the material removal from two aspects: the number of *active* abrasives, and the size of the active abrasives. In this chapter, a model for material removal rate explaining the effects of abrasive size distribution has been proposed and verified. In the future, the application of the model for process optimization, for example, improving the non-uniformity by changing the standard deviation or minimizing the surface scratching and maintaining material removal rate by using optimal standard deviation, may be attempted.

2.3 Overview of CMP characteristics and agglomeration

The ultimate goal of CMP is to achieve an optimal material removal rate creating an atomically smooth surface with a minimal number of defects while maintaining global planarity. The chemical effect in CMP is provided by the addition of pH regulators, oxidizers, or stabilizers depending on the process. The mechanical action, on the other hand, is mostly provided by the submicron-sized abrasive particles contained in the slurry, as they flow between the polishing pad and the wafer surface. Due to this motion, slurry

particles are motivated to interact with each other as well as with the wafer surface. consequently, combinations of static elements (pH, van-der Waal forces, double layer forces, metal oxidation, …) with the dynamic elements (friction forces, velocities, …etc.) derive the agglomeration generation.

The relationship between the size of nanoparticles and the agglomeration mechanism plays a vital role to understand the nature of agglomerates. Luan et al. [47] used dynamic light scattering (DLS) for particle size investigation. They have deduced the large particles (or soft agglomerates) through the peak of distributions. They have mentioned that these large particles (agglomerates) have been established at weakly alkaline barrier slurry without BTA and the oxidizer (FA/O barrier slurry). Moreover, they have elucidated that this phenomenon back to the high mechanical grinding activity of colloidal silica, as well as, it was observed that the chemical action had declined.

Matijevic and Babu[3] have highlighted that when the rotational speed of the carrier and the platen are the same, the relative velocity of each point on the wafer with respect to the pad is the same, facilitating a uniform material removal rate from across the entire wafer surface. authors drew attention to the difficulty to compare published results of using silica particles as abrasives because we shall not only consider the size parameter, but also the slurry concentration, and other conditions. Due to different substrates and various chemical compositions of slurries (pH, additives), certain trends should be discussed.

In this review article, we introduce a comprehensive study on the researches altitudes that have attempted to realize the particle agglomeration at CMP and its complex implications. Where firstly a study of possible cases of agglomeration agitation has been offered. It is highlighted the seriousness of features of slurries that are affected in particle

6 7

agglomeration in its constituents. Thus, many researchers discovered a substantial relationship between the agglomeration production and the stability status of the used slurry. Moreover, researchers have found out prominent complications at <u>material removal rate</u>, surface finishing treatments, contaminations, consumables, and others which pointed us to the economic feedback as an industrial/manufactural view of point. Secondly, many comparisons have been discussed about the methodologies followed to detect and identify the agglomeration through the concentration and size analysis. So, if one wants to check about the grade of slurry under usage, this section is very feasible for that. Thirdly, we deal with a crucial scope at this topic, that is the vital function of the friction and shear forces at surface finishing under the effect of agglomeration. Ultimately, we have cited the researchers' conductance to decipher the puzzling interconnectedness among different factors of CMP characteristics and agglomeration.

References

1. F. Preston, "The theory and design of plate glass polishing machines," Journal of the Society of Glass Technology, Vol. 11, pp. 214-256, 1927.

2. J. F. Archard, "Contact and rubbing of flat surfaces," Journal of Applied Physics, Vol. 24, pp. 981-985, 1953.

3. A. Maury, D. Ouma, D. Boning, J. Chung, "A modification to Preston's equation and impact on pattern density effect modeling," Program Abstracts, Advanced Metalization and Interconnect Systems for ULSI Applications, Sept. 30-Oct. 2, 1997.

4. P. Wrschka, J. Hernandez, Y. Hsu, T. S. Kuan, G. S. Oehrlein, H. J. Sun, D. A. Hansen, J. King, M. A. Fury, "Polishing parameter dependencies and surface oxidation of chemical mechanical polishing of Al thin films," Journal of the Electrochemical Society, Vol. 146, No. 7, pp. 2689-2696, 1999.

5. N. J. Brown, P. C. Baker, R. T. Maney, "Optical polishing of metals," Proceedings of SPIE, Vol. 306, pp. 42-57, 1981.

6. L. M. Cook, "Chemical processes in glass polishing," Journal of Non-Crystalline Solids, Vol. 120, pp. 152-171, 1990.

7. K. L. Johnson, Contact Mechanics. Cambridge University Press, Cambridge, 1985.

8. C. W. Liu, B. T. Dai, W. T. Tseng, C. F. Yeh, "Modeling of the wear mechanism during chemical-mechanical polishing," Journal of the Electrochemical Society, Vol. 143, No. 2, pp. 716-721, Feb., 1996.

9. S. R. Runnels, "Feature-scale fluid-based erosion modeling for chemicalmechanical polishing," Journal of the Electrochemical Society, Vol. 141, No. 7, pp.1900-1904, July 1994.

10. W. T. Tseng, Y. L. Wang, "Re-examination of pressure and speed dependence of removal rate during chemical mechanical polishing processes," Journal of the Electrochemical Society, Vol. 144, pp. L15-L17, 1997.

11. F. Zhang, A. Busnaina, "The role of particle adhesion and surface deformation in chemical mechanical polishing processes," Electrochemical and Solid-State Letters, Vol. 1, No. 4, pp. 184-187, 1998.

12. F. Zhang, A. A. Busnaina , G. Ahmadi, "Particle adhesion and removal in chemical mechanical polishing and post-CMP cleaning," Journal of the Electrochemical Society, Vol. 146, No. 7, pp. 2665-2669, 1999.

13. G. Ahmadi, X. Xia, "A model for mechanical wear and abrasive particle adhesion during the chemical mechanical polishing process," Journal of the Electrochemical Society, Vol. 148, No. 3, pp. G99-G109, 2001.

14. A. R. Mazaheri , G. Ahmadi, "Modeling of the effect of bumpy abrasive particles on chemical mechanical polishing," Journal of the Electrochemical Society,

Vol. 149, No. 7, G370-G375, 2002.

15. A. R. Mazaheri , G. Ahmadi, "A model for effect of colloidal forces on chemical mechanical polishing," Journal of the Electrochemical Society, Vol. 150, No. 4, G233-G239, 2003.

16. Y-T Su, "Investigation of removal rate properties of a floating polishing process," Journal of the Electrochemical Society, Vol. 147, No. 6, pp. 2290-2296, 2000.

17. Y. Moon, "Mechanical aspects of the material removal mechanism in chemical mechanical polishing (CMP)," Ph.D. Dissertations, 1999, Department of Mechanical Engineering, University of California at Berkeley, Berkeley, CA, U. S. A.

18. J. Z. Zhang, S. K. Huang, W. S. Toh, W. S. Tay, F. Chen and B-B. Zhou, "Optimization of pad conditioning for stable oxide CMP process," 1997 CMP-MIC Conference, pp. 315-321, Santa Clara, CA, U.S. A., Feb. 13- 14, 1997.

19. T. Yu, C. Yu, M. Orlowski, "A statistical polishing pad model for chemical-mechanical polishing," IEEE International Electron Devices Meetings, pp. 865-868, Dec. 1993.

20. J. M. Steigerwald, S. P. Murarka and R. J. Gutmann, Chemical Mechanical Planarization of Microelectronic Materials. New York, John Wiley & Sons., 1997.

21. B. Zhao, F. G. Shi, "Chemical mechanical polishing in IC processes: new fundamental insights," 1999 CMP-MIC Conference, pp. 13-22, Santa Clara, CA, Feb. 11-12, 1999.

22. J. Luo, D. A. Dornfeld, "Material removal mechanism in chemical mechanical polishing: theory and modeling," IEEE Transaction: Semiconductor Manufacturing, Vol. 14, No. 2, pp.112- 133, May 2001.

23. J. Luo, D. A. Dornfeld, "Effects of abrasive size distribution in chemical mechanical planarization: modeling and verification," IEEE Transaction on Semiconductor Manufacturing, Vol. 16, Issue3, pp. 469-476, 2003, DOI: 10.1109/TSM.2003.815199.

24. J. Luo, D. A. Dornfeld, "Material removal regions in chemical mechanical planarization for sub-micron integrated circuit fabrication: coupling effects of slurry chemicals, abrasive size distribution, and wafer-pad contact area," IEEE Transaction: Semiconductor Manufacturing, Vol. 16, No. 1, pp. 45-56, 2003.

25. G. Fu, A. Chandra, S. Guha and G. Subhash, "A plasticity-based model of material removal in chemical-mechanical polishing (CMP)," IEEE Transaction: Semiconductor Manufacturing, Vol. 14, No. 4, pp. 406-417, 2001.

26. K. Osseo-Asare, "Surface chemical processes in chemical mechanical polishing: relationship between silica material removal rate and the point of zero charge of the abrasive material," Journal of the Electrochemical Society, Vol. 149, No. 12, G651-G655, 2002.

27. F. B. Kaufman, D. B. Thompson, R. E. Broadie, M. A. Jaso, W. L. Guthrie, D. J. Pearson and M. B. Small, "Chemical-mechanical polishing for fabricating patterned W metal features as chip interconnects," Journal of the Electrochemical Society, Vol.

138, No. 11, pp. 3460-3465, Nov. 1991.

28. E. Paul, "A model of chemical mechanical polishing," Journal of the Electrochemical Society, Vol. 148, No. 6, G355-G358, 2001.

29. Y. Zhao, L. Chang and Kim SH, "A mathematical model for chemical mechanical polishing based on formation and removal of weakly bonded molecular species," Wear, Vol. 254 No. 3-4, pp. 332-339, FEB 2003.

30. C. L. Borst, D. G. Thakurta, W. N. Gill, R. J. Gutmann, "Surface kinetics model for SiLK chemical mechanical polishing", Journal of the Electrochemical Society, Vol. 149, No. 2, pp. G118-G127, 2002.

31. C. A. Sainio, D. J. Duquette, J. Steigerwald, S. P. Murarks, "Electrochemical Effects in the Chemical-Mechanical Polishing of Copper for Integrated Circuits," Journal of Electronic Materials, Vol. 25, No. 10, pp. 1593-1598, 1996.

32. D. Castillo-Mejia, S. Gold, V. Burrows and S. Beaudoin, "The effect of interactions between water and polishing pads on chemical mechanical polishing removal rates," Journal of The Electrochemical Society, Vol. 150, No. 2, pp. G76-G82, 2003.

33. Y. Xie , B. Bhushan, "Effects of particle size, polishing pad and contact pressure in free abrasive polishing," Wear, Vol. 200, pp. 281- 295, 1996.

34. Y. Zhao, L. Chang "A micro-contact and wear model for chemical mechanical polishing of silicon wafers," Wear, Vol. 252, No. 3-4, pp.220-226, Feb. 2002.

35. A. Bastawros, A. Chandra, Y. J. Guo and B. Yan, "Pad effects on material removal rate in chemical-mechanical planarization," Journal of Electronic Material, Vol. 31, No. 10, pp. 1022-1031, 2002.

36. J. Seok, C. P. Sukam, A. T. Kim and J. A. Tichy and T. S. Cale, "Multiscale material removal modeling of chemical mechanical polishing," Wear, Vol. 254, No. 3-4, pp. 307-320, 2003.

37. M. C. Pohl, D. A. Griffith, "The importance of particle size to the performance of abrasive particles in the CMP processes," Journal of ElectronicMaterials, Vol. 25, pp. 1612- 1616, 1996.

38. R. Xu, G. Smart and M. Zhang, "Particle characteristics and removal rate in CMP process", 1999 CMP-MIC Conference, pp. 253- 255, Santa Clara, CA, U.S. A., Feb. 11-12, 1999.

39. M. Bielmann, U. Mahajan and R. K. Singh, "Effect of particle size during tungsten chemical mechanical polishing," Electrochemical and Solid-State Letters, Vol. 2, pp. 401- 403, 1999.

40. R. Jairath, M. Desai, M. Stell, R. Tolles , D. Scherber-Brewer, "Consumables for the chemical mechanical polishing (CMP) of dielectrics and conductors," Material Research Society Symposium Proceedings, Vol. 337, pp. 121-131, 1994.

41. G. B. Basim, J. J. Adler, U. Mahajan, R. K. Singh, and B. M. Moudgil, "Effect of particle size of chemical mechanical polishing slurries for enhanced polishing with

minimal defects," Journal of the Electrochemical Society, Vol. 147, pp. 3523-3528, 2000.

42. J. Huang, H. C. Chen, J. Y. Wu and W. Lur, "Investigation of CMP micro-scratch in the fabrication of sub-quarter micron VLSI circuits," 1999 CMP-MIC Conference, pp. 77- 79, Santa Clara, CA, U.S. A., Feb. 11-12, 1999.

43. K. Nicholes, R. Singh, D. Grant and M. Litchy, "Measuring particles in CMP slurries," Semiconductor International, Vol. 24, No. 8, pp. 201-206, 2001.

44. J. Luo and D. A. Dornfeld, "Improvement of non-uniformity in chemical mechanical polishing from the viewpoint of consumable effects based on a developed material removal model: a research proposal," ESRC Reports (01-2001), University of California at Berkeley, Berkeley, CA, U.S.A, Jan., 2001.

45. J. Luo, David A. Dornfeld, "Optimization of chemical mechanical planarization from the viewpoint of consumable effects," 2001 VMIC Conference, pp.281-289, Santa Clara, CA, U. S. A., Sept. 25-26, 2001.

46. C. H. Zhou, L. Shan, J. R. Hight, S. Danyluk, S. H. Ng and A. J. Paszkowski, "Influence of colloidal abrasive size on material removal rate and surface finish in SiO2 chemical mechanical polishing," Tribology Transactions, Vol. 45, No. 2, pp. 232-238, 2002.

47. Xiaodong Luan, Yuling Liu, Baoguo Zhang, Shengli Wang, Xinhuan Niu, Chenwei Wang, Juan Wang, "Investigation of the barrier slurry with better defect performance and facilitating post-CMP cleaning", Microelectronic Engineering, Vol. 170, pp. 21-28, 2017.

Chapter 3:

Material Removal Mechanism and Particle Agglomeration

Chapter 3: Material Removal Mechanism and Particle Agglomeration

3.1 Smoluchowski approach and Collision Mechanisms

Most discussions of the rate of aggregation [1] start from the classic work of Smoluchowski [2], which laid the foundations of the subject. It is convenient to think in terms of a dispersion of initially identical particles (primary particles), which, after a period of aggregation, contains aggregates of various sizes and different concentrations - n_i particles of *size* i, n_j particles of size *j* etc. Here, n_i etc. refer to the number concentrations of different aggregates and 'size' implies the number of primary particles comprising the aggregate; we can speak of 'i-fold' and 'j-fold' aggregates. A fundamental assumption is that aggregation is a second-order rate process, in which the rate of collision is proportional to the product of concentrations of two colliding species. (Three-body collisions are usually ignored in treatments of aggregation - they only become important at very high particle concentrations). Thus, the number of collisions occurring between *i* and j particles in unit time and unit volume, J_{ij}. is given by:

$$J_{ij} = k_{ij}n_in_j \quad (1)$$

where k_{ij} is a second-order rate constant, which depends on a number of factors, such as particle size and transport mechanism. In considering the rate of aggregation, we must recognize that, because of interparticle forces, not all collisions may be successful in producing aggregates. The fraction of successful collisions is called the collision efficiency and given the symbol *a*. If there is strong repulsion between particles then practically no collision gives an aggregate and *a* = 0. When there is no significant net repulsion or when there is an attraction between particles, then the collision efficiency can approach unity.

Although there are some theoretical difficulties, it is usual to assume that the collision rate is independent of colloid interactions and depends only on particle transport. This assumption can often be justified on the basis of the short-range nature of interparticle forces, which operate over a range which is usually much less than the particle size, so that particles are nearly in contact before these forces come into play. The 'decoupling' of transport and attachment steps greatly simplifies the analysis of aggregation kinetics and a similar assumption is common in simple treatments of particle deposition.

A very important case where this approach is not justified is that of hydrodynamic or viscous interaction, which involves much longer-range effects.

For the present, we shall assume that every collision is effective in forming an aggregate (i.e. the collision efficiency, $a = 1$), so that the aggregation rate constant is the same as the collision rate constant. It is then possible to write the following expression for the rate of change of concentration of k-fold aggregates, where $k=i+j$:

$$\frac{dn_k}{dt} = \frac{1}{2} \sum_{\substack{i+j \to k \\ i=1}}^{i=k-1} k_{ij} n_i n_j - n_k \sum_{k=1}^{\infty} k_{ik} n_i \ (2)$$

The first term on the right-hand side represents the rate of formation of k-fold aggregates by collision of any pair of aggregates, i and j, such that $i + j = k$. Carrying out the summation by this method would mean counting each collision twice and hence the factor 1/2 is included. The second term accounts for the loss of k-fold aggregates by collision, and aggregation, with any other aggregates. The terms k_{ij} and k_{ik} are the appropriate rate constants. It is important to note that is for irreversible aggregation, since no allowance is made for break-up of aggregates.

For continuous particle size distributions, an integral version of equation can be written. In principle, it is then possible to derive the evolution of the aggregate size distribution

with time, but there are formidable difficulties, especially in assigning values to the rate coefficients. These depend greatly on the nature of the particles and on the way in which collisions are brought about. The simplest assumption is that spherical particles coalesce on contact to form a larger sphere with the same total volume. This is physically unrealistic except for liquid (emulsion) droplets, but has often been assumed in earlier treatments of aggregation kinetics. There are three important transport mechanisms in practice: (1) Brownian diffusion (giving *perikinetic* aggregation); (2) fluid motion (orthokinetic aggregation); and (3) differential settling. These will be considered in the next section. In all cases, we shall assume that the particles are spherical and that the collision efficiency is unity (every collision is effective in forming a permanent aggregate). Also, hydrodynamic interaction will be neglected for the time being. Although these assumptions are not realistic for practical systems, they enable simple results to be derived which can be used to illustrate the essential features of the various aggregation mechanisms.

3.1.1 Collision Mechanisms

Small particles in suspension can be seen to undergo continuous random movements or Brownian motion. The diffusion coefficient of a spherical particle is given by the Stokes-Einstein equation:

$$D_i = \frac{kT}{6\pi a_i \mu} \qquad (3)$$

where k is Boltzmann's constant, T the absolute temperature, ai the particle radius and p the viscosity of the suspending fluid. Smoluchowski [2] calculated the rate of diffusion of spherical particles of type i to a fixed sphere j. If each i particle is captured by the central sphere on contact, then the i particles are effectively removed from the suspension

and a concentration gradient is established in the radial direction towards the sphere, *j*.
After a very brief interval, steady-state conditions are established and it can easily be
shown that the number of *i* particles contacting *j* in unit time is:

$$J_i = 4\pi R_{ij} D_i n_i \quad (4)$$

where D_i is the diffusion coefficient of particles of type *i* and n_i is their concentration in
the bulk suspension. R_{ij} is the collision radius for particles *i* and *j*, which is the center-to-
center distance at which they may be taken to be in contact. In practice, it can usually be
assumed that this is simply the sum of the particle radii, i.e.:

$$R_{ij} = a_i + a_j \quad (5)$$

When there is significant long-range attraction between particles they may be
effectively 'captured' at greater distances, so that the collision radius is rather larger
than that given by Eq. 5. However, there is usually very little error in using this
approximation. Of course, in practice, the central sphere j is not fixed, but is itself
subject to Brownian diffusion. It is only necessary to replace *Di* in (4) by the *mutual
diffusion coefficient, D_{ij},* to account for the motion of the j particle, with:

$$D_{ij} = D_i + D_j \quad (6)$$

If the concentration of *j* particles is n_j, then the number of *i-j* collisions occurring in unit
volume per unit time is simply:

$$J_{ij} = 4\pi R_{ij} D_{ij} n_i n_j \quad (7)$$

Therefore;

$$k_{ij} = \frac{2kT}{3\mu} \frac{(a_i + a_j)^2}{a_i a_j} \quad (8)$$

This result has the very important feature that, for particles of approximately equal size, the collision rate constant becomes almost independent of particle size. The term $\frac{(a_i+a_j)^2}{a_i a_j}$ has a constant value of about *4* when $a_i \approx a_j$. Physically, this is because increasing particle size leads to a lower diffusion coefficient, but a larger collision radius and these two effects cancel each other out when the particles are of nearly the same size. Under these conditions, the rate constant becomes:

$$k_{ij} = \frac{8kT}{3\mu} \quad (9)$$

Inserting values appropriate to aqueous dispersions at 25°C gives $k_{ij} = 1.23 \times 10^{-17} m^3 s^{-1}$.

3.1.2 Orthokinetic aggregation:

We have seen that collisions brought about by Brownian motion do not generally lead to the rapid formation of very large aggregates, especially in dilute suspensions. In practice, aggregation (flocculation) processes are nearly always carried out under conditions where the suspension is subjected to some form of shear, either by stirring or by flow. Particle transport brought about by fluid motion can give an enormous increase in the rate of interparticle collisions, and aggregation brought about in this way is known as *orthokinetic aggregation.* The first treatment of the rate of orthokinetic aggregation was also due to Smoluchowski [2], who considered only the case of uniform laminar shear. Such conditions are rarely, if ever, encountered in practice, but it is convenient to start from this simple case and then to modify the result for other conditions.
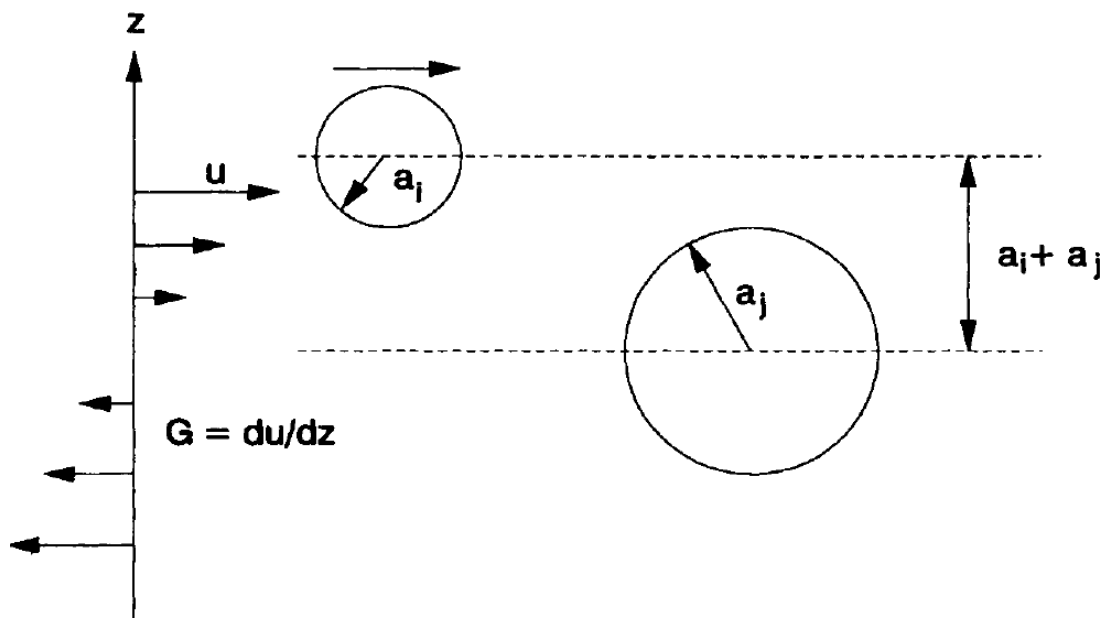
Fig. 1 Model of the orthokinetic collision of spheres in a uniform shear field. The particles are on streamlines which are separated by a distance equal to the collision radius, $a_i + a_j$, and so will just collide.

A uniform laminar shear field is one in which the fluid velocity varies linearly in only one direction, perpendicular to the direction of flow. Smoluchowski assumed that particles would follow straight fluid streamlines and collide with particles moving on different streamlines, according to their relative position. The collision frequency depends on the sizes of the particles and on the velocity gradient or shear rate, G. By considering a fixed central sphere of radius a_j and flowing particles of radius ai, it can be assumed that those moving particles on streamlines that bring their centers within a distance $a_i + a_j$ (the collision radius, R_{ij}) of the central particle will collide with it. The collision frequency can then be calculated by considering the flux of particles through a cylinder of radius $R_{ij}l$ the axis of which passes through the center of the sphere j. For the conditions of previous figure, it is clear that the particles in the upper half of the cylinder will move from left to right and vice versa.

3.1.3 Collision efficiencies

Assumption that all particle collisions are successful in producing aggregates. In practice, this is very often not the case and allowance has to be made for the reduced *collision efficiency* (i.e. the fraction of successful collisions). Formally, all that is needed is to incorporate the collision efficiency, *a,* into the rate expressions discussed earlier. For example, the rate of change of the primary particle concentration, given by equation, becomes:

$$(\frac{dn_1}{dt})_{t\to 0} = -\alpha k_{11} n_1^2 (10)$$

There remains the problem of assigning a value to *a* and this presents some difficulties. The collision efficiency can be very significantly reduced as a result of repulsive colloidal interactions, such as double layer repulsion or steric interaction. Another major effect is due to hydrodynamic or viscous interaction, which tends to hinder the approach of colliding particles. Collisions brought about by diffusion or by induced particle motion are affected in different ways by these interactions and a comprehensive treatment is difficult. Initially, we will consider the effect of colloidal interactions on Brownian collisions and then go on to discuss hydrodynamic effects.

3.1.4 Orthokinetic collision efficiencies

For collisions of non-Brownian particles (greater than a few micrometers in size), the Fuchs concept of diffusion in a force field is not appropriate and we have to consider the relative motion of particles induced by fluid shear or by external forces such as gravity. In such cases it may be possible for colliding particles to overcome potential energy barriers as a result of their relative motion. It has been observed that aggregation of otherwise stable colloids can sometimes be achieved by the application of sufficiently

high shear. For instance, Zollars and Ali [3] found that latex particles which were stable against Brownian aggregation for up to 4 years could be coagulated in a few minutes by the shearing at very high rates. The phenomenon of *shear flocculation* [4] is probably an example of such an effect. It should be clear that, for a given suspension, the collision efficiency for Brownian aggregation could be very different from that for orthokinetic collisions. In some cases, similar values are found (Swift and Friedlander, [5]), but the agreement is probably fortuitous.

3.1.5 Form of aggregates
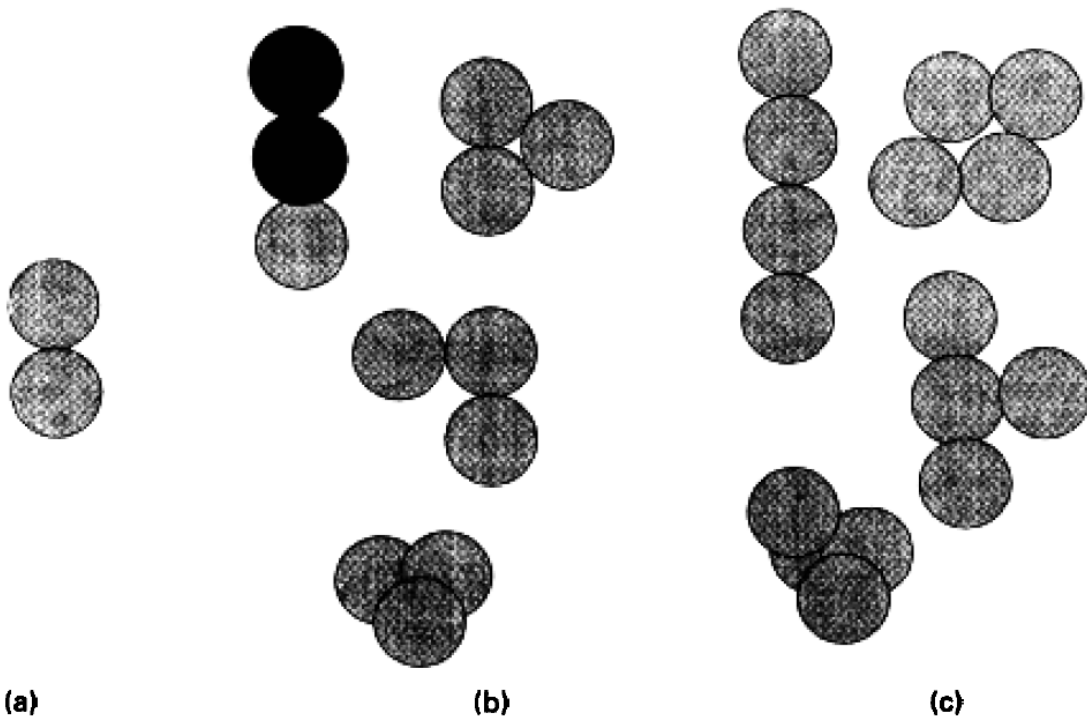
Fig. 2 Showing possible forms of aggregates of equal spheres: (a) doublets, (b) triplets, and (c) quadruplets

When solid particles aggregate, no coalescence can occur and the resulting clusters may adopt many different forms. In the simplest case of equal spheres, there is no doubt about the shape of a doublet, which must be in the form of a dumbbell. However, a third particle can attach in several different ways and with higher aggregates the number of possible

structures rapidly increases, as indicated in Fig. 2. In real aggregation processes, aggregates containing hundreds or thousands of primary particles can arise and it will never be possible to provide a detailed description of their structure. Some convenient method is needed which enables aggregate structure to be characterized in general terms, but still conveys useful information. A great deal of progress was made in this area during the 1980s, largely as a result of computer simulation of aggregate formation and the study of model aggregates.

3.1.6 Aggregate strength and break-up

It was stated at the beginning of our discussion of aggregation kinetics that aggregation would be regarded as irreversible, and this assumption is implicit in expressions. This is a convenient assumption, since the breakup of aggregates is very difficult to model. However, since nearly all aggregation processes are carried out with some form of agitation, the break-up process cannot be ignored. In practice, it is often found that aggregates (flocs) reach a certain, limiting *size,* which depends on the applied shear or energy dissipation and on the *floc strength.* Empirically, the *size* may depend on the energy dissipation according to (e.g. Muhle and Domasch, [6]):

$$d_{max} = C\epsilon^{-n} \quad (11)$$

where *C* and *n* are constants. There are several theoretical approaches for floc break-up in turbulent flow which lead to expressions of the form of eqn. (11) (Tambo and Francois, [7]; Muhle [8]). The exponent depends on the size of the floc relative to the turbulence microscale; for instance, for flocs large compared to the microscale an exponent of around -0.4 may be found, whereas for much smaller flocs the dependence on energy input is not *so* great and $n = 0.3$. However, these values are difficult to check experimentally and may be highly system-specific. As a convenient rule of thumb, it is sometimes assumed that

the limiting floc size in a turbulent flow field is of the same order as the Kolmogoroff microscale. Even in laminar shear, it is not easy to predict maximum aggregate size. Torres et al. (Torres, F. E., Russel, W. B. and Schowalter, W. R., "Floc structure and growth kinetics for rapid shear coagulation of polystyrene colloids", J. Colloid Interface Sci., Vol. 142, pp. 554-574, 1991.) used the following expression to model break-up of large flocs in simple shear, derived by balancing the van der Waals force between two particles with the hydrodynamic force acting to separate two aggregates:

$$R_{Hi} + R_{Hj} = (\frac{A}{18\pi\mu Ga\delta^2})^{1/2} \quad (12)$$

where R_{Hi} and R_{Hj} are the dimensionless hydrodynamic radii of two colliding aggregates (scaled by the primary particle radius, *a),* A is the Hamaker constant and δ is the separation of particles in the primary minimum. The parameter δ is subject to considerable uncertainty and is often treated as a fitting parameter, with a value of the order of 1 nm or less. Although the equation applies to simple shear and is based on simplifying assumptions, it does highlight some important factors governing aggregate strength. For instance, the maximum floc size is predicted to vary as G-0.5, which is equivalent to a dependence on and this exponent is of the same order as those found experimentally in some cases (Tambo and Frangois [7]).

The criterion for limiting floc size assumes that a collision between two aggregates can only lead to attachment if the sum of their hydrodynamic radii does not exceed a certain critical value. For larger aggregates, the shear force tending to separate them is greater than the binding force. This is equivalent to finding the size of colliding aggregates, under given shear conditions, for which the collision efficiency becomes zero. Such an approach

was adopted by Brakalov [9] for turbulent conditions and the predictions of his model agree quite well with measurements on aggregates of metal hydroxides.

However, there are many cases where the concept of a limiting size based on a vanishing collision efficiency is not appropriate. For instance, aggregates formed under low-shear conditions may break when subjected to higher shear. In that case, floc breakage may occur in several ways, not necessarily into the aggregates from which the floc was formed at the last collision. Experimental observations (e.g. Glasgow and Liu, 1991) indicate that floc breakage is a complex phenomenon, with large-scale fragmentation as well as surface erosion of small components occurring simultaneously. At present, there is no satisfactory model to account for the observed effects, and progress is hampered by the lack of an accepted experimental method for studying floc breakage. Also, there is no widely accepted definition of common terms such as 'floc strength'. Intuitively, the strength of an aggregate must depend on the attractive forces between component particles and the number of particle-particle contacts. The latter must depend on the density of the aggregate, which determines the effective 'coordination number' of the component particles. Because of the fractal nature of aggregates, an increase in size means a decrease in density and a reduced number of particle-particle contacts per unit volume of aggregate. Since the disruptive force increases with size, the limiting size may be reached when the aggregation number is still quite small. The same number of primary particles in a smaller, more compact aggregate could be said to be 'stronger' in that it resists a shearing force which would disrupt the larger, lower density aggregate. For this reason, assessment of 'floc strength' on the basis of the limiting hydrodynamic size achieved under given shear conditions may be misleading. Information on the *muss* of the aggregate would also be relevant.

Inclusion of floc break-up in modelling of aggregation processes usually involves an assumption of the limiting aggregate size under given conditions. Aggregates exceeding *this* size are assumed to break into two or more 'daughter' aggregates and the precise form of breakage assumed can greatly influence the computed aggregate size distribution.

3.2 Proposed MRR Model

3.2.1 Introduction

The progressive shrinkage in device feature size and increase in the process complexity has generated severe issues in the form of scratches and abrasive particle agglomeration. These defects are highly critical and unacceptable to devise yields and performance. During defect analysis, sometimes it is hard and complex to investigate the source of defect formation and become a serious issue during the CMP process. Therefore, to improve the device's performance and increase its efficiency, it is important to identify the root cause of the defects generated during the CMP process. This can help in resolving the defect level in a shorter and quicker time scale via developing an efficient CMP process.

Therefore, a Higley stable CMP slurry is critical to reducing process-dependent defectivity such as scratches and particle residues. The consumables such as pads and slurries play a critical role in CMP process performance. To meet the strict requirements of advanced nodes, novel types of abrasives such as ceria coated silica particles have been handled to extend the capability of commercial CMP slurries [11]. On the other hand, the Long-term stability of nanoparticle suspensions, by making small (1- to 10-nm) nanoparticles and dispersing them without agglomeration using special mechanical dispersing techniques and the creative use of chemical dispersants, is critical to fully

appreciate the benefits of nanofluids (slurry underuse). It has been observed that the modification of nanoparticle surfaces with surface-modifying additives such as surfactants has a strong influence on the thermal conductivity of nanofluids. For example, copper nanoparticle surfaces modified with thioglycolic acid can significantly increase the effective thermal conductivity of nanofluids (Eastman et al. [12]).

3.2.2 Agglomeration assessments between CMP and nanofluid technology

In that same context, there is a robust connection between stability and CMP characteristics through agglomeration activity. Material removal mechanism which represents the core of (CMP) process has been experienced by many models from decades ago, based on the domination of either mechanical or chemical effects. Based on the research field of CMP, there are three fundamentals; Shear particle force, MRR, and agglomeration which most researchers interest to correlate between them. Treatments have been achieved between the shear and agglomeration theoretically and experimentally [14]. Also, the relation between MRR and shear has been built qualitatively [15,16]. There are a few bit results for experimental outputs in this treatment. However, the direct relation between agglomeration and MRR has not been completely understood yet, which is our concern in this study. In *aggregation*, the particles retain their individuality, but part of their surface area is lost due to the interaction. This interaction is based on the molecules/groups (e.g. hydrogen bonding) on the surface of nanoparticles. Whereas electrostatic interactions try to keep the particles away from each other, van der Waals interactions between the particle cores bring them together. This results in a net energy minimum.

These van der Waals interactions are strong at short distances and the particles coalesce in the absence of a shell that imparts repulsion. The repulsion can, additionally, be due to steric forces, as in the case of a molecule covering a particle. The nature of repulsive interactions changes depending on the type of shell. For the van der Waals forces to be effective, the distance has to be short and there is a barrier that prevents this interaction from being dominating. If the height of this barrier is greater than the thermal energy k_B T, the system is kinetically stable. As can be seen, the particles possess greater energy to overcome this barrier at higher temperatures, and the colloidal system aggregates beyond a critical value called the critical flocculation temperature.
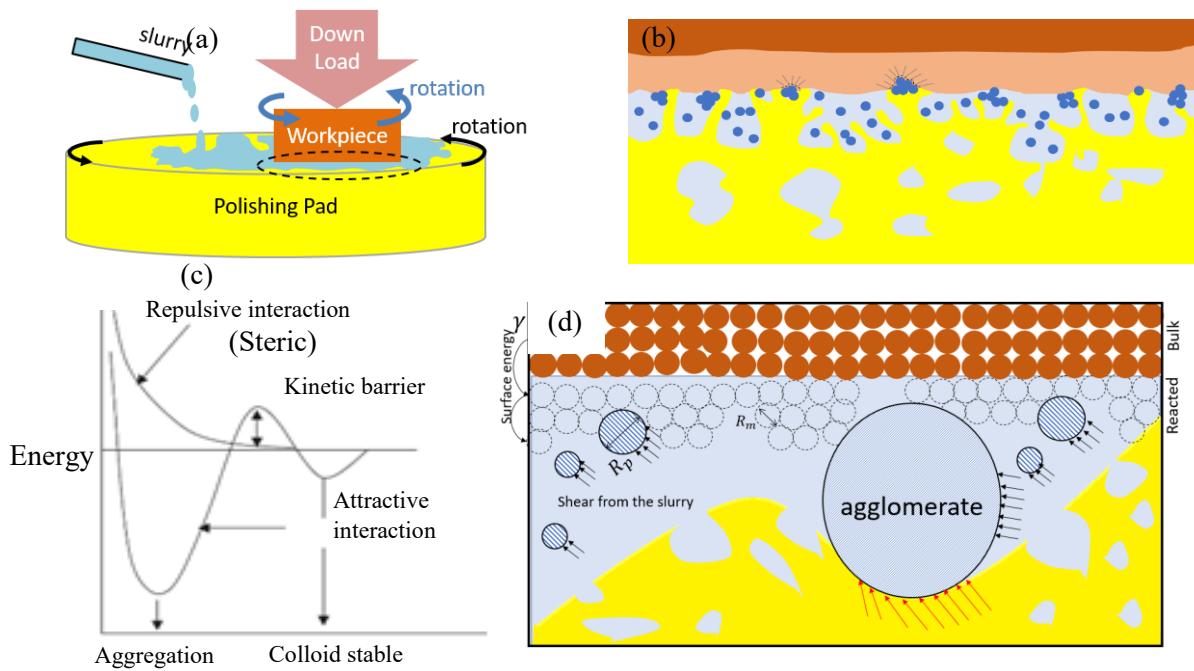
Fig.3 CMP system and the removal mechanism using nanoparticle action.

It may be noted that the stability of the shell over the nanoparticle is also temperature-dependent. Consequently, it's necessary to focus on the energy balance principle as a key

to the removal mechanism. The required particle force of pulling off the molecules on the reacted layer at the wafer surface is stipulated under the condition [16]:

$$F\left(\frac{\pi R_p{}^2}{4}\right) R_m \geq 2\gamma \left(\frac{\pi R_m{}^2}{4}\right) N \qquad (13)$$

where F is the resultant particle force, R_p the particle diameter, R_m the molecule diameter, γ the surface energy, and N is the number of removed molecules from the wafer surface. Inequality (13) is implemented at the proposed model to substitute with the material removal resulted in the particle force (Eqs. 27, 28). It should be stressed that the agglomeration effect could be justified by investigating the surface roughness for the wafer under CMP process. Yeon-Ah Jeong et al. [13] stated that the nanoparticle agglomerates massively bind the wafer surface molecules due to the large created drag forces generated from aggregates (Fig. 3(d)). While Gao et al. [17] noted that the fabricated aggregate silica achieves low surface roughness. Moreover, well-manufactured nanofluids can help develop better lubricants. The recent nanofluid activity involves the use of nanoparticles in lubricants to enhance tribological properties of lubricants, such as load-carrying capacity and anti-wear and friction-reducing properties between moving mechanical components. In lubrication application, it has been reported that surface-modified nanoparticles stably dispersed in mineral oils are very effective in reducing wear and enhancing load-carrying capacity (Que et al. [18]). Li et al. [19] performed experiments on lubricant nanofluids containing IrO_2 and ZrO_2 nanoparticles. The results showed that nanoparticles decrease friction remarkably on the surface of 100 C6 steel. Conversely, Crawford [20] showed how agglomerates at high salinity slurry worse the surface finishing. That's could be yielded from the intensive friction force achieved by

the agglomerates. Hence, the agglomeration intensifies the defect level of surface roughness through stability analysis of the slurry. Upon that, it's appealed that the agglomeration and nanofluid instability are two faces for the same coin, so it is critical to reduce and control the formation of agglomeration during the CMP process.

Basim and Moudgil [21] studied the effects of soft aggregates on CMP removal rates and surface roughness using slurries of silica particles spiked with different concentrations of polymer-flocculated or salt-coagulated silica particles and observed that they can alter the MRR, increase the surface roughness, and cause damage to the surface from polishing.

Therefore, the relation between agglomeration, MRR, and surface roughness is ambiguous and influences many complex conditions. However, if MRR is kept to be stable, this greatly decreases the surface defects. So that, this is the aim of the current study to correlate directly between MRR and agglomeration.

As stated before, the researchers have connected the agglomeration and CMP slurry shear as a qualitative investigation. They have matched between the material removal mechanism and the shear forces and the normal forces as well. The remaining corner of the fundamental CMP elements which is the direct relationship between the material removal rate and the slurry agglomeration which is investigated in the current study through the effect of shear forces which greatly dominate the wafer/pad interfacial region.

3.2.3 Methodology

Particle aggregation occurs due to particle collisions. Based on Smoluchowski's theory, assume that n_i, n_j are the initial concentrations of the primary particles of sizes $\{i, j\}$ respectively. Agglomeration is a second-order rate process, in which the rate of collision

is proportional to the product of concentrations of two colliding species. Thus, the number of collisions between i and j particles in unit time in unit volume is given by

$$J_{ij} = k_{ij}n_in_j \quad (14)$$

where k_{ij} is the rate constant [22]. Assuming every collision is effective, the rate of change of concentration of k-fold agglomerates [1] (agglomerate of size k where $k=i+j$) is:

$$dn_k/dt = (1/2)\sum_{i=1}^{i=k-1} k_{ij}n_in_j - n_k\sum_{k=1}^{\infty} k_{ik}n_i \quad (15)$$

Define the total concentration as:

$$n_T = n_1 + n_2 + n_3 + \cdots \quad (16)$$

where $[n_T]_{t=0} = n_0$,

substituting (4) in (3), yields [42];

$$dn_T/dt = -(1/2)(k_{11}n_1^2 + k_{12}n_1n_2 + \cdots) \quad (17.1)$$

Regarding all rate constants are equal, for any i,j; $k_{ij} = k$ (18)

$$dn_T/dt = -(1/2)(k)(n_1^2 + n_1n_2 + n_1n_3 + \cdots + n_2^2 + n_2n_1 + n_3n_1 + \cdots) \quad (17.2)$$

$$dn_T/dt = -(1/2)(k)(n_1 + n_2 + n_3 + \cdots)(n_1 + n_2 + n_3 + \cdots) \quad (17.3)$$

Applying the definition of Eq. (16) at Eq. (17.3):

$$dn_T/dt = -(1/2)kn_T^2 \quad (19)$$

Performing integration on both sides of equation (19):

$$\int \frac{dn_T}{n_T^2} = \int \frac{1}{2} k dt \ (20)$$

$$n_T = \frac{n_0}{1 + \frac{k}{2} n_0} \frac{1}{t} \quad (21)$$

Total concentration n_T is depicted from Eq. (21) as a descending function of time and it suffers from damping (Fig. 4) due to particle collisions which divide into three types; (1) Brownian diffusion (perikinetic aggregation), (2) fluid motion (orthokinetic), (3) differential settling. Often, the second mechanism is more sensible to be implemented because the abrasives (colliding particles) are dispersed under the effect of the turbulent flow [47] especially that the nanofluids provide the turbulence intensity than that in case of base fluid. By the way, the dispersions bearing such nanoparticles have so different attributes other than the bulk fluid as Kumer et al. [23] have concluded that the dilatant fluid is better heat transporter than Newtonian and pseudo plastic fluids. It's implied that the total concentration strictly decreases to the steady-state concentration as the parameter k increases so the slurry stability increases as "k" decrease. Regarding the orthokinetic collision rate [1]:

$$J_{ij} = \frac{4}{3} G R_{ij}^3 n_i n_j \ (22)$$

Comparing Eq. (22) to Eq. (14):

$$k_{ij} = \frac{4}{3} G R_{ij}^3 \ (23)$$
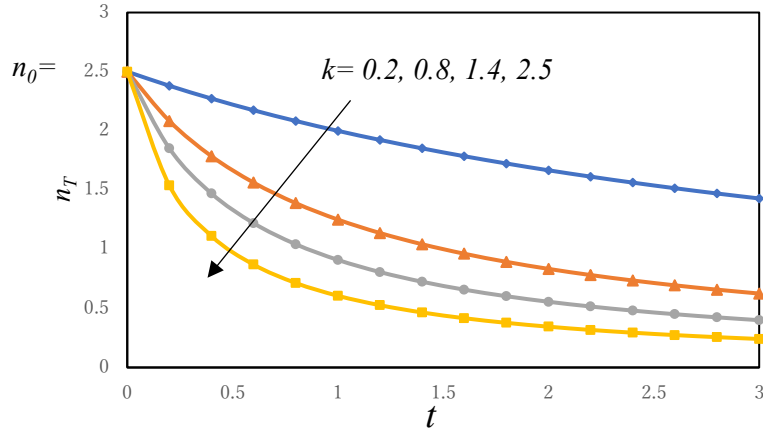
Fig.4 History of total particle concentration "n_T".

where R_{ij} is the distance between the centers of two spherical particles and G is the shear of the slurry. Invoke condition (18);

$$k = \frac{4}{3} G R_{avg}^3 \quad (24)$$

where R_{avg} the average overall R_{ij}'s. From (24) into (21):

$$n_T = \frac{n_0}{1 + \frac{2}{3} G R_{avg}^3 n_0 t} \quad (25)$$

which reflexes the relation between particle concentration and the slurry shear. The shear frequency f_τ could be as [24]:

$$f_\tau = \frac{V A_\tau}{A_n} \left(2 R_p \sqrt{\frac{E_{sp}}{H_w}} \right) \left(\frac{6 \rho_s \alpha}{\pi \rho_a R_p^3} \right)^{\frac{2}{3}} (1 - \phi(3\sigma_s - d)) \quad (26)$$

where V, sliding velocity, E_{sp}, equivalent particle pad modulus, H_w, wafer hardness, ρ_s/ρ_a, slurry/particles densities respectively, α, weight concentration of slurry (%), and ϕ, the normal distribution [25] of pad asperities is in terms of d which is the separation distance

9 2

between the wafer and the polishing pad surface after force balancing, and σ_s which is the root mean square of the pad surface asperities height. Invoking Eq. (13), then the MRR could be formulated as [15]:

$$MRR \propto removed\ volume \cdot N \cdot f_\tau \quad (27)$$

where the removed volume ($= \frac{4}{3}\pi(\frac{R_m}{2})^3$) is the volume of the material units (molecule) at the wafer surface, $N = \frac{2F}{\gamma R_m}$ is the amount number of the removed material units (molecules), and f_τ is the shear frequency on the wafer surface.

$$MRR \cong \frac{1}{3}\frac{F}{\gamma}R_m^2 f_\tau \quad (28)$$

3.2.4 Model quantification

Due to the turbulent flow at the wafer/pad interface layer is dominant or the slurry is non-Newtonian (shear thinning/thickening), the dispersion techniques such as high shear and ultrasound (very large sliding velocity between the polishing pad and the wafer surface) can be used to create various particle–fluid combinations. Hence, the nanofluids are prepared by the two-step method during the CMP.

Not only the slurry shear dominates the resultant particle force, but also the wafer is an underlying hydroplaning motion (Tsai et al. [26]). Hence, from Eq. (25), the shear is given by:

$$G = \frac{3}{2}\frac{1}{R_{avg}^3 n_0 t}\left(\frac{n_0}{n_T} - 1\right) (29)$$

Define the shear force using the viscosity (v) as:

$$F = \frac{3}{2} \frac{v}{R_{avg}^3 n_0 t} \left(\frac{n_0}{n_T} - 1\right) \quad (30)$$

Substituting Eq. (30) into Eq. (28), yields:

$$MRR = \frac{1}{2\gamma} \frac{v}{R_{avg}^3} \frac{1}{t} \left(\frac{1}{n_T} - \frac{1}{n_0}\right) R_m^2 f_\tau \quad (31)$$

which correlates with MRR, particle concentration, and time.

3.2.5 Model verification

By substituting the definition of f_τ from (26) into (31), and rearrange the equation:

$$MRR = \frac{v R_m^2}{\gamma\left(\frac{R_m + R_p}{2}\right)^3 R_p} \frac{A_\tau}{A_n} \left(\frac{6\rho_s \alpha}{\pi \rho_a}\right)^{\frac{2}{3}} (1 - \phi(3\sigma_s - d)) \frac{1}{t} \left(\frac{1}{n_T} - \frac{1}{n_0}\right) V \sqrt{\frac{E_{sp}}{H_w}} \quad (32)$$

The term $\left(\frac{1}{n_T} - \frac{1}{n_0}\right)$ for the stable slurry case is so slow to change so it is relatively constant. This is implied from Fig.4, after a certain period (on the horizontal axis), the slurry state becomes stable and the curve approximately moves parallel to the horizontal axis (time). This means that the difference between initial concentration n_0, and n_T is fixed. Therefore,

$$MRR = k(t) V \hat{P} \quad (33)$$

which represents the Preston Equation, where $k(t) = \frac{v R_m^2}{\gamma\left(\frac{R_m + R_p}{2}\right)^3 R_p} \frac{A_\tau}{A_n} \left(\frac{1}{n_T} - \frac{1}{n_0}\right) \frac{1}{t}$ is the

modified Preston coefficient, and $\hat{P} = \sqrt{\frac{E_{sp}}{H_w}}$ is the resultant pressure
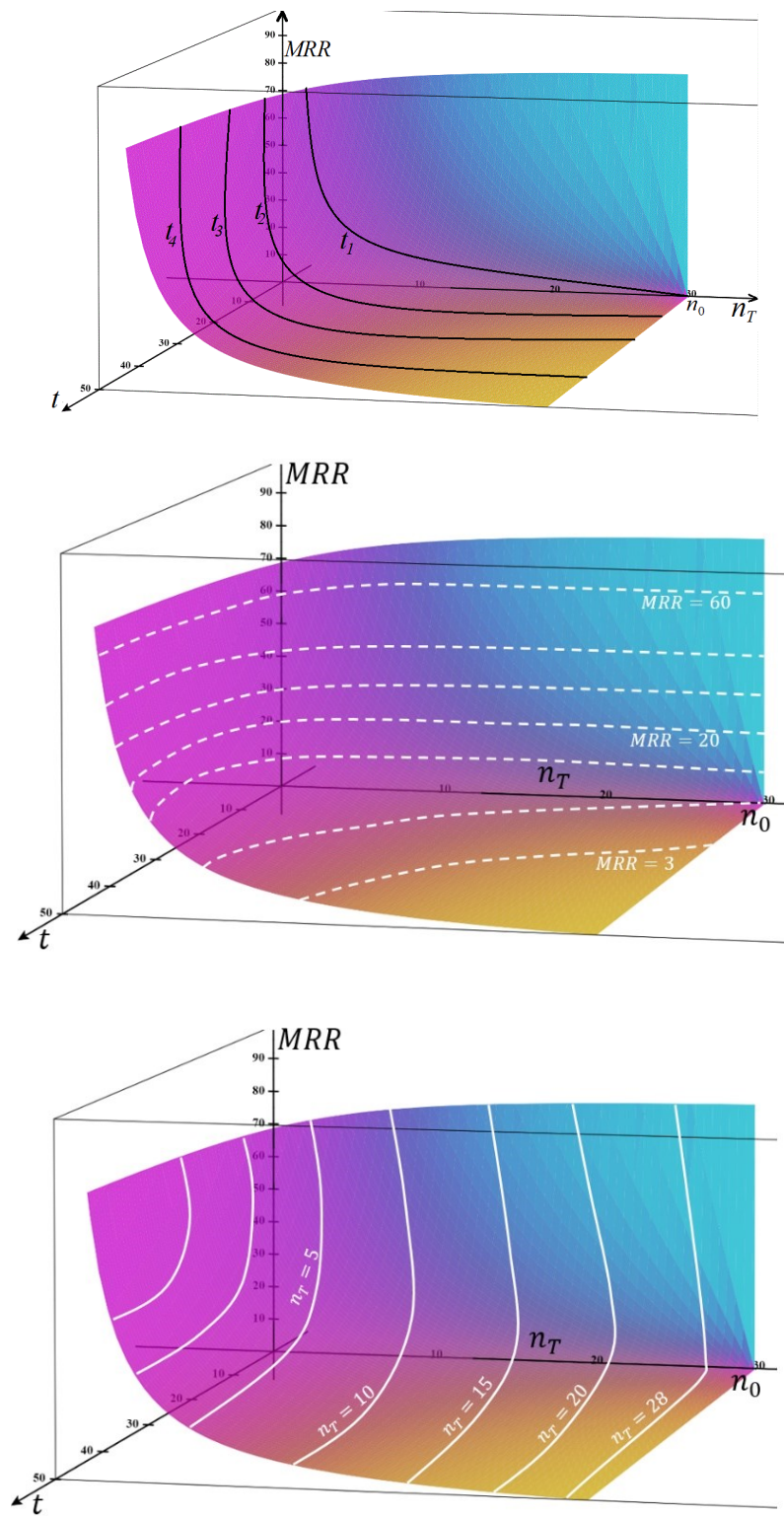
Fig. 5 MRR as a function of time and particle concentration.
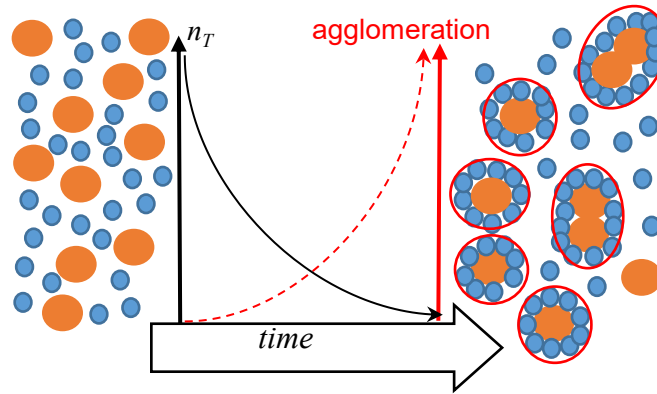
Fig. 6 Relation between particle concentration and agglomeration.

3.2.6 Behaviour of MRR function

During CMP, it is possible to assume that the slurry viscosity and the shear frequency have negligible changes, besides, the surface energy and the radius of molecules and particles are constants. Then the term $\frac{\nu R_m^2 f_\tau}{2\gamma R_{avg}^3}$ in Eq. (31) becomes a constant relatively "c".

Hence, $MRR = MRR(t, n_T) = c\frac{1}{t}\left(\frac{1}{n_T} - \frac{1}{n_0}\right)$ as shown in Fig. 5 where the removal mechanism records high rates at the initial time, $t \neq 0$ as well as for low particle concentrations and dramatically descends, therefore it tends to settle near zero as {$t\to\infty$, $n_T \to n_0$}. The Sharp drop of MRR could be mitigated by increasing the value of the parameter "c".

If we consider time fixing (Fig. 5 (top)), MRR decreases as n_T increases up to the value n_0 due to the lack of active nanoparticles because n_0 is the initial case where there is no abrasion action. However, as n_T decreases (moves far from n_0), the slurry shear implicitly increased and MRR accordingly increases (Fig. 5 (top)). The initial value, n_0, is the upper limit, then n_T decreases (moves in inverse direction on concentration axis) with time regarding MRR is constant (Fig. 4, Fig.5 (bottom)). Therefore, In the beginning,

the total primary nanoparticles concentration, n_0 , is larger than the agglomerates concentration (Fig. 6). As time goes on (during CMP processing) the particle concentration gradually decreases and the agglomerates grow up (Fig. 6). So, if MRR is an explicit function of particle concentration, inevitably this means that MRR is a function of the particle agglomeration implicitly. Accordingly, MRR could be stabilized as n_T is maintained through the controlling of the nanoparticle agglomeration.

3.3 Relation among MRR, n_T, and the agglomeration

As shown in Fig. 5, provided that time is fixed, MRR decreases as n_T approaches n_0, meaning that, MRR decreases as $n_0 - n_T$ decreases. To understand that at real CMP process, both $\{n_0, n_T\}$ are considered such that at the beginning of CMP process, n_0, should be larger than n_T (the instantaneous value) as shown from the model (Eq. 31). Hence, as time goes on (Fig.6), the concentration decreases, meaning that $n_T < \cdots < n_0$. Inevitably, the term $n_0 - n_T$ enlarges, which also means that the term $\frac{1}{n_T} - \frac{1}{n_0}$ enlarges more and more, directly implying that MRR increases (Eq. 31). Besides, we can track agglomerate rate as in (Eq.31). The practical results (Fig. 7) depict that as the nanoparticle concentrations {both n_0, n_T} decrease, MRR decreases, which agrees in general with the results reported by B. Park et al. [27] as shown in Fig.7 (inset). The difference at the relatively large concentration values could back to the approximation which is based on the cubic polynomial. Also, the same phenomenon had been captured by [28]. On the other hand, the model (Fig. 5) depicts the relativity between $\{n_0, n_T\}$. The superficial view may suggest a contradiction between Eq. (31) and Fig. 7 if all parameters are supposed to be constant as well as the time except for the MRR and n_T; but this is not a real case because the polishing time could not be totally fixed while the meaning offered

by Fig. 5 (bottom) is that the decline of the MRR decreases as n_T decreases. in other words, the range of MRR values shrinks as n_T decreases.
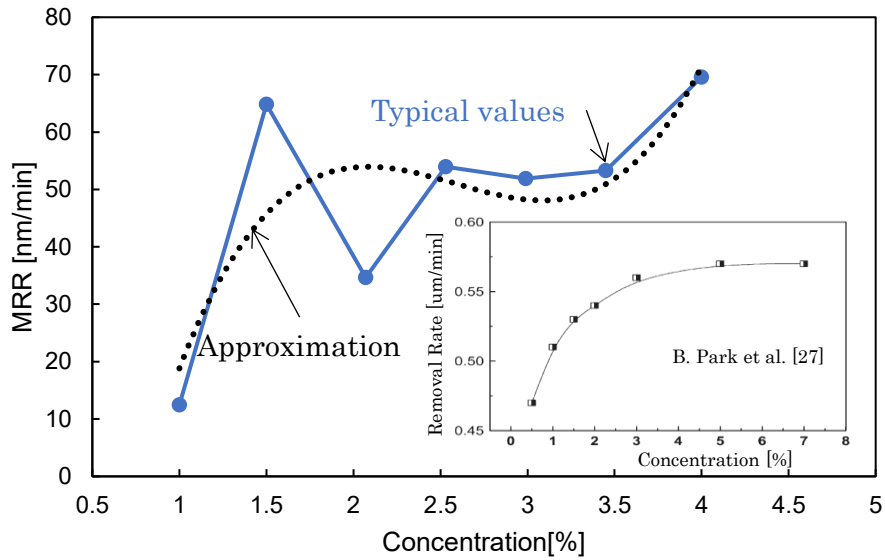
Fig. 7 MRR measurements along with different concentrations (colloidal Silica PL-7).

Current CMP is performed on SiO_2 wafer under a load of 5.728 PSI for 5 mins using the colloidal silica slurry (75 nm) at alkaline medium (pH:10.54~12.54) using KOH+DIW (deionized water). The polishing pad (IC1000) and the head (workpiece carrier) have the same rotation speed (~72 cycles/min) (Fig.3(a)) and the environment temperature was sustained at (25.2~25.9 °C) (Fig. 19).

it's worthy to mention that a dense treatment is needed to avoid the aggregation of silica nanoparticles. Dai et al. [29] had attempted surface modification with vinyltriethoxysilane and 2-mercaptobenzimidazole in order to fabricate a new kind of self-dispersing silica nanoparticle for enhanced oil recovery applications.

Well-dispersed stable nanoparticle suspensions are produced by fully separating nanoparticle agglomerates into individual nanoparticles in a host liquid. In most

nanofluids prepared by the two-step process, the agglomerates are not fully separated, so nanoparticles are dispersed only partially. Although nanoparticles are dispersed ultrasonically in liquid using a bath or tip sonicator with intermittent sonication time to control overheating of nanofluids, this two-step preparation process produces significantly poor dispersion quality [10]. Because the dispersion quality is poor, the conductivity of the nanofluids is low.

Therefore, the key to success in achieving significant enhancement in the thermal properties of nanofluids is to produce and suspend nearly monodispersed or non-agglomerated nanoparticles in liquids. A promising technique for producing non-agglomerating nanoparticles involves condensing nanophase powders from the vapor phase directly into a flowing low-vapor-pressure fluid. This approach, developed in Japan (by Akoh et al. [30]), is called the VEROS (vacuum evaporation onto a running oil substrate) technique. VEROS has been essentially ignored by the nanocrystalline materials community because of subsequent difficulties in separating the particles from the fluids to make dry powders or bulk materials. Based on a modification of the VEROS process developed in Germany (Wagener et al. [31]). Eastman et al. [32] developed a direct evaporation system that overcomes the difficulties of making stable and well-dispersed nanofluids. The direct evaporation–condensation process yielded a uniform distribution of nanoparticles in a host liquid.

In this much-longed-for way to making non-agglomerating nanoparticles, they obtained copper nanofluids with excellent dispersion characteristics and intriguing properties. The thermal conductivity of ethylene glycol, the base liquid, increases by 40% at a Cu nanoparticle concentration of only 0.3 vol%.
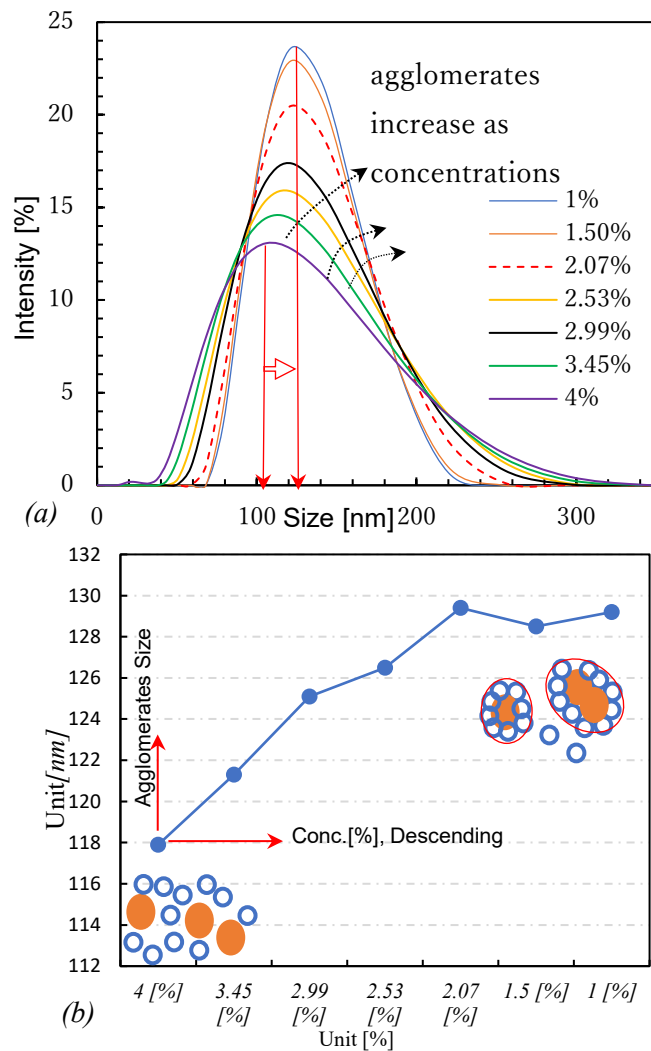
Fig. 8 Size distributions of slurry samples for different concentrations.

This is the highest enhancement observed for nanofluids except for those containing carbon nanotubes. However, the technology used by Eastman et al. has two main disadvantages. First, it has not been scaled up for large-scale industrial applications. Second, it applies only to low-vapor-pressure base liquids.

Zhu et al. [33] developed a one-step chemical method for producing stable Cu-in-ethylene glycol nanofluids by reducing copper sulfate pentahydrate ($CuSO_4 \cdot 5H_2O$) with sodium hypophosphite ($NaH_2PO_2 \cdot H_2O$) in ethylene glycol under microwave irradiation. They

claim that this one-step chemical method is faster and cheaper than the one-step physical method. The thermal conductivity enhancement approaches that of Cu nanofluids prepared by a one-step physical method developed by Eastman et al. [12]. Although the two-step method works well for oxide nanoparticles, it is not as effective for metal nanoparticles such as copper. For nanofluids containing high-conductivity metals, it is clear that the single-step technique is preferable to the two-step method.

To track the effect of agglomerates growth; invoking the reciprocal relation between the nanoparticle concentration and the agglomeration, the size distributions of the agglomerates are obtained (Fig. 8(a)) for different concentrations of CMP slurry using the dynamic light scattering technology (Zetasizer measurement set) which shows the horizontal shift of the peaks along the size axis. Consequently, the agglomerates increase as the concentration of slurry used at CMP decreases which agrees with (Eq. 19). Moreover, Caterina Minelli et al. [34] have found that during the dilution the nature of the surface chemistry of the particles may be altered because of a decrease in the concentration of the stabilizing agents. This often results in an increase in particle agglomeration with sample dilution. From the previous discussion, as agglomeration increases (Fig. 8(b)), the nanoparticle concentrations decrease $\{n_0, n_T\}$, globally the material removal rate MRR decreases (Fig. 7), also locally it decreases (Fig.5) as $n_0 - n_T$ becomes small (large n_T). Therefore, controlling the agglomeration is an important factor to maintain the concentration along with time progress, moreover, obtaining a stable removal mechanism.

3.4 Measurement of Agglomeration

For the 1st method for the estimation of nanoparticle agglomeration is based on the change of the intensity of scattered light, as it is shown in figures 9-11.

This could be noticed when the concentration of slurry is changed. As the concentration decreases, the noise of accumulation function decays (Fig. 12). Moreover, the correlation coefficient continues longer time which means the scattered lights spout from large particles which represent the agglomerates. By the way, the dynamics of large particles is described that its Brownian velocity is so slow. Caterina Minelli et al. [34] have mentioned that for the DCS method, they used the are under the peak of the monodisperse particles in the mass-weighted size distribution to measure the number concentration of these particles.
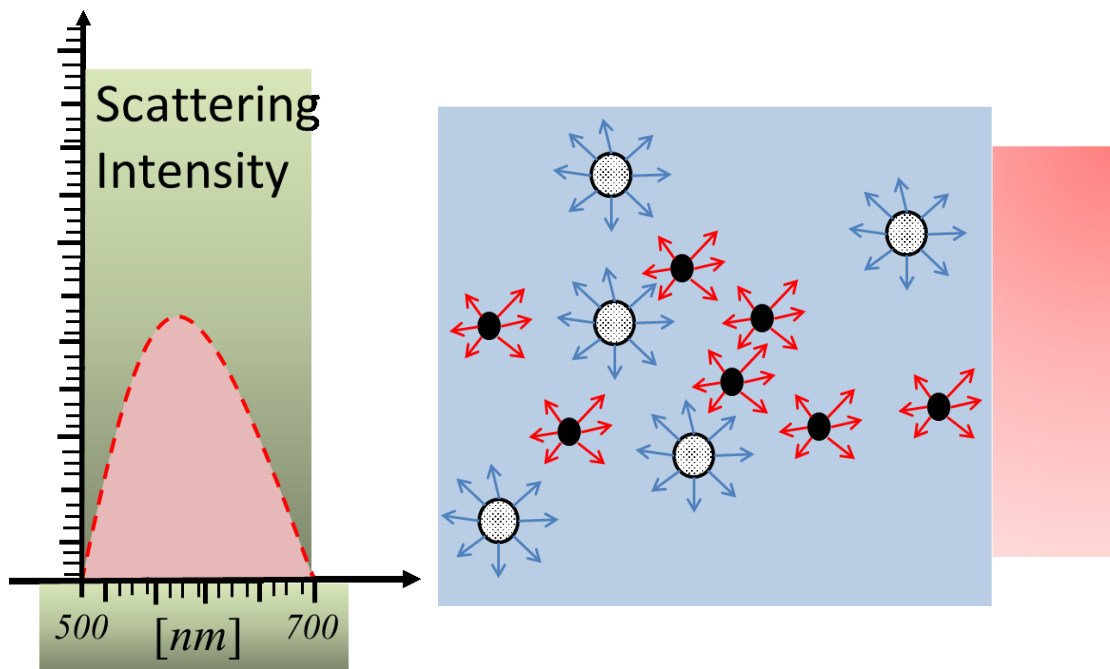
Fig. 9 Different sizes of nanoparticles scatter the incedent laser at the dispersion.
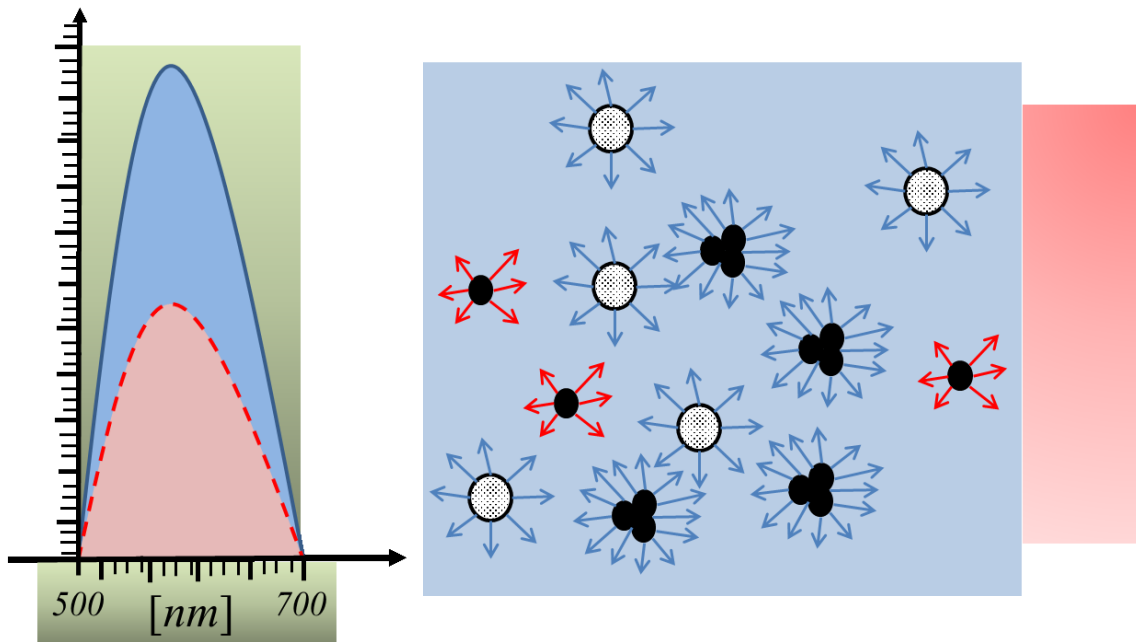
Fig. 10 Change at scattering intensity due to particle agglomeration.

1 0 3
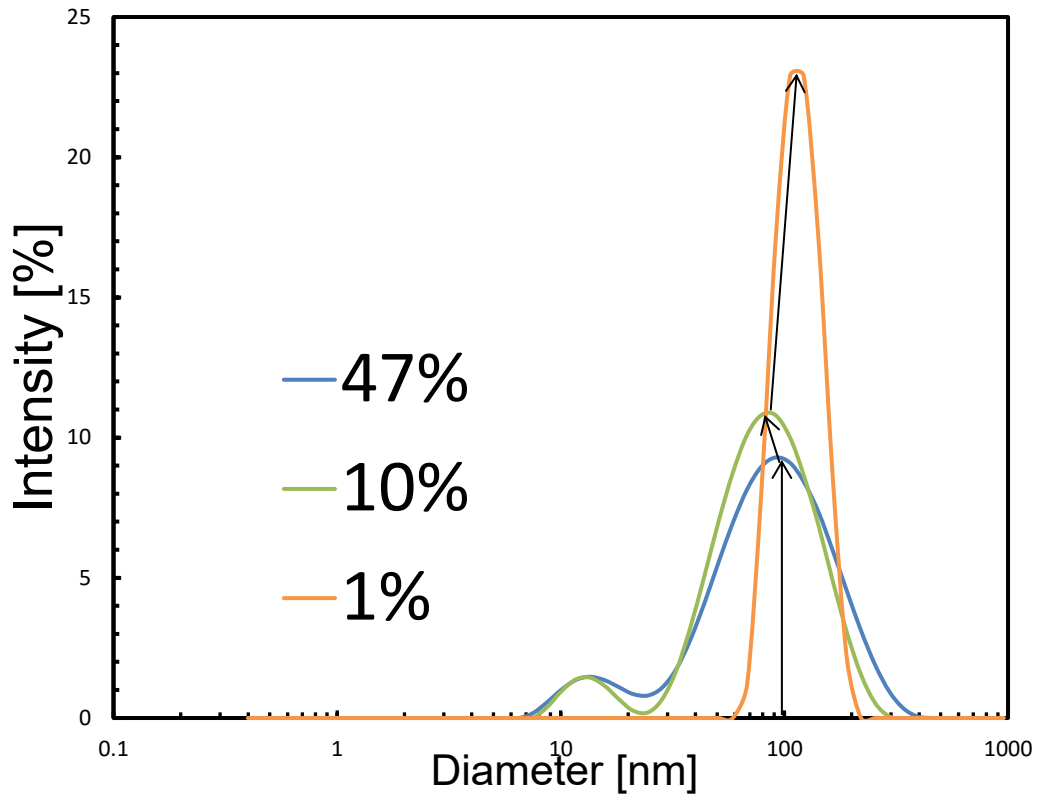
Fig. 11 Paticle size distribution for different concentrations.
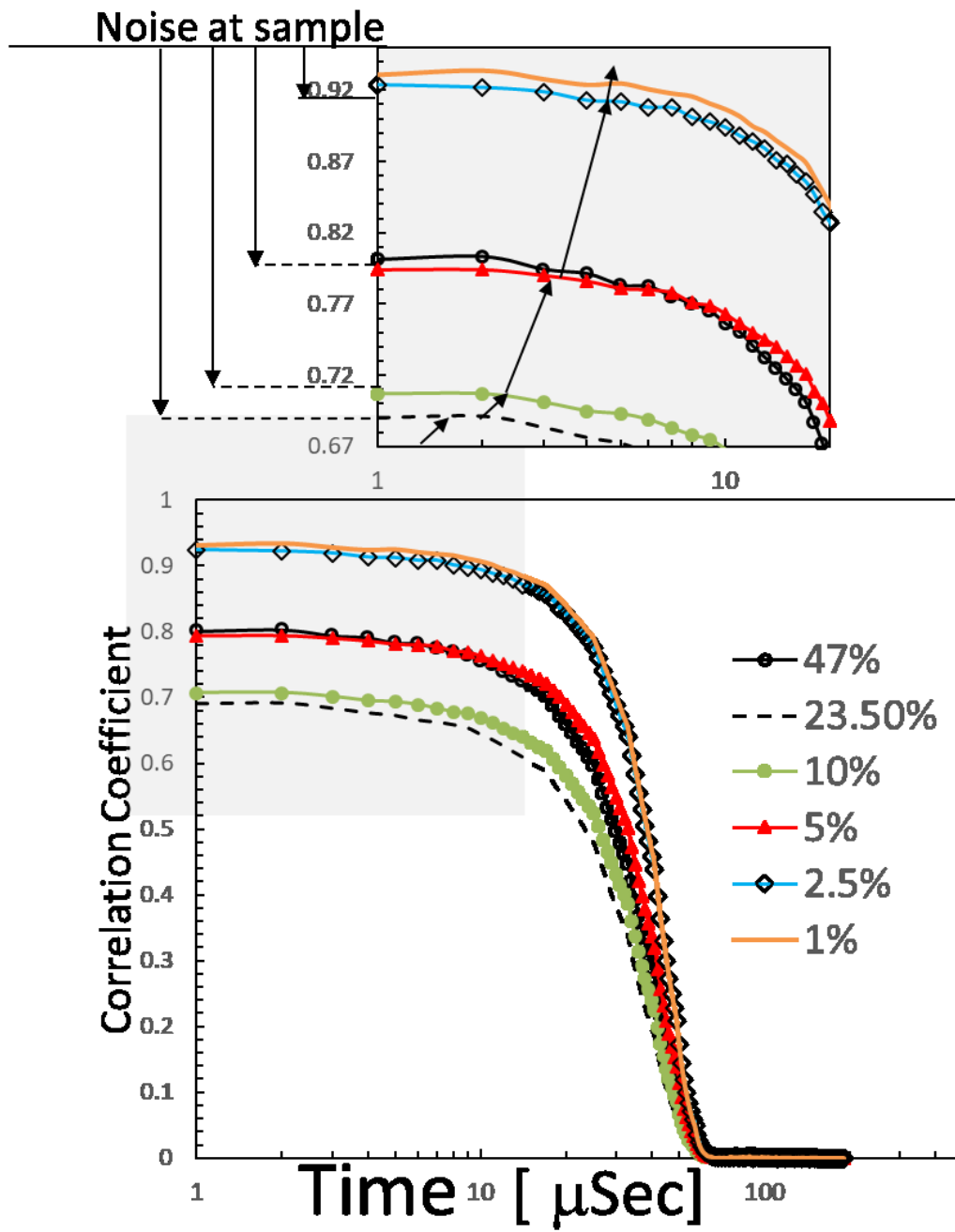
Fig. 12 Cumulant correlation function curve for different slurry concentrations.

However, it could be considered that the increase at intensity back to increase at concentration but not always means that it's conformation of agglomerates. The 2nd method is more appropriate based on change on the size axis (horizontal axis) for the size distribution of DLS curves. At this method, we track the position of the peak of size distribution; if it moves vertically along the intensity axis for different test cases; this means change has been occurred for the concentrations of slurry particles which have the same size approximately. If the peak moves horizontally along the size axis for different cases this means the aggregates have been generated.

We can track agglomerates behaviour using results of DLS, where the size distributions for samples of different cases (when we monitor the slurry behaviour under change of certain "Effect" like Pressure, Velocity, … so on) are obtained. If the Peaks of distributions change vertically (along the Intensity axis) this means Peaks have almost same size (say r*; Fig. 13) for different test cases, i.e. change the concentration of particles of almost same size. However, when the Peaks of different test cases change along the size axis [Malvern Panalytical Ltd. Grovewood Road, Malvern, Worcestershire, WR14 1XZ, UnitedKingdom, ISO:22412DLS second edition, JISZ：88282019.], this means change at size and agglomerates are generated as peak moves right.
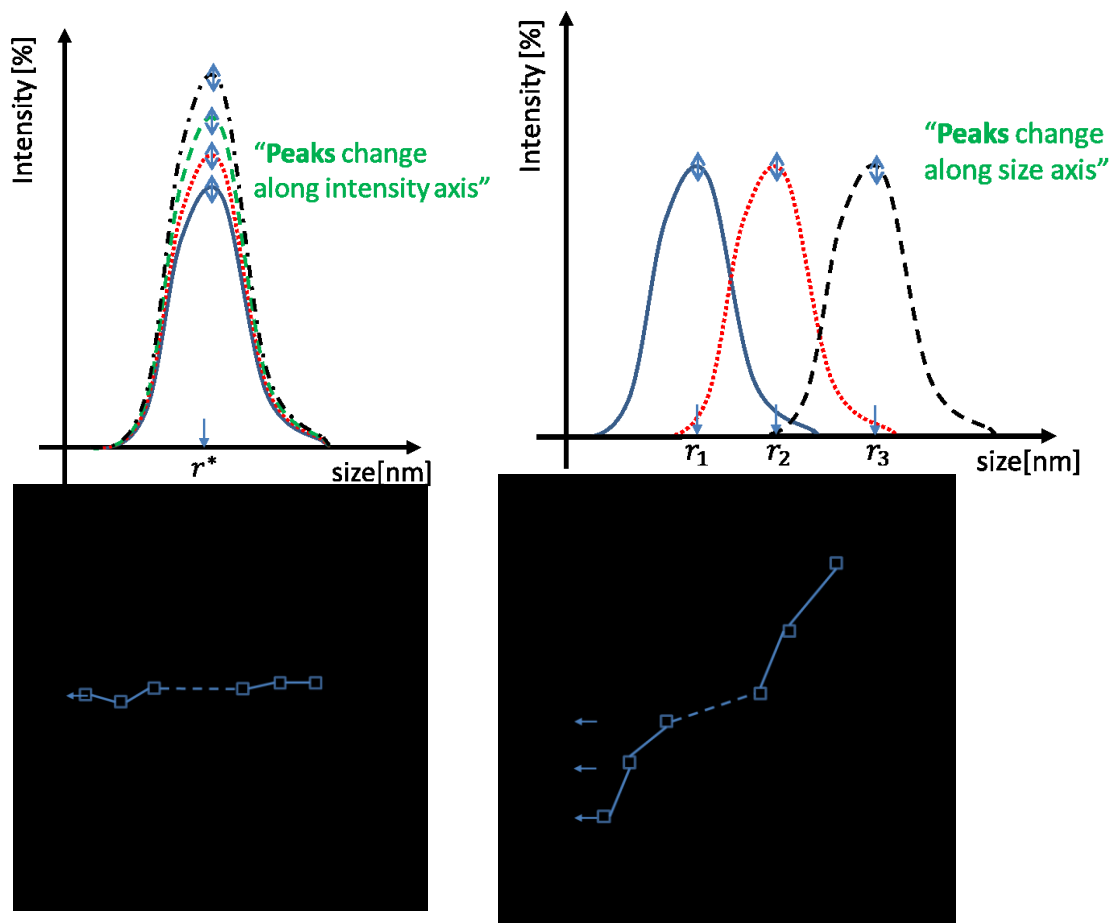
Fig. 13 The relation between somewhat effect and the particle size distribution

3.5 pH and Agglomeration

It was found that pH had a dominant effect on the aggregation behaviour [36], when the aggregation rate and mechanism of 150 nm alumina particles in 1 mM KNO_3 with different additives used in Cu CMP were investigated [36]. it was observed that alumina aggregated in acidic suspensions when sodium dodecylsulfate was present, a behaviour that was not observed with any other suspension. Basim and Moudgil [21] studied the effects of soft aggregates on CMP removal rates and surface roughness using slurries of silica particles spiked with different concentrations of polymer-flocculated or salt-

coagulated silica particles and observed that they can alter the MRR, increase the surface roughness, and cause damage to the surface from polishing.

It is found that above the minimum shear rate [11] is needed to induce agglomeration, the duration of application of shear rate also has a similar effect on agglomeration. Therefore, the degree of agglomeration increases with time. This behaviour is consistent with Smoluchowski's theory of agglomeration. If the shear rate does not exceed the threshold Camp number 10^5, no agglomeration is observed even though for longer duration since the particle attraction force does not overcome the interparticle repulsive force. The shear rate threshold at basic medium is larger than acidic. Repulsive inter-particle forces in the slurry keeps the slurry stable and the reduction in it have shown to decrease slurry stability [35]. The isoelectric point (IEP) of silica particle is at ~pH 2, and an increase in the pH induces higher amounts of negatives charges on the surface of silica particles. Silica particles are high stable in pH>=10, and as the slurry pH is lowered from basic to acidic and approaches IEP, repulsive inter-particle force decreases [35]. Agglomeration within lower pH silica slurry can be expected to get severe once the slurry subjected to shear. Moreover, zeta potential can be used to represent differences in the inter-particle forces between silica particles at different pH values. Moving away from the isoelectric point of silica, it is observed that negative surface charge increases as the pH of silica slurry increases (2~10). This agrees with our findings (Fig. 14) when we applied NaOH for justifying the alkaline slurry medium. It is found that size distributions of agglomerates for different polishing durations (0 min. ~ 10 min.) for neutral and alkaline mediums did not variate along horizontal axis greatly. Conversely, distributions were clearly distinguished at acidic slurry (where we justify pH of silica slurry using nitric acid

(HNO$_3$)). At acidic slurry, distribution peaks greatly shifted on size axis as time increase; simultaneously, increase polydispersity. Which means larger and harder agglomerates were generated.
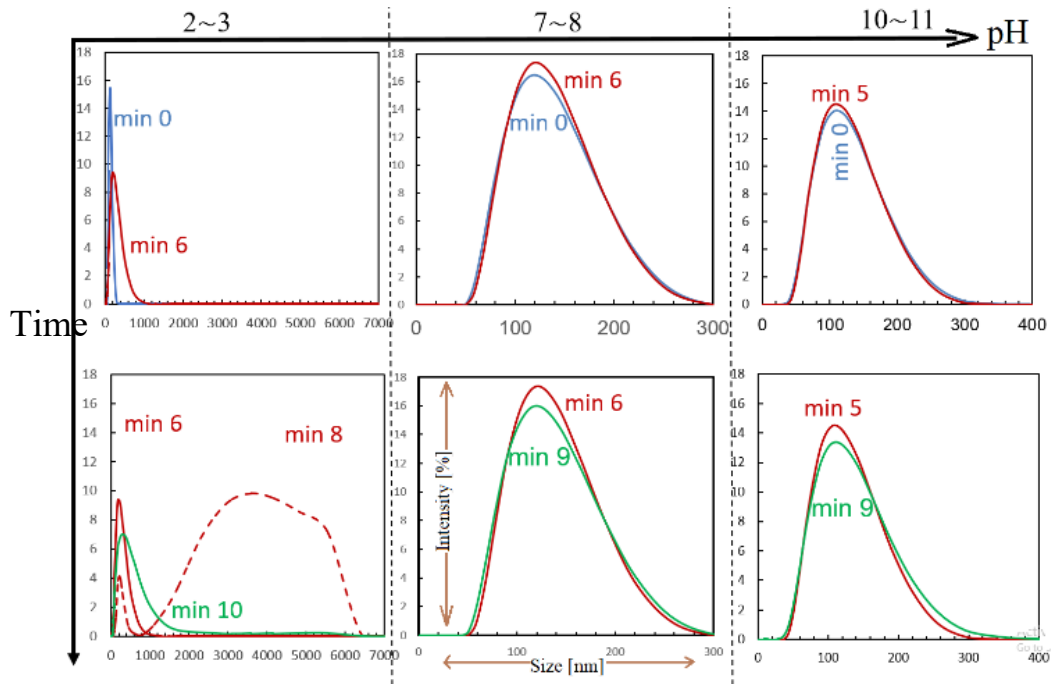
Fig. 14 Effect of pH on size distribution during CMP.

3.6 Agglomeration's Variables

The CMP slurry silica with a particle size of ~75nm used was a dispersion manufactured by Fuso Chemical Industry Co., Ltd. containing 23% ultra-high purity colloidal silica which is

1- Milky-appearance, has specific gravity (20/4°C) =1.14,

2- Produced by sol-gel synthesis from ultra-high purity alkyl silicate,

3- A uniform dispersible and has sharp particle size distribution with less sedimentation.

4- Stable at neutral and alkaline pH,

5- Less lot to lot variation, Alkali metals contents less than 300 ppb, and for heavy metals less than 100 ppb.
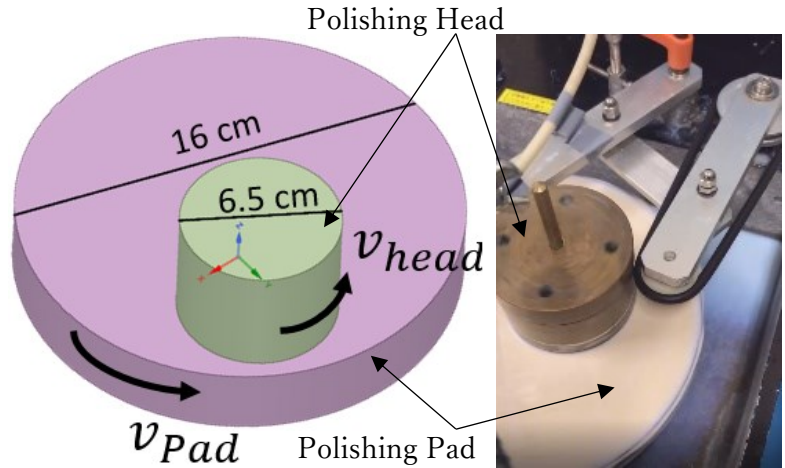
Fig. 15 Polishing pad and head motion during CMP.

The pH was adjusted using KOH+DIW. Firstly, we clean the polishing machine (all route way where the slurry will move through) by DIW, then dressing is done to polishing pad (IC1000) for ~5mins, the SiO_2 wafer is attached to the bottom side of the head during providing the slurry as 30 cc/min. the polishing pad and head rotate (Figs. 15, 19) simultaneously with same velocity (increase it gradually up to the target ~72 cycles/min). During the polishing (5 mins), the slurry samples are withdrawn during CMP testing at compact closed tubes to be investigated. Necessary precautions have been considered to prevent contaminations during experiment processing.

The slurry particles are investigated, at the same day, after CMP event, of experiment performance to avoid effect of history storage and to assure that size data were obtained before particles settling, using dynamic light scattering (DLS) technology to measure the effective size (mean of hydrodynamic diameter) using a Zetasizer (Malvern Panalytical Ltd.-Japan) at a scattering angle of 173°. A sample from prepared slurry was withdrawn

before CMP processing "initial case" to exclude external effects at results comparisons. Sample temperature is justified slowly and gradually by software setup before investigation along 5 minutes. Data of intensity of scattered light by particles detected ~14 times, then it is repeated 10 times separated by 10 sec. in between for maintaining sample condition and to prevent any speciality. The distributions showed in current study are the average over 10 repetitions to exclude any abnormal behaviour. In addition, the distributions were almost monodispersed (Polydispersity Index PDI<<0.7). It is worthy to mention here that in our study we did not consider any catalyst or oxidizers at the prepared slurry contrary to some relative researches that had done. For instant, the study by [13] considered the catalyst factor at slurry, as well as the temperature was greatly changing during the existence of O_2 bubbles, meaning that slurry flow was turbulent. Such interaction between two different phases can establish particle forces of high order. In other word, such medium is not easy to thermodynamically controlled. Therefore, the slurry is unstable as the peaks of size distributions have large steps along size axis (e.g. Fig.7 at [13]). However, in our study we avoided all such additives, maintained the experiment medium to be compact to far extent.

We chose to study the agglomeration behavior at the alkaline medium for the slurry. Hence, the initial state could be regarded as no agglomeration case. Therefore, we test the effective factors (such as pressure, velocity, concentrations, polishing time, …) that able to change this state to agglomeration case. There are other factors such as temperature, humidity, viscosity, flow rate, … and so on. But they considered for far extent that they are constant and stable at our experiment since our polishing time is so short (almost, not more than 6 mins). It's believed that we can add more factors in future work if we

experience more longer time to check variations at these factors.

For concentration effect, we maintained to apply low concentrations of tested slurry to assure stability of the medium, keep temperature during CMP processing, … etc. At concentration of 4% the distribution was minimum intensity and the peak of it point to the minimum size on horizontal axis as shown in Fig. 8 (Sec.3.3). Gradually, the peaks rise and moves right along size axis, so the agglomeration mechanism increases at the direction of increase dilution (Fig. 8(Sec. 3.3)). This agrees with findings of Caterina Minelli et al. [34] who had found that during the dilution, the nature of the surface chemistry of the particles may be altered because of a decrease in concentration of the stabilizing agents. This often results in an increase in particle agglomeration with sample dilution.

| 47 % | 10 % | 1% |
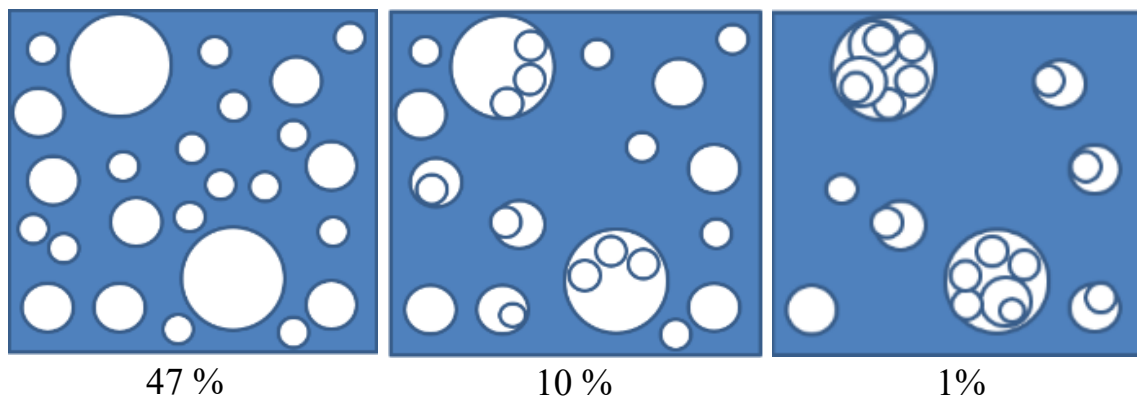
Fig.16 Agglomeration mechanism with different concentrations

For the broadness of distributions which is called the polydispersity (PDI). The maximum value for PDI (is for case 4[%]) equals to 0.2, which is still confined at the suitable range over which the distribution algorithms best operate over. This broadness means that particles have not symmetric shape. This could back to generation of soft agglomerates or the DLA agglomerates [21] which classified as open, fast, and loosely packed

agglomerates. Since particle repulsion forces are small, particles stick together almost as soon as they contact. In addition, as concentration increases, the random particle collisions allow establishment many of such large agglomerates
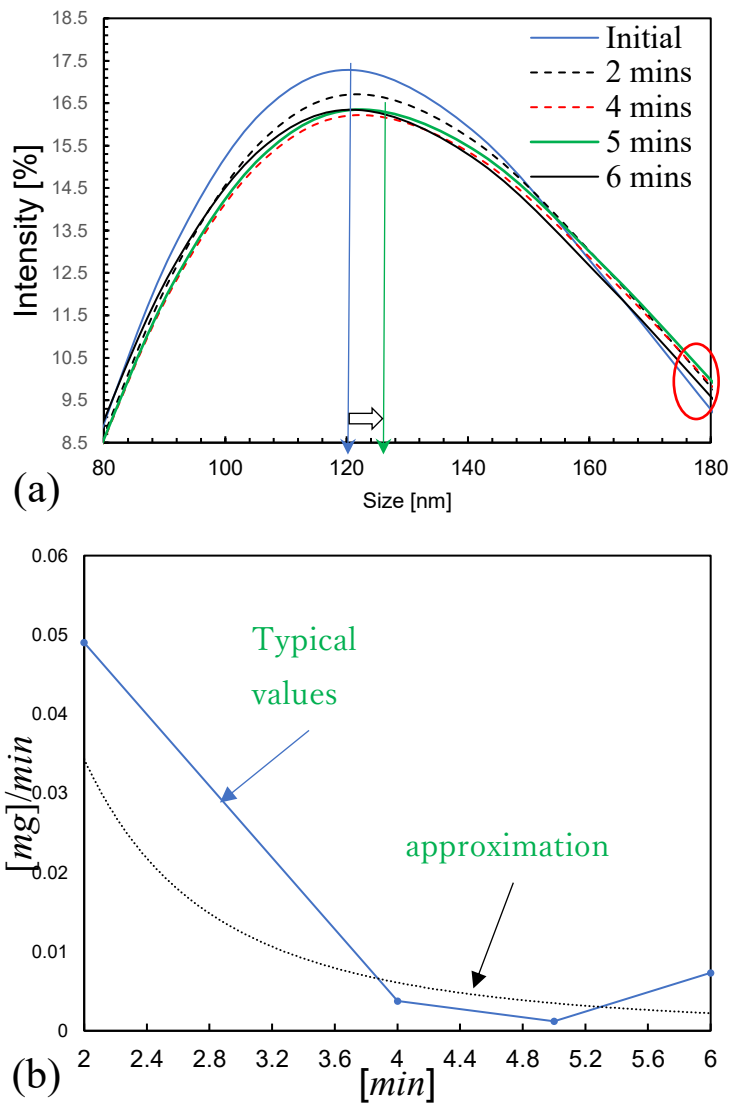
Fig. 17 Effect of polishing time on (a) size distribution during CMP, (b) material removal rate of SiO_2 wafer.

structures. At the same time, it is easy for these agglomerates to collapse into many smaller particle assemblages. Moreover, the right figure shows that MRR increase as agglomeration decreases, which agrees with many researchers, for example; S. Ozbek et

al. [49] found that MRR increases as pH of silica slurry increase, implicitly means that when agglomeration decreases (alkaline medium), MRR increases.

A. J. Kanna et al. [38] showed that increase in shear rate and polishing time lead to increase of agglomerates. Also, Fig.17(a) shows that size distributions are arranged in the interval (80~180 nm) where the maximum intensity is for the peak of the least size at initial case. However, the peak of the larger size is for case of 5 mins. It is questionable to correlate between PDI and intensity, because the minimum PDI gives the max. intensity, and vice versa. It is worthily to mention here that it is difficult to correlate between PDI and size; since as it is thought that polydispersity relies on the experiment history for the test sample more than size value on horizontal axis. Furthermore, Fig.17(b) depicted that MRR decreases with the polishing time (it is represented as an exponential function of time by applying curve fitting) which agrees with findings of [39, 40, 43]. Similarly, Tae-Young KWON et al. [41] have expressed the relation between abrasive silica particles and MRR as a decreasing function of size (as agglomerates size increases).

The polishing pad revolution velocity [cycles/min] is tested under applied loading 5.34 PSI using slurry with concentration ~3% of pH (10.2~10.7) where the temperature is maintained at [27.5~29 C] along 5 mins polishing as shown in Fig.18(a), the vertical represents the sizes of distribution peaks for the generated agglomerates.
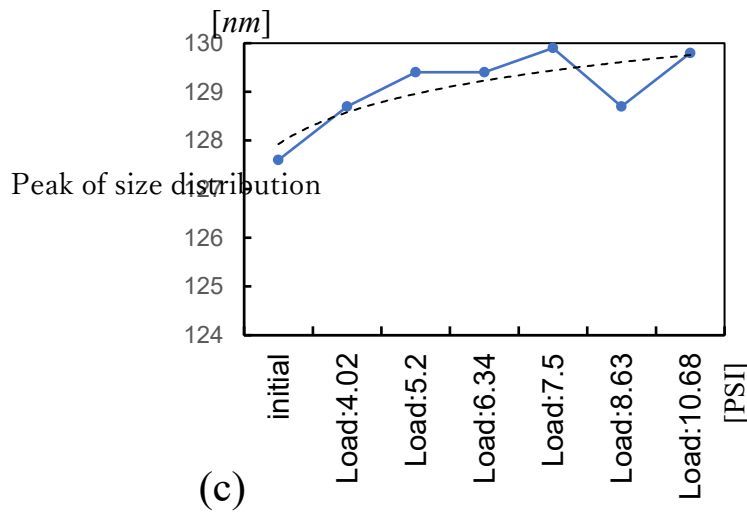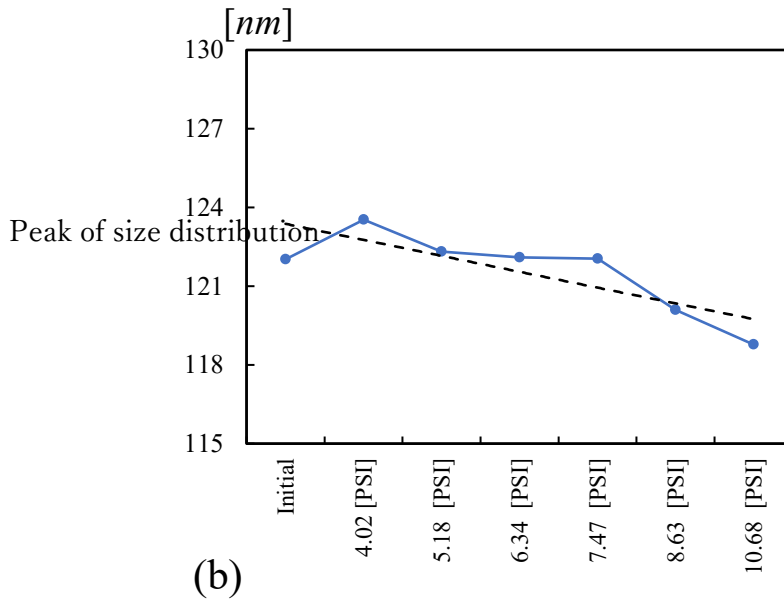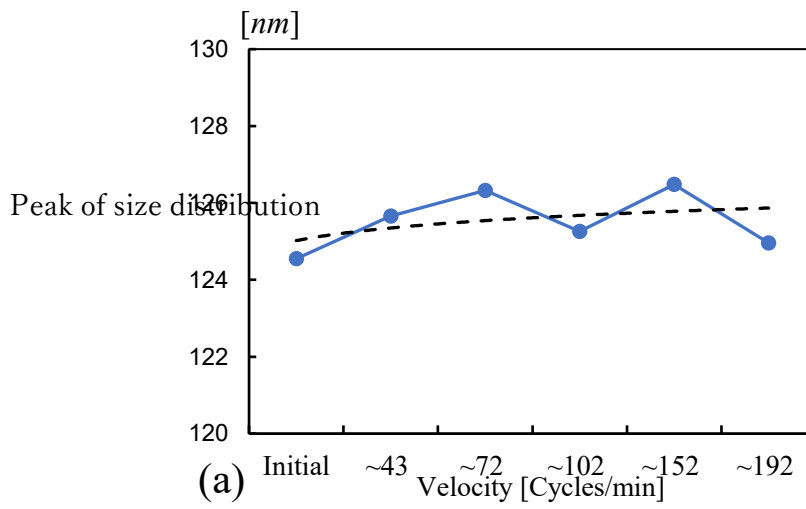
Fig. 18 Effect of (a) Sliding velocity and (b, c) Pressure on size distribution of agglomerates during CMP.

It is implied from approximations that as velocity increases, the agglomerates size increase. The reason is that the high sliding velocity leads to slurry with high shear rate. Therefore, increase degree of agglomeration as clarified by A. J. Khanna et al. [26]. On other hand the pressure (load) effect which appears at Fig.18(b) is studied subjected to almost same conditions (pH (10.4~10.6), temperature (27.3~29), velocity; ~72 cycles/min) where the behaviour is opposite to velocity, so it decays the agglomeration. To understand that, S. Ozbek et al. [37] interpreted the relation between pressure and particle in general as if the pressure increases more than certain level, the contact area starts to decrease, then the load per particle increases, which leads to decrease at MRR. However, MRR increases as pressure increases if only the contact area is increasing. Therefore, if slurry contains soft agglomerates, then the load increase breaks up the agglomerates (may be destroys them) and decrease the agglomeration, while if slurry contains hard agglomerates, considering other factors (such that softness of polishing pad material, low temperature, low velocity, relative low pH, …), the pressure increase enhances the agglomerates size. That back to that the cohesion forces of the agglomerate structure are larger than the load per particle. Based on that, we can conclude that the effect of pressure on agglomeration is two sided, so when the velocity become very low (~14 cycles/min) (Fig.18(c)) as a solid-solid contact model, and the temperature also decreased (24~25.7 C, pH [9.63~10.64]), the agglomeration is enforced by applying pressure, while for our moderate parameters (higher velocity and temperature), the agglomeration decays by applying more pressure units. It is worthy to mention that we found that pressure effect greatly enhances the agglomeration action when the alkaline medium was justified by NaOH, as also has been referred by AINA et al. [44].
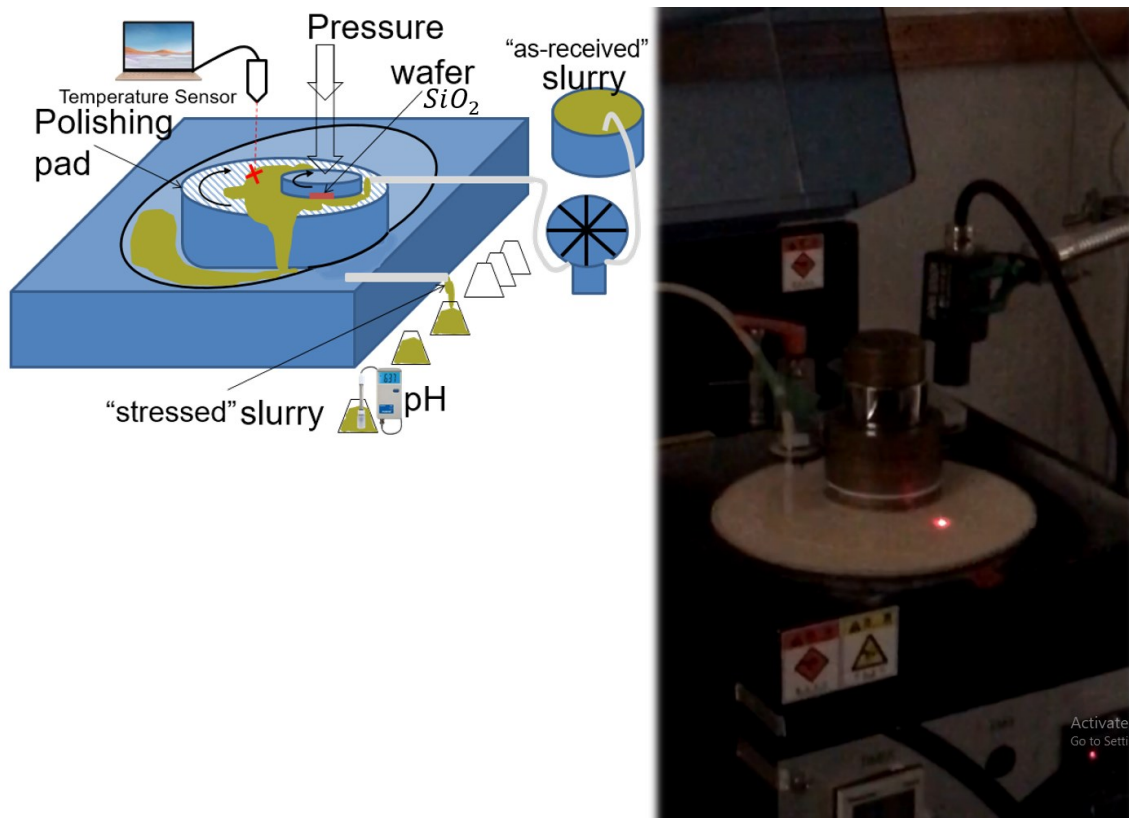
Fig. 19 Schematic figure (left) for the slurry transfer during CMP (right).

3.7 How far typical CMP characteristics clear up the agglomeration's behaviour

There are several size analysis techniques available for detecting the agglomerates in the CMP slurries. Among these, the number counting techniques are the most promising in detecting the agglomerates at the lowest concentrations. However, as the slurries are diluted for counting, some of the techniques may not be effective in detecting the soft agglomerates formed during slurry preparation. Therefore, a combination of sizing techniques that can analyze both the dilute and concentrated slurries must be used for effective detection of coarser size particulates.

Table 1. Optical methods for the estimation process

Method	Purpose	Characteristics
UV-visible spectrophotometer	understanding how the spectra depend on the agglomerate size	Structural differences within agglomerate sizes larger than dimers may change the absorbance spectra.
Absorbance	Works within the absence of diffusion or other dispersion	each agglomerate size will form a sharp sedimentation boundary that moves from the inside of the centrifugal cell to the outside
	absorbance spectrum of various agglomerate sizes could be calculated from the time derivative of the measured absorbance,	When measuring the absorbance spectra at a single position, the contributions to the measured absorbance from each agglomerate size will cease as its sedimentation boundary crosses that position
Bulk Absorbance	most accurate in the limit of small amounts of agglomeration, because the spectra change the most for the smallest agglomerates	It is a much simpler methodology since no need for separation techniques, Provide higher time resolution of modern UV-visible spectrophotometers than DLS or AUC instruments, It is a greater prevalence of UV-vis instruments than the other techniques
	achieve a very good estimate of the actual size distribution, especially for monomers, dimers, and trimers, for which the differences were less than 6%.	
	For slightly larger agglomerates, the calculated size distribution tends to significantly overestimate the size of agglomerates.	

Considering that a key difficulty for many of the frequently used techniques is that the entire distribution of particles within a sample is concurrently sampled, and thus any differences in properties within the particle distribution are convoluted into the reported values [57]. Moreover, careful sample preparation procedures are very serious when measuring agglomerates because additional agglomeration, or agglomerate rupture, can occur during drying. Thus, Table 1 for example depicts the importance of the electromagnetic waves that are incident on the nanoscale particles. such effect resolves the problem of capturing the tiny floating populations (nanoparticle agglomerates) in the spacious investigated domain. Nevertheless, the classification among broad scale of agglomerates sizes is still a puzzlement point needed for modifications. Conversely to Table 1 which is attributed to it is more reliable and its results are reproducible, the comparing faces at Table 2 depend on the physical features of agglomerates. Therefore, recording the outputs is required excessive sensitivity and high resolution, and for experiment situations as well.

Table 2. Sensitive instruments for particle tracking

TEM (Transmission Electron Microscope)	Analytical Ultracentrifugation (AUC)
visualize particle size distribution and agglomeration with particles in complex media,	allows dynamic monitoring of particle motion during spatial differentiation of particles according to their sedimentation coefficient,
can provide precise information on the shape and size of the primary nanoparticles	sedimentation coefficient increases with a particle's density and size.
	Peaks for monomers, dimers, and trimers are separated for small agglomerates
Particle Counting: by making use of the image resolution.	Larger agglomerates can be measured up to a few hundred nanometers in size.
Disadvantage: Agglomeration data could not be quantitative,	Disadvantage: Structural differences within agglomerate sizes larger than dimers may affect the sedimentation coefficients implying error measurements.

Table 3. Some monitors of dynamics of nanoparticle agglomeration
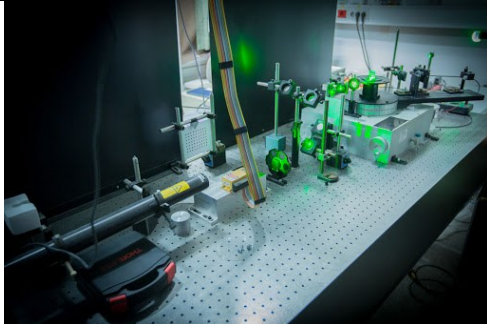
Accusizer	DLS (Dynamic Light Scattering)
It's Single-particle optical sensor (SPOS) system, and a direct method for measuring oversize particle distribution above 500 nm [29],	Identifies the particle size within the Brownian motion,
Accusizer has two-stage dilution system that allows the user to measure samples with any concentration,	Any particle is restricted at its hydrodynamic diameter*,
It is able to give the actual counts of the particles of different sizes accurately in a given volume of slurry sample and hence is a relative method for particle concentration,	Depends on the ionic concentration by changing the thickness of the electric double layer covered the surface of a floating particle,
It enables its photo-zone sensor to detect single particles in the 0.51–200 μm range,	Depends on the activities on the particle surface,
Various semiconductor companies consider it as a mandatory Certificate of Analysis (CoA) item as these can be quantified and easily co-related to the level of the defect.	The performance of a DLS instrument is normally verified by measurement of a suitable polystyrene latex standard.

*notes about DLS [50-54]: Hydrodynamic diameter: presents how a particle diffuses within a fluid, $\frac{kT}{3\pi\eta D}$; D: The velocity of the Brownian motion/the translational diffusion coefficient; η:fluid viscosity.

Brownian motion is realized by measuring the rate at which the intensity of the scattered light fluctuates. Size is obtained from the correlation function by using different algorithms such as; Cumulants analysis and Non-negative least square. It is inferred from Table 2 that the agglomeration data are instantaneous and gathered locally. So that, for the certain sample under investigation, more typical constraints are needed in addition to high technical accuracy. Otherwise, massive invariance will appear in the collected results. If the plot shows a substantial tail or more than one peak, then Mie's theory converts the intensity distribution to a volume distribution to give a more realistic view of the importance of the tail or second peak present.

The differences between the three distributions {Number, Volume, Intensity} are: If there are particles that have two different sizes with equivalent ratios at Number distribution, the ratio of the bigger size is 1000-times multiplied at volume distribution, and further, 10^6-times multiplied at Intensity distribution. The object beyond Table 3 is holding a comparison to supply clear identification about two measurement instruments that are share at some points although the mechanism of action for each of them differs. On the other hand, Table 4 represents a trial to understand how to make use of theoretical attributes of nanoparticles practically within the implemented tools as well as software. It is noticed that the results diversify greatly due to the software potentiality on contact between theoretical properties and practical application. Hence, the arriving from abstract view to functional technique needs an extensive study for the needed and available abilities.

Table 4. Comparison between particle sizing-machines

TEM (transmission electron microscope) [55]	PCS (photon correlation spectroscopy) [56]
characterizing sub-100 nm particles	
Slow in automating image analysis depending on the width of the size distribution	Rapid technique
Very accurate but time-consuming method to produce statistically significant PSDs,	Very sensitive to oversize particles

It was shown that when using a standard density of 2.2 g/cm^3 for the silica, the three methods (Table 5) although very consistent gave a significantly lower value than that found from image analysis by TEM (median volume diameter 50 nm cf 78 nm). When considering the porosity measured from nitrogen adsorption measurements and the thickness of the electrical double layer for the HCl dispersed silica, a hydrodynamic density of 1.52 g/cm^3 was computed and good correspondence between XDC and image analysis was found (77 and 78 nm respectively). For the broader distributions investigated (one boehmite and two gamma aluminas) the three instruments (Table 5) showed a divergence. Moreover, XDC gives a very good measure of the particle size distribution for inorganic powders in the sub-100 nm size range.

1 2 3

Table 5. Three methods for quantifying the agglomerations

Photo centrifuge (CAPA)	x-ray centrifuge (XDC)	PCS (photon correlation spectroscopy)
cover the 10–100 nm range		
Slowest	Slow	Fast
	Needs a sufficient x-ray absorption, and assumes spherical shape for the particles	The results are very reproducible
Good agreement at size range 25~50 nm		
Overestimates the fraction of the fine particles (Sub-30nm).	The XDC values are always intermediate and without the complications of the scattering phenomenon, because of its x-ray the detection system is probably the most reliable results.	overestimate the number of agglomerates (50~200 nm)
It is giving the finest values	The XDC had a better resolution in the <50 nm regime in particular	It's giving the highest values

The accuracy of the sizes measured by the XDC was shown to be highly dependent on having an accurate figure of the hydrodynamic density of the powder under investigation. (which was left at the theoretical density of 3.01 g/cm^3). Ultimately, Table 6 is capable to reveal the disparities points between the two methods that are largely identical at theoretical roots. That magnifies the critical effect produced from a small change at either physical/chemical input values of tested particles or instantaneous situations of the specified problem. It is revealed the power relation between the agglomeration rate and CCC (**critical coagulation concentration**). In addition, the standard software settings for stock solution analysis using nanoparticle tracking analysis (NTA) [47] were: camera

level 7, screen gain 10, detection threshold 15, and blur: auto.

Table 6. Comparisons between nanoparticle detectors.

Nanoparticle tracking analysis (NTA)	DLS (Dynamic Light Scattering)
The size distribution of the primary particle size varied in the range (50~150) nm,	The size distribution of the primary particle size varied in the range (50~250) nm,
The peak area is smaller	The peak area is larger
NTA tracks individual particles and yields their size distribution along with a real-time view of the nanoparticles being measured, independent of the particle density,	The DLS method is used to determine z-average hydrodynamic diameter and the size distribution of CeO_2 NPs in different salt solutions [47]
All NTA measurements were performed on the NanoSight 300 system and analyzed by NTA 3.2 software (Malvern Instruments Ltd., UK). The samples used for the NTA measurements were obtained by diluting each stock suspension (100 mg/L) to suitable multiples.	Traditional light-scattering techniques (such as DLS) measure the fluctuation in scattering intensity of NPs and then use this information to calculate the size of the particles through the Stokes-Einstein equation (Zetasizer Nano User Manual, Malvern Instruments, UK).

Table 6. (Continuous)

Nanoparticle tracking analysis (NTA)	DLS (Dynamic Light Scattering)		
The unknown modifications to the data probably eliminate large particles, which are considered to be experimental errors by the NTA software.	DLS is very sensitive to the presence of large particles, Nur et al. [48] reported that it was difficult to obtain a suspension of primary NPs even after sonication		
The most important finding in Figs. 19-21 was that NTA can measure samples with concentrations ranging (0.1~100) mg/L, which would satisfy the requirements of most studies on the life cycle and behavior of NPs.	According to study [47], some of the small aggregates were neglected by DLS in various solutions. Unfortunately, they may play a decisive role in toxicological experiments.		
the shear can affect the aggregation state during NTA measurements so the results indicated that NTA may not be suitable for measuring the aggregation kinetics. Further, at electrolyte concentrations above the CCC, the aggregation rate is completely dependent on the particle number	ionic strength (IS) [mM]		rate of aggregation
	KCl	CaCl$_2$	
	2.5	0.5 and 2	No aggregation
	5<	4<	increased with increasing cation concentration
	20<	6<	maximum
The size of the aggregated particles was far smaller than the value obtained in the aggregation kinetics experiment, due to collision efficiency consideration.	The size given by DLS was 304.4 ± 34.1 nm at a stock concentration of 0.1 mg/L, which is much larger than normal.		

Table 6. (Continuous)

Nanoparticle tracking analysis (NTA)	DLS (Dynamic Light Scattering)
The disadvantage of NTA is that it requires a higher sample concentration than DLS. Although the particle concentration of the stock solution did not exceed the detection range of the instrument (107–109 total particles / mL), the optimal result could not be obtained if the mass concentration was too high or too low.	The disadvantage: Considering that the samples were monodisperse stock suspensions, such a big error cannot be ignored. Thus, the scattering intensity can be directly related to the solution molecular mass of the sample [49]. Therefore, a large error was obtained probably because the light-scattering intensity was too low for accurate calculation when the NP concentration was too low.
NTA was unable to reflect the actual behavior of NPs in an aquatic environment because of the narrow range of measurements, which means high concentration samples always need to be diluted before each measurement	DLS can provide misleading results since the average particle size can easily be skewed by a few large particles in a mixture compared to many small particles. In addition to this, the technique is not material specific and therefore cannot differentiate between natural particles in solution or agglomerates of natural and engineered particles.
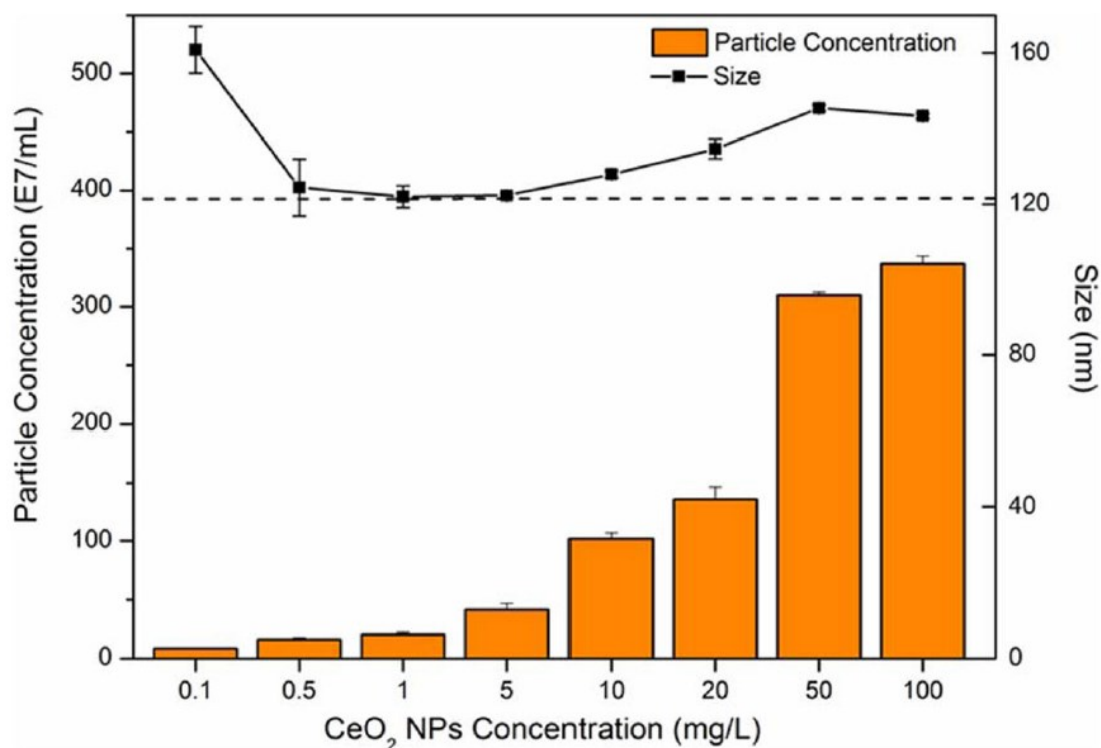
Fig. 19 Agglomeration Sizing and growth based on CeO_2 concentrations [47].

All measurements were performed in triplicate at 25 ± 0.3 °C. When ionic strength IS in the solution reaches the CCC (Table 6), which usually refers to the minimum electrolyte concentration that could completely eliminate the surface charge of particles, the aggregation rate tracked by DLS reaches maximum. The CCC values in this study were about 50 and 6 mM for KCl and $CaCl_2$. Nevertheless, when the mass concentration of CeO_2 NPs (measured by NTA) was lower than 1 mg/L, the size of CeO_2 NP was stable even when the KCl concentration was higher than the CCC.
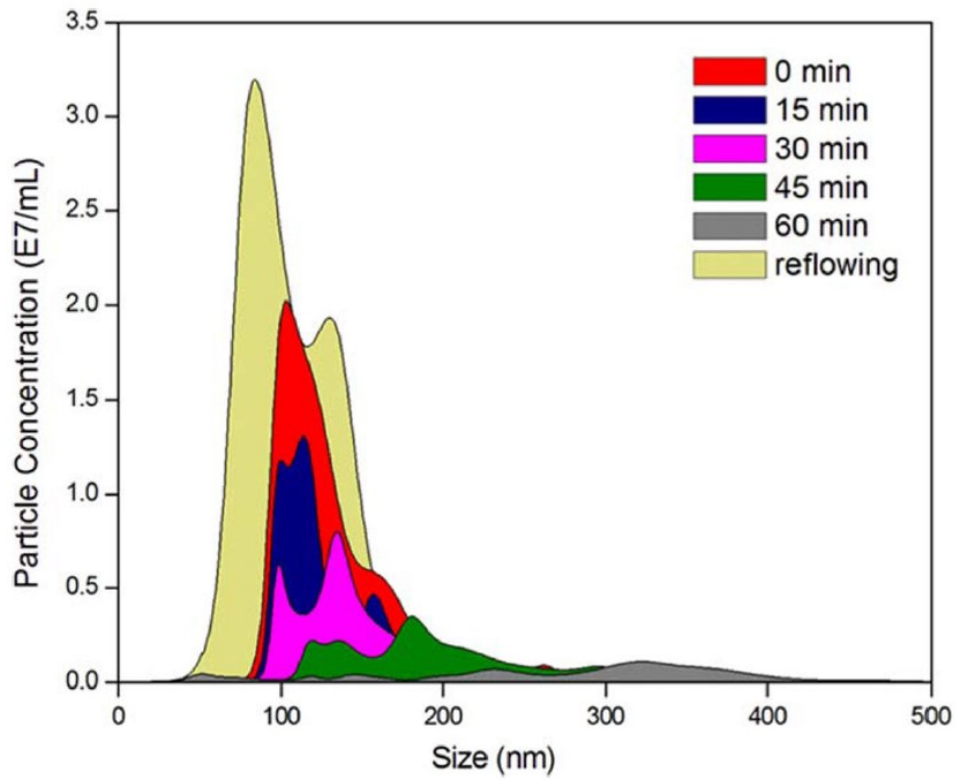
Fig. 20 Agglomerates population according to size discretization and reaction time [47].
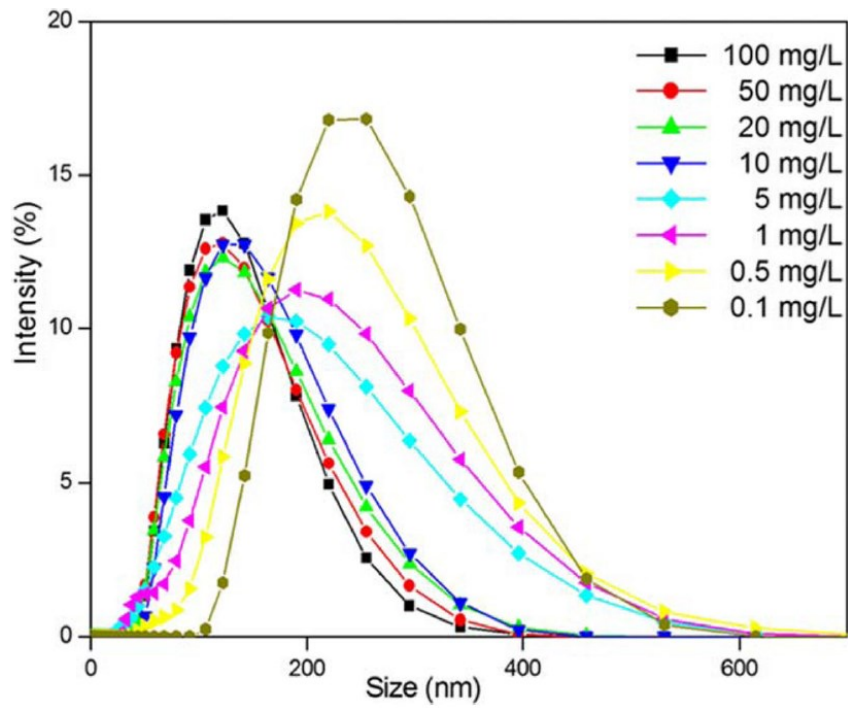
Fig. 21 Particle Size Distribution (PSD) for different con slurry concentrations [47].

1 2 9

Aggregation occurs invariably between particles in samples when the electrolyte concentration is above the CCC. This happens because when the sample concentration is extremely low and the particle concentration decreases during the aggregation process with time, the scattering intensity detected by DLS is too low for accurate calculations. This result indicates that there exists limited detection concentration in the measurement of aggregation kinetics by DLS. It is worthy to mention that the effect of measurement time shows that the particle concentration decreased significantly with the measuring time.

References

1. M. Elimelech, J. Gregory, X. Jia, R. A. Williams, "Particle Deposition and Aggregation Measurement, Modelling and Simulation", ISBN: 0-7506-7024-X, (1995) by Butterworth-Heinemann, http://www.bh.com.

2. M. Smoluchowski, "Versuch einer mathematischen Theorie der Koagnlationskinetik kolloider Lösungen", Z. Phys. Chem., 92, 129-168, 1917, https://doi.org/10.1515/zpch-1918-9209.

3. R. I. Zollars, S. I.Ali, "Shear coagulation in the presence of repulsive interparticle forces", J. Colloid Interface Sci., 114, 149-166, 1986.

4. L. J.Warren, Shear flocculation. Chemtech, 11(3), 180-185, 1981, CODEN: CHTEDD; ISSN: 0009-2703, http://pascal-francis.inist.fr/vibad/index.php?action=getRecordDetail&idt=PASCAL8130320558.

5. D. L. Swift, S. K.Friedlander, "The coagulation of hydrosols by Brownian motion and laminar shear flow", J. Colloid Sci., 19, 621-647, 1964.

6. K.Muhle, and K. Domasch, "Stability of particle aggregates in flocculation with polymers", Chem. Eng. Process., 29, 1-8, 1991.

7. N.Tambo, R. J. Francois,"Mixing, breakup and floc characteristics" In text book: "Mixing in Coagulation and Flocculation" (edited by Aminharajah, A., Clark, M. M. and Trussell, R. R.), , pp. 256-281, 1991, ISBN 0898675618 9780898675610, American Water Works Association Research Foundation, Denver CO.

8. Klaus Muhle, "Floc stability in laminar and turbulent flow" In text book: "Coagulation and Flocculation Theory and Applications" (edited by Bohuslav Dobias; University of Regesburg, Regensburg, Germany), pp. 355-390, 1993, ISBN 0-8247-8797-8, Marcel Dekker Inc., New York.

9. L. B. Brakalov, "A connection between the orthokinetic coagulation capture efficiency of aggregates and their maximum size", Chem. Eng. Sci., Vol. 42, pp. 2373-2383, 1987.

10. Sarit K. Das, Stephen U. S. Choi, Wenhua Yu, T. Pradeep, "Nanofluids: Science and Technology", John Wiley & Sons, Inc., Hoboken, New Jersey (2008), ISBN 978-0-470-07473-2, https://www.wiley.com/en-us/Nanofluids%3A+Science+and+Technology-p-9780470180686.

11. Aniruddh J. Khanna, Sushant Gupta, Purushottam Kumar, Feng-ChiChang, Rajiv K. Singh, "Quantification of shear induced agglomeration in chemical mechanical polishing slurries under different chemical environments", Microelectronic Engineering, Vol. 210, pp. 1–7, 2019.

12. J. A. Eastman, S. U. S. Choi, S. Li, W. Yu, and L. J. Thomson, "Anomalously increased effective thermal conductivities of ethylene glycol based nanofluids containing copper nanoparticles", Appl. Phys. Lett., Vol. 78, pp. 718–720, 2001.

13. Yeon-Ah Jeong, Maneesh Kumar Poddar, Heon-YulRyu, Nagendra Prasad Yerriboina, Tae-Gon Kim, Jaehyun Kim, Jong-Dai Park, Mingun Lee, Chang-Yong Park, Seongjun Han, Myeong-Jun Kim, Jin-Goo Park, "Investigation of particle agglomeration with in-situ generation of oxygen bubble during the tungsten chemical mechanical polishing (CMP) process", Microelectronic Engineering, vol. 218, 111133, pp. 1-6, 2019.

14. H. Hocheng, H. Y. Tsai, and Y. T. Su, "Modeling and Experimental Analysis of the Material Removal Rate in the Chemical Mechanical Planarization of Dielectric Films and Bare Silicon Wafers", Journal of Electrochemical Society, Vol. 148(10), G581-G586 (2001).

15. J. Xin, W. Cai, J.A. Tichy, "A fundamental model proposed for material removal in chemical–mechanical polishing", Wear, Vol.268, pp. 837-844, 2010.

16. B. V. Derjaguin and L. D. Landau, "Theory of the stability of strongly charged lyophobic sols and of the adhesion of strongly charged particles in solution of electrolytes", Acta Physicochim. URSS, Vol. 14, pp. 633-662, 1941.

17. Qi GAO, Yasuhiro TANI, Gang DONG, "Polishing characteristics of micron particles aggregated by nanosilica", Journal of Advanced Mechanical Design, Systems, and Manufacturing, Vol.9, No.3 (2015), Paper No.14-00461, DOI: 10.1299/jamdsm.2015jamdsm0027, https://doi.org/10.1299/jamdsm.2015jamdsm0027.

18. Q. Que, J. Zhang, Z. Zhang, Synthesis, "structure and lubricating properties of dialkyldithiophosphate-modified Mo– S compound nanoclusters", Wear, Vol. 209(1– 2) pp. 8–12, 1997.

19. J. F. Li, H. Liao, X. Y. Wang, B. Normand, V. Ji, C. X. Ding, C. Coddet, "Improvement in wear resistance of plasma sprayed yttria stabilized zirconia coating using nanostructured powder", Tribol. Int., Vol. 37, pp. 77–84, 2004.

20. Nathan C. Crawford, "Shear thickening and defect formation of fumed silica CMP slurries", Colloids and Surfaces A: Physicochem. Eng. Aspects, Vol. 436, pp. 87– 96, 2013.

21. G.B. Basim, B.M. Moudgil, "Effect of Soft Agglomerates on CMP Slurry Performance", J. Colloid Interface Sci., Vol. 256, pp. 137-142, 2002.

22. J. Gregory, "Flocculation of Fine Particles" In NATO ASI Series (Series E: Applied Sciences): "Innovations in Flotation Technology" (edited by Mavros P., Matis K.A.), vol 208, 1992. Springer, Dordrecht. https://doi.org/10.1007/978-94-011-2658-8_4.

23. K. Ganesh Kumar, M. Gnaneswara Reddy, M. V. V. N. L. Sudharani, S. A. Shehzad, Ali J. Chamkha, "Cattaneo-Christov heat diffusion phenomenon in Reiner-Philippoff fluid through a transverse magnetic field", Physica A, Vol. 541, 123330, 2020.

24. Yongguang Wang, Yao Chen, Fei Qi, Zhanwen Xing, Weiwei Liu, "A molecular-scale analytic model to evaluate material removal rate in chemical mechanical planarization considering the abrasive shape", Microelectronic Engineering, Vol. 134, pp. 54–59, 2015.

25. Yeau-Ren Jeng, Pay-Yau Huang, "A Material Removal Rate Model Considering Interfacial Micro-Contact Wear Behavior for Chemical Mechanical Polishing", Journal of Tribology, Vol. 127(1), pp. 190-197, JANUARY 2005.

26. Sant Tsai, Rashid Mavliev, Liang-Yuh Chen, "United States Patent", US 6,869,498 B1, Mar. 22, 2005, Applied Materials Inc., Santa Clara, CA (US).

27. Boumyoung Park, Sukhoon Jeong, Hyunseop Lee, Hyoungjae Kim, Haedo Jeong, and David A. Dornfeld, "Experimental Investigation of Material Removal Characteristics in Silicon Chemical Mechanical Polishing", Japanese Journal of Applied Physics, Vol. 48, 116505, pp.1-9, 2009.

28. H.S. Lee, H.D. Jeong, D.A. Dornfeld, "Semi-empirical material removal rate distribution model for SiO2 chemical mechanical polishing (CMP) processes", Precision Engineering, Vol.37, pp. 483– 490, 2013.

29. C. Dai, X. Wang, Y. Li, W. Lv, C. Zou, M. Gao, M. Zhao, "Spontaneous imbibition investigation of self-dispersing silica nanofluids for enhanced oil recovery in low-permeability cores", Energy & Fuels, Vol. 31, pp. 2663–2668, (2017).

30. H. Akoh, Y. Tsukasaki, S. Yatsuya, A. Tasaki, "Magnetic properties of ferromagnetic ultrafine particles prepared by a vacuum evaporation on running oil substrate", J. Cryst. Growth, Vol. 45, pp. 495–500, (1978).

31. M. Wagener, B. S. Murty, B. G¨unther, "Preparation of metal nanosuspensions by high-pressure dc-sputtering on running liquids", in Nanocrystalline and Nanocomposite Materials II , (edited by S. Komarnenl, J. C. Parker, and H. J. Wollenberger), Vol. 457, pp. 149–154, 1997, Materials Research Society, Pittsburgh, PA.

32. J. A. Eastman, S. U. S. Choi, S. Li, L. J. Thompson, S. Lee, "Enhanced thermal conductivity through the development of nanofluids", Proc. Symposium Nanophase and Nanocomposite Materials II, Vol. 457, pp. 3–11, 1997, Materials Research Society, Boston, MA.

33. H. Zhu, Y. Lin, Y. Yin, "A novel one-step chemical method for preparation of copper nanofluids", J. Colloid Interface Sci., Vol. 277, pp. 100–103, (2004).

34. Caterina Minelli, Dorota Bartczak, Ruud Peters, Jenny Rissler, Anna Undas, Aneta Sikora, Eva Sjöström, Heidi Goenaga-Infante, and Alexander G. Shard, "Sticky Measurement Problem: Number Concentration of Agglomerated Nanoparticles", Langmuir, Vol. 35, pp. 4927−4935, 2019.

35. Feng-Chi Chang, "Externally induced agglomeration during chemical mechanical polishing of metals and dielectrics", Materials Science & Engineering, Ph.D Thesis, pp. 1-123, 2008, ISBN 978-1-109-32147-0, University of Florida, Gainesville, Florida, US.

36. Neil Brahma, Jan B. Talbot, "Effects of chemical mechanical planarization slurry additives on the agglomeration of alumina nanoparticles II: Aggregation rate analysis", Journal of colloidal and interface Science, Vol. 419, pp. 25-30, 2014.

37. S. Ozbek, W. Akbar, G. B. Basim, "Optimized Process and Tool Design for GaN Chemical Mechanical Planarization", ECS Journal of Solid State Science and Technology, Vol.6 (11), pp. S3084-S3092, (2017).

38. Aniruddh J. Khanna, Sushant Gupta, Purushottam Kumar, Feng-Chi Chang, Rajiv K. Singh, "Study of Agglomeration Behavior of Chemical Mechanical Polishing Slurry under Controlled Shear Environments", ECS Journal of Solid State Science and Technology, Vol. 7(5), pp. p238-p244, (2018).

39. Lele Ren, Feihu Zhang, Shijie Zhao, Defeng Liao, Ruiqing Xie, Jian Wang, Qiao Xu, "Correlation between polishing pad's properties and material removal during full-aperture polishing", International Journal of Applied Glass Science, Vol. 10, pp. 287–301, 2019.

40. Markus Forsberg, "Effect of process parameters on material removal rate in chemical mechanical polishing of Si (1 0 0)", Microelectronic Engineering, Vol. 77, pp. 319–326, 2005.

41. Tae-Young KWON, Manivannan RAMACHANDRAN, Jin-Goo PARK, "Scratch formation and its mechanism in chemical mechanical planarization (CMP)", Friction, Vol. 1(4), pp. 279–305, (2013), DOI 10.1007/s40544-013-0026-y.

42. Malvern Panalytical Ltd. Grovewood Road, Malvern, Worcestershire, WR14 1XZ, UnitedKingdom, ISO:22412DLS second edition, JISZ：88282019.

43. M.A.Y.A. Bakier, Keisuke Suzuki, Panart Khajornrungruang, "Study on relationship between nano particle agglomeration action and polishing characteristics in CMP", Extended Abstracts of the 2020 International Conference on Solid State Devices and Materials, pp. 139–140, 2020.

44. Mohamad Zuki NOOR AINA, Jing Yao SIN, Amane JADA, Arezoo Fereidonian DASHTI, Mohd Omar FATEHAH, "AGGLOMERATION OF SILICON DIOXIDE

NANOSCALE COLLOIDS IN CHEMICAL MECHANICAL POLISHING WASTEWATER: INFLUENCE OF pH AND COAGULANT CONCENTRATION", CIVIL AND ENVIRONMENTAL ENGINEERING REPORTS, Vol. 3(29), pp. 252-271, 2019, DOI: 10.2478/ceer-2019-0040, E-ISSN 2450-8594.

45. G. Bahar Basim, Brij M. Moudgil, "Slurry Design for Chemical Mechanical Polishing", KONA Powder and Particle Journal, Vol.21, pp. 178-184, 2003.

46. Aniruddh J. Khanna, Feng-Chi Chang, Sushant Gupta, Purushottam Kumar, and Rajiv K. Singh, "Characterization of the nature of shear-induced agglomerates as hard and soft in chemical mechanical polishing slurries", Journal of Vacuum Science & Technology B Vol. 37, 011207, (2019); doi: 10.1116/1.5065516.

47. Chao Wang, Bowen Lv, Jun Hou, Peifang Wang, Lingzhan Miao, Hanlin Ci, "Quantitative measurement of aggregation kinetics process of nanoparticles using nanoparticle tracking analysis and dynamic light scattering", J. Nanopart Res., Vol.21, article no. 87, pp. 1-15, 2019, https://doi.org/10.1007/s11051-019-4527-0.

48. Y.Nur, J.R. Lead, M. Baalousha, "Evaluation of charge and agglomeration behavior of TiO_2 nanoparticles in ecotoxicological media", Sci Total Environ, Vol. 535, pp.45–53, 2015.

49. John S. Philo, "A critical review of methods for size characterization of non-particulate protein aggregates". Curr Pharm Biotechnol 10 (4), pp. 359-372, 2009.

50. International Standard ISO13321 Methods for Determination of Particle Size Distribution Part 8: Photon Correlation Spectroscopy, International Organisation for Standardisation (ISO) 1996.

51. W. T. Winter, "Measurement of suspended particles by quasi-elastic light scattering", Journal of Polymer Science: Polymer Letters Edition, (Barton E. Dahneke, Ed.), Vol. 21 issue 12, pp. 570, 1983, Wiley, New York, https://doi.org/10.1002/pol.1983.130211210.

52. R. Pecora, Book: Dynamic Light Scattering: "Applications of Photon Correlation Spectroscopy", DOI: 10.1007/978-1-4613-2389-1, eBook ISBN 978-1-4613-2389-1, 1985, Plenum Press, New York.

53. Clive Washington, "Particle Size Analysis" In Pharmaceutics And Other Industries: Theory And Practice, 1992, ISBN 0-203-98417-X, West Sussex, Ellis Horwood LIMITED, England.

54. C.S. Jr. Johnson, D.A. Gabriel, "Laser Light Scattering", Dover Publications; Corrected edition (January 9, 1995), ISBN-10: 9780486683287, ISBN-13: 978-0486683287.

55. https://uwaterloo.ca/metrology/tem-stem.

56. http://www-f7.ijs.si/facilities/photon-correlation-spectroscopy-pcs-dls/

57. J. M. Zook, V. Rastogi, R. I. MacCuspie, A. M. Keene, J. Fagan, "Measuring Agglomerate Size Distribution and Dependence of Localized Surface Plasmon Resonance Absorbance on Gold Nanoparticle Agglomerate Size Using Analytical Ultracentrifugation", ACS Nano, VOL. 5, NO. 10, pp. 8070–8079, 2011.

Chapter 4:
Removal Mechanisms
at Pattern Trapping
Model

Chapter 4: Removal Mechanism at Pattern Trapping Model

4.1 Challenges of CMP simulations

4.1.1 Indications of computational approaches

Planarization in semiconductor device fabrication is, from the perspective of materials physics and chemistry [1], an almost perfect example of a chemo-mechanical process. Such processes depend critically upon the interplay of chemistry and mechanical stress. Atomistic simulations of chemo-mechanical processes with real predictive power are not yet available. An obvious barrier is computational cost. Underlying those costs is the inherently multi-scale nature of the problem. The challenges of straight-forward multi-scale simulation, while large, are reasonably well-understood, with major progress made already. The current big step is inclusion of chemical reactivity.

From the advantage point of computational materials scientists, chemo-mechanical processes are an intellectual gold mine of fascinating problems. But the challenges are many and immense, hence the perceptible intellectual horror expressed by such workers upon encountering these problems: quantum mechanics and classical mechanics both are important in the same problem. Ordinarily we can keep to the one or the other but not here. Another challenge is that chemical reactivity must be treated with both fluid and solid dynamics included. In contrast, most computational progress on reactions has been via calculations that correspond to the dilute gas phase. Another challenge is breaking of bonds, a characteristic that suggests strongly that models using clever potentials may not be adequate.

The objective is assumed to be an inclusive simulation. It would address the following problem: Given a comprehensive description of a specific chemo-mechanical process,

provide reliable computed predictions of the key outcomes of that process before it is tried in the laboratory. We assume that the comprehensive description would provide such information as the size ranges, composition, and state of the solid elements, the chemical and hydrodynamical nature of fluids in the interface, and the range of speed of motions and their duration. Even the ability to distinguish which processes have high or low prospects for meeting a specified set of needs would be a success. We assume therefore that the simulations must be predictive. Obviously, it is valuable to parameterize data in models that can be used as design tools but that is not our focus.

Since it must start at atoms and end up with predictions about material samples of ponderable size (e.g. a wafer), the inclusive simulation clearly is involved with the issue of length scales from the start. The issue becomes particularly evident upon considering the methods that must be ingredients in the inclusive scheme. Multiple time scales are not quite as obvious, but they are there.

4.1.2 Model description using finite element implementations

Start at the sample level, planarization or polishing for example. At these length scales atoms are invisible as such and continuum mechanics treatments are the tool of choice. Key system and material parameters - density, viscosity, bulk modulus, etc., develop as a function of time according to differential equations for mass motion, fluid flow, concentration and so forth, subject to appropriate boundary conditions. The time scales involved may range from milliseconds to minutes or longer. The way this domain is treated varies but the underlying "finite element" scheme is common to all approaches. Focus on the kinetic and elastic energy densities for the continuum. Both are functions of the displacement field and therefore for all times r, the system energy is calculable as an

1 3 9

integral over the continuum volume. The integral is handled numerically by introducing a mesh of points, called nodes, throughout the volume. Assume that the displacements u, and velocities $\dot{u}$, are known at all the nodes i. The nodes define irregular tetrahedra that fill the system volume (to whatever accuracy is desired or affordable). Within each tetrahedron, the required energy integrals can be approximated by introducing a scheme to interpolate from the values of variables on the nodes to all of the interior of the tetrahedron. The result is a discretized expression for the energy of the whole object

$$E = \frac{1}{2}\sum_{i=1}^{N_{cells}}\sum_{\mu v}\{u_{\mu,i}K_{\mu v}^i + \dot{u}_{\mu,i}M_{\mu v}^i\dot{u}_{v,i}\} \quad (1)$$

The matrices K and M are the "local stiffness" and "local mass" matrices that characterize the particular cell as a result of the tetrahedral integration.

From a computational point of view this discretization is much more than conversion of an integral into a numerically manageable finite sum because it introduces a particulate character to the continuum problem. Once we have these macroscopic pseudo-particles (for lack of a better term), the energy expression can be treated as a Hamiltonian for those pseudo-particles and it follows that we can derive dynamical equations for them. That opens the opportunity for coupling the dynamics of the pseudo-particles to the dynamics of atomic-scale particles. We defer discussing how such coupling is done.

Almost nothing is known about chemically realistic calculation of solvent effects that include solvent dynamics, that is, fluid flow. Molecular Dynamic simulations of fluid motion and continuum treatments by computational fluid dynamics (CFD) today are specialties rather different from the simulation and modeling sketched above. Another area of simulation that today is a separate specialty and in which relatively little has been done is atomic-level calculations of bare (i.e. no solvent or reactivity contributions)

frictional effects. So far as we are aware, there is no work at the electronic structure level on this problem; it is not even obvious how to formulate the problem.

4.2 Copper interconnections for IC manufacturing

Another important application of CMP in recent years is in the copper damascene process (Fig. 1 [2]). The semiconductor roadmap [3] predicts that the interconnect delay will dominate the circuit performance in the sub-micron era, Fig. 2. Replacing the Al alloys (Al-Cu alloys), which have been used for over thirty years as the interconnect metal with copper has already been attempted to reduce the interconnect delay because of the copper's lower resistance. Fig. 3 shows a multilevel IC chip fabricated by IBM using the copper as the interconnect material.

However, the copper is difficult to be patterned using the conventional dry and wet etching methods. Instead, a method called the **damascene process** has been used.

During the copper damascene process, the copper is deposited over a dielectric layer

with trenches and vias patterned using conventional etching methods. The coppers deposited in the dielectric trenches and via are the interconnection lines. Overburden copper left over the dielectric surface has to be removed to isolate the lines in different trenches. CMP is currently the only method that is able to remove the overburden copper with good global planarity. Fig. (1) shows schematically the process steps of a dual copper damascene process. Besides copper, CMP is also used in the planarization of aluminum interconnects and tungsten vias under a similar inverse metallization scheme. In addition, a barrier layer such as Ti and TiN is usually used as an <u>interfacial layer between metal</u>

interconnects and dielectrics to avoid the metal diffusion. The CMP of them also needs
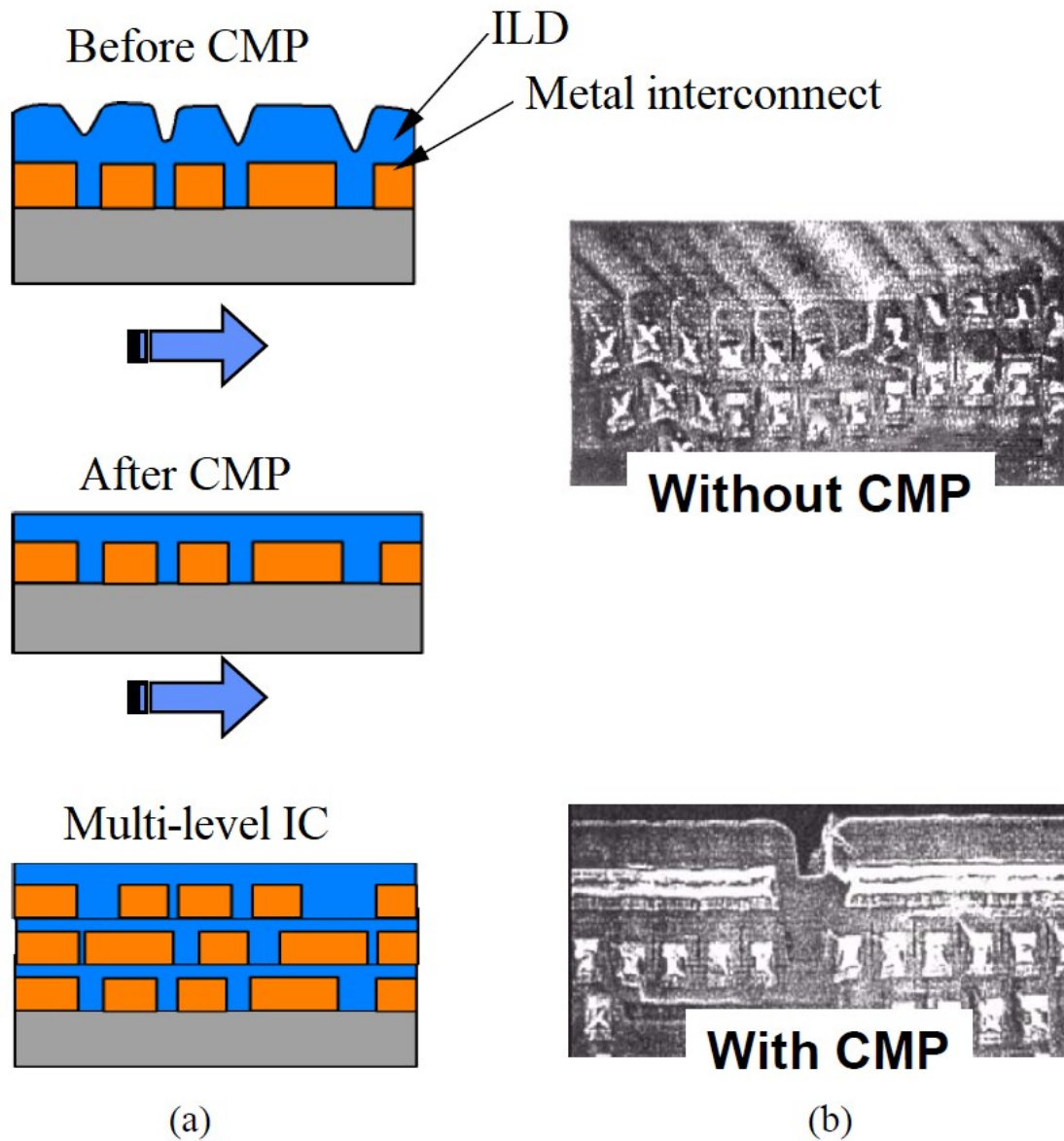
investigation.

Fig. 1. (a) Process flow of CMP of ILD and (b) Comparison of ILD surface with CMP and without CMP
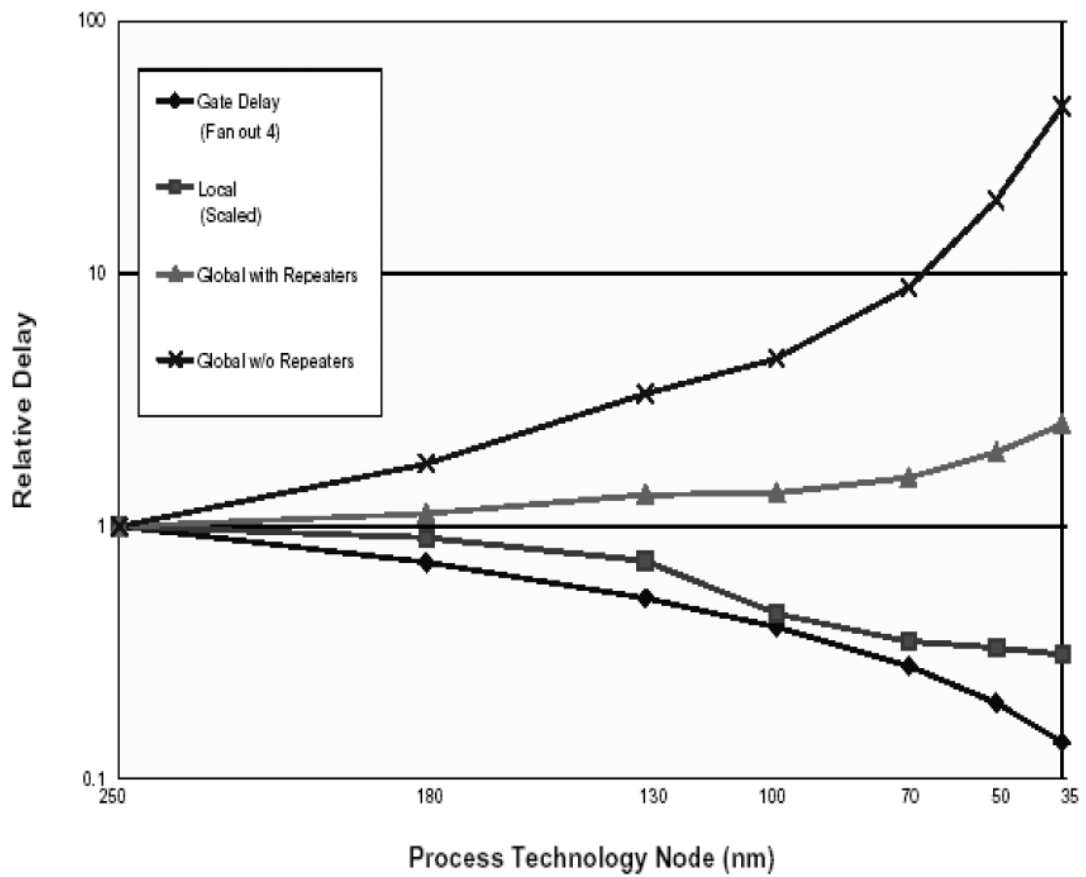
Fig. 2 The relative IC delay for different process technology nodes [3].
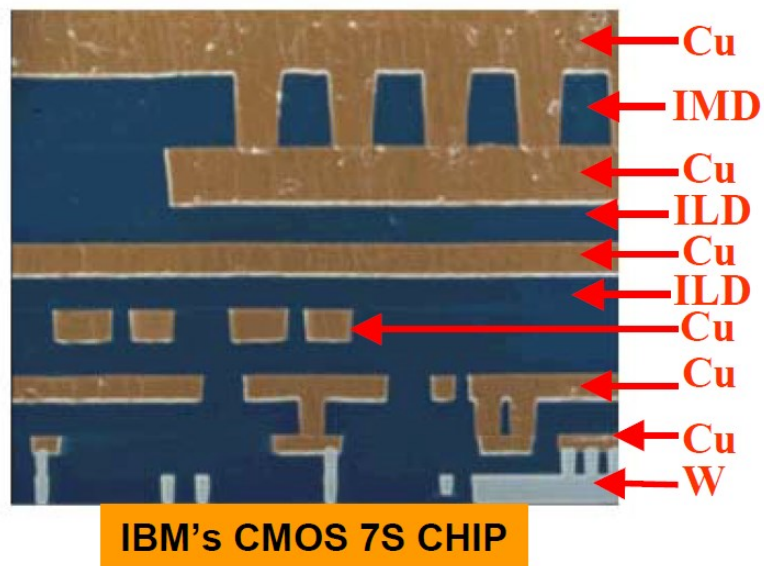

Fig. 3 A multi-level chip using copper as interconnects by IBM

Both of the ILD planarization and copper damascene process belong to the back-end of the processes, which deal with the interconnection between different modulus. Another important application of CMP, called shallow trench isolation is applied in the front-end processes of IC fabrication. The isolation is needed between adjacent devices to prevent the establishment of parasitic channels. Conventionally, LOCOS (local oxidation of silicon) is used which involves the formation of a semirecessed oxide in the non-active (or field) areas of the substrate [4]. Due to the bird's beak encroachment problem, LOCOS has been replaced by the shallow trench isolation with the CMOS technology scaled down to the sub-micron generation. Similar as the copper damascene process, the shallow trench isolation is a damascene process as well. Silicon oxides are deposited into the shallow trenches etched on the field area of the silicon substrate and CMP is then used to remove the overburden oxide.

There are a number of output variables with CMP. They include the material removal rate (*MRR*), the with-in die non-uniformity (WIDNU) of material removal rate, the with-in wafer non-uniformity (WIWNU) of material removal rate, scratching, surface roughness and dishing & erosion in damascene process. Although CMP has obtained broad applications in the IC fabrication, mature modeling efforts are needed that can help systematic optimization and development of the process. Based on the outputs of interest, there are issues at three scales of CMP to be modeled, namely, the particle scale, die scale and wafer scale.

barrier layer

Copper

Si/SiO_2

Si/SiO_2

Copper

Barrier layer

Si/SiO_2
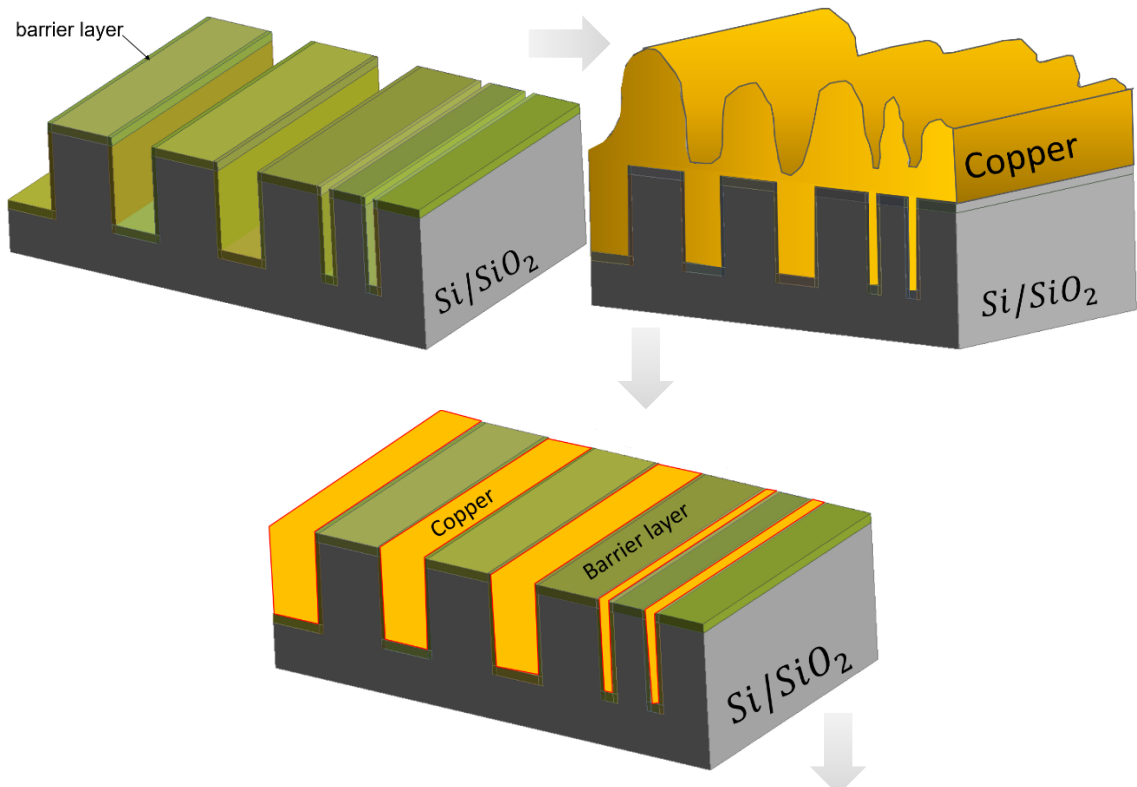
Interconnections at "IC"
Integrated Circuits
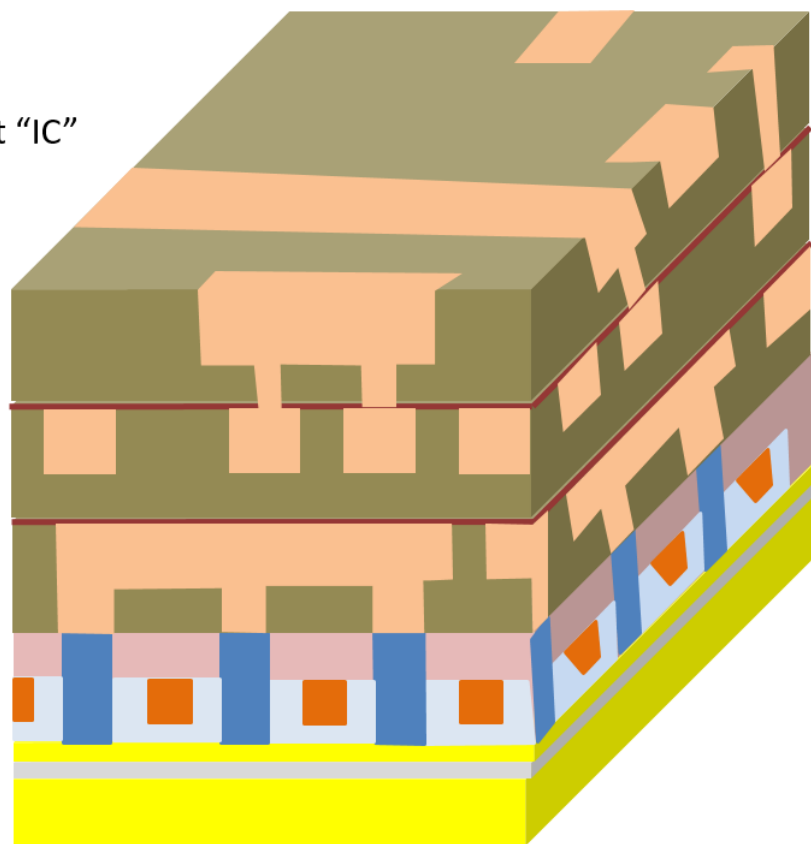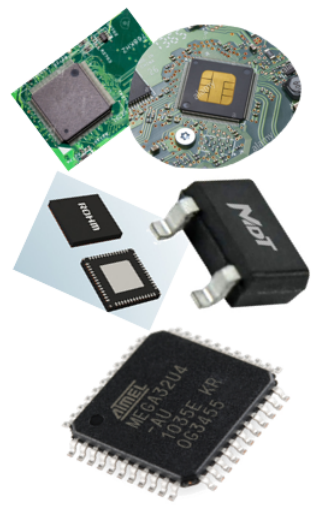
Fig. 4 Fabrication steps in dual damascene process

1 4 5

4.3 Cu-CMP model setting

It is not easy to etch the copper material, especially that the damascene process starts by trenches at the silicon wafer (which is considered as a mould), then a barrier layer (Ti/TiN) is deposited because the copper diffuses at Si bulk body (Fig. 4). Hence, we have to discuss the core of our study which is the polishing and treatment the overburden copper to achieve planar chip surface composes of different regions of copper, Ti barrier material, and Si/SiO_2. Whenever the Cu-CMP has been successfully achieved, multilayers could be created by repetition process. Then the integrated circuits (ICs) become qualified for different microelectronic devices chips (Fig. 4)
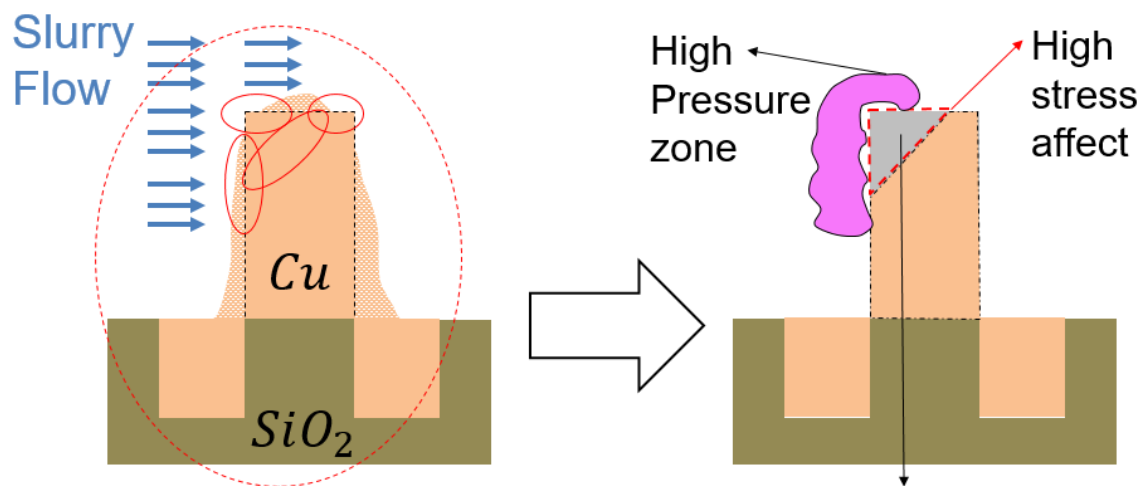
Fig. 5 schematic of removal status at CMP mechanism

Fig. 6 Progress of material decreasing as Slurry flow field continue during CMP.

The main point of our interest (step of CMP) is the typical identification for the material removal status. All implementations are depending on the reality description of the removal mechanism and the proposed assumptions. Specially we focus on the effect of

slurry flow on the protrusive copper body where the flow field carries the important physical effects such as velocity and pressure. An interaction must be occurred between slurry flow and the copper body which aligned with fluid solid interaction phenomenon. Hence, we seek the weakest part at the solid body which is affected greatly by slurry. It can be proposed that the weakest part at solid body suffers from the highest stress a response to the high pressure comes from slurry flow over the solid copper body. Therefore, by investigating the pressure contours of slurry flow at the domain under consideration as well as the stresses contours at the copper body, we can expect the most fragile parts at the solid body. When the brittle pieces at the copper body are determined, the removal process could be performed on mass property (Fig. 5). representing the previous approach consequently, regarding the up to date changes at the solid geometry due to mass decrease, we can predict the final stage where the optimum planarity criterion is satisfied (Fig. 6).
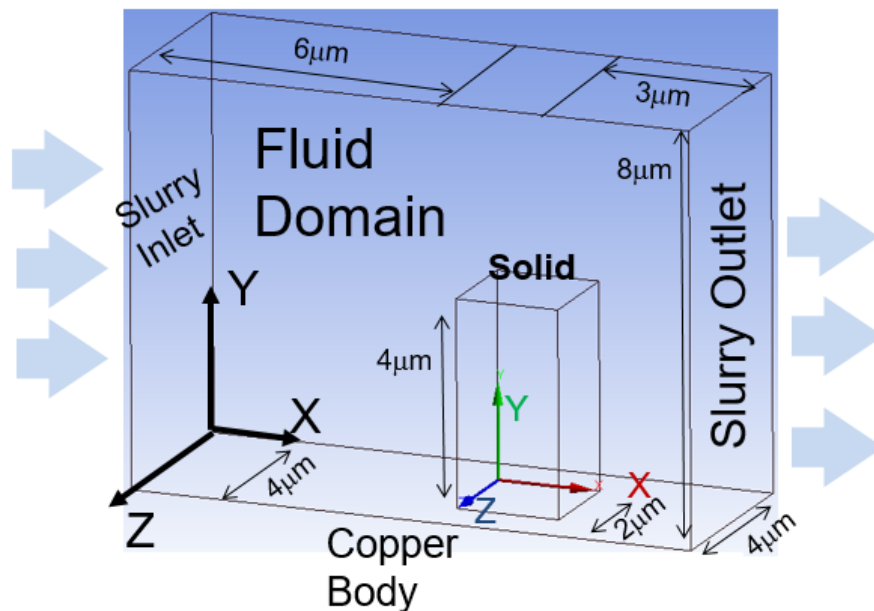
Fig. 7 Geometrical description of the problem under consideration.

For <u>flow direction</u>; basically, slurry is constrained under rotation motion. By deep insight to material mechanism strength points, we can notice that it's effect at the micro level, in addition, the circular motion at macro scale is represented by transfer motion at micro scale. For <u>problem geometry</u>; since the slurry flow is assumed to be at one direction only (here is assumed to be x-direction), it is worthy to mention that these constrains are only outside and around the boundary of the domain under consideration. While inside the domain, the velocity (its value and direction) is unknown and subjected to the solution of the governing equations which represent the physical model. The fluid domain under study (Fig. 7) is considered as $4 \times 8 \times 11 \ [\mu m^3]$ which represent the slurry motion space surrounding the copper protrusive body ($2 \times 2 \times 4 \ [\mu m^3]$).
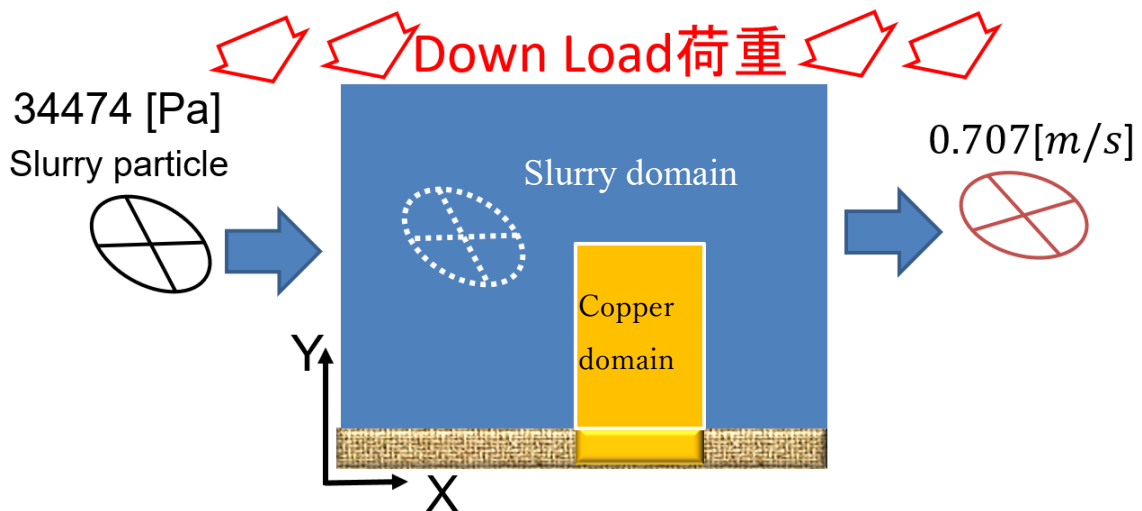
Fig. 8 Fluid boundary conditions of the problem under consideration.

The slurry height is assumed to be double of solid height to guarantee the stability of the slurry flow at the mainstream (streamlines far from the obstacle copper body and the bottom side). Moreover, this is important to exclude the mutual effect between the top boundary conditions and the fluid-solid interaction. Besides, the distance from the inlet to the copper body is larger than the distance beyond the copper body due to two important reasons. The first, is the entering fluid particles gain an auxiliary velocity to be capable

of performing the collision with the solid body. The second is the numerical instabilities, where it is known that during the ANSYS(Fluent) software treatment for the problem under proposed conditions, many numerical instabilities are generated during the execution process when the obstacle is located near to the inlet.

For the domain of study, it is required when we simulate the physical model of the problem, to take care of the mesh setting. The geometry of the physical model is converted to a mesh; therefore, it can be handled by the software. Software is the work environment of the mathematical model which much depends on the justification of the boundary conditions of the problem geometry and the harmonization of the governing equations which represent the physical model mathematically. When the numerical solution is achieved on the mathematical model, the values of unknowns (variables) such as pressure, position coordinates, velocities, density, temperature, … could be identified at each node at the mesh. More than 20000 nodes and 100000 tetrahedron elements are included in mesh under study.
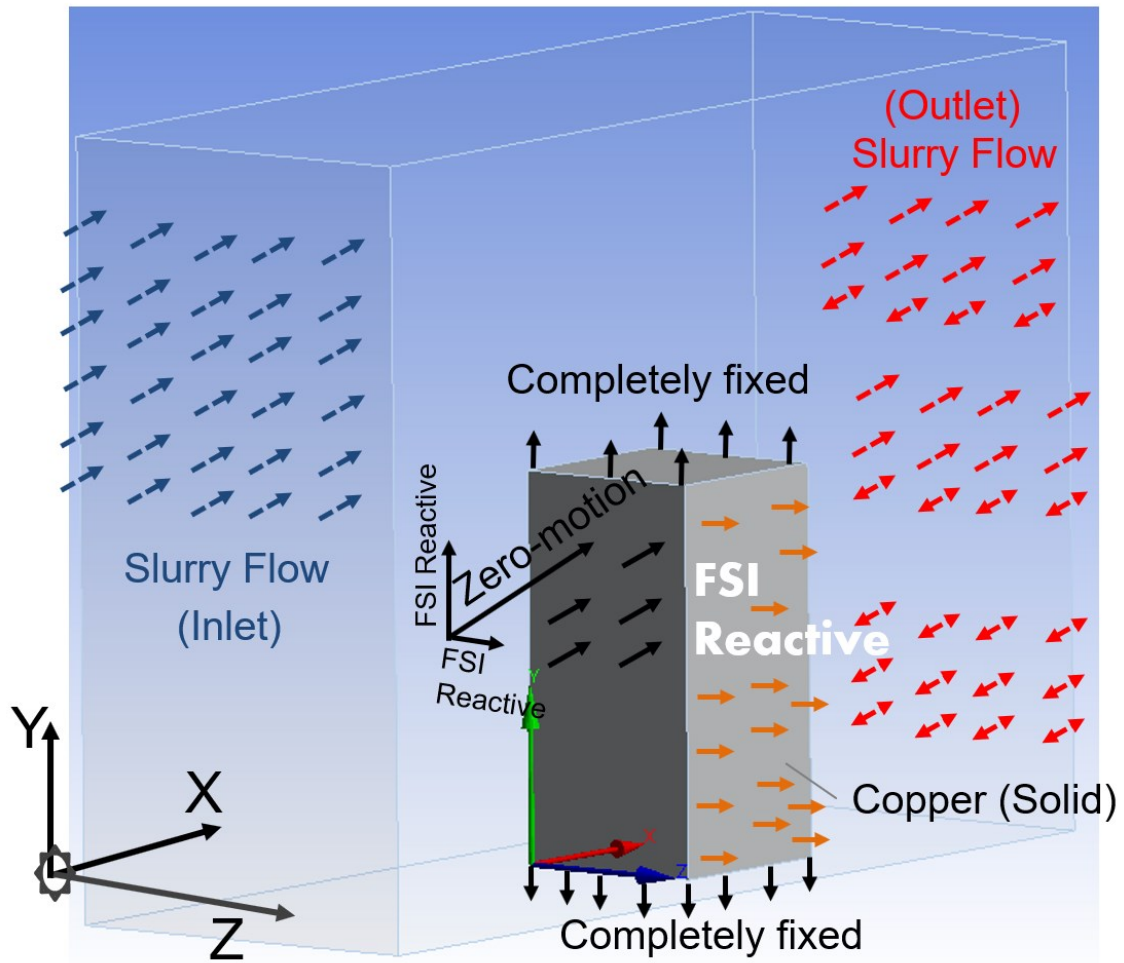
Fig. 9 Fluid-Solid Interaction and the boundary/interface condition implementation.

The coupled method for pressure-velocity coupling scheme is implemented and the second order approximation on spatial discretization is considered for pressure, momentum, …etc. The time step size is assumed 0.00015 (s) along 3000 steps. Actually, the model arrives the steady case after ~189 steps when the maximum corrections per time step is 5.

Fluid Boundary Conditions (Fig. 8):

It is very important to distinguish between the state of fluid-particle before entering the

domain of study and after it goes out. Hence, we need to apply conditions that coincide with each other and satisfy the real action at the same time. When the fluid particle moves from the free space to the domain under study, it is subjected to download comes from the top side (polishing pad here) which pull the particle to move inside the domain. Recall that the pressure is distributed at the domain under the assumption of Pascal rule which assumes that when an external pressure is applied on some part of a surface including the fluid inside, the pressure value is transferred completely to all parts of fluid and to all walls (surfaces) adjacent to the fluid. Far from complexity, the changes of fluid variables are imposed to be at x and y directions, and keep z-direction (the width) to be an univariant (changes are so small so that it could be neglected relatively).

After the fluid particles enter the domain, they are exerted under the treatment of the governing equations that control the dynamics inside the domain. A great push force is required to expel the fluid particle from the inside domain to the outside. Such this force is created from the relative of rotation motion of both polishing pad (top side) and wafer (bottom side). Hence, for all particles leaving the domain, they must gain velocity of the top side (0.707 m/s) which is calculated from the rotation speed (regarding the rotation speed 60 cycles/min and the radius of polishing pad and wafer carrier as well).

Fluid solid Interaction:

The basic important action effect at removal mechanism is the interaction between slurry flow and the copper body which is under linear elastic treatment (calculations of the stresses in the case of slight bending of the bars [5]).

The conditions are applied at interface mesh established between solid domain (Copper: 8978 kg/m^3) and slurry (silica: 320 kg/m^3; 0.00108 Pa-s) domain (Fig. 9). The interface

mesh is implemented to be coupled and matched at Fluent settings. This means that the nodes at the interface domain under effect of coupled degree of freedoms. Which means that this node is subjected to effect of coupled variables from both fluid and solid. This is classified under FSI intrinsic term which is introduced by Fluent boundary conditions options. Whenever we apply such conditions, the fluid force vectors at the fluid nodes are transferred to the solid node through the interface domain in the form of displacement vectors. Another important condition is called "completely fixed" which means that the solid nodes are constrained such that keep its position coordinates during the execution process (as the computational time grows up).

Investigation the domain under consideration, we can imply that the change of variables at Z-direction could be neglected with respect to the change in x and y direction. Also, for the solid body, it suffers from high stress at y and x direction to resist the slurry flow. Therefore, we can assume a symmetric plane ($z = 1\mu m$) as a standard plane in which we can inspect the change of the required variables at both fluid and solid domains. At the symmetric plane, the variation for all variables take place at x and y direction which decreases the degrees of freedoms of the problem. For solid body boundary conditions (Fig. 9), it is assumed that the two faces parallel to YZ plane are affected to the fluid solid interaction except for the x direction where it is subjected to zero-displacement condition. This to reassure that the copper body will not be shifted from its original place during the simulation. The two faces parallel to XY plane are completely under effect of fluid solid interaction, where the two faces parallel to ZX plane (top and bottom) are completely fixed.

4.4 Results and Discussion
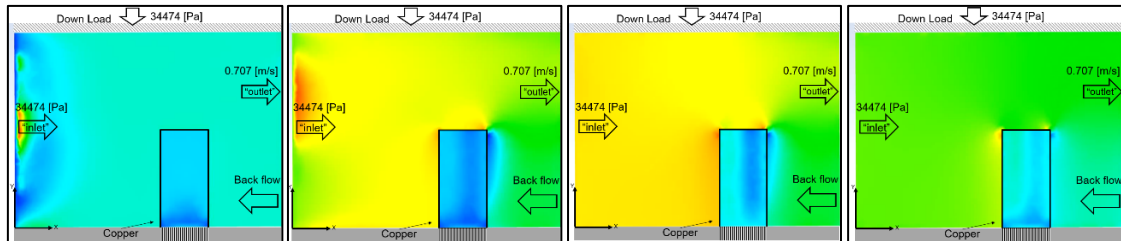
Fig. 10 Different configuration for pressure-contours progress at unsteady treatment.
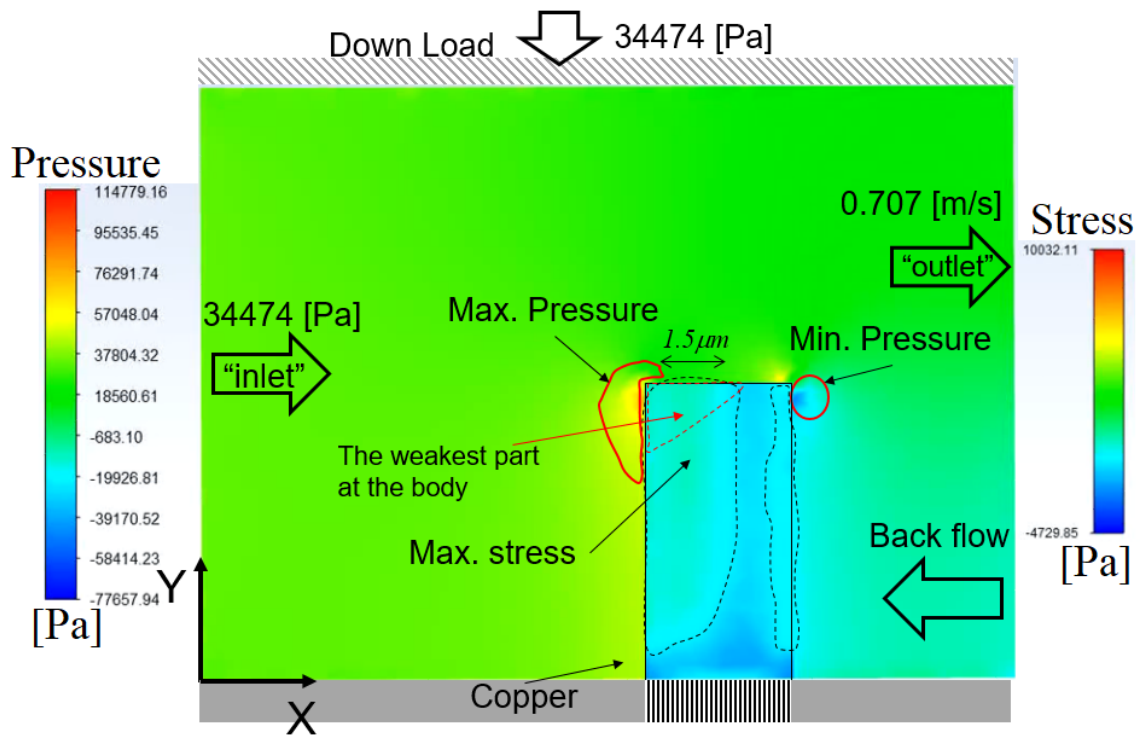
Fig. 11 Pressure-stress contours for slurry-copper interaction at steady case.

At the beginning the pressure inlet boundary condition implies to concentrate the entering particles which have high kinetic energy at the top centre of the inlet face due to the collision between the particles (Fig. 10) which is provided by the surface forces and the turbulent kinetic energy under the $k - \varepsilon$ turbulent model powerful. Moreover, the particles at bottom inlet also gain high pressure due to effect of hydrostatic pressure. However, these particles tend to move out the domain, therefore, the high energy

generated at the inlet is dissipated or mitigated which in turn helps for establishment more
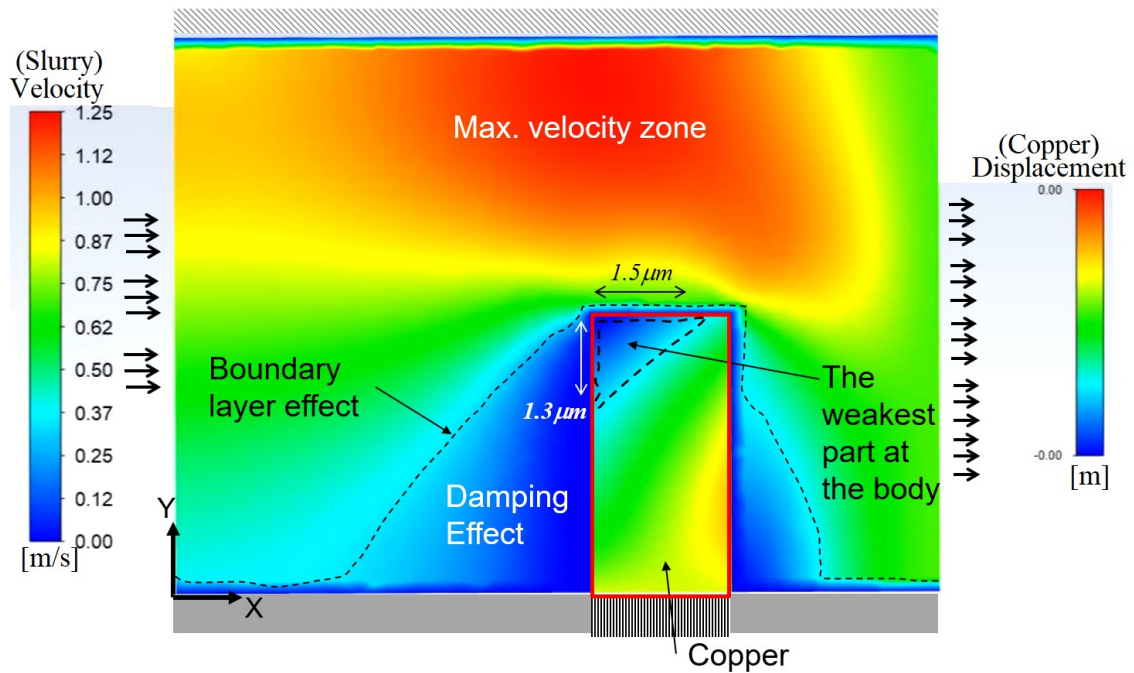
Fig. 12 Velocity-displacement contours at steady case.

stable flow field (Fig. 11).

By the time, the velocity of the particles at bottom inlet fall down while the particles at

the top centre of the inlet zone are remaining to keep their high speed. At the same time,

there are high velocity regions appear inside the domain (but not higher than velocities at

inlet region) adjacent to the top surface due to the direct contact pressure coming from

the down load. Simultaneously, high velocity regions appear on the back of the copper

body could be considered as a result of the back-flow current which comes from the outlet.

The back-flow interaction increases with time progress. As time goes on, the high velocity

region at the inlet is transferred to the top-centre inside the domain, dominates more larger

volume and expands around the copper body. Moreover, this high kinetic energy of slurry

mass is concentrating at the back of copper body due to increase the collision between

the entering fluid particles and the back-flow current. As state closes more to the steady case; the interaction between the two opposite fluid currents (entering and back flow) decays and the effect of boundary layer of the bottom side dominates the adjacent zone as well as the copper body (which is considered as flow barrier). Therefore, the high velocity region is dedicated only at the upper half of the domain especially at zone trapped between copper tip and the top side (Fig. 12).
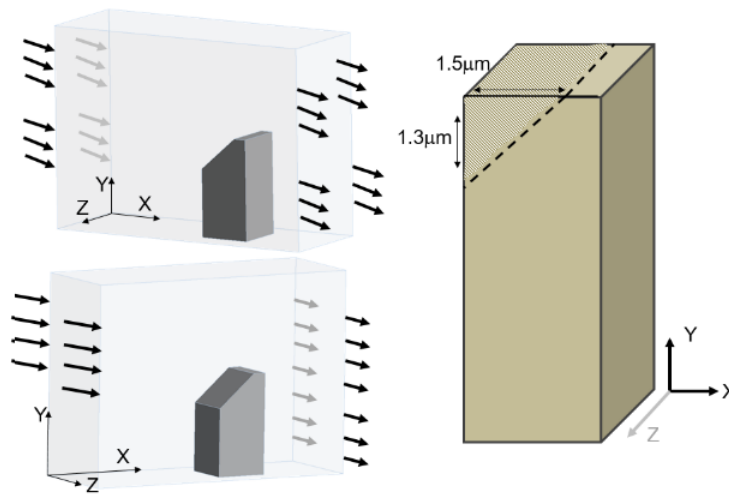
Fig. 13 Mass loss due to removal mechanism of Cu-CMP (step2).

The fixed velocity at the outlet is due to the effect of rotating wafer and the polishing pad. It keeps the pressure growth inside the domain to not be wasted outside as possible. Moreover, it prevents the particles with eccentric velocities (velocity spikes) from developing. After the fluid arrive the steady case, and we could denote the weakest region at copper body, then the removal process (Fig. 13) is performed by using the geometry coordinates of the contours. By this action we are transferring to step 2 with the new geometry configuration of the copper body (Fig. 14). The distinguishable character at this step is that the tip of the copper body is sharper, therefore, it is exposed to more intensive slurry flow (Fig. 14). Moreover, the tilted face which is new side (was not exist at first

step) greatly affect the stress diffusion within the solid body. Firstly, for the slurry flow field, the highest kinetic energies of fluid particles are located at the top side far from the effect of boundary layer and under the effect of main stream flow. While around the copper body and the bottom side, the effect of boundary layer dominates the flow field. This effect which is interpreted as a damping effect for the energetic fluid particles. A large part of the copper body bottom suffers from high displacement or lower stress response due to the fixed base at the bottom and the high stress at the top especially at the tip of copper body which is converted by balance of momentum calculation at static case to high displacement at the opposite limit, which is the bottom side here. It is worthy to mention that the trapped mass between the copper tip and top surface of fluid domain decreases the mass flow rate and increase the fluid particle velocity.
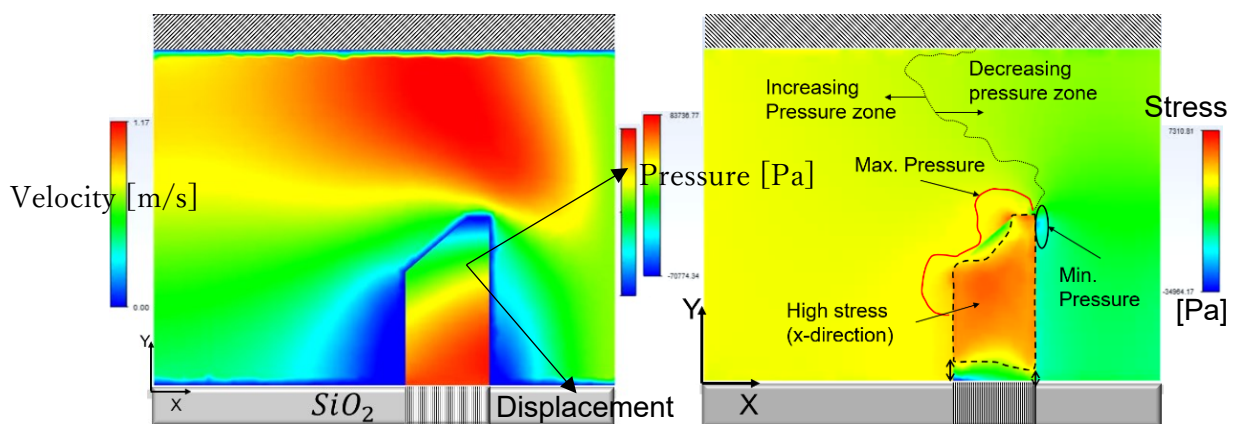
Fig. 14 Slurry flow field effect on copper body (left), and Pressure-Stress interaction (right) at steady case.

Consequently, it is noticed that (Fig. 14 right) the tip of the copper body divides the flow field into two separated regions at steady case; the right region is the pressure-increasing region, where the pressure of fluid particles monotonically increases due to the boundary condition at the inlet. While the left region is the pressure-decay zone due to the fluid particles loss their kinetic energy by the effect of dissipation of velocity

boundary condition. So that we can understand why the maximum pressure zones exist on the limits of the tilted side (simple corners) while the minimum pressure zone locates near the tip of back side of the copper body. It is worthy to mention that at Fig. 14 (left), where the distribution of velocity-displacement contours is displayed, the base of the copper body shows the highest displacement. This could explain as if we consider the copper body as same as a cantilever, then the high stress at the top tip of the body will generate inevitably high displacement at the opposite limit (the base of the body) due to the momentum balance within the solid body.

As stated before, the tilted side enhances the high stress distribution at copper body, such that we can determine the weakest region which will be removed under flow action. It is worthy to notice that the mass removal at this step is larger than the previous because the number of sides at solid body which are exposed to the direct effect of slurry increases, in addition, the sharp corners number is decreased. Fig. 15 shows the dimensions of the new configuration of the stressed copper body (step 3) where a medium pressure value dominates the flow field for all domain. In addition, slurry flow tends to more stable case with relatively high speed. However, the solid body suffers from high stress effect especially at the vertical direction where the dimensions are much small (Fig. 16). Therefore, the probability of removing the protrusive copper is very high at this step. We can conclude that completion of the polishing process depends on how control the strength of flow intensity during the remain time.
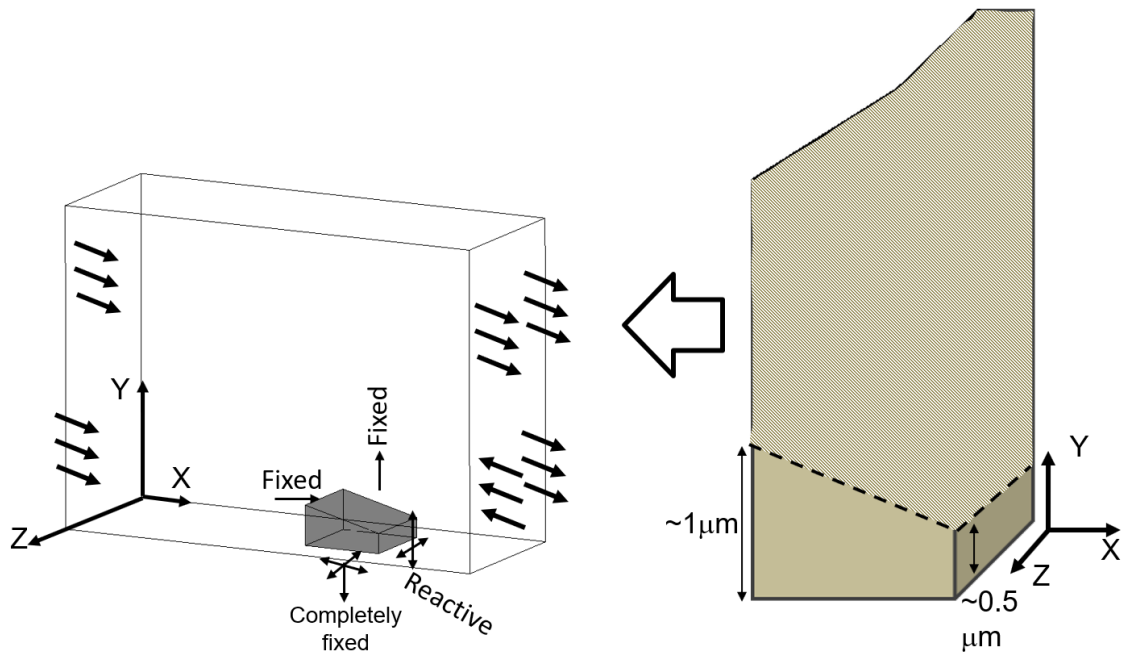
Fig. 15 Mass loss due to removal mechanism of Cu-CMP (step 3).
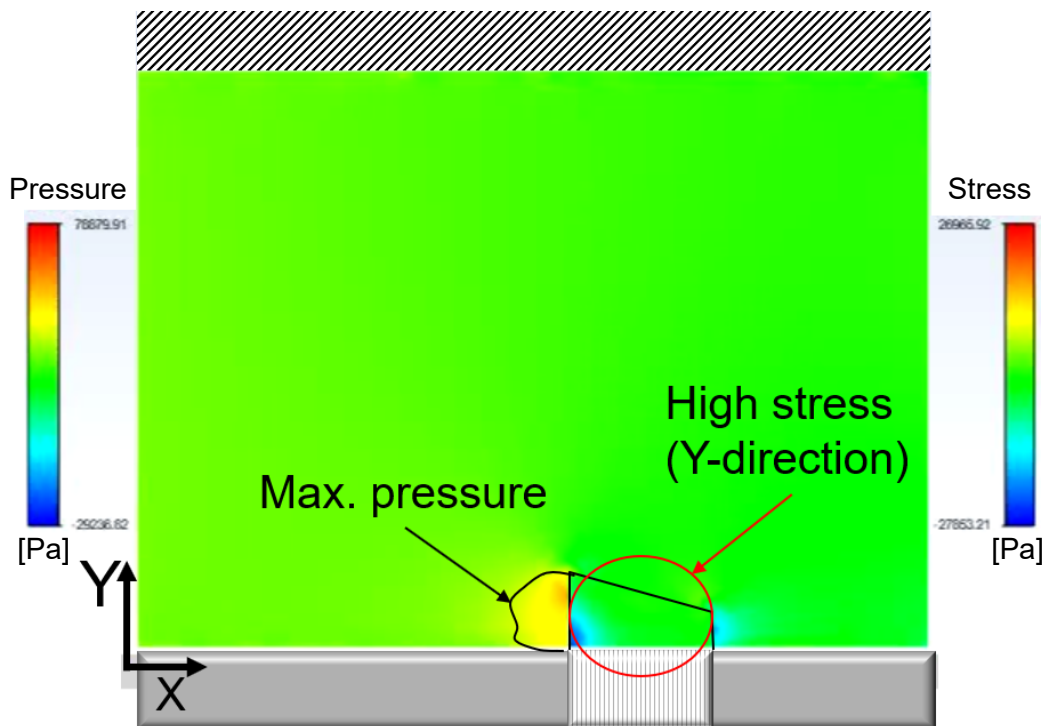
Fig. 16 Steady case for pressure distribution (slurry) and copper vertical-stress response (inside black polygon) for the step 3 of removal mechanism Cu-CMP.
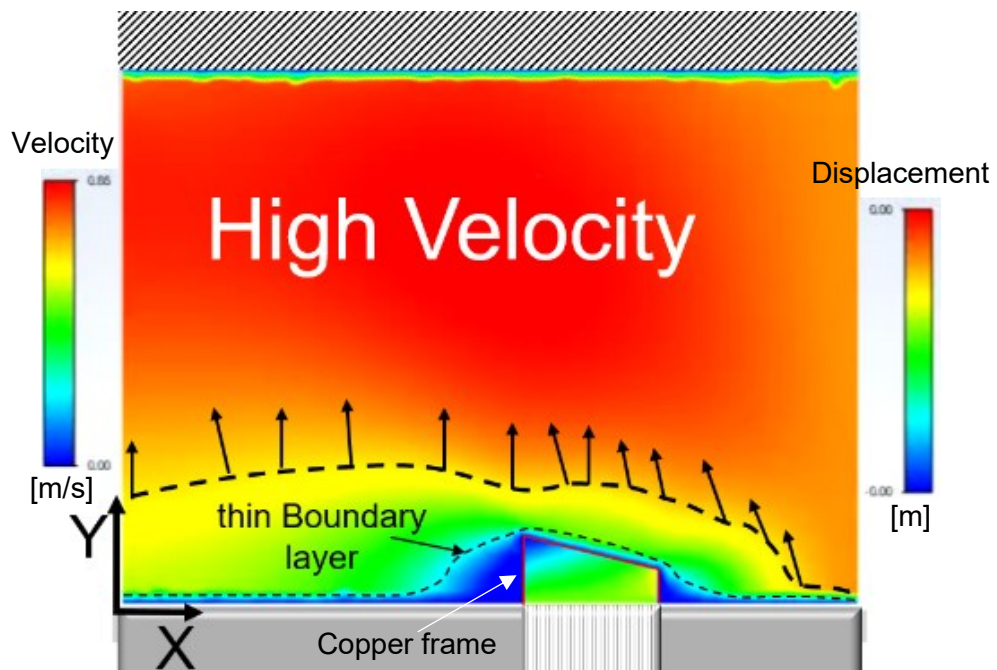
Fig. 17 The greatest velocity values dominates the majority of the domain at removal step 3.

References

1. S. B. Trickey, P.A. Deymier , CHALLENGES AND STATE OF THE ART IN SIMULATION OF CHEMO-MECHANICAL PROCESSES, CHEMICAL MECHANICAL PLANARIZATION IV Proceedings of the International Symposium, Proceedings Volume 2000-26, Copyright 2001 by The Electrochemical Society, Inc. All rights reserved, The Electrochemical Society, Inc. 65 South Main Street Pennington, New Jersey 08534-2839, USA, Library of Congress Catalogue Number: 2001086381, ISBN 1-56677-293-1.

2. Jianfeng Luo, Integrated Modeling of Chemical Mechanical Planarization / Polishing (CMP) for Integrated Circuit Fabrication: from Particle Scale to Die and Wafer Scales, PhD Thesis, Copyright © University of California, Berkeley, Spring 2003.

3. P. Gargini, "The International Technology Roadmap for Semiconductors", GaAs IC Symposium. IEEE Gallium Arsenide Integrated Circuits Symposium, DOI: 10.1109/GAAS.2000.906261, Print ISBN:0-7803-5968-2, Semiconductor Industry Association, 1999.

4. Stanley Wolf, Richard N. Tauber, Silicon Processing for the VLSI Era, Vol. 1, Process Technology, 2000, ISBN-13: 978-0961672164, ISBN-10: 0961672161, Lattice Press, Sunset Beach, California, U. S. A.

5. A. P. Boresi, R. J. Schmidt, O. M. Sidebottom, "Advanced mechanics of materials", 1993, ISBN: 9780471551577, 0471551570, John Wiley and Sons, New York

Chapter5:

Classification by

Fluid Dynamics

Chapter 5: Classification by Fluid Dynamics

5.1 Background for fluid dynamic models for CMP

5.1.1 Model of Pressure-Stress Interaction based on film thickness [1]

One suggests that the workpiece is separated from the polishing pad by a hydrodynamic film of slurry, and polishing is done by collision of the slurry particles with the surface (erosion). The other more promising suggestion is that the hydrodynamic effect is not strong enough to separate the workpiece from the pad and the asperities of the pad contact the wafer with entrained slurry particles (abrasion).

The current study expands on this work with a more thorough investigation by the finite element method of the magnitude and distribution of the contact stress and fluid pressure. In addition, we present a finite element analysis at the feature scale of an individual pad asperity in contact with the wafer.

Wafer scale:

The externally applied force F_z is the integrated sum of the contact stress a on the asperities and the fluid pressure p. Contact stress is the local normal force per unit area that one surface exerts on the other at a solid-solid interface. The equations that result from any model, and relevant simulation strategies, must include a force balance and a momentum balance, namely,

$$\frac{F_z}{A} = \int_A (\sigma + p)dA, \qquad M_y = \int_A x(\sigma + p)dA \quad (1)$$

In the above equation, the applied moment M is due to the global contact friction force $F_x = C_{friction}F_z$ multiplied by an effective moment arm between the interface and the pivoted support of the wafer.

The simplified conceptual model proposed below appears to capture the basic physics of the wafer-pad contact mechanics and slurry fluid flow of the CMP process. In particular, the model can predict the counter-intuitive experimental determination of <u>suction fluid pressure below the pad introduced above</u>. If the model continues to successfully predict observed trends, better predictions are expected as model features and parameter values are refined.

The essential description of the mechanical problem is that the wafer is subject to an externally applied normal load and undergoes a displacement into a compliant pad surface. The pad surface is very rough by usual tribology standards - for the purposes of this study, both the roughness/pore height and the spacing of the asperity peaks are assumed to be about 50 μm. The pad material is porous but largely impermeable, except near the surface. The process of 'conditioning' (roughening) the pad surface exposes the rough pore structure. Both the contact forces of the pad asperities and the slurry fluid forces balance the externally applied normal download. The contact stress, while treated in the wafer-scale model as continuously varying, is visualized as an ensemble of discrete contact points, transmitted through the asperities. Thus, we assume the fluid and solid forces are both distributed over the same area **without** influencing each other. Due to the small size of the slurry particles, and the relatively small solids fraction of the slurry, the fluid is assumed to **be Newtonian**. The fluid is assumed to flow through a film of varying height, which is essentially the effective height of the compressed asperities it was proposed the following model to explain the interfacial pressure profile, portrayed schematically in Fig. 1.

Relative motion of the interface produces a shear stress due to rubbing, which produces an applied moment on the wafer. The applied normal load and moment produces an

asymmetric bowl-shaped contact stress (9, 10). The stress shape leads to a thinner fluid film around the fixture (wafer) edge and a thicker film at the center due to the non-uniform deformation of pad asperities. This spatial distribution of fluid film thickness, together with the pad-wafer relative motion, generates a fluid pressure in accord with Reynolds' equation of hydrodynamic lubrication theory. The net divergence of the film (becoming thinner to thicker in the flow direction) causes the suction pressure.
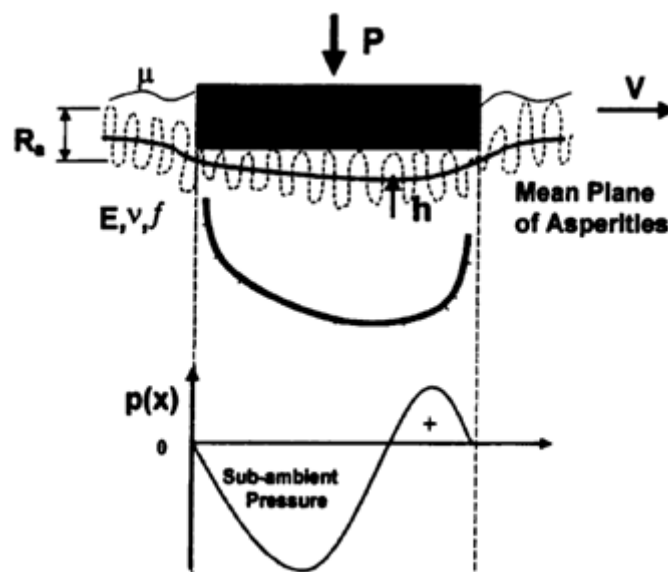
Fig. 1 Schematic of wafer scale model and fluid pressure at wafer/pad interface.

The solid line that runs beneath the wafer in Figure 3 shows a profile of the mean position of the asperities, $h(x, y)$. This curve diverges and converges as a result of the relative motion of the fixture and the rebound of the asperities. The mesoscale model described below relates the contact stress of asperities a to the local mean separation of the surfaces h.

Assuming we know the film thickness $h(x, y)$, the fluid flow problem is addressed by assuming a continuous fluid flow at the interface. The Reynolds equation of hydrodynamic lubrication can be used to calculate the interfacial fluid pressure (11),

$$\frac{\partial}{\partial x}\left(h^3 \frac{\partial p}{\partial x}\right) + \frac{\partial}{\partial y}\left(h^3 \frac{\partial p}{\partial y}\right) = 6\mu(V_x \frac{\partial h}{\partial x} + V_y \frac{\partial h}{\partial y}) \quad (2)$$

where μ is the liquid viscosity and (V_x, V_y) are the relative sliding velocities. The simplified model of Ref. (1) uses one-dimensional analysis, $V_y = \partial/\partial y = 0$. For the case of the wafer rotating at the same speed as the platen (normal industrial practice), it is easy to show that the motion is linear, $V_y = 0$.

Assuming Hertzian contact of individual asperities, the equivalent liquid film thickness can be calculated by using the Greenwood and Williamson (12) contact model for curved surfaces:

$$\sigma(x,y) = \frac{4E}{3(1-v^2)}\eta\sqrt{R_{asp}}\int_{h(x,y)}^{\infty}[z - h(x,y)]^2\varphi(z)dz \quad (3)$$

where, E is the elastic modulus of the pad, v is Poisson's ratio, η and R_{asp} are density (number/area) and average radius of the asperities, respectively, h is the distance between the rigid flat and the mean plane of asperities (equivalent fluid film thickness), and $\varphi(z)$ is the distribution function of asperity heights. For convenience, an exponential distribution can be assumed, $\varphi(z) = \exp\left(\frac{z}{s}\right)/s$, where, s is the RMS of the pad surface roughness.

Performing the indicated integration and solving the resulting equation for h, we obtain,

$$h(x,y) = s\ln(\frac{\eta E\sqrt{\pi R_{asp}s^3}}{(1-v^2)\sigma(x,y)}) \quad (4)$$

5.1.2 Slurry motion model and pressure balance [2]

This study is concerned primarily with the modeling of slurry flow and transport process in CMP in general. Here we show that the interaction between wafer, pad, and slurry need to be modeled on a multiple-scale basis (from wafer scale to pad-asperity and feature scale). Slurry flow can be modeled based on a new unit-cell approach proposed herein. This approach applies to the modeling of flows between pad asperities and flow between (and within) pad grooves. Thermal simulation is also discussed by extending the unit-cell approach to heat and mass transfer. Mass-transfer layer profile is analyzed based on the slurry flow scaling, and polish kinetics is discussed for regimes that are dominated by transport and by abrasion, respectively.

Wafer-scale model:

A 3-D slurry flow solver was developed for CMP simulation. As stated earlier, for simplicity, we use the lubrication model as an example in the following discussion. In the lubrication model, the three-dimensional slurry velocity field can be determined by the two-dimensional pressure distribution within the slurry p (x, y), and the velocity at the wafer and pad boundaries (U_1 and U_2). The unknowns are the slurry thickness and the pressure distribution p (x, y). The dynamic pressure in the slurry can be described as

$$\frac{\partial}{\partial x}\left(\frac{h^3}{12\mu}\frac{\partial p}{\partial x}\right) + \frac{\partial}{\partial y}\left(\frac{h^3}{12\mu}\frac{\partial p}{\partial y}\right) = \frac{\partial}{\partial x}\left[\frac{h(U_1+U_2)}{2}\right] + \frac{\partial h}{\partial t} \quad (5)$$

where h is the distance between wafer and pad. The clearance at the wafer center is h_0. Coupled with the slurry flow is the deformation of wafer and pad under hydrodynamic (and possible contact) pressures. To determine the slurry thickness and the wafer position above pad, the overall force and moment balance on the polisher need to be solved. the slurry thickness is on the same order of pad roughness, and pad asperity effect must be

included to model the slurry dynamics. Similar issues exist in elasto-hydrodynamic lubrication of rough surfaces: The state of lubricating fluid between two solid surfaces can be classified as either boundary lubrication, mixed lubrication, or hydrodynamic lubrication, based on the ratio between lubrication fluid thickness, h, and the solid surface roughness, σ, i.e. h/σ. Conventional CMP process can be classified in the mixed lubrication regime in elasto-hydrodynamic lubrication. the average slurry thickness h can be expressed as

$$\frac{h}{D} = F(\frac{\mu U}{PD}, \frac{R}{D}) \qquad (6)$$

where D is the wafer diameter, μ is the slurry viscosity. P is polish pressure, U is the linear (relative) velocity. Wafer dome height (wafer shape) R is equal to the height difference between wafer edge and wafer center, and is a measure of the wafer curvature. It affects the slurry thickness scaling because changes in wafer curvature shift the load and moment balance for the wafer and therefore redistributes the hydrodynamic stress. Figure 2(a) shows (the freely rotating) wafer tilting downward in the pad velocity direction. This generates a (positive) hydrodynamic pressure that can balance the downward polish pressure P. For convex wafer shapes (wafer center closer to the pad than the wafer edge), negative and positive pressure are generated in the slurry. It creates a clock-wise moment on the wafer, which balances possible moment due to tilting. The moment arrow in figure 2(a) and (b) illustrates this balance.
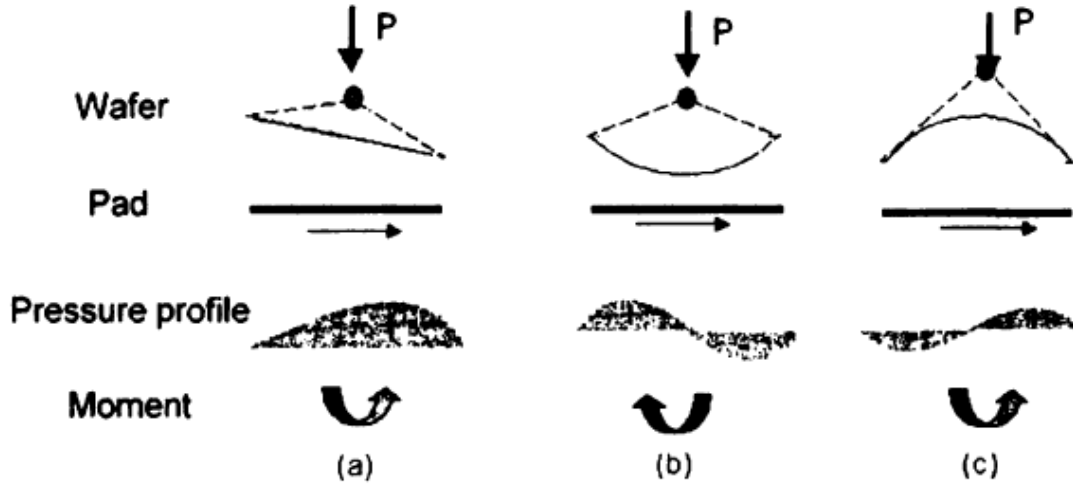
Fig.2 Simulated slurry pressure distribution on the wafer for (a) wafer tilting downward in the pad velocity direction, (b) convex wafer shape, (c) concave shape. Vertical arrow represents pressure and horizontal arrow represents relative velocity. Moment arrow represents moment on the wafer due to pressure distribution about the loading point above the wafer.

For concave shapes, however, the pressure distribution creates a moment that is in the same direction as those due to wafer tilting (figure 2c). Thus, the wafer tends to rotate until there is solid pad-wafer contact. This is also true for random wafer shape variations. Over the wafer scale, it is reasonable to assume that flow balance across the boundaries of a unit cell can still be represented by the first equation at the chapter, but with correction factors due to the roughness. The local flow field can be averaged over the unit cell. The effect of roughness on pressure-drive flux and shear-drive flux can be represented by the pressure factor ϕ_x, ϕ_y, and shear flow factor ϕ_s, respectively. The average lubrication equation for the slurry pressure on the wafer-scale becomes

$$\frac{\partial}{\partial x}\left(\phi_x \frac{\bar{h}_T^3}{12\mu}\frac{\partial p}{\partial x}\right) + \frac{\partial}{\partial y}\left(\phi_y \frac{\bar{h}_T^3}{12\mu}\frac{\partial p}{\partial y}\right) = \frac{\partial}{\partial x}\left[\frac{U_1+U_2}{2}\bar{h}_T + \frac{U_1-U_2}{2}\sigma\phi\right] + \frac{\partial h_T}{\partial t} \quad (7)$$

where $\bar{h}_T$ the average gap. The flow factors are expressed as function of dimensionless slurry thickness h/σ based on extensive simulations over the unit-cell level. In the limit

168

of large h/σ (pad separated from wafer by a thick slurry film), is equivalent to the equation for smooth surface, i.e. $\phi_x \to 1, \phi \to 0$. In the limit of small h/σ (slurry thickness small compared to pad roughness), slurry is trapped in pockets formed by contact between wafer and pad asperities, and the pressure-drive flow is minimal (i.e. $\phi_x \to 0$). authors developed a laminar flow solver for the slurry velocity on the unit-cell level. The flow field within the pad grooves is first calculated using wafer-scale boundary condition (including wafer and pad speed, slurry thickness). Averaged flow properties can be estimated based on the average of detailed flow field. These parameters are then used in the wafer-scale model to calculate wafer-scale pressure distribution and velocity field. In the case of slurry dispensing through the pad (figure 5c), wafer-scale distribution is also coupled with slurry dispensing rate and dispensing pressure.
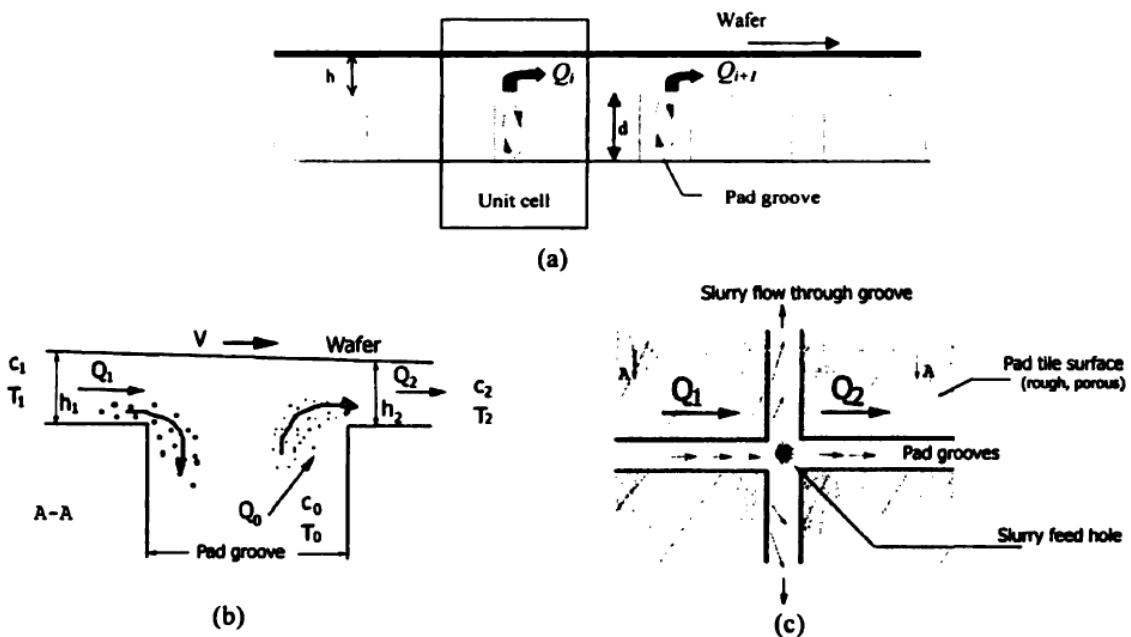
Fig. 3 Schematics of the unit-cell approach for slurry flow with pad groove effect, (a) Location of unit-cell window for slurry flow simulation, (b) Illustration of the flux balance and mass/heat transfer around pad grooves (c) Top view of a unit cell with X-Y type grooves and possible slurry dispensing through the pad (slurry feeding hole).

This multi-scale approach is extendable to mass and heat transfer, as indicated in figure 3(b). The boundary conditions for the unit-cell level simulation then include not only wafer-scale flux (Q), but also concentration and temperature. Convection-diffusion equation can be solved based on the multi-scale velocity field and appropriate boundary conditions at pad and wafer surface. A typical unit-cell simulation is shown in figure 6, with an imposed (arbitrary) temperature at the slurry inlet (left). Flow streamline and temperature fields are shown within the pad groove in figure 5. Groove geometry and slurry thickness can be varied in the simulation to examine their impact on overall polish system performance.
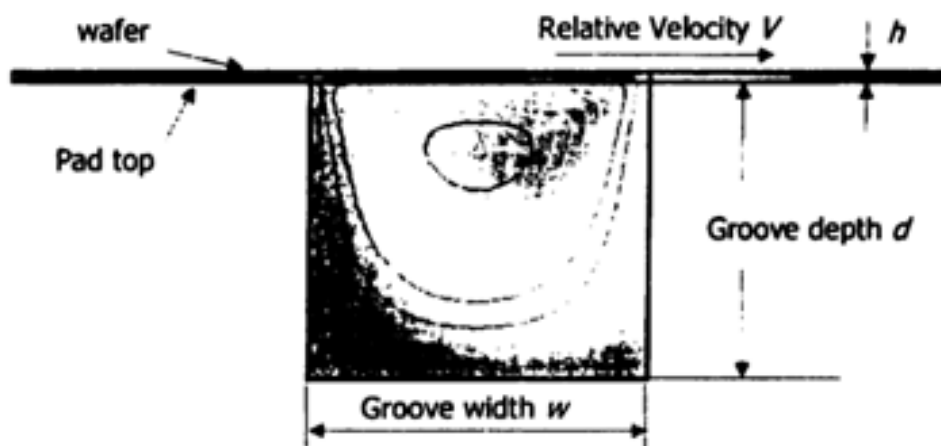
Fig. 4 Flow and temperature field streamlines for a unit cell with pad groove

5.2 Slurry Film Thickness Effect

In CMP, the material removal is created due to the contact between the wafer surface and the polishing pad charged with abrasive slurry.

According to the geometrical relationship illustrated, it is believed that the material removal rate will be influenced by the actual pad contact area on the wafer surface since

the actual pad contact area on the wafer surface controls the number of active abrasives which are in contact with the wafer surface and abrade material from the wafer surface. Under a certain pad and slurry combination, the actual pad contact area, therefore, will heavily depend on the wafer-pad contact mode or the slurry film thickness, which is defined as the distance between the bottom of the wafer and the base surface of the polishing pad in this study.

Given a certain consumable set (abrasive slurry and polishing pad), the major factor which dominates the wafer-pad contact mode is slurry film thickness between the wafer surface and the polishing pad. It has been acknowledged that understanding the behavior of slurry film thickness in CMP is fundamental to the investigation of material removal mechanisms and the development of a process model for CMP [3]. The slurry viscosity, rotation speed, normal pressure, and wafer curvature are critical variables determining the slurry film thickness in CMP [3]. The variation of slurry film thickness has been numerically calculated in terms of rotation speed and slurry viscosity [3,4] and was measured in-situ by using capacitance air gap probes [5]. A simplified two-dimensional numerical model of slurry flow under a wafer surface has been developed to predict the pressure and shear stress under a wafer [6]. Wafer drag force and slurry film thickness have been measured experimentally.

The characteristics of lubrication (boundary lubrication, elasto-hydrodynamic lubrication, and hydrodynamic lubrication) were determined and shown to depend on the lubrication film thickness [7]. In order to explain the behavior of the slurry

film during CMP, hydrodynamic lubrication theory has been adopted [3]. The slurry layer thickness was assumed to be in the range from 10 to 50 um depending on the relative velocity of the wafer.

The wafer-pad contact mechanics will be consider using three wafer-pad contact modes. In addition, the concept of hydrodynamic lubrication theory as applied to CMP will be explained. A general relation of the friction coefficient and the lubrication film with viscosity, velocity, and normal load has been characterized by the Stribeck curve [7]. At low viscosity, low velocity, and high pressure, the lubrication film thickness is small and the state of contact of two surfaces is in direct contact. When two surfaces are in direct contact, the state of lubrication is called boundary lubrication. At boundary lubrication, the friction force in the interface of two surfaces is extremely high. As the viscosity and velocity increase and the normal pressure decreases, the lubrication film thickness between two surfaces increases and the contact modes will change from direct contact to semi-direct and hydroplane sliding contact. The lubrication in semi-direct and hydroplane sliding contact mode correspond to the elasto-hydrodynamic and the hydrodynamic lubrication, respectively. The friction coefficient will initially decrease until elasto-hydrodynamic lubrication is the dominant lubrication; then it will start to increase after the lubrication between two surfaces reaches a state of hydrodynamic lubrication. The effect of three contact modes on CMP performance has been studied [8]. By controlling the thickness of slurry film between the wafer and the pad, it was

found that the material removal of an oxide wafer is independent of normal pressure, relative velocity, and the pad surface properties. Three possible erosion models (padabrasion-based erosion, slurry-shear-based erosion, and pad-abrasion and slurry shear combined erosion) were proposed according to the wafer-pad contact mode and a phenomenological-physical hybrid model was developed to predict CMP performance [9].

The ideal indicator of slurry film thickness, Hersey number, is given as

$$Hersey \ number = \frac{viscosity \cdot velocity}{pressure}$$

Slurry film thickness is proportional to the square root of the wafer velocity and the Hersey number if pressure and viscosity are kept constant in the hydrodynamic lubrication regime [3].

Slurry supplies the direct chemical reaction, distributes the abrasives evenly on the wafer, helps the wafer to slide over the polishing pad without excessive friction, and dissipates undesirable heat generated between the wafer and the pad surface. The width of wafer is assumed to be infinite, which simplifies the problem to a two-dimensional problem. The Navier-Stokes equations for the two dimensional, Newtonian, and incompressible flow with steady state conditions are

$$\frac{\partial p}{\partial x} + \rho \left(u \frac{\partial u}{\partial x} + v \frac{\partial u}{\partial y} \right) = \rho g_x + \mu (\frac{\partial^2 u}{\partial x^2} + \frac{\partial^2 u}{\partial y^2}) \quad (8.1)$$

$$\frac{\partial p}{\partial y} + \rho \left(u \frac{\partial v}{\partial x} + v \frac{\partial v}{\partial y} \right) = \rho g_y + \mu (\frac{\partial^2 v}{\partial x^2} + \frac{\partial^2 v}{\partial y^2}) \quad (8.2)$$

where ρ: density of wafer, p: hydrodynamic pressure, u: flow velocity in x-direction, v: flow velocity in y-direction, gx, gy: acceleration of gravity in x and y axis, and μ: viscosity. Regarding $v \ll u$, and neglecting of the gravity force, therefore

$$\frac{\partial p}{\partial y} = 0 \rightarrow \frac{dp}{dx} + \rho u \frac{\partial v}{\partial x} = \mu (\frac{\partial^2 u}{\partial x^2} + \frac{\partial^2 u}{\partial y^2}) \quad (9)$$

Since wafer surface, h, is much less than wafer length, L, and the inertia force ($\rho u \frac{\partial v}{\partial x}$) can be neglected with respect to viscous force ($\mu(\frac{\partial^2 u}{\partial x^2} + \frac{\partial^2 u}{\partial y^2})$), it yields the reduced form of special Navier Stokes Eq.:

$$\frac{\partial^2 u}{\partial x^2} \ll \frac{\partial^2 u}{\partial y^2} \rightarrow \frac{dp}{dx} = \mu\left(\frac{\partial^2 u}{\partial y^2}\right) \qquad (10)$$

The boundary conditions:

$$x = -\frac{L}{2}; p = p_a, y = 0; u = -U \qquad (11)$$

$$x = \frac{L}{2}; p = p_a, y = h; u = 0 \qquad (12)$$

5.3 Colloidal hydrodynamics and Transports:

5.3.1 Brownian Motion [10,11]

The chaotic, or Brownian, motion of colloidal particles is a direct result of collisions between the colloids and the fluid molecules surrounding them. The trajectory of a colloidal particle undergoing Brownian motion, obtained by tracking its movements at the usual experimental timescale intervals (e.g. seconds), is of the self-similar nature. That is, if any portion of a given Brownian trajectory is magnified (i.e. the sampling time interval is decreased), the magnified trajectory will look qualitatively similar to the original one. Thus, a Brownian trajectory is not a mathematically smooth curve, and the apparent velocity of a Brownian particle derived from it does not represent the true, physically well-defined, velocity of the particle. For this reason, the mean-square displacement is generally used to describe the motion of Brownian particles. To estimate the order of magnitude of Brownian motion, the Brownian motion may be modelled by a series of independent *random walks,* with each walk being described by classical mechanics (such as Newton's second law and Stokes' law). If, at the start of a random

walk, the particle acquires an initial velocity ~0 due to collisions with fluid molecules, then its subsequent motion may be described by:

$$m\frac{d^2x}{dt^2} = -\xi\frac{dx}{dt} \qquad (13)$$

where m is the mass of the particle, x the distance of the particle from the origin at time t, and ξ **is called the friction coefficient**. Hence the solution

$$x(t) = \tau_B u_0\left[1 - e^{-\frac{t}{\tau_B}}\right], u(t) = u_0 e^{-t/\tau_B} \qquad (14)$$

where $\tau_B = m/\xi$ and has the dimension of time. τ_B can be regarded as the typical timescale for a single random walk, also known as the *relaxation time* for the particle's momentum. The **length scale** of a typical random walk, l_B can be considered to be equal to $\tau_B u_0$. The initial velocity may be estimated from the equipartition theorem of kinetic energy:

$$\frac{1}{2}m < u_0^2 >= \frac{1}{2}kT \rightarrow u_0 = (kT/m)^{1/2}, l_B = (mkT)^{1/2}/\xi \qquad (15)$$

where $<>$ denotes statistical mean. Given a hydrosol of 1 μm radius and 1 kg dm^{-3} mass density in water at room **temperature**, it follows that the relaxation time is about 0.2 μs and the typical length of a single walk is about 0.3 nm. By treating Brownian motion as a series of random walks, Einstein (1906) showed that the mean-square displacement of a Brownian particle in one-dimensional projection, averaged over a long period of time ($t \gg \tau_B$) can be expressed as:

$$< x^2 > = 2D_0 t \qquad (16)$$

Due to its isotropic nature, the mean-square displacement of Brownian motion in two dimensions and three dimensions is thus; respectively:

$$< r^2 > = < x^2 + y^2 > = 4D_0 t \qquad (17)$$

$$< r^2 > = < x^2 + y^2 + z^2 > = 6D_0 t \quad (18)$$

where the **diffusion coefficient** D_o is a constant for a single particle in an unbounded fluid, and is related to the friction coefficient I; by the Stokes-Einstein relation [10, 11]:

$$D_0 = kT/\xi \qquad (19)$$

5.3.2 Navier-Stokes Equation

A fluid whose mass density ρ remains constant in time *and* space is called an *incompressible* fluid. If the viscous properties of a fluid can be characterized by a single constant viscosity μ, the fluid is referred to as a *normal* or *Newtonian* fluid. Examples of Newtonian fluids include water and aqueous solutions of inorganic and some organic substances. Fundamental fluid mechanics shows that, under the continuum hypothesis, an incompressible Newtonian fluid can be fully described by the following equations

$$\frac{\partial v}{\partial t} + v \cdot \nabla v = -\frac{\nabla p}{\rho} + \frac{\mu}{\rho}\nabla^2 v + f \qquad (20)$$

$$\nabla \cdot v = 0 \qquad\qquad (21)$$

where **v** is the fluid velocity vector, p the hydrostatic pressure, ρ the mass density of the fluid, and f the external body force exerted on a unit **mass** of the fluid. Eqs. (20-21) is known **as** the Navier-Stokes equation which is, in essence, a reformulation of Newton's second law for a unit volume of the fluid. Equation (21) is called the continuity equation and is actually the conservation law of matter, expressed specifically for the incompressible fluid. Under steady state, i.e. $\partial v/\partial t = 0$, and assuming that the external forces are absent, the Navier-Stokes equation, Eqs. (20-21), can be greatly simplified. For the sake of numerical analysis, the resulting equation may be written in a

dimensionless form, by scaling the velocity and pressure with a reference length *Lo* and velocity *Uo,* as follows:

$$Re\tilde{\boldsymbol{v}} \cdot \boldsymbol{\nabla}\tilde{\boldsymbol{v}} = -\frac{\nabla\tilde{p}}{\rho} + \frac{\mu}{\rho}\nabla^2\tilde{\boldsymbol{v}} \qquad (22)$$

where $\tilde{v} = \frac{v}{U_0}$, $\tilde{p} = \frac{pL_0}{\mu U_0}$, $Re = \rho L_0 U_0/\mu$ is called the Reynolds number, and is one of the most important parameters in fluid mechanics. Physically, it is interpreted **as** the ratio of inertial force to the viscous force, and its value often signifies the prevailing fluid flow regime. For instance, at small Reynolds numbers, the fluid flow is steady and well-behaved (the laminar-flow regime): at large Reynolds numbers beyond a critical value, the fluid flow becomes unsteady and chaotic (the turbulent-flow regime). Different flow regimes entail different treatments to solve the governing equations. It should be noted that the value of the Reynolds number, and hence the flow regime, is determined by the characteristic length scale and velocity used for reference. Thus, although a suspension flowing through a pipe at high speed may be turbulent, the local flow field around each suspended particle may still be laminar.

Mathematically, the Reynolds number can be used to justify simplifications of the Navier-Stokes equation. When Re << **1** and under steady state, the left-hand side terms in eqn (20) can all be neglected. By further assuming that external forces are absent or negligible, eqn (20) becomes:

$$\nabla^2\boldsymbol{v} = \frac{\nabla p}{\mu} \qquad (23)$$

This equation is known as the *Stokes* or *creeping flow* equation and is usually the starting point for theoretical analyses of colloidal hydrodynamics. It's worthy to mention that First, it should be recognized that the Stokes equation is for steady-state laminar flows with

inertial effects being neglected. For example, for a spherical particle of 1 μm diameter in water, Re approaches unity only when the relative speed of the particle is as high as 1 ms⁻¹. Thus, for colloidal systems, the condition that Re << 1 can be satisfied in almost all cases. Secondly, it is a linear differential equation. This is a very useful properly, allowing the superposition technique to be invoked to decompose a complex flow field into simpler ones. This can greatly simplify the effort in deriving a solution to the equation for the complex flow field.
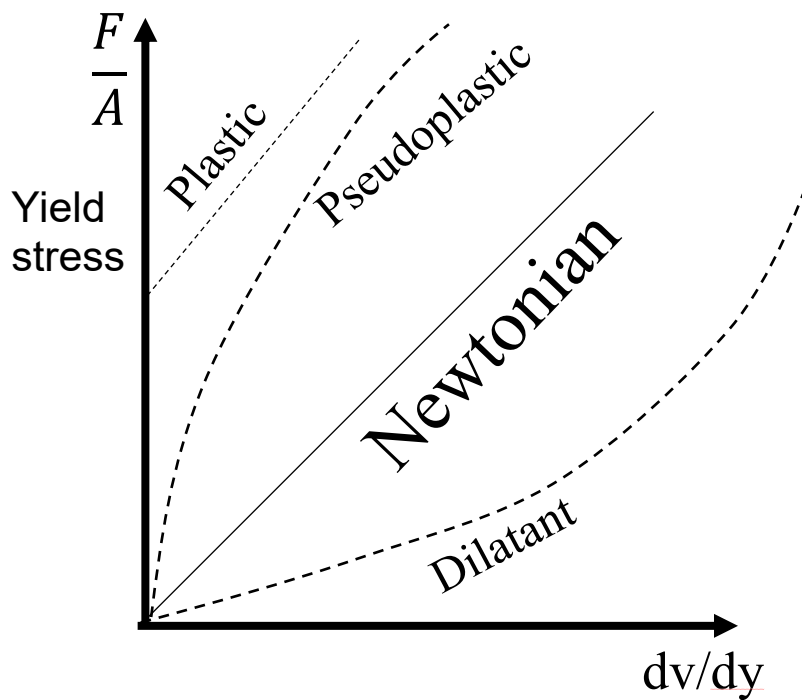

Fig. 5 Effect of stress (vertical) on fluid sandwiched between two parallel plates.

5.3.3 NEWTON's and of viscosity of Dispersion

If force F in x-direction is applied on one of two parallel plates of area A, sandwiched a liquid of viscosity η, its motion was described by Newton's law. It states that the shear

stress $\tau = F/A$, is propotional to dv/dy, where the viscosity of the sandwiched fluid is the factor of proportionality:

$$\tau = \frac{F}{A} = \eta \frac{dv}{dy} = \eta \dot{\gamma} \qquad (24)$$

where $\dot{\gamma}$ is the rate of shear strain (flow deformation per unit length). Previous equation hypothesizes that the shear stress is linearly proportional to the rate of strain. Fluids that obey the form predicted are said to be Newtonian. Non-Newtonian fluids generally show their viscosity; the slope of the tangent to the curve at various points, is a function of the rate of shear.

5.4 Nanofluids characteristics at CMP

5.4.1 The prominent characteristics of the CMP

Chemical Mechanical Planarization/Polishing (CMP) can be deployed for generation engineered surface textures such as microlens array for LEDS, OLEDS applications [12, 13]. The continuous decrease in node size has resulted in an ever-increasing demand for low defectivity during the CMP process. One of the reasons for defectivity during the CMP process is the presence of large agglomerates (over-sized particles) in the slurry nanofluid [14, 15]. Moreover, they affect the viscosity, thermal conductivity, stability, …etc [16] of the slurry. Because the particles smaller than 100 nm exhibit properties different from those of conventional solids. Such solid particles conduct heat much better than do liquids. It is well known that at room temperature, metals in solid form have orders-of-magnitude higher thermal conductivities than those of fluids [17]. Concurrently, Menni et al. [18] have reported that nanoparticles at fluid enhance slurry flow field, turbulence and affect friction values much greater than the base fluid. Simultaneously,

the nanoparticles Ag and TiO2 intensively affect the complex thermo-magneto hydrodynamic flow fields as shown by Krishna and Chamkha [19]. Also, Increasing the nanoparticle volume fraction with the suspensions enhances the temperature over the wedge, plate and stagnation point [20].

5.4.2 Stability of nanofluids and agglomeration

The thermal, mechanical, optical, magnetic, and electrical properties of nanophase materials are superior to those of conventional materials with coarse grain structures [18, 21,22]. The noble properties of nanophase materials come from the relatively high surface area/volume ratio, which is due to the high proportion of constituent atoms residing at the grain boundaries. The number of atoms present on the surface of nanoparticles, as opposed to the interior, is very large. Therefore, these unique properties of nanoparticles can be exploited to develop nanofluids with an unprecedented combination of the two features most highly desired for heat transfer systems: extreme stability and ultrahigh thermal conductivity. Keep in mind that heat transfer phenomenon is associated with other material attributes complexity. For instant, the heat transfer coefficients, in contrary to the skin friction, coincides with viscous dissipation of slurry fluid constituents [23-26]. Moreover, the thermodynamic irreversibility of some fluid parts could greatly variate due to the change of heat transfer rate [27]. Furthermore, because nanoparticles are so small, they may reduce erosion and clog dramatically. Consequently, research and development investigation of nanophase materials has drawn considerable attention from both material scientists and engineers (Duncan and Rouvray [28]).

Most nanofluids containing oxide nanoparticles and carbon nanotubes reported in the open literature are produced by the two-step process. If nanoparticles are produced in dry

powder form, some agglomeration of individual nanoparticles may occur due to strong attractive van der Waals forces between nanoparticles. The two-step method is the most widely used method for preparing nanofluids. The nanomaterials are first produced as dry powders by chemical or physical methods and then dispersed into a fluid in the second processing step with the help of magnetic force agitation, ultrasonic agitation, high-shear mixing, homogenizing, and ball milling [29]. The process of drying, transportation, and storage of nanoparticles cannot be avoided in a two-step method. The two-step method is the most economic method to produce nanofluids on a large scale because several nano-powder synthesis techniques have already been scaled up. The major disadvantage of the two-step method is that the formation of agglomerates is easy due to high surface energy of nanoparticles, while this can be minimized in the one-step method. On the other hand, the two-step method can be used almost with every kind of fluid. The main factor which makes the nanofluid unstable is the tendency of nanoparticles to coagulate/aggregate due to the presence of a high surface charge present on them [30]. Aggregation of nanoparticles within the nanofluid can block the channels of the heat exchanger used for heat transfer. Also, instability of the nanofluid can alter its thermophysical properties like thermal conductivity, viscosity, density, etc. with time, leading to the loss of potential benefits of nanofluids [31].

5.4.3 Nanofluids and agglomeration growth

In terms of the Derjaguin-Landau-Verwey-Overbeek, [32,33] (DLVO) theory of coagulation/agglomeration of colloidal dispersions, a dispersion is stable if a potential energy barrier, larger than the average kinetic energy of the particles, exists. When the mathematical devices are used to describe this state of coagulation in terms of the energy

barrier that is experienced by particles during the collision, and stability ratio as well, they predicted that small nanoparticles will exhibit more rapid coagulation than larger particles [34]. The experimental results pointed out that the stability appears to decrease with increasing the particle size. Or first increases then decreases with increase in the particle size [35].

Hence, the stability of a particle in solution, according to DLVO theory is determined by the sum of van der Waals attractive and electrical double layer repulsive forces that exist between particles as they approach each other due to the Brownian motion they are undergoing. This interaction depends on the distance between particles and the total interface energy F_{DLVO} that is the sum of the van der Waals attraction and the electrostatic repulsion between them.

$$F_{DLVO} = k\varepsilon\varepsilon_0 d_p \varphi_0^2 e^{-k(L)} - \frac{Ad_p}{24L^2} \qquad (25)$$

where φ_0 is the surface potential (created by the surface charge), ε is the relative permittivity of base fluid, L is the separation distance between the particles, A is the Hamaker constant, dp is the diameter of nanoparticle, k is inverse of Debye length ($k = 3.29\sqrt{c}$ (nm^{-1})), (c) is the molar concentration of monovalent electrolyte, and $\varepsilon0$ is the permittivity of free space ($\varepsilon0 = 8.854 \times 10^{-12} \, c^2 m^{-1}$) [36]. However, each of these forces has a particular range of effectiveness and some limitations to be effective. If the attractive force is larger than the repulsive force, the two particles will collide, and the suspension is not stable. For stable nanofluids, the repulsive forces between particles must be predominant. The attractive interaction energy between the nanoparticles depends on the volume fraction. Besides, it also depends strongly on the surface energy (zeta potential) and surface area, which vary with the shape of the particles. For instance, Kim et al. [37]

reported that alumina nanofluids with brick-shaped nanoparticles had the best suspension stability and showed the highest enhancement of thermal conductivity, while the nanofluids with blade-shaped nanoparticles were least stable and showed the lowest enhancement of thermal conductivity despite having the same volume faction and thermal conductivity. Therefore, to prepare a stable homogeneous suspension of nanofluids, the challenge is to overcome the strong van der Waals interactions between nanoparticles that induce the formation of aggregates.

The most widely applied methods for nanofluid stabilization are mechanical dispersion, electrostatic stabilization, and steric stabilization. In mechanical dispersion, a high energy force is applied within the nanofluid to break the clusters of nanoparticles. Electrostatic stabilization occurs when nanoparticles present in nanofluids attain some charge due to the adsorption of ions. This results in an electrical double layer around nanoparticles which creates repulsive forces between nanoparticles. This is a pH-sensitive method. Chemical treatment (surface treatment of nanoparticles) such as the addition of surfactant (polymers) and change in pH of nanofluid are adopted for electrostatic and steric stabilization. Some of the researchers applied all of these methods to gain better stability.

5.4.4 Mechanical methods for agglomeration remedy

Mechanical mixing such as ultrasonication is effective in dispersing agglomerated nanoparticles into the base fluid. Cavitation and bubbles are formed and collapse during the process of ultrasonication. However, heat generated during the ultrasonication process increased the temperature of the nanofluid affecting various parameters like density, viscosity, thermal conductivity, stability, etc. Ideally, ultrasonication time must be optimized because excessive ultrasonication might introduce some defects [38] or may

reduce the size of the nanoparticles. Incidentally, the hybrid nanoparticles were dispersed in polar base fluids with the help of an ultrasonicator [39].

The high pressure/shear homogenization method is more efficient to break the agglomerates of nanoparticles in the nanofluid due to the combined effects of cavitation and high shear force [43] than ultrasonication. Filho et al. [41] prepared a silver/deionized water nanofluid which was found to be stable for more than 3 months. A homogenizer consists of two micro-channels that divided the feed stream into two parts that are again combined in the mixing chamber. There was a huge increase in velocity inside the mixing chamber because the diameter of the feed stream was very less which resulted in high shearing, a large impact on the walls of the chamber, and the formation of strong cavitations within the nanofluid. All these effects were thought to be responsible for the breaking of agglomerates present within the nanofluids. Mechanical or sonic agitation is only effective in temporarily dispersing dilute water-based dispersion, so it is used as a secondary technique for the preparation of nanofluids with long-term dispersion stability.

5.4.5 Nanofluids and Chemical methods for agglomeration remedy

Certain additives like surfactants/dispersants or polymers possess the ability to prevent the aggregation of nanoparticles dispersed in nanofluids. The surfactants cover the surface of nanoparticles with a long loop and tail which extend out into the nanofluids stabilizing them sterically and electrostatically for a long period either in polar or nonpolar solvents as the need arises [42]. The interactions between surfactants and nanoparticles are generally noncovalent interactions such as van der Waals, hydrogen bonding, hydrophobic, and π-π interactions.

1 8 4

In general, when the base fluid is polar, water-soluble surfactants are used, while for nonpolar base fluids, nonpolar surfactants are used. On the other hand, the solubility of nonionic surfactants is described by the hydrophilic/lipophilic balance value. The lower the hydrophilic/lipophilic balance number, the more oil-soluble the surfactants, while a higher hydrophilic/lipophilic balance number surfactant will solubilize polar base fluids. However, care should be taken to use an appropriate amount of surfactant since the use of less surfactant will not produce an efficient coating that creates an electrostatic repulsion and compensate the van der Waals attractions. Generally, a lot of surfactants is required to completely cover the particles, which affects the thermophysical properties of the nanofluids. Further, surfactants may produce foam during heating in heat exchange systems. Therefore, the nanofluid will lose its stability, and the sedimentation of nanoparticles will occur.

For steric stabilization, polymers such as polymethylmethacrylate, Polyvinylpyrrolidone, and polyacrylamide are added into the suspension system, and they will adsorb onto the surface of the particles, producing an additional steric repulsive force [43]. The steric effect of polymer dispersant is determined by the concentration of the dispersant.

Grafting water-miscible polymer chains onto the surface of **nanoparticles (NPs)** has also been proved to be able to suppress inter-particle attraction. The grafted long chains could physically separate neighboring NPs, thus minimizing the van der Waals attraction force [44]. Generally, there are two grafting technologies: "grafting-to" and "grafting-from." The former one directly attaches polymer chains onto NP surface. The latter approach first anchors initiators and then starts the polymerization process to grow polymer chains out from the surface of NPs. The "grafting to" approach may hold better potential for the

preparation of stably dispersed nanofluids at a large scale because of its simplicity. The "grafting-from" approach is more complicated than "grafting-to" method, but it has better control over the grafting density and grafted chain length. The Fe_3O_4 NPs were modified with (3-mercaptopropyl) trimethoxy silane to obtain the Fe_3O_4-SH NPs. The attached initiators then started the polymerization of MMA monomers. The steric repulsion between the grafted polymethylmethacrylate chains rendered the grafted NPs excellent dispersion stability in organic solvents. However, the densely grafted polymer chains would also reduce the thermal energy transfer efficiency among different particles. Moreover, nonionic surfactant mixtures of sorbitan trioleate and polysorbate have shown to be effective stabilizers of *n*-decane/water emulsions due to steric effects of their large, polar head groups.

Controlling pH can lead to electrostatic stabilization through a high surface charge density due to strong repulsive forces. At the isoelectric point pH, the surface charge density equals the charge density of the bulk solution and the zeta potential (the potential difference between the surface of a solid particle immersed in a base fluid and the bulk of the fluid) is zero (point of zero charge). Therefore, the charge density in this layer is zero. At this pH the nanofluids become unstable as the repulsive forces between NPs suspended in a base fluid are zero. As the pH of the solution departs from the isoelectric point of particles, zeta potential becomes large and the nanoparticles get more stable. For instance, it was observed that Cu NPs modified with sodium dodecyl benzene sulfonate have improved dispersion stability within the water when the pH of the solution was increased from 2 to 9.5 [45]. Peterson et al. investigated the effect of pH on the stability of Al2O3 nanofluids. The experiments indicated that the nanofluid was more stable at a

pH of 1.7 than at 7.66. When Al2O3 particles are immersed in water, hydroxyl groups (-OH) are produced at the surface of the Al2O3 particle. When the pH of the solution is lower than the point of zero charges (PZC), the hydroxyl groups react with H^+ from water, which leads to a positively charged surface. On the other hand, when the pH of the solution was higher than the PZC, the hydroxyl groups reacted with OH– from water and created a negatively charged surface.

References

1. Andrew Kim, John A.Tichy, Timothy S. Cale, CMP FINITE ELEMENT CONTACT MODEL: WAFER AND FEATURE SCALE, CHEMICAL MECHANICAL PLANARIZATION IV Proceedings of the International Symposium, Proceedings Volume 2000-26, 2001, Copyright by The Electrochemical Society, Inc. 65 South Main Street Pennington, New Jersey 08534-2839, USA, Library of Congress Catalogue Number: 2001086381, ISBN 1-56677-293-1.

2. Lei Jiang, Harsono Simka, Sadasivan Shankar, MULTI-SCALE MODELING OF FLOW AND MASS-TRANSFER IN CHEMICAL MECHANICAL POLISHING, CHEMICAL MECHANICAL PLANARIZATION IV Proceedings of the International Symposium, Proceedings Volume 2000-26, 2001, The Electrochemical Society, Inc. 65 South Main Street Pennington, New Jersey 08534-2839, USA, Library of Congress Catalogue Number: 2001086381, ISBN 1-56677-293-1.

3. Scott R. Runnels, L. Michael Eyman, "Tribology Analysis of Chemical-Mechanical Polishing", Journal of Electrochemical Society, Vol. 141, No. 6, pp. 1698-1701, 1994.

4. J.Ticky, J. A. Levert, L.Shan, S. Danyluk, "Contact Mechanics and Lubrication Hydrodynamic of Chemical-Mechanical Polishing", Journal of Electrochemical Society, Vol. 146, No. 4, pp. 1523-1528, 1999.

5. J.Levert, , R.Baker, , F.Mess, , S.Danyluk, , R.Salant, L. Cook, "In-Situ Slurry Film Measurements for Chemical-Mechanical Polishing", Proceeding of the American Society for Precision Engineering (ASPE), Vol. 14, pp. 80-85, 1996.

6. C.Rogers, , J. Coppeta, L. Racz, A.Philipossian, F. B. Kaufman, D. Bramono, , "Analysis of Flow Between a Wafer and Pad during CMP Processes", Journal of Electronic Materials, Vol. 27, No. 10, pp. 1082-1087, 1998.

7. John Austin Williams, "Engineering Tribology", ISBN: 0198565038, 9780198565031, 488 pages, 1994, (Oxford University Press), Oxford.

8. M.Bhushan, , R.Rouse, J. E. Lukens, "Chemical-Mechanical Polishing in Semidirect Contact Mode", Journal of Electrochemical Society, Vol. 142, No. 11, pp. 3845-3851, 1995.

9. S. R. Runnels, "Advances in Physically Based Erosion Simulators for CMP", Journal of Electronic Materials, Vol. 25, No. 10, pp 1574-1580, 1996.

10. M. Elimelech, J. Gregory, X. Jia, R. A. Williams, "Particle Deposition and Aggregation Measurement, Modelling and Simulation", chapter 4, ISBN: 0-7506-7024-X, 1995, Copyright by Butterworth-Heinemann, 225 Wildwood Avenue, Woburn, MA 01801-2041, http://www.bh.com.

11. Paul C. Hiemenz, Raj Rajagopalan, "Principles of colloid and surface chemistry", chapter 4, third edition, rev. and expanded, ISBN 0-8247-9397-8, 1997, Copyright by Marcel Dekker, Inc., 270 Madison Avenue, New York, New York 10016.

12. P. Kumar, A. Khanna, S. Son, J. Lee, R.K. Singh, "Analysis of light out-coupling

from microlens Array", Opt. Commun., Vol. 284, NO. 19, pp. 4279–4282, 2011.

13. G.B. Basim, J.J. Adler, U. Mahajan, R.K. Singh, B.M. Moudgil, "Effect of particle size of chemical mechanical polishing slurries for enhanced polishing with minimal defects", J. Electrochem. Soc., Vol. 147, pp. 3523–3528, 2000.

14. T.Y. Teo, W.L. Goh, V.S.K. Lim, L.S. Leong, T.Y. Tse, L. Chan, "Characterization of scratches generated by a multiplaten copper chemical–mechanical polishing process", J. Vac. Sci. Technol. B, Vol. 22, pp. 65–69, 2004.

15. Aniruddh J. Khanna, Sushant Gupta, Purushottam Kumar, Feng-Chi Chang, Rajiv K. Singh, "Quantification of shear induced agglomeration in chemical mechanical polishing slurries under different chemical environments", Microelectronic Engineering, Vol. 210 pp. 1–7, 2019.

16. Sarit K. Das, Stephen U. S. Choi, Wenhua Yu, T. Pradeep, "Nanofluids, Science and Technology", ISBN 978-0-470-07473-2, 2008, John Wiley & Sons, Inc., Hoboken, New Jersey, USA.

17. Y. S. Touloukian, R. W. Powell, C. Y. Ho, P. G. Klemens, "Thermophysical Properties of Matter", TPRC data series, Vol. 2, ISBN: 0306670208, 1970, Plenum Press, New York, LCCN 73129616, https://apps.dtic.mil/sti/pdfs/ADA951936.pdf.

18. Younes Menni, Ali J. Chamkha, Nicola Massarotti, Houari Ameur, Noureddine Kaid, Mohammed Bensafi, "Hydrodynamic and thermal analysis of water, ethylene glycol and water-ethylene glycol as base fluids dispersed by aluminum oxide nano-sized solid particles", International Journal of Numerical Methods for Heat & Fluid Flow, Vol. 30 No. 9, pp. 4349-4386, 2020. https://doi.org/10.1108/HFF-10-2019-0739.

19. M. Veera Krishna, Ali J. Chamkha, "Hall and ion slip effects on MHD rotating boundary layer flow of nanofluid past an infinite vertical plate embedded in a porous medium", Results in Physics, Vol. 15, 102652, 2019.

20. H. Thameem Basha, R. Sivaraj, A. Subramanyam Reddy, and A.J. Chamkha, "SWCNH/diamond-ethylene glycol nanofluid flow over a wedge, plate and stagnation point with induced magnetic field and nonlinear radiation - solar energy application", The European Physical Journal Special Topics, vol. 228, pp. 2531-2551, (2019), https://doi.org/10.1140/epjst/e2019-900048-x.

21. P. Sudarsana Reddy, P. Sreedevi, Ali. J. Chamkha, "MHD boundary layer flow, heat and mass transfer analysis over a rotating disk through porous medium saturated by Cu-water and Ag-water nanofluid with the chemical reaction", Powder Technology, Vol. 307, pp. 46–55, 2017.

22. G. K. Ramesh, S. A. Shehzad, A. Rauf, A. J. Chamkha, "Heat transport analysis of

aluminum alloy and magnetite graphene oxide through the permeable cylinder with heat source/sink", Physica Scripta, Vol. 95, Issue 9, 10 pp., 2020, id.095203, DOI: 10.1088/1402-4896/aba5af.

23. A. J. Chamkha, "Solar radiation assisted natural convection in uniform porous medium supported by a vertical flat plate", J. Heat Transfer., Vol. 119(1), pp. 89-96, 1997, https://doi.org/10.1115/1.2824104.

24. B. Kumar, G.S. Seth, R. Nandkeolyar, A.J. Chamkha, "Outlining the impact of induced magnetic field and thermal radiation on magneto-convection flow of dissipative fluid", International Journal of Thermal Sciences Vol. 146, 106101, 2019.

25. M. Veera Krishna, Ali J. Chamkha, "Hall and ion slip effects on MHD rotating flow of elastico-viscous fluid through porous medium", International Communications in Heat and Mass Transfer, Vol. 113, 1044942, 2020.

26. H. S. Takhar, A. J. Chamkha, G. Nath, "Combined heat and mass transfer along a vertical moving cylinder with a free stream", Heat and Mass Transfer, Vol. 36, pp. 237-246, 2000.

27. Abderrahim Wakif, Ali Chamkha, I. L. Animasaun, M. Zaydan, Hassan Waqas, R. Sehaqui, "Novel Physical Insights into the Thermodynamic Irreversibilities Within Dissipative EMHD Fluid Flows Past over a Moving Horizontal Riga Plate in the Coexistence of Wall Suction and Joule Heating Effects: A Comprehensive Numerical Investigation", Arabian Journal for Science and Engineering, Vol. 45, pp. 9423–9438, (2020), https://doi.org/10.1007/s13369-020-04757-3.

28. Michael A. Duncan, Dennis H. Rouvray, "Microclusters", Scientific American, Vol. 261, No. 6, pp. 110–115, 1989, by Scientific American a division of Nature America, Inc., https://www.jstor.org/stable/24987519.

29. K. R. Sreelakshmy, S. N. Ashwathy, K. M. Vidhya, T. R. Saranya, C. N. Sreeja, "An overview of recent nanofluid research", International Research Journal of Pharmacy, Vol. 5, pp. 239–243, 2014.

30. A. Ghadimi, R. Saidur, H. S. C. Metselaar, "A review of nanofluid stability properties and characterization in stationary conditions", International Journal of Heat and Mass Transfer, Vol. 54, pp. 4051–4068, 2011.

31. S. Mukherjee, S. Paria, "Preparation and stability of nanofluids: A review", IOSR Journal of Mechanical and Civil Engineering, Vol. 9, pp. 63–69, 2013.

32. E. J. W. Verwey and J. Th. G. Overbeek, "Theory of the Stability of Lyophobic Colloids", pp. 164-177, 1948, (Elsevier Publishing Company, Inc. New York), http://www.damtp.cam.ac.uk/user/gold/pdfs/teaching/VerweyOverbeek.pdf.

E. J. W. Verwey and J. Th. G. Overbeek, "Theory of the Stability of Lyophobic Colloids" (Dover Books on Chemistry), ISBN-10: 0486409295, 218 pps, July7 (1999), by Dover Publications.

33. R. H. Ottewill and J. N. Shaw, "Stability of monodisperse polystyrene latex dispersions of various sizes", Discussions of the Faraday Society, Vol. 42, pp. 154, 1966.

34. Yeon-Ah Jeong, Maneesh Kumar Poddar, Heon-Yul Ryu, Nagendra Prasad Yerriboina, Tae-Gon Kim, Jaehyun Kim, Jong-Dai Park, Mingun Lee, Chang-Yong Park, Seongjun Han, Myeong-Jun Kim, Jin-Goo Park, "Investigation of particle agglomeration with in-situ generation of oxygen bubble during the tungsten chemical mechanical polishing (CMP) process", Microelectronic Engineering, Vol. 218, 111133, 2019.

35. G. R. Wiese and T. W. Healy, "Effect of particle Size on Colloid Stability", Trans. Faraday Soc., Vol. 66, pp. 490-499, 1970, https://doi.org/10.1039/TF9706600490.

36. M. J. Rhodes, "Colloids and fine particles" In Book: "Introduction to Particle Technology", 2nd ed., pp. 117-152, 2008, John Wiley & Sons, Print ISBN: 9780470014271, Online ISBN:9780470727102, DOI:10.1002/9780470727102.

37. H. J. Kim, S.-H. Lee, J.-H. Lee, S. P. Jang, "Effect of particle shape on suspension stability and thermal conductivities of water-based bohemite alumina nanofluids", Energy, Vol. 90, pp. 1290-1297, 2015.

38. A. Amrollahi, A. A. Hamidi, A. M. Rashidi, "The effects of temperature, volume fraction and vibration time on the thermo-physical properties of a carbon nanotube suspension (carbon nanofluid)", Nanotechnology, Vol. 19, 315701, 2008.

39. T. Theres Baby, R. Sundara, "Synthesis of silver nanoparticle decorated multiwalled carbon nanotubes-graphene mixture and its heat transfer studies in nanofluid", AIP Advances 3, 012111, 2013.

40. Y. Hwang, J.-K. Lee, J.-K. Lee, Y.-M. Jeong, S. Cheong, Y.-C. Ahn, S. H. Kim, "Production and dispersion stability of nanoparticles in nanofluids", Powder Technology Vol. 186, pp. 145–153, 2008.

41. E. P. B. Filho, O. S. H. Mendoza, C. L. L. Beicker, A. Menezes, D. Wen, "Experimental investigation of a silver nanoparticle-based direct absorption solar thermal system", Energy Conversion and Management, Vol. 84, pp. 261–267, 2014.

42. T. J. Choi, S. P. Jang, M. A. Kedzierski, "Effect of surfactants on the stability and solar thermal absorption characteristics of water-based nanofluids with multi-walled carbon nanotubes", International Journal of Heat and Mass Transfer, Vol. 122, pp. 483–490, 2018.

43. R. S. Kumar, T.Sharma, Stability and rheological properties of nanofluids stabilized

by SiO2 nanoparticles and SiO2-TiO2 nanocomposites for oilfield applications, Colloids and Surfaces A: Physicochemical and Engineering Aspects, Vol. 539, pp. 171–183, 2018.

44. Y. Li, T. M. Krentz, L. Wang, B. C. Benicewicz, L. S. Schadler, "Ligand engineering of polymer nanocomposites: From the simple to the complex", ACS Applied Materials & Interfaces, Vol. 6, pp. 6005–6021, 2014.

45. X. F. Li, D. S. Zhu, X. J. Wang, N. Wang, J. W. Gao, H. Li, Thermal conductivity enhancement dependent pH and chemical surfactant for Cu-H_2O nanofluids. Thermochimica Acta, Vol. 469, pp. 98–103, 2008.

Chapter 6:

Essence points and Summary

Chapter 6: Essence points and Summary

6.1 Catch up the agglomeration

From advanced chapters, a conclusion has been constituted of how researchers could grasp the existence of agglomerates at the solution/dispersion suffers from different conditions due to CMP operation.

6.1.1 Slurry Stability

The fundamental feature discriminating the chemical mechanical polishing CMP is the steadiness and settling of all different kinds of its operations. Any disturbance or fluctuations that occur at CMP components is directly suppressing the general performance of the process. Therefore, studying the stability of used slurry has a dominant effect on all outputs. One of the most promising ways to do that is to know the isoelectric point (IEP) of slurry, on which the slurry particle activity much depends. For instance, to keep colloidal stability, we have to maintain slurry close to IEP. Anyhow, stability handling of the slurry forced us to deal with the agglomerates in our priorities.
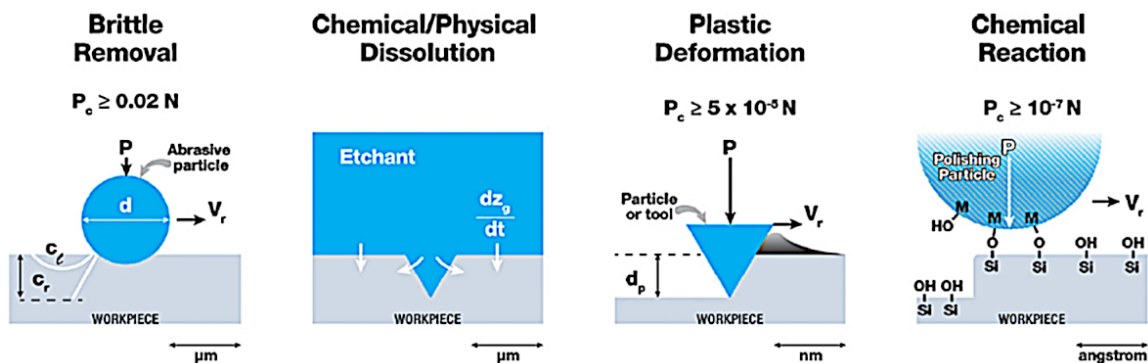

Fig. 1 Various removal mechanisms from a workpiece surface after grinding and polishing [1].
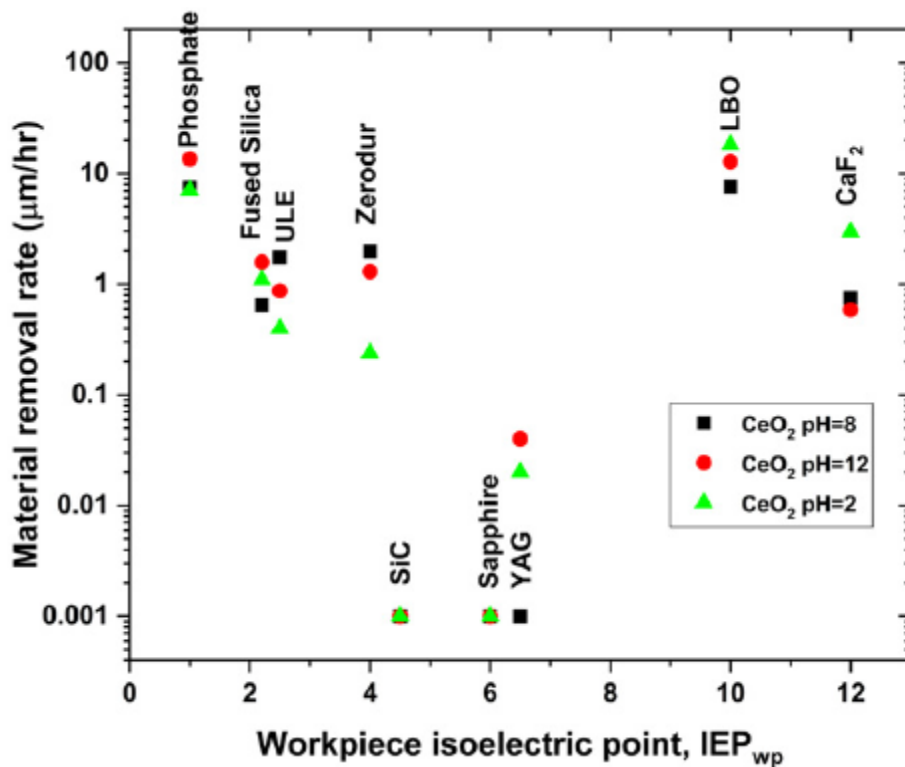
Fig 2. Material removal rate over various workpieces polished using CeO_2 colloidal slurries at different pH values as a function of workpiece isoelectric point [1].

Tayyab Suratwala et al. [1] have stated that colloidal silica is preferable over other slurry types for optical workpiece polishing and material removal rate. It shows nanoplasticity behaviour (Fig.1). When pH>IEP, net surface charge (measured through zeta potential) is negative, and vice versa. So, pH greatly affects the agglomeration and material removal rate as well (Fig. 2). When the charge on the surface is vanishing, it is called the point of zero charge (PZC). However, the weakness is that there is confusion about the definition of large particles and agglomerates features. Also, they are interested only in large sizes (>500nm) of primary particles although those small particle surveys are very relevant in this field.

New perception to describe the stability grade of the slurry was offered by Khanna et al. [2] who have discriminated between what is called soft and hard "shear-induced agglomerates" based on agglomeration and de-agglomeration occurred at slurry either before the process (they have named it as-received slurry) or after the process (they called it stressed slurry) as shown at Fig. 3. However, the adopted consideration by authors which is built on that no existence for intermediate cases other than these two completely
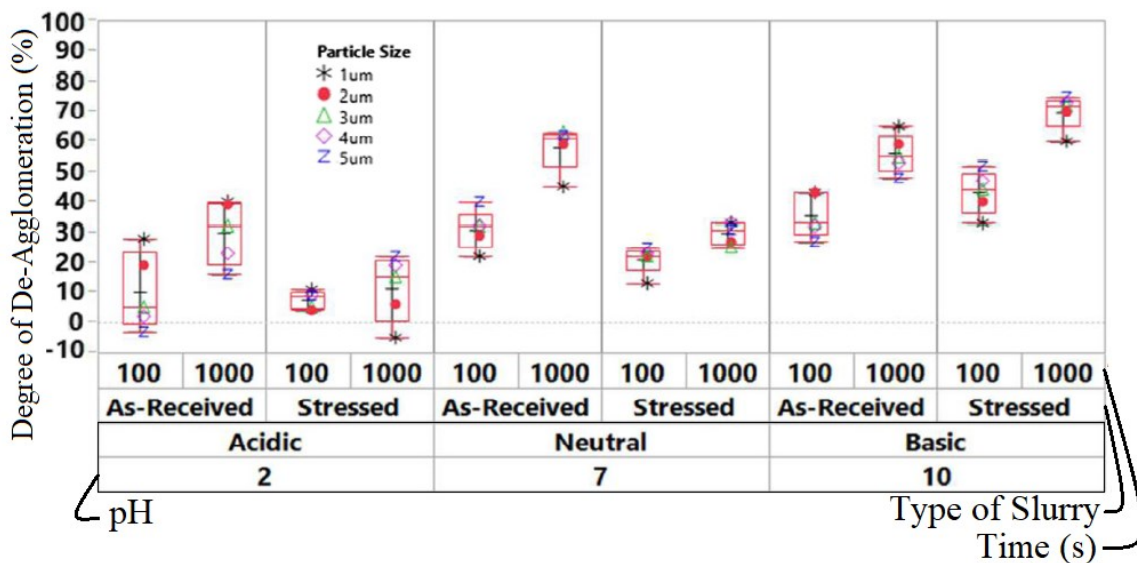
Fig 3. Comparisons of the degree of de-agglomeration of different particle sizes [um] for the two slurry types for shear rate 100 s-1 at different pH for 100 and 1000 seconds [2].
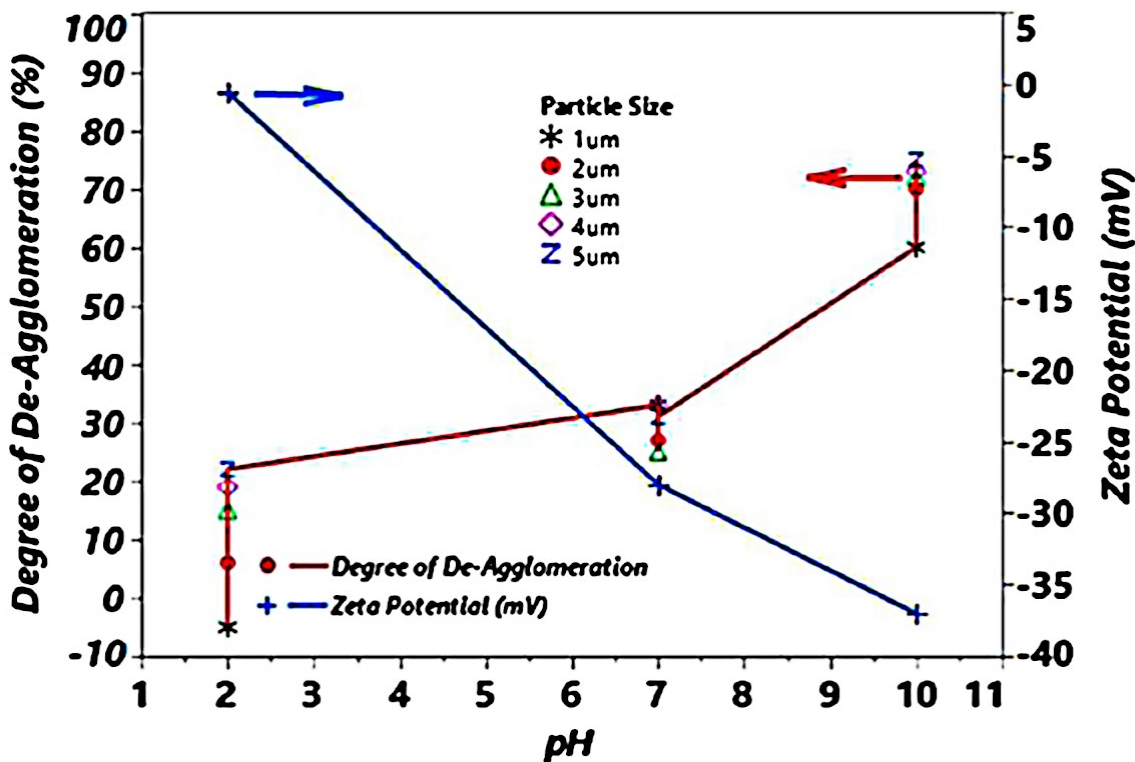

Fig 4. Overlay plot for the degree of de-agglomeration of "stressed" silica slurry samples for different particle sizes and Zeta potential for different pH subjected to a shear rate of 100 s-1 for 1000 seconds [2].

separated opposite classes of agglomeration may be so impractical. For an instant, at stable slurry, the inexistence of agglomeration does not mean that de-agglomeration has taken place. In addition, the possibility of the existence of hard shear-induced

agglomerates at "as-received" slurry, principally draws to the confusion about the main point beyond the particle agglomeration. Nevertheless, the existence of complexity in slurry situations gets us to move away from issuing generalized judgments. For example, they stated that the (de-agglomeration) increases as pH increases, meaning that agglomerates at alkaline slurry are relatively weak (Fig. 4). However, in another literature [3], they proved the opposite idea. Besides, they depicted that the strength of agglomerates is assorting in the opposite of interparticle repulsive force order. But there is no argument about such contradiction. Differently, the comparisons between "as-received/stressed" slurries in the case of basic pH show that de-agglomeration at the stressed slurry has been dominant than what had been investigated in the as-received case. Strictly speaking, the low shear stress has decreased the agglomerates ratio, indicating the high stability of slurry. On the contrary of the acidic case, where the low shear has increased the agglomerates population meaning that there is a high slurry instability impact.

6.1.2 Mutual effect of concentration and particle size

6.1.2.1 Particle size identification

Luan et al. [4] have used dynamic light scattering (DLS) for particle size investigation. They have depicted the effect of slurry filtration on the tails of distribution curves (Fig. 5). Nevertheless, there is confusion about the filtration technique, because it is expected that the right tail of the curve is only affected by filtration (as a large size side). Uncommonly, the shrinkage has occurred at both the right and left tails of the normal distribution curve. So, what had happened for small sizes (<50nm) regarding that only large particles (>0.2um) are restrained by the filtration is not yet obvious. In addition, why intensities of large and small particles are so comparable. As it is outstanding, the scattered light intensity from (agglomerates) must overshadow that from the small particles.
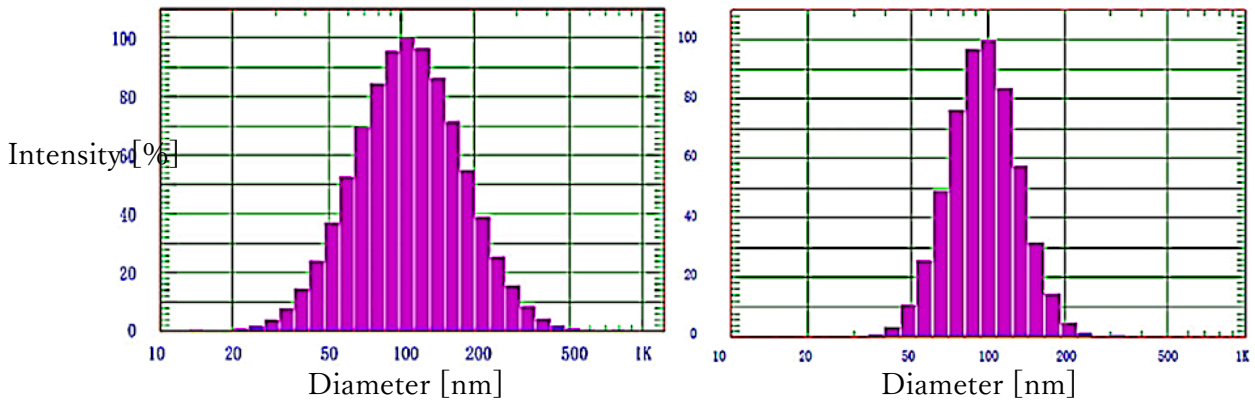
Weight Gauss distribution

Intensity [%]

Diameter [nm]　　　　　Diameter [nm]

Fig 5. Particle size distribution of slurry with 0.5 um slurry filter (left) and 0.2 um slurry filter (right) [4].

6.1.2.2 Abrasives properties from dynamic light scattering

Agglomeration mechanisms had been surveyed through dynamic light scattering (DLS) characterization [5,6]. Hoekstra et al. [7] tracked the agglomerates' growth through evaluation change of the concentration and shear, as well as the dynamic light scattering curves. For instant, they stimulated that the concentration increasing supplies the diffusion-limited aggregation, DLA, while the concentration decrement enhances the reacted limited aggregation, RLA, based on potential barrier *"$k_B T$"*. The defectivity appears from the existence of sodium among the actants, therefore salinity greatly motivates aggregates generation at such unstable slurry. That was explicitly stated by authors by the expression of the rapid nucleation and crystallization. The other drawback is that the relationship between shear and aggregation rate could not be established due to large scatter in the experimental results which outweighed the inaccuracy of the collected data.

6.1.2.3 Relationship between size particle and concentration homogeneity

Lattuada et al. [8] have handled the polymer particles (75nm) for the agglomeration investigation and they have tracked their behaviour by using dynamic light scattering (DLS). They indicated that aggregation controlling is so sensitive because of the scarcity of information on the aggregation kinetics and the limitations of set up conditions as well. Moreover, they believed that particle concentration homogeneity automatically takes place at mixing two solutions where one of them has large primary particles and the other has small primary particles without the need to mechanical action.
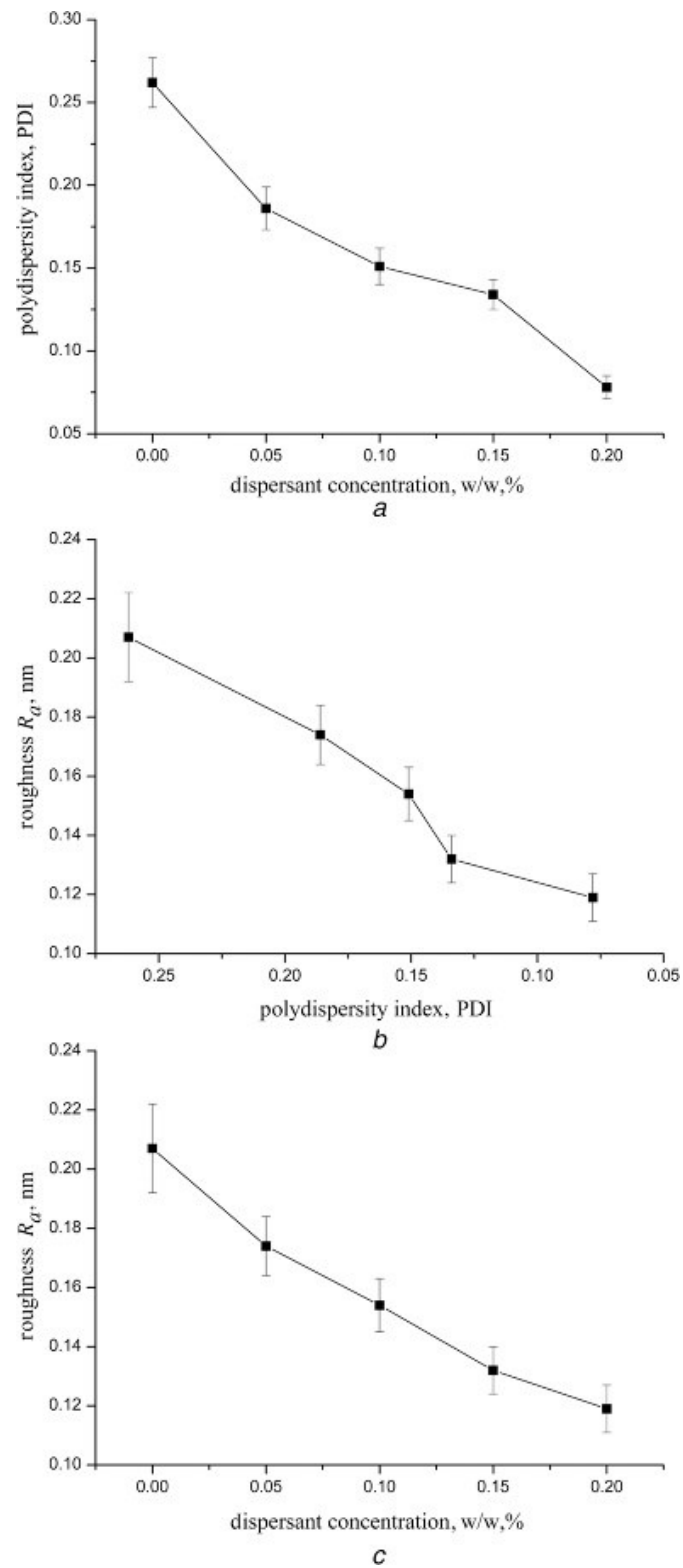
Fig 6. Effect of dispersant concentration on PDI (top), Effect of PDI on surface roughness (middle), Effect of dispersant concentration on MRR (bottom) [9].

Using polymer colloidal could be considered as a fault point. Because it is unaccustomed what is voiced that addition of sodium dodecylsulfate is required to improve the stability but, in reality, this contradicts with sodium property at many of unstable mediums.

It is worthy to mention that Luan et al. [10] were able to correlate among the alternative quantities: large particles (Agglomerates), concentration (percent solids), and the number of particles. Gaopan Chen et al. [9] have deduced that the polydispersity index (PDI) of dynamic light scattering (DLS) curves decreases as concentration increases (Fig. 6). Sensibly, PDI could be affected in the residue from CMP operations. Yet, the existence of ethylenediamine (EDA), the chemical etchant which is conducted to the slurry, here causes problems at slurry, therefore, as slurry concentration increases, EDA effect gradually decreases, so PDI decreases. Although the authors mentioned the benefits of slurry which contains micelles, they admitted the drawbacks that arise the agglomeration (large particle generation) specifically. Still, there is an extraordinary style of MRR and concentration, since the increasing of concentration is proposed to get more stable slurry, though MRR decreases. The uncertainty of the offered hermeneutics rises here due to the expected effectivity of other strong CMP components such as pressure and velocity.

6.1.2.4 Concentration and agglomeration growth mechanisms

Brahma and Talbot [6] have experienced aggregation growth by implementing diffusion-limited aggregation (DLA) and reaction-limited aggregation (RLA) features. But the problem is that they expect the fractal dimension for so large sizes (>500 nm) while ignored study aggregates which are demonstrated from small primary particles that represent a huge portion of agglomeration. In addition, this estimation needs a long time (10 mins) to be accomplished comparable to the timing of other types (such as silica particles) which is known to be much little.

On the other hand, there is a robust attraction between the rate of removal mechanism and the concentration. When the MRR has begun to decline, it means that the concentration level has adjoined to the saturation level. Although the model introduced by Bozkaya and Müftü[11] could predict critical particle concentration (for saturation state) regardless of the particle size value, the ambiguity appears at the experiment that it had not observed the saturation effect for large particle (agglomerates). It could be interpreted as because

the saturation state depends on the real contact area where the particles are trapped between polishing pad asperities and the wafer surface. In the case of agglomerates, they able to make indentations or deformations at the polishing pad surface. In addition, the agglomerates could increase the contact area by causing great indentations at the softer regions on the wafer surface (which in turn cause huge surface damages).
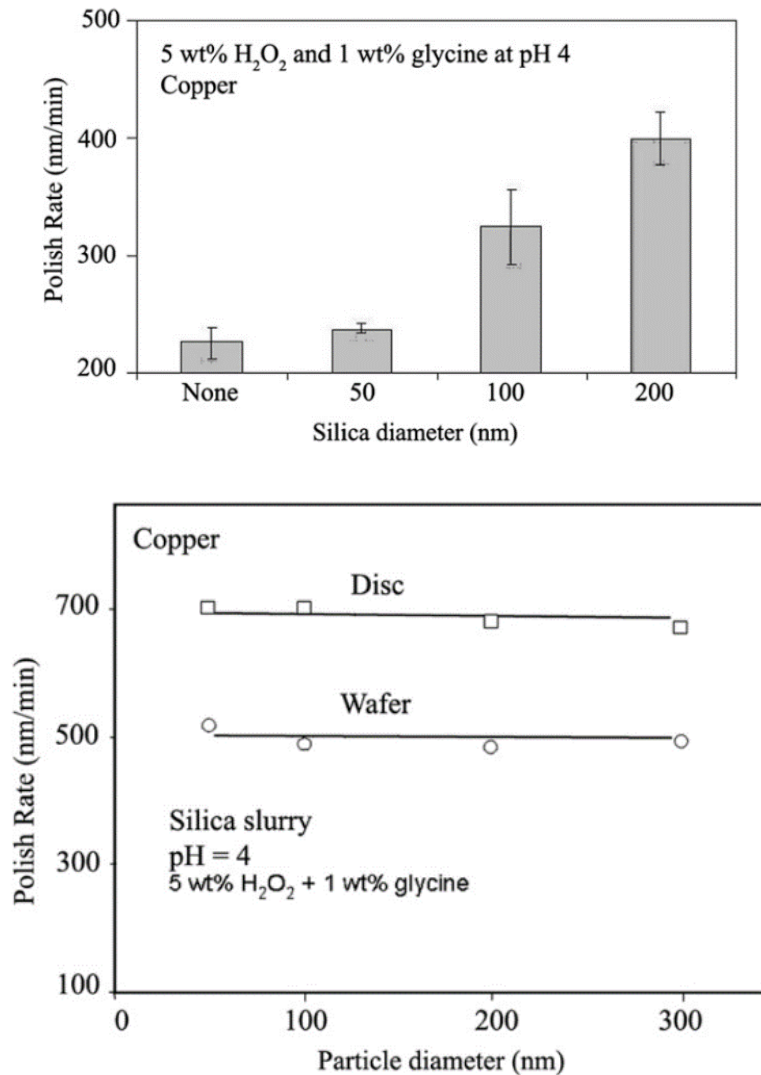

Fig 7. Effect of the silica size on the rates of Cu polishing using aqueous slurries containing the same number of particles (~8.7 × 1012 per 1 g slurry) (top), Effect the polishing rate of Cu with silica slurries, containing this abrasive in terms of the same specific surface area (bottom) [16].

6.1.3 Material removal rate (MRR) patterns

The removal rate on oxide surfaces as a function of the slurry concentration of larger silica particles depends on their sizes [12]. The effects of the particle size on the removal also depend on the substrates to be polished.

The removal rate for Ta and low-*k* [13] surfaces increased with a larger size (Fig. 7, top). On the other hand, the maximum removal rate has been detected when nanosized silica abrasives have been implemented [14, 15]. By the recalculation for these data, it was established [16] that the polish rate was independent of the silica size for slurries of the same total surface area of dispersed abrasives (Fig. 7, bottom). Analogous results were obtained in polishing tantalum disks with these slurries

6.1.4 External operators

The shear-induced agglomeration could be found at conventional polishing, not only the rheo-polishing. Because the shear rate is demonstrated in between two surfaces, one of them is movable and the else is constant and they are separated by fluid region. This phenomenon is myriad in microscale at the intermediate region between the polishing pad (certainly at pores or non-contact areas) and wafer surface as it clearly appears in simulation results. So, based on the fracture of a contact area of the polishing pad (~3%), the effectivity of shear is magnified.

6.1.4.1 Shear as an interface between agglomeration and deagglomeration

Dogon and Golombok [17] have stated that shear rate and availability of slurry ions are the keys of agglomeration study. As concentration increases, agglomeration growth decreases. Farther, they drew attention to the comprehensive expression of suspension ability of the fluid. Moreover, it has been found that as particle size increases, agglomeration growth decreases. Still, the defective point here is that the examined sizes are too large (0.1~300 um) which are tracked using the particle sizer (Gali CIS). However, they concluded that high shear affects only the large particles (agglomerates) and breaks them apart which is contradict with findings exerted by Khanna et al. [7].
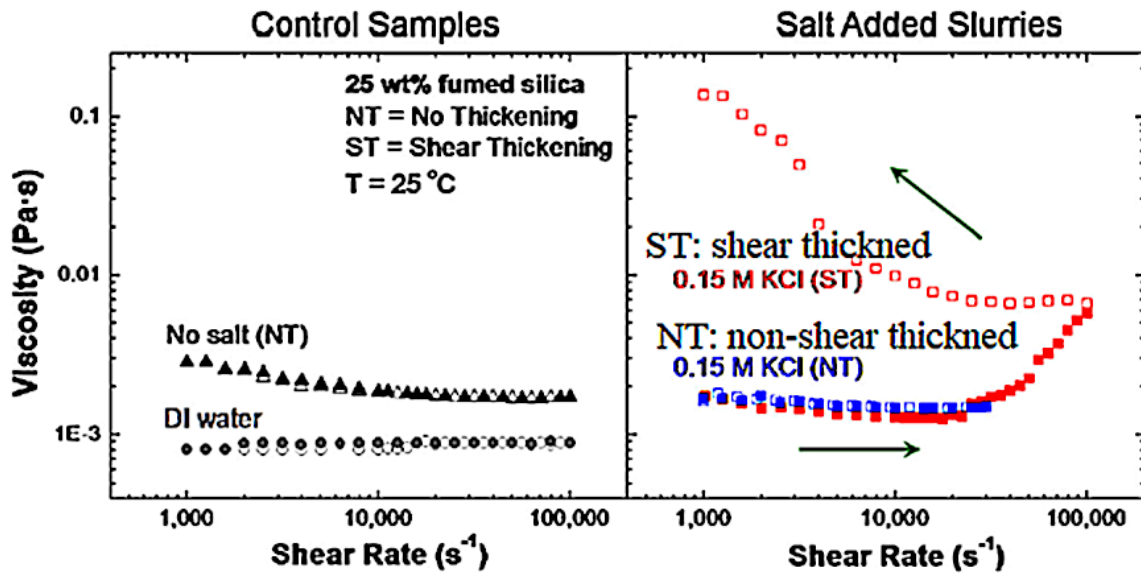
Fig 8. Steady-state shear rate ramp (filled symbols) and reduction (open symbols) for different slurry types [18].

On the other hand, Khanna et al. [3] experienced the slurry shear-induced agglomerates resulted in the activity of surfactants and salts [19]. They proved that the applied shear can increase viscosity (Fig. 8) and enhance agglomeration64. Nevertheless, Khanna et al. [3] have proved also that alkaline slurry is the most stable medium and discovered that slurry shear act as a border between agglomeration and de-agglomeration when it equals 1000 s-1. Although the puzzlement is that slurry which had been used was 35 nm silica particles (10%wt) means that the velocities of the particles are much high due to their many small sizes. In other words, there are myriads of collisions facilitating agglomeration development. That is, it is difficult to control the components which affect the status of the particle.

6.1.4.2 Slurry nature in terms of the Shear

Crawford et al. [18] have investigated the fumed silica slurry 160 nm (25wt%) where the size distributions detected by dynamic light scattering (DLS). They have mentioned that agglomeration caused slurry thickening, hence cause surface scratching. They have also proved that if shear intensity is more than 10000 s-1, agglomeration capable to change the slurry viscosity [20, 21]. Moreover, they have considered that shear thickening is accompanied by the irreversible process which produces hydro clusters. Further, they have pointed out the hydro-interparticle bridging to be the main reason beyond that and proved that DLS could not be suitable for detecting particles larger than 2 μm.

Crawford et al. [18] also have thought that the normal polishing likely implies the shear-thinning due to the polishing pad deformation with the supply of pores and patterns (Fig. 9). But the embarrassment is that why the viscosity remarkably dropped when they used non-thickening slurry as shear increases. This point which is remaining ambiguous.

6.1.4.3 Friction and agglomeration

Gaopan Chen et al. [9] have focused on the friction of CMP (either from the polishing pad or from abrasives) as one of the most critical elements of CMP. Friction treatment depends on the supplication of cellulose polymer layer on silicon wafer and silicon dioxide particles too. Therefore, this the target of adding water-soluble polymer to the slurry. Nevertheless, this induces agglomeration, as well, the high flow rate (50 ml/min), low pressure, and large velocity which all synergies enhancing the agglomeration. Anyhow, the deficiency point that they did not mention the size of primary particles, and the polishing time was relatively long (10mins). However, they demonstrated that the basic pH is applied for stabilizing the slurry due to the existence of chemical etchant.
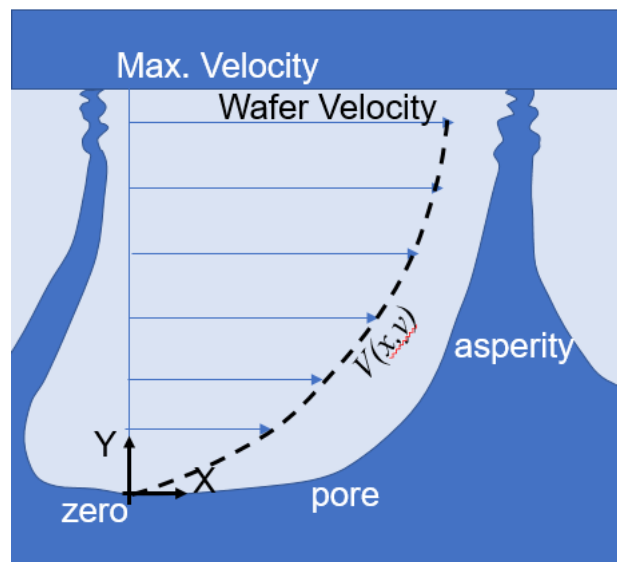

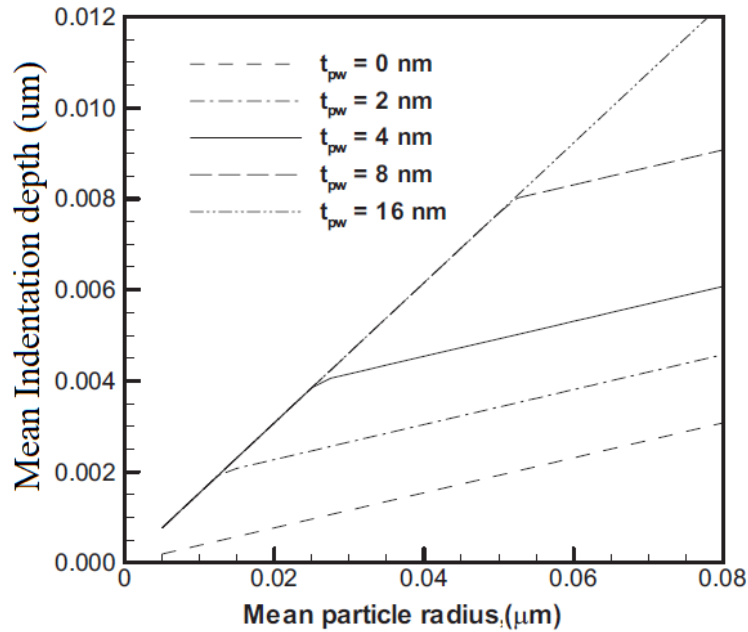Fig 9. Effect of the shear at conventional polishing

Fig 10. Effect of particle size on the indentation [11].

In a related study, the indentation depth which yields from the strength degree of the effective friction force has been observed by Bozkaya and Müftü [11]. They have found that as the particle size increases, the indentation becomes larger (Fig. 10). That's due to the increasing friction force created between the tip of the particle and the wafer surface. The particle size effect has been investigated for different passivated layer thickness "t_{pw}". The previous linear proportionality relationship was been found that holds for very small passivated layer thickness or very large thickness. But for intermediate values, change in this relation has occurred because the particle size increasing implies to exceedance of the critical value at which the particles start to indent through the passivated layer.

6.1.4.4 Triple-sided mechanism with agglomeration: Shear, Pressure, and velocity

It is possible to track the behavior style between the agglomeration and one of the typical CMP characteristics provided that all other remaining elements are kept fixed. Nevertheless, it is somewhat difficult to consider two or more CMP components in the dynamic case with the agglomeration. However, Mariscal et al. [22] applied ceria slurry for polishing SiO_2 wafer to study the relation between MRR and each of Friction, sliding velocity, and pressure. They magnified the serious role of slurry shear on particle behaviour through studying of stribeck+ curves [22] for Mixed Layer (ML) as the dominant tribological mechanism where the wafer and the pad are not in intimate contact

with one another and the fluid layer, which partially separates the two, becomes thicker as pressures drop and velocities rise, leading to lower Coefficient of Friction (COF) values. At polishing pressures of 2 and 3 PSI, the removal rate becomes immune to changes in velocity. COF results show further that at the lowest sliding velocity, COF increases with applied pressure, while at medium and high velocities, COF values drop and become totally independent of pressure.

In addition, Xu et al. [23] have declared the advantages of using composite abrasive slurry as following. The polymers which represent the large particles could be acted as micro polishing pads during the removal mechanism. Hence any deterioration at the removal mechanism resulted in the fluidity decline of the slurry because the shear has been deteriorated therefore, the friction of the micro polishing pad has deteriorated as well. Oftentimes, MRR has a directly proportional relation with silica concentrations and sliding particle velocity due to the chemical cauterization and mechanical friction. Whereas MRR steadily increases with pressure. Thus, it is sensible to predict that the agglomeration effect decays for the dominated-pressure situations. While the agglomeration booster medium is where the concentrations and velocities suffer from broad changes.

6.2 Essence points for Material Removal Model based on nanoparticle agglomeration and Patterned Trapping Model

At the previous chapters, the material removal mechanism has been discussed at different cases of various chemical mechanical polishing criteria. We focused on the effect of particle agglomeration on the material removal behavior and the investigated its state for Cu-CMP by numerical simulation. The following points are extracted from previous discussions.

A new correlation method between material removal mechanism at CMP and particle agglomeration has been studied. Controlling particle agglomeration yields stable concentrations required to obtain uniform material removal rate. The relation between the polishing time and the agglomerates size which is inferred from the proposed model, coincides with the general practical findings as well as the general Preston model. The experimental outputs confirm that the velocity enhances the role of shear force on the particle agglomeration. While the pressure clarifies the effect of the contact area at the deformed asperities at the interface region between the wafer surface of the workpiece

and the polishing pad.

A new technique based on the numerical simulations (using ANSYS) sheds light on the great velocity and pressure variations with respect to micro changes at slurry thickness at CMP operation. Therefore, clear interconnection between flow velocity and pressure appears at unsteady case. This treatment capable us to estimate the final stage of the material removal at the pattern trapped copper CMP process and the optimum criterion as well. From the pressure distribution (at slurry flow domain) and the stress distribution (at Copper material), the removal action is determined. Prominent interaction between pressure-stress appears during the simulation, moreover, it appears at the velocity-displacement contours as well. In general, the stress at the same flow direction (X-direction): (1) dominates the Copper body, (2) coincides with pressure distribution. As the copper body becomes shorter, the normal stress dominates the solid domain. Which, in turn, accelerates the rate of the copper removing, supports arriving the required planarization level, and maintains the amount of manufacturing consumables which are considered very economically expensive.

References

1. Tayyab Suratwala, Rusty Steele, Philip E. Miller, Lana Wong, Joel F. Destino, Eyal Feigenbaum, Nan Shen, Michael Feit, "Influence of partial charge on the material removal rate during chemical polishing", Journal of American Ceramic Society, Vol. 102, pp. 1566–1578, 2019.

2. Aniruddh J. Khanna, Feng-Chi Chang, Sushant Gupta, Purushottam Kumar, and Rajiv K. Singh, "Characterization of the nature of shear-induced agglomerates as hard and soft in chemical mechanical polishing slurries", Journal of Vacuum Science & Technology B, Vol. 37, 011207, (2019); doi: 10.1116/1.5065516, https://doi.org/10.1116/1.5065516.

3. Aniruddh J. Khanna, Sushant Gupta, Purushottam Kumar, Feng-Chi Chang, Rajiv K. Singh, "Quantification of shear induced agglomeration in chemical mechanical polishing slurries under different chemical environments", Microelectronic Engineering, Vol. 210, pp. 1–7, 2019.

4. Xiaodong Luan, Yuling Liu, Baoguo Zhang, Shengli Wang, Xinhuan Niu, Chenwei Wang, Juan Wang, "Investigation of the barrier slurry with better defect performance and facilitating post-CMP cleaning", Microelectronic Engineering, Vol. 170, pp. 21-28, 2017.

5. G.B. Basim, B.M. Moudgil, "Effect of Soft Agglomerates on CMP Slurry Performance", J. Colloid Interface Science, Vol. 256, pp. 137–142, 2002.

6. Neil Brahma, Jan B. Talbot, "Effects of chemical mechanical planarization slurry additives on the agglomeration of alumina nanoparticles II: Aggregation rate analysis", Journal of Colloid and Interface Science, Vol. 419, pp. 25–30, 2014.

7. L. L. Hoekstra, R. Vreeker, W. G. M. Agterof, "Aggregation of colloidal Nickel Hydroxycarbonate studied by light scattering", Journal of Colloid and Interface Science, Vol.151, Issue 1, pp. 17-25, June 1992.

8. Marco Lattuada, Peter Sandkuhler, Hua Wu, Jan Sefcik, Massimo Morbidelli, "Aggregation kinetics of polymer colloids in reaction limited regime: experiments and simulations", Advances in Colloid and Interface Science, Vol. 103, pp. 33–56, 2003.

9. Gaopan Chen, Guihai Luo, Guoshun Pan, Yuhong Liu, Haimen Luo, "Influence of colloidal silica dispersion on the decrease of roughness in silicon chemical mechanical polishing", Micro & Nano Letters, Vol. 11, Issue 7, pp. 382–385, 2016, doi: 10.1049/mnl.2015.0592.

10. Myung-Geun Song, Jin-ho Lee, Yoon-Gyu Lee, Ja-ho Koo, J. Colloid Interface Sci. Vol. 300, Issue 2, pp. 603–611, 2006.

11. Dinçer Bozkaya, and Sinan Müftü, "A Material Removal Model for CMP Based on the Contact Mechanics of Pad, Abrasives, and Wafer", Journal of The Electrochemical Society, Vol. 156, Number 12, H890-H902, 2009.

12. E. Matijevic, S.V. Babu, "Colloid aspects of chemical–mechanical planarization", Journal of Colloid and Interface Science, vol. 320, pp. 219–237, 2008.

13. K. Cooper, J. Cooper, J. Groschopf, J. Flake, Y. Solomentsev, J. Farkas, "Effects of Particle Concentration on Chemical Mechanical Planarization", Electrochemical and Solid-State Letters, Vol. 5 Number 12, G109, 2002.

14. C. Zhou, L. Shan, S.H. Ng, R. Hight, A.J. Paszkowski, S. Danyluk, "Effects of Nano-scale Colloidal Abrasive Particle Size on SiO2 by Chemical Mechanical Polishing", MRS Online Proceedings Library, 671, Article Number: 16 (2001). https://link.springer.com/article/10.1557%2FPROC-671-M1.6.

15. C. Zhou, L. Shan, J.R. Hight, S. Danyluk, S.H. Ng, A.J. Paszkowski, "Influence of Colloidal Abrasive Size on Material Removal Rate and Surface Finish in SiO2 Chemical Mechanical Polishing", Tribology Transactions, Vol. 45 Issue 2, pp. 232-238, 2002.

16. Z. Lu, S.-H. Lee, S.V. Babu, E. Matijevic, "The use of monodispersed colloids in the polishing of copper and tantalum", Journal of Colloid and Interface Science, Vol. 261, pp. 55–64, 2003.

17. David Dogon, Michael Golombok, "Particle agglomeration in sheared fluids", Journal of Petroleum Exploration and Production Technology, Vol.5, pp.91-98, 2015, DOI 10.1007/s13202-014-0121-2.

18. Nathan C. Crawford, S. Kim R. Williams, David Boldridge, Matthew W. Liberatore, "Shear thickening and defect formation of fumed silica CMP slurries", Colloids and Surfaces A: Physicochem. Eng. Aspects, Vol. 436, pp. 87– 96, 2013.

19. F.C. Chang, "Externally induced agglomeration during chemical mechanical polishing of metals and dielectrics", Materials Science & Engineering, Vol. Ph.D, University of Florida, Gainesville, Florida, 2008, pp. 1–123.

20. N.J. Wagner, J.F. Brady, "Shear thickening in colloidal dispersions", Physics Today, Vol. 62 (10), pp. 27–32, (2009).

21. J.M. Brader, "Nonlinear rheology of colloidal dispersions", Journal of Physics: Condensed Matter, Vol. 22, Number 36, Article number = 363101, 2010.

22. Juan Cristobal Mariscal, Jeffrey McAllister, Yasa Sampurno, Jon Sierra Suarez, Mark O'Neill, Hongjun Zhou, Malcolm Grief, Dave Slutz, Ara Philipossian, "Tribological, Thermal and Kinetic Characterization of SiO2 and Si3N4 Polishing for STI CMP on Blanket and Patterned Wafers", ECS Journal of Solid State Science and Technology, Vol.9, Number 4, article number: 044008, 2020.

23. Xue Feng Xu, H.F. Chen, H.T. Ma, B.X. Ma, Wei Peng, "The Mechanism of Polymer Particles in Silicon Wafer CMP", Materials Science Forum, Vols. 626-627, pp 231-236, 2009.